Universidad de Las Palmas de Gran Canaria
Departamento de Bioquímica y Biología Molecular, Fisiología, Genética e Inmunología
Instituto Universitario de Investigaciones Biomédicas y Sanitarias

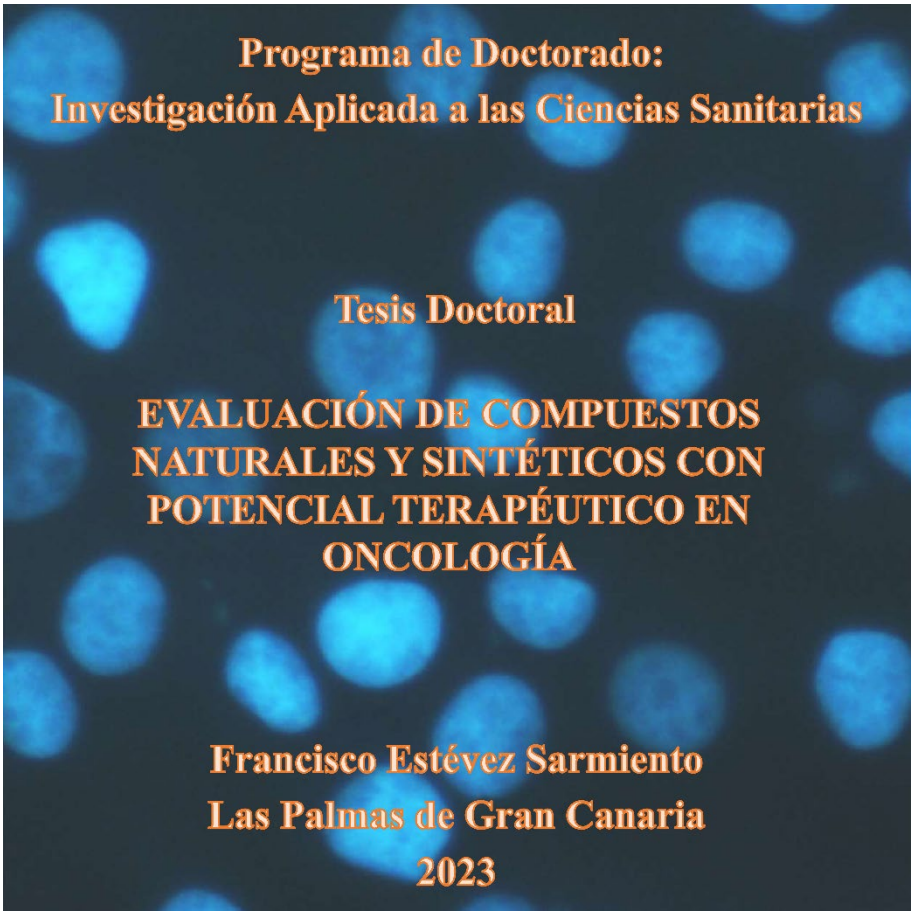

Portada: Microfotografía fluorescente de un campo representativo de células de melanoma humano SK-MEL-1 teñidas con Hoechst 33258 y visualizadas utilizando un microscopio de fluorescencia Zeiss.

Agradecimientos

Esta Tesis ha sido realizada en el Departamento de Bioquímica y Biología Molecular, Fisiología, Genética e Inmunología de la Universidad de Las Palmas de Gran Canaria, Unidad Asociada al CSIC, bajo la dirección del Catedrático Dr. D. Francisco Estévez Rosas y del Catedrático Dr. D. José Quintana Aguiar, a quienes expreso mi más profundo agradecimiento.

Igualmente quiero hacer extensivo mi agradecimiento a todos los compañeros del laboratorio por la ayuda y aliento que me han dispensado en todo momento.

ÍNDICE DE CONTENIDOS

1. Introducción

El objetivo de esta Tesis ha sido evaluar un grupo de productos naturales y sintéticos inspirados en productos naturales con potencial valor terapéutico. La razón de la elección de los productos naturales es debido a que éstos han servido como una fuente clave para el descubrimiento de nuevos agentes terapéuticos y representan aproximadamente el 50% de fármacos a nivel mundial [1]. En el área de oncología los compuestos derivados de productos naturales constituyen más del 70% de todos los fármacos disponibles contra el cáncer [2]. En las últimas tres décadas la resistencia a fármacos ha sido reconocida como un importante obstáculo para los pacientes. Los tratamientos farmacológicos que eran inicialmente eficaces se vuelven menos eficaces. El desarrollo de la resistencia a fármacos puede tener lugar por numerosos mecanismos moleculares [3-5]. Actualmente, la combinación de terapias es una de las elecciones más eficaces y seguras en el tratamiento de las enfermedades oncológicas, puesto que es menos probable la generación de resistencia y es más eficaz que la monoterapia [6-8]. En esta Tesis hemos evaluado los efectos de tres series de compuestos sobre la viabilidad de varias líneas celulares de cáncer humanas. Los productos evaluados fueron derivados de quince átomos de carbono que incluían (i) flavonoides sintéticos; (ii) lactonas sesquiterpénicas naturales del grupo de las guayanolidas

caracterizadas por poseer átomos de cloro y (iii) guanidinas trisustituidas conteniendo un núcleo 1,3-difenilpropenona.

La justificación de la evaluación de estos productos sobre la viabilidad de las células de cáncer se basa en el hecho que aproximadamente el 63% de los fármacos contra el cáncer introducidos en los últimos 30 años son productos naturales o inspirados en ellos [1].

Los flavonoides son metabolitos secundarios presentes en los alimentos vegetales y constituyen un componente en la dieta humana. Químicamente, son compuestos polifenólicos y poseen una estructura fenil benzopirona (C6-C3-C6). Se caracterizan por poseer 15 átomos de carbono dispuestos en un anillo de cromano (A y C) unido a un anillo B en el C2 (flavonoides) o C3 (isoflavonoides). Se clasifican principalmente de acuerdo con el grado de saturación, el patrón de sustitución y el grado de oxidación del anillo C y la apertura del anillo central de pirano en al menos 7 clases principales: chalconas, flavanonas, flavonas, flavonoles, flavanoles, isoflavonas y antocianidinas (Figura 1). Cada clase difiere en el grado de hidroxilación y sustitución. Las chalconas son los precursores biosintéticos de los flavonoides y se caracterizan por poseer el esqueleto 1,3-diaril-2-propen-1-ona. Las flavanonas, también conocidas como dihidroflavonas, se caracterizan por poseer un anillo C saturado y oxidado. Los flavanoles (flavan-3-oles, conocidas también como catequinas) de manera similar a las flavanonas se

caracterizan por poseer un anillo C saturado que normalmente no está oxidado y un grupo hidroxilo en C3.

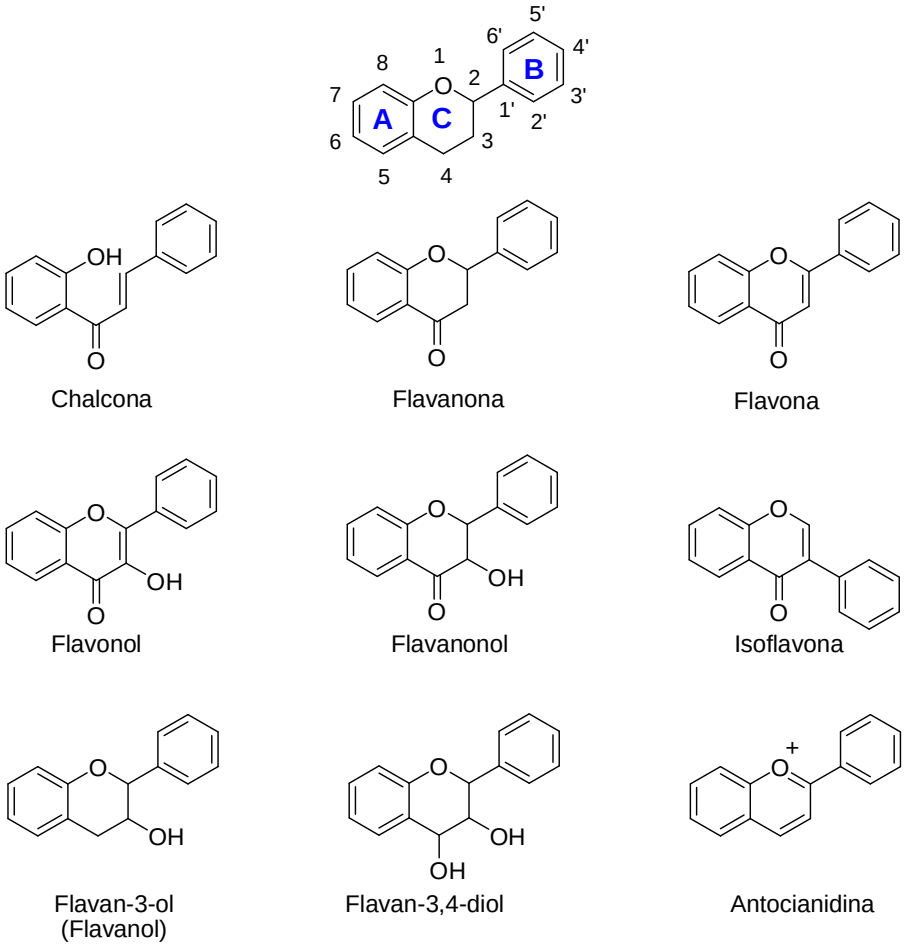

Figura 1. Estructura básica de los flavonoides y principales clases.

Los flavonoles se caracterizan por poseer un anillo C con un doble enlace en C2-C3, oxidado en C4 y un grupo hidroxilo en C3. Los flavanonoles son

análogos a los flavonoles, pero carecen del doble enlace C2-C3. Las flavonas contienen un doble enlace en C2-C3 y un grupo ceto en C4, pero a diferencia de los flavonoles carecen del hidroxilo en C3. Las antocianidinas son una clase de flavonoides insaturados, no oxidados y solubles en agua y son responsables del color de las plantas dependiendo del pH. Los isoflavonoides contienen el anillo B unido al C3, un doble enlace en C2-C3 y un grupo ceto en C4.

Muchos flavonoides presentan un amplio espectro de actividades biológicas incluyendo propiedades antitumorales [9,10]. Estas están mediadas por diferentes tipos de parada del ciclo celular y la inducción de apoptosis. Esta modalidad de muerte celular regulada se caracteriza por la translocación de la fosfatidilserina a la cara externa de la membrana plasmática, por la fragmentación internucleosómica del DNA, la condensación de la cromatina y la formación de los cuerpos apoptóticos. La inducción de apoptosis es una respuesta importante a muchos agentes utilizados en quimioterapia. La apoptosis está mediada por la activación de una clase de cisteína proteasas, denominadas caspasas, a través de dos vías principales denominadas vía intrínseca y vía extrínseca, dependiendo del tipo de célula [11-13]. La vía intrínseca implica la translocación de la hemoproteína citocromo *c* desde la mitocondria al citoplasma, el ensamblaje del apoptosoma y la activación de la caspasa-9, que hidroliza y activa a las caspasas ejecutoras o efectoras

(caspasas-3, -6 y -7), que a su vez producen la hidrólisis de proteínas estructurales y reguladoras clave para efectuar la muerte celular [14]. La vía extrínseca está mediada por receptores de muerte de la superficie celular, tales como los receptores para el factor necrótico tumoral, Fas y TRAIL (Ligando Inductor de Apoptosis relacionado con el Factor Necrótico Tumoral), y es dependiente de la activación de la caspasa iniciadora caspasa-8 que rompe y activa a las caspasas efectoras [15]. Ambas, la caspasa-8 y la caspasa-9, activan a la caspasa-3, que es la responsable de la hidrólisis de múltiples proteínas celulares específicas durante la apoptosis incluyendo el enzima nuclear poli(ADP-ribosa)polimerasa que normalmente está implicado en la reparación del DNA [16,17].

Investigaciones previas han puesto de manifiesto que los flavonoides con un grupo hidroxilo en posición 3 son potenciales agentes contra el cáncer y que la metilación de estos compuestos aumenta su actividad antiproliferativa frente a células tumorales humanas [18-20]. El conocimiento de los efectos de los perfiles de sustitución del esqueleto flavonoide sobre su actividad antitumoral y sobre su actividad inhibidora de la polimerización de tubulina ha progresado notablemente en los últimos años. La casticina y la centaureidina (Figura 2), son dos miembros importantes de la familia de las flavonas que presentan dos grupos metoxi en las posiciones C4´ y C3 y un

grupo hidroxi en la posición C3´ y son prometedores agentes contra el cáncer debido a su alta citotoxicidad frente a una variedad de células de cáncer.

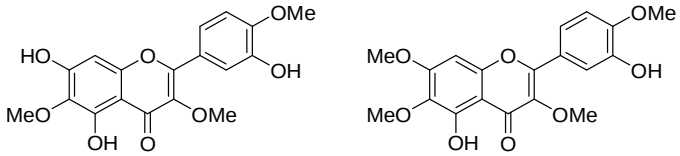

Figura 2. Estructuras químicas de 3-metoxiflavonas.

La centaureidina fue la primera flavona citotóxica descrita como un agente que interaccionaba con la tubulina y esto fue seguido por la identificación de una flavona que contenía el mismo perfil de sustitución que la centaureidina y que inhibía la incorporación de tubulina en los microtúbulos [21,22]. Posteriormente, las flavonas metoxiladas se usaron como compuestos líderes en el diseño de nuevos análogos como inhibidores de tubulina [23]. El análisis de las relaciones estructura-actividad mostró que: (i) los compuestos que contienen el perfil de sustitución previamente indicado fueron más activos como inhibidores de la polimerización de tubulina que aquellos que carecían de él, (ii) la sustitución de un grupo metoxi en C3 por un hidroxi disminuyó dramáticamente la actividad del compuesto, y (iii) las sustituciones en el anillo A no parecen ser relevantes en absoluto [24]. Los estudios llevados a cabo por nuestro grupo de investigación confirmaron que el perfil de sustitución

(metoxi en C3, C4´ e hidroxi en C3´) conduce a compuestos con actividad antileucémica e inhibidora de la polimerización de tubulina [25]. El potencial de flavonoides conteniendo este patrón de sustitución en la terapia antimelanoma no ha sido explorado hasta el momento.

La segunda serie de compuestos explorados en esta Tesis han sido lactonas sesquiterpénicas naturales. Estos son compuestos de 15 átomos de carbono que contienen tres unidades de isopreno y un grupo lactona, presentan un amplio espectro de actividades biológicas y son potenciales agentes en la lucha contra el cáncer [26,27]. Estas especies químicas que contienen el agrupamiento α-metilén-γ-lactona son de naturaleza lipofílica, incoloras y amargas, y actúan como agentes alquilantes a través de una reacción de adición tipo Michael (Figura 3). Las lactonas sesquiterpénicas poseen actividad anti-inflamatoria e inhiben el factor de transcripción NF-κB [28]. Estas moléculas son también prometedoras en el descubrimiento de fármacos contra el cáncer debido a su selectividad hacia células tumorales y células madre de cáncer [29]. Estos compuestos fueron seleccionados de nuestra biblioteca de sesquiterpenos generada en estudios previos que habían puesto de manifiesto que las lactonas sesquiterpénicas del grupo de las guayanolidas son los compuestos más citotóxicos frente a diferentes líneas celulares de cáncer [30]. Hasta ahora, el uso potencial de estas guayanolidas halogenadas

en la terapia anti-leucémica y anti-melanoma no ha sido explorado. En esta Tesis hemos llevado a cabo un estudio de las relaciones estructura-citotoxicidad de ocho guayanolidas halogenadas -siete de ellas han sido aisladas de plantas del género *Centaurea*, perteneciente a la familia *Asteraceae*, en células de leucemia y de melanoma humanas.

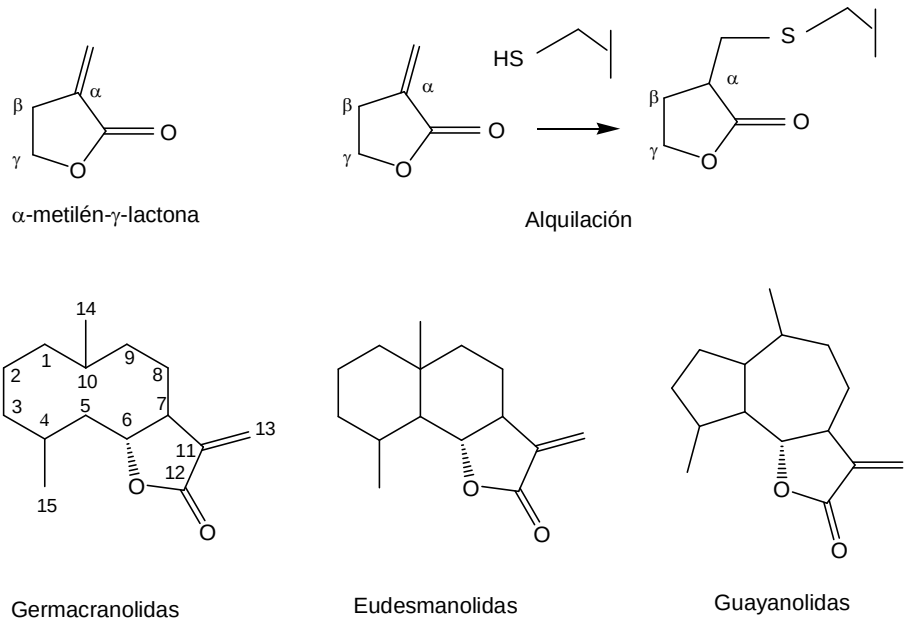

Figura 3. Agrupamiento α-metilén-γ-lactona, reacción de adición tipo Michael y estructuras de los esqueletos carbonados de las principales clases de lactonas sesquiterpénicas.

La tercera serie de compuestos evaluados en esta Tesis han sido nuevos compuestos híbridos constituidas por guanidinas trisustitutidas conteniendo un núcleo 1,3-difenilpropenona (Figura 4).

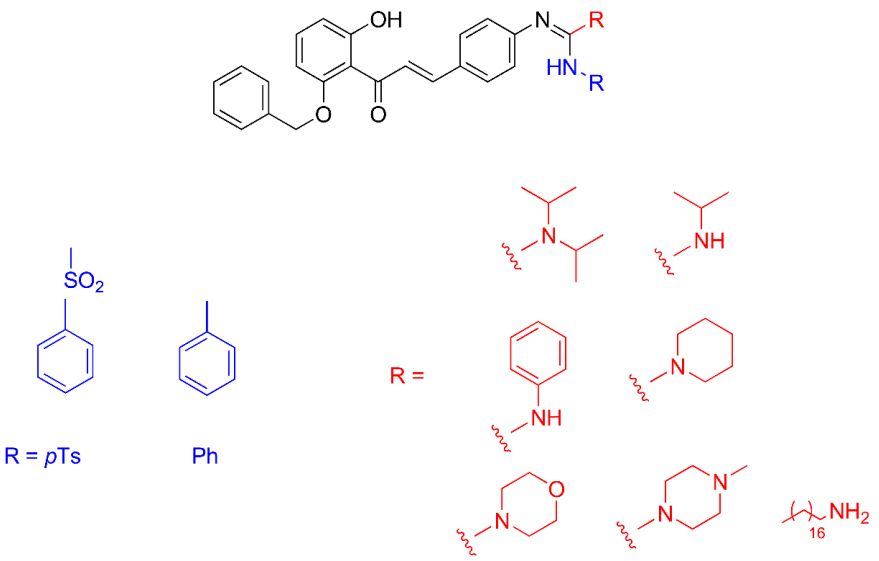

Figura 4. Estructura general de los compuestos híbridos constituidos por guanidinas trisustituidas conteniendo un núcleo 1,3-difenilpropenona.

Los compuestos híbridos, obtenidos por síntesis orgánica, resultan de la combinación de dos o más moléculas relevantes biológicamente activas. La justificación de generar y desarrollar nuevos compuestos híbridos en la lucha contra el cáncer es que éstos pueden mejorar su actividad biológica, su especificidad y ayudar a superar la multirresistencia a fármacos. Un excelente

punto de partida para desarrollar nuevos fármacos es la incorporación de una estructura privilegiada de un producto natural, por ejemplo una chalcona, como una de las moléculas originales [31]. Las chalconas (1,3-diaril propenonas) son precursores biosintéticos de los flavonoides y pueden interaccionar con múltiples dianas, exhibiendo actividades prometedoras *in vitro* e *in vivo* en diferentes células de cáncer susceptibles y que han desarrollado resistencia [32]. El núcleo de chalcona se considera una entidad química apropiada para implementar estrategias racionales en el descubrimiento de fármacos basados en la hibridización molecular (asociación molecular de partes distintas o mixtas por formación de enlace covalente) en la búsqueda de nuevos agentes anticancerígenos [33]. Estas entidades químicas son muy apropiadas para una posterior optimización basada en la funcionalización sistemática del fragmento núcleo de partida, de acuerdo con sus propiedades fisicoquímicas y farmacológicas. Recientemente se han preparado y evaluado como potenciales agentes anticancerígenos numerosas chalconas híbridas. Algunas de ellas han mostrado una potencia excelente en células tumorales *in vitro* e *in vivo*, indicando que estos compuestos pueden tener valor terapéutico [33,34].

2. Objetivos planteados

1. Analizar el efecto sobre la viabilidad celular de tres series de compuestos incluyendo flavonoides, guayanolidas y guanidinas derivadas del núcleo 1,3-difenilpropenona, utilizando como modelo varias líneas de cáncer humanas.

2. Seleccionar los inhibidores de la viabilidad más potentes y explorar su mecanismo de acción.

3. Resultados y discusión

3.1. Primera serie: Flavonoides

3.1.1. Objetivos específicos planteados

El principal objetivo de la primera publicación científica de esta Tesis fue investigar los efectos de 15 flavonoides sintéticos (Figura 5) sobre la viabilidad de las células de melanoma humanas SK-MEL-1 y elucidar el mecanismo de muerte celular del compuesto más potente. Los resultados mostraron que la 3´-hidroxi-3,4´-dimetoxiflavona es el compuesto más citotóxico frente a esta línea celular y, por primera vez, se presentan evidencias que este flavonoide induce muerte celular regulada mediada por activación de caspasas e inhibición de la polimerización de tubulina.

3.1.2. Primera serie. Resultados y discusión

En el artículo científico publicado en la revista *Bioorganic & Medicinal Chemistry* hemos descrito la síntesis de 15 flavonoides, incluyendo ocho flavonoles y siete 3-metil éteres, con uno o dos sustituyentes en el anillo B y un sustituyente adicional en el anillo A, y evaluado sus efectos sobre la viabilidad celular de la línea de melanoma humana SK-MEL-1 [35]. Los sustituyentes en el anillo B incluían las parejas 3´-hidroxi-4´-metoxi, 4´-

hidroxi-3´-metoxi o simplemente un grupo hidroxi. Las estructuras de los compuestos ensayados están relacionadas en la Figura 5.

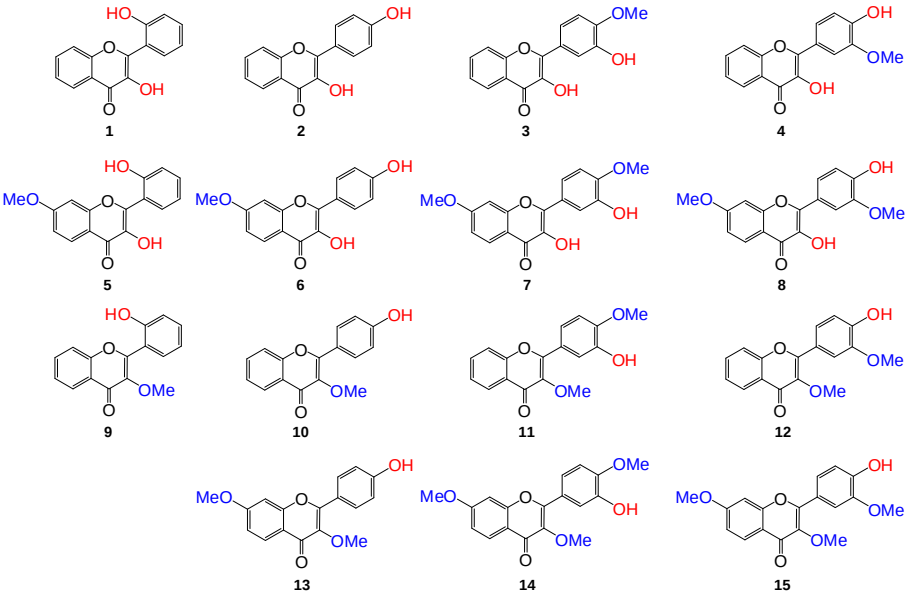

Figura 5. Estructuras químicas de los flavonoides sintéticos, incluyendo ocho flavonoles y siete 3-metil éteres, con uno o dos sustituyentes en el anillo B y un sustituyente adicional en el anillo A, ensayados en células de melanoma humanas SK-MEL-1.

Una 3-metoxiflavona, que contiene la pareja de sustituyentes 3´-hidroxi-4´-metoxi en el anillo B (compuesto **11,** Figura 5), fue el compuesto más citotóxico frente a las células de melanoma y presentó baja citotoxicidad frente a linfocitos humanos. El hecho que las células de melanoma humanas SK-MEL-1 fueran sensibles al compuesto sintético es extremadamente interesante ya que el melanoma es el tipo de cáncer de piel más agresivo y letal y frecuentemente resiste la quimioterapia.

Pocos estudios han analizado el potencial de los flavonoides en terapia antimelanoma. La tamarixetina (3,5,7,3´-tetrahidroxi-4´-metoxiflavona) y la dihidromiricetina (3,3´,4´,5,5´,7-hexahidroxi-flavanona) son dos flavonoides que han sido descritos como compuestos con capacidad antiproliferativa frente a células de melanoma [36,37]. La tamarixetina exhibe propiedades citotóxicas en células SK-MEL-1 pero las vías implicadas en la muerte celular no han sido exploradas [36], y los estudios comparativos indican que su capacidad citotóxica, determinada por el valor de IC_{50} (concentración de inhibidor necesaria para reducir la viabilidad un 50% de su valor en ausencia de inhibidor), es tres veces más baja que la 3´-hidroxi-3,4´-dimetoxiflavona (IC_{50} = 23.1±2.1 µM vs. 6.9±1.1 µM). La dihidromiricetina inhibe la proliferación celular de las células de melanoma SK-MEL-28 a través de la parada del ciclo celular en la fase G_1 y apoptosis, aunque esto tiene lugar a

concentraciones más altas que las que se usaron con la 3´-hidroxi-3,4´-dimetoxiflavona.

3.1.3. Primera serie. Conclusiones

En conclusión, el presente estudio en células de melanoma humanas SK-MEL-1 demuestra que la 3´-hidroxi-3,4´-dimetoxiflavona detiene el ciclo celular en la fase G_2-M, induce muerte celular por apoptosis e inhibe la polimerización de tubulina (Figura 6). La apoptosis fue confirmada por (i) microscopía fluorescente, (ii) el aumento del porcentaje de células hipodiploides y (iii) la activación de la caspasa-3. El efecto antiproliferativo del compuesto sintético está asociado con la liberación de la proteína citocromo *c* del espacio intermembrana mitocondrial y con la activación de las caspasas iniciadoras implicadas en las vías extrínseca e intrínseca de muerte celular.

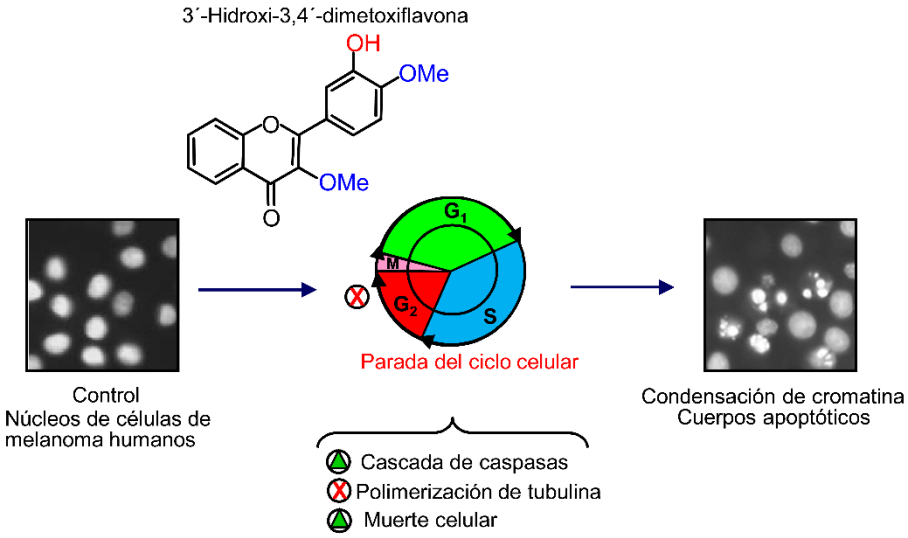

Figura 6. La flavona 3´-hidroxi-3,4´-dimetoxiflavona es el compuesto inhibidor de la viabilidad más potente de los quince flavonoides sintéticos ensayados en células de melanoma humanas. Las microfotografías de fluorescencia obtenidas después de la tinción con el fluorocromo trihidrocloruro de bisbencimida ponen de manifiesto la condensación y fragmentación de la cromatina y la formación de cuerpos apoptóticos. La inducción de apoptosis estuvo precedida por una parada del ciclo celular en la fase G_2-M y la muerte celular estuvo asociada con la activación de las vías intrínseca y extrínseca de apoptosis e inhibición de la polimerización de tubulina.

Estos resultados han sido publicados en la revista *Bioorganic & Medicinal Chemistry* en el año 2017.

Autores (p.o. de firma): Estévez-Sarmiento F, Said M, Brouard I, León F, García C, Quintana J, Estévez F.

Título: 3'-Hydroxy-3,4'-dimethoxyflavone blocks tubulin polymerization and is a potent apoptotic inducer in human SK-MEL-1 melanoma cells.

Revista: *Bioorganic & Medicinal Chemistry* 2017 Nov 1;25(21):6060-6070. https://doi.org/10.1016/j.bmc.2017.09.043

Indicios de calidad:

(A) Base de datos de indexación: *Journal Citation Reports*

(B) Año: 2017

(C) Índice de impacto: 2,881

(D) Posición que ocupa en la categoría: 24/59, Q2

(E) Categoría: Chemistry, Medicinal

3.2. Segunda serie: guayanolidas

La segunda serie de compuestos explorados en esta Tesis han sido lactonas sesquiterpénicas naturales (Figura 7). Las guayanolidas pertenecen a una clase de lactonas sesquiterpénicas caracterizadas por tres anillos fusionados, consistentes en una estructura de dos anillos de cinco miembros y un anillo de siete miembros que poseen múltiples actividades biológicas [38]. Algunos compuestos de esta clase presentan actividad anti-inflamatoria debido a la inhibición del factor de transcripción NF-κB [28,39].

Los compuestos halogenados generalmente contienen un átomo de cloro y se han aislado alrededor de 5.000 de fuentes naturales. Estos poseen un amplio espectro de actividades farmacológicas que han conducido a aplicaciones en la industria farmacéutica. Actualmente, la mitad de las moléculas en cribados de alta resolución contienen átomos de halógenos [40]. Muchos de estos compuestos halogenados son clorohidrinas que han sido aisladas junto con sus correspondientes epóxidos [41]. Las lactonas sesquiterpénicas halogenadas naturales y sus derivados sintéticos exhiben actividades antitumorales y citotóxicas y tienen potencial como agentes contra el cáncer [42,43]. Hasta ahora, el uso potencial de estas guayanolidas halogenadas en la terapia antileucémica y/o antimelanoma no ha sido explorado.

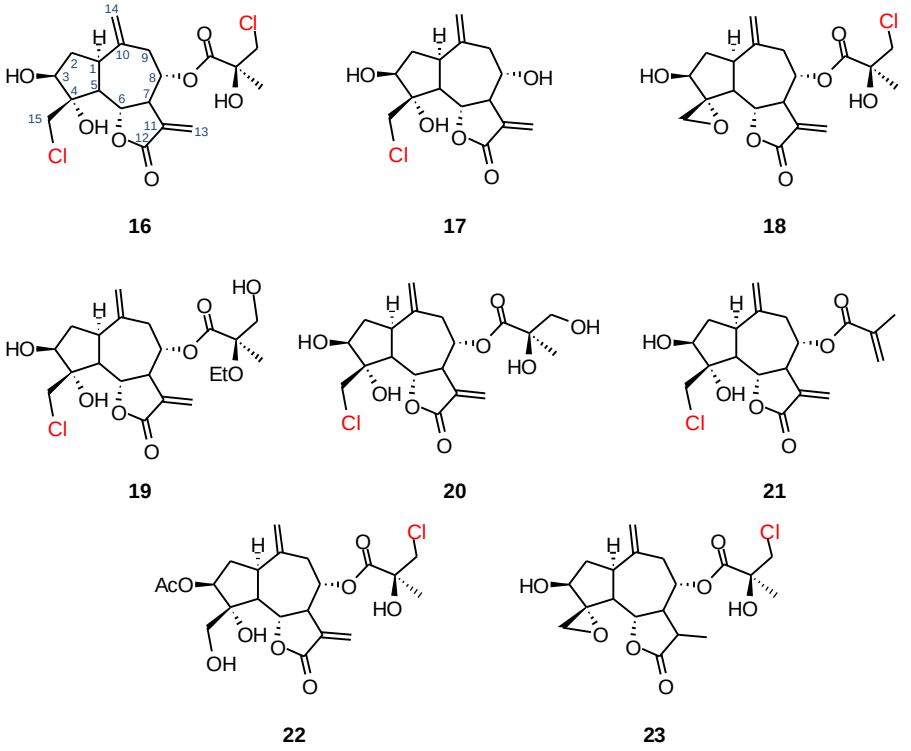

Figura 7. Estructuras químicas de las lactonas sesquiterpénicas del grupo de las guayanolidas evaluadas en estudios de viabilidad en células de cáncer humanas.

3.2.1. Segunda serie. Objetivos específicos planteados

Determinar las relaciones estructura-citotoxicidad de ocho guayanolidas halogenadas (siete de ellas han sido aisladas de plantas del género *Centaurea*, perteneciente a la familia *Asteraceae*) en células de leucemia y de melanoma humanas.

3.2.2. Segunda serie. Resultados y discusión

Las guayanolidas ensayadas fueron aisladas de fuentes naturales como se ha descrito previamente [44-46]. La determinación de la pureza y los estudios espectroscópicos de las guayanolidas utilizadas en esta Tesis fueron llevados a cabo en el Instituto de Productos Naturales y Agrobiología del Consejo Superior de Investigaciones Científicas bajo la dirección del Dr. Ignacio Brouard Martín. Las guayanolidas cloradas clorohyssopifolinas A **16**, B **17**, C **18**, D **19** y E **20** fueron aisladas de *Centaurea hyssopifolia* Vahl. La liniclorina A **21** y la liniclorina C **22** se aislaron de *Centaurea linifolia* Vahl. La 11,13-dihidroclorohyssopifolina C **23** se obtuvo a partir de la clorohyssopifolina A **16**, por reducción con Zn-Cu seguido por formación de un epóxido con $AgNO_3$ [46]. Las guayanolidas evaluadas poseen en común (i) la presencia de un doble enlace como un grupo metileno en posición 10 (C10); (ii) la presencia de un grupo hidroxi y/o un grupo acetilo en posición 3 del anillo de ciclopentano; (iii) diferentes sustituyentes en C8 y (iv) la presencia de un átomo de cloro tanto en posición C-15, en el grupo éster o en ambos (Figura 7). Algunos de los compuestos más potentes en células tumorales humanas como las clorohyssopifolinas A **16** y D **19**, y la liniclorina A **21**, se seleccionaron para determinar si los efectos sobre la viabilidad celular fueron debidos a la activación de la vía apoptótica. Específicamente se estudiaron los efectos sobre la inducción de apoptosis y la activación de caspasa. El objetivo

de este estudio fue explorar las relaciones estructura-citotoxicidad de ocho lactonas sesquiterpénicas seleccionadas, pertenecientes a la clase de las guayanolidas, en células de leucemia y de melanoma humanas y también evaluar el mecanismo de acción de los compuestos más potentes sobre la inducción de apoptosis usando las células de leucemia humana U-937. Estas células se eligieron puesto que son un modelo útil para el estudio de las neoplasias y la terapéutica [47,48].

La importancia del agrupamiento α-metilen-γ-lactona sobre la citotoxicidad en presencia de grupos electrofílicos reactivos adicionales se ha descrito para la repina, una guayanolida aislada de *Centaurea repens* [49]. Estudios previos han mostrado que la clorohyssopifolina A **16** inhibe la viabilidad celular de varias líneas celulares de cáncer incluyendo las líneas 1A9 (cáncer de ovario), KB (cáncer de nasofaringe) y KB-V (sublínea de KB resistente a vincristina) y que la clorohyssopifolina C **17** mostró citotoxicidad significativa frente a MCF-7 (cáncer de mama receptor de estrógeno positivo). En este estudio las clorohyssopifolinas A **16** y C **18** no fueron ensayadas en células de melanoma humanas y el mecanismo de muerte celular no fue explorado [42]. De una manera similar a nuestros resultados en células de leucemia y de melanoma humanas, la clorohidrina en C4 puede modificarse a un epóxido en el esqueleto cíclico sin ningún cambio en la citotoxicidad como se observa al

comparar los valores de IC_{50} de la clorohyssopifolina A **16** y la clorohyssopifolina C **18**. Además, la presencia de un diol en la cadena lateral en C8 (clorohyssopifolina E **20**) más que una clorohidrina (clorohyssopifolina A **16**) abolió la actividad. Una observación similar se ha descrito por la comparación entre babylina A, que contiene un diol en la cadena lateral, y la clorohyssopifolina C **18** que contiene una clorohidrina en la cadena lateral [42].

Un resultado relevante de este estudio es que las guayanolidas fueron capaces de inhibir la viabilidad de U-937/Bcl-2, una sublínea que expresa niveles elevados de la proteína humana Bcl-2, que está implicada en la resistencia a la quimioterapia especialmente en las neoplasias hematológicas [50]. Estos resultados sugieren que las guayanolidas son capaces de bloquear la proliferación de células tumorales humanas por inactivación de la protección mitocondrial conferida por Bcl-2. Además, las células de melanoma SK-MEL-1 fueron sensibles a las clorohyssopifolinas A **16**, C **18** y D **19**, y a la liniclorina A **21**, enfatizando el potencial de estas lactonas sesquiterpénicas, debido a la agresividad y letalidad de este tipo de cáncer de piel.

Los resultados de este trabajo revelan que la liniclorina A **21** es una de las guayanolidas inhibidoras más potentes de la viabilidad celular de las cuatro

células de cáncer ensayadas. La liniclorina A **21** ha sido reconocida como un regulador negativo de la degradación del inhibidor de las proteínas quinasas dependientes de ciclinas $p27^{Kip1}$. Esta guayanolida inhibe la ubiquitinación de $p27^{Kip1}$ por el complejo multiproteico ubiquitina ligasa SCF^{Skp2} *in vitro*, estabiliza los niveles de $p27^{Kip1}$ en células HeLa e inhibe la proliferación de células de cáncer humana y de ratón [51]. La liniclorina A **21** presenta una actividad antiproliferativa selectiva en células de cáncer y transformadas en el rango de micromolar. Los valores de IC_{50} publicados para la liniclorina A **21** en HeLa (carcinoma de cérvix humano), tsFT210 (células tumorales de ratón) y NIH3T3 (células inmortalizadas de ratón) fueron 3.2, 1.6 y 12.7 μM, respectivamente, determinadas por el ensayo de WST-8 durante 48 h. Sin embargo, se conoce muy poco sobre el mecanismo de muerte celular inducido por la liniclorina A **21**.

Los experimentos de citometría de flujo realizados en esta Tesis revelaron que la inhibición de la viabilidad celular por las clorohyssopifolinas A **16**, C **18**, D **19**, y la liniclorina A **21** estuvo acompañada por un aumento en el porcentaje de células en sub-G_1. Las guayanolidas seleccionadas, las clorohyssopifolinas A **16** y D **19**, y la liniclorina A **21**, indujeron cambios morfológicos nucleares como la fragmentación y la condensación de la cromatina, característicos de muerte celular apoptótica. Los experimentos usando las células U-937 como

modelo confirmaron que estos compuestos son inductores potentes de muerte celular regulada demostrado por la inducción de la externalización de la fosfatidilserina y la hidrólisis del enzima de reparación del DNA poli(ADP-ribosa)polimerasa. Además, las guayanolidas seleccionadas indujeron liberación del citocromo *c* mitocondrial apoptogénico indicando que la vía apoptótica intrínsica puede jugar un papel clave en la muerte celular. Los estudios enzimáticos revelaron la activación de la caspasa-9 y de la caspasa-3, resultados que concuerdan con la liberación de citocromo *c*. En estos experimentos también se detectó la activación de la caspasa-8 en los extractos de células U-937 tratadas con las guayanolidas seleccionadas. Para identificar las dianas primarias y el mecanismo de acción de las lactonas sesquiterpénicas evaluadas en las células U-937 se utilizaron concentraciones próximas o tres veces superiores a los valores de IC_{50}, que fueron determinados después de 72 h de tratamiento, mientras que los experimentos de citometría de flujo y los ensayos de determinación de la actividad caspasa se analizaron a las 24 h de tratamiento. Las concentraciones próximas a los valores de IC_{50} de las lactonas sesquiterpénicas fueron suficientes para inducir apoptosis. Una baja concentración (3 μM) de las clorohyssopifolinas A **16** y D **19** y de la liniclorina A **21** fue capaz de inducir la liberación de citocromo *c* en las células U-937. Estos resultados indican que ambas rutas, la vía intrínseca y la vía

extrínseca, desempeñan un importante papel en la muerte celular inducida por las clorohyssopifolinas A **16** y D **19**, y la liniclorina A **21**.

3.2.3. Segunda serie. Conclusiones

En este estudio sobre las lactonas sesquiterpénicas de la clase guayanolidas desplegado en esta Tesis se ha explorado las relaciones estructura-citotoxicidad de ocho guayanolidas cloradas, siete de ellas obtenidas de fuentes naturales y un derivado semisintético, usando como modelos líneas celulares de leucemia y de melanoma humanas. Estos compuestos se caracterizan por la presencia de dobles enlaces exocíclicos en los carbonos C10 y C11, y diferentes sustituyentes en los carbonos C3, C4 y C8.

Los resultados de las relaciones estructura-citotoxicidad revelaron que: (i) la reducción del doble enlace 11,13 bloqueó la actividad inhibidora de la viabilidad en células de cáncer, independientemente de la presencia de un grupo electrofílico reactivo adicional; (ii) la acetilación de un grupo hidroxi en C3 no potenció la citotoxicidad en comparación con el correspondiente alcohol; (iii) la introducción de un grupo ester en C8 amplificó o disminuyó la citotoxicidad; (iv) el aumento de la polaridad de la cadena hidrocarbonada del grupo ester en C8 redujo la citotoxicidad; y (v) la introducción de un grupo

alquilante como un epóxido en C4 no potenció la citotoxicidad pero la introducción de una enona en C8 sí amplificó la citotoxicidad (Figura 8).

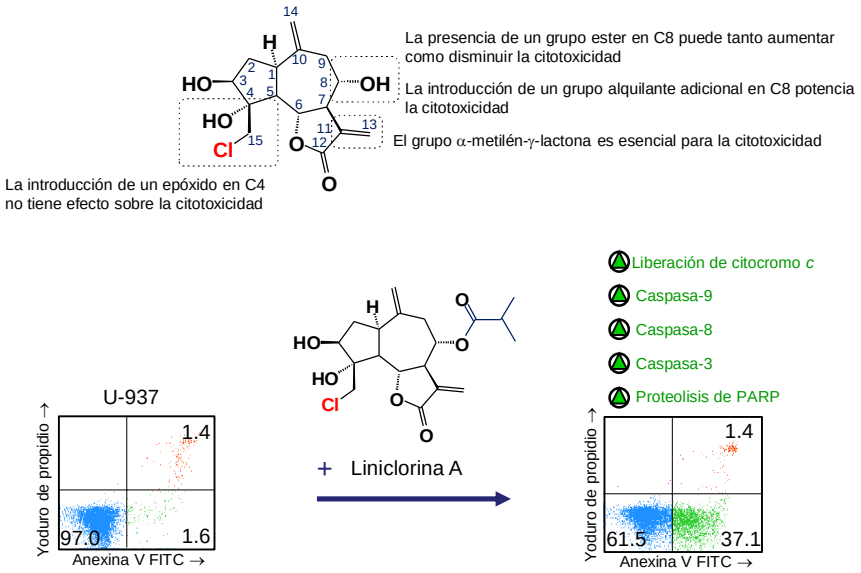

Figura 8. Las relaciones estructura-actividad de las guayanolidas estudiadas ponen de manifiesto que la introducción de un grupo alquilante en C8 potencia la citotoxicidad y que el grupo α-metilén-γ-lactona es esencial. La liniclorina A fue una de las más potentes inhibidoras de la viabilidad de células de cáncer humanas y es un potente inductor de apoptosis. El mecanismo de muerte celular implica la liberación de citocromo *c* mitocondrial, la activación de las caspasas involucradas en las vías intrínseca y extrínseca y la proteolisis del enzima de reparación del DNA poli(ADP-ribosa)polimerasa.

Los resultados de los estudios de la segunda serie de compuestos se han publicado en la revista *International Journal of Molecular Sciences* en el año 2020 [52].

Autores (p.o. de firma): Estévez-Sarmiento F, Saavedra E, Ruiz-Estévez M, León F, Quintana J, Brouard I, Estévez F.

Título: Chlorinated Guaiane-Type Sesquiterpene Lactones as Cytotoxic Agents against Human Tumor Cells.

Revista: *International Journal of Molecular Sciences* 2020 Dec 21;21(24):9767.

https://doi.org/10.3390/ijms21249767

Indicios de calidad:

(A) Base de datos de indexación: *Journal Citation Reports*

(B) Año: 2020

(C) Índice de impacto: 5,924

(D) Posición que ocupa en la categoría: 67/295, Q1

(E) Categoría: *Biochemistry & Molecular Biology*

3.3. Tercera serie: compuestos híbridos

La tercera serie de compuestos evaluados han sido nuevos compuestos híbridos constituidos por guanidinas trisustituidas conteniendo un núcleo 1,3-difenilpropenona (Figura 9). Las guanidinas son organosuperbases versátiles y son capaces de unirse por interacciones electrostáticas a grupos carboxilatos y fosfatos y a metales. A pH fisiológico, el catión guanidinio participa en interacciones especiales entre ligandos y receptores o enzimas y sustratos y pueden desempeñar propiedades biológicas importantes y con implicaciones químicas y farmacológicas. Las guanidinas son de gran interés en química médica y constituyen un motivo clave de muchos fármacos utilizados en clínica como por ejemplo el anti-diabético dimetildiguanida y el anti-ulceroso cimetidina. Los derivados de guanidina están también ampliamente distribuidos en la naturaleza y han atraído mucha atención debido a su diversidad química y múltiples actividades biológicas [53,54].

3.3.1. Tercera serie. Objetivos específicos planteados

El objetivo específico principal ha sido explorar los efectos de una serie de once compuestos híbridos chalcona-guanidina trisustituida **25**-**35** incluyendo el precursor **24** sobre la viabilidad de seis líneas celulares de cáncer humanas. Específicamente los compuestos fueron benciloxichalconas conteniendo un grupo funcional guanidina trisustituído con diferentes sustituyentes.

Chalcona	Isocianato	Amina	Producto
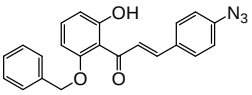 **24**	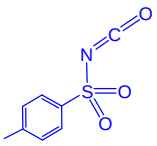		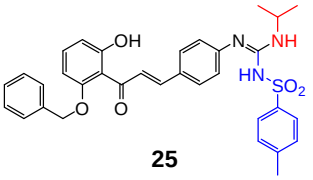 **25**
			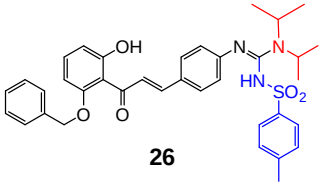 **26**
			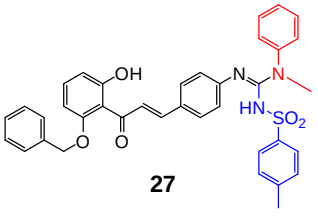 **27**
			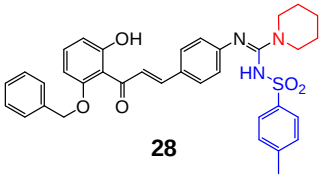 **28**
			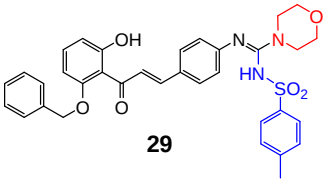 **29**
			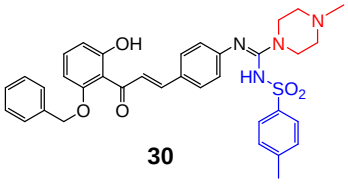 **30**
		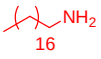	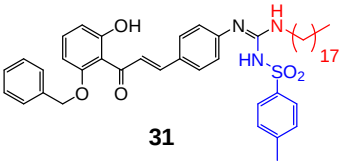 **31**

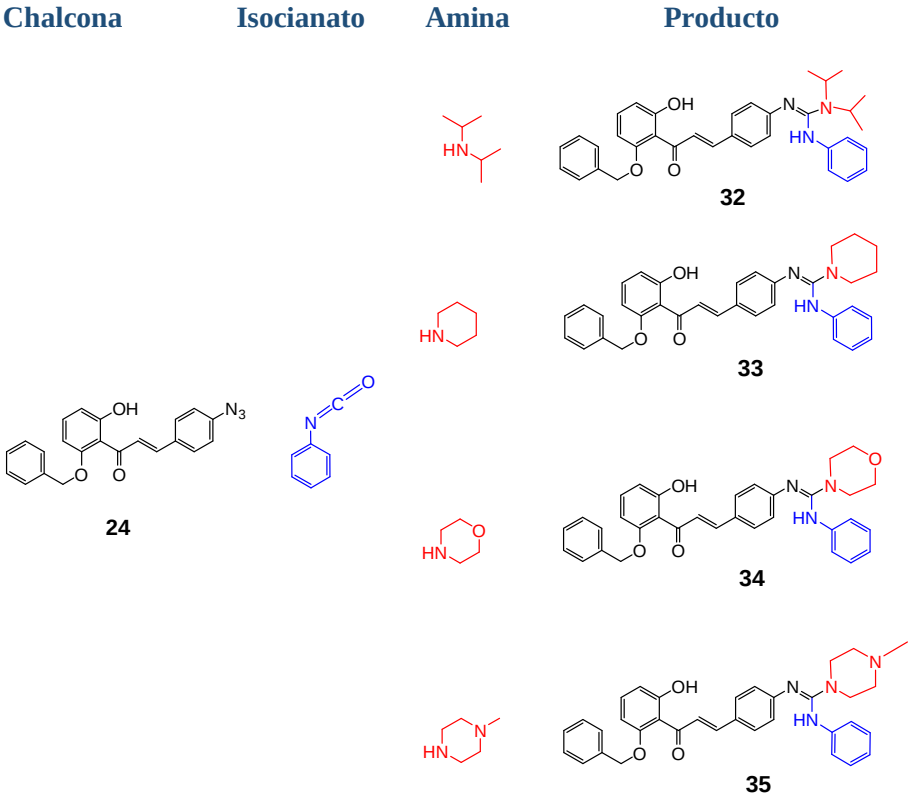

Figura 9. Estructuras químicas de la azidochalcona precursora (**24**) y de los 11 compuestos híbridos resultantes (**25-35**) que fueron ensayados en seis líneas celulares de cáncer humanas.

Los sustituyentes incluían: (i) la presencia de un grupo *p*-tosilsulfonamida o un radical fenilo en uno de los átomos de nitrógeno del grupo funcional guanidina y (ii) la presencia de diferentes grupos como el isopropilo, diisopropilo, fenilo o un heterociclo en el otro átomo de nitrógeno del grupo funcional guanidina. Además, los compuestos más citotóxicos fueron

ensayados como inductores de muerte celular regulada en células de leucemia humanas.

3.3.2. Tercera serie. Resultados y discusión

La potencial citotoxicidad de los compuestos híbridos conteniendo un esqueleto chalcona y un grupo guanidina se evaluó usando seis líneas de cáncer humanas. Estas líneas fueron U-937 (linfoma histiocítico), HL-60 (leucemia promielocítica aguda), MOLT-3 (leucemia linfoblástica aguda), NALM-6 (leucemia de precursor de célula B), U-937/Bcl-2 (línea que expresa altos niveles de Bcl-2) y SK-MEL-1 (melanoma). Los estudios del efecto sobre la viabilidad celular de esta serie de compuestos revelaron que en el caso de compuestos híbridos conteniendo el grupo *p*-toluensulfonilo, la citotoxicidad depende de la correspondiente amina: el derivado isopropilamino **25** y el derivado fenilmetilamino **27** fueron más potentes que el correspondiente derivado diisopropilamino **26**. Hubo un importante cambio en la citotoxicidad en los compuestos con una estructura heterocíclica como sustituyente, dependiendo si el grupo amino forma parte de una piperidina **28**, una morfolina **29** o una *N*-metilpiperazina **30**. En general, el compuesto híbrido más citotóxico fue **30**. Las diferencias más importantes en citotoxicidad se observaron en U-937 en las que el orden fue **30** > **29** > **28**. En MOLT-3 estos tres derivados fueron casi igualmente potentes con valores de

IC_{50} entre 1.5 µM y 3.3 µM, y en U-937/Bcl-2 el derivado conteniendo morfolina **29** presentó una potencia similar al derivado conteniendo *N*-metilpiperazina **30**. El derivado conteniendo *N*-metilpiperazina **30** fue el compuesto inhibidor más potente de la viabilidad en todas las células de cáncer ensayadas incluída la de melanoma SK-MEL-1. Los valores de IC_{50} fueron similares al del antineoplásico etopósido, que fue usado como control positivo en los ensayos de citotoxicidad.

En el caso de los *p*-toluensulfonil derivados, el compuesto más potente contiene una *N*-metilpiperazina **30** y el orden de potencia fue: *N*-metilpiperazina **30** > morfolina **29** > piperidina **28**, principalmente en U-937 y SK-MEL-1. Sin embargo, los compuestos **29** y **30** presentaron valores de IC_{50} similares en HL-60, NALM-6 y U-937/Bcl-2, y los compuestos **28**, **29** y **30** fueron igualmente potentes en MOLT-3.

Entre los *N*-fenil derivados, el compuesto conteniendo un anillo de piperidina **33** fue, en general, el compuesto más citotóxico con valores de IC_{50} que fueron menores (U-937, HL-60, MOLT-3 y U-937/Bcl-2) o próximos (NALM-6, SK-MEL-1) a 10 µM. La sustitución de un anillo de piperidina **33** por una *N*-metilpiperazina **35** disminuyó la citotoxicidad. En cambio, la sustitución de la piperidina **33** o una morfolina **34** aumentó la citotoxicidad en MOLT-3, NALM-6 y SK-MEL-1.

En general, la expresión de niveles elevados de Bcl-2 no confiere protección frente a la inhibición de la viabilidad, puesto que los valores de IC_{50} fueron similares e incluso más bajos que en la línea parental U-937. La mayoría de los compuestos ensayados en MOLT-3 fueron igualmente potentes, presentando valores de IC_{50} por debajo de 10 µM, exceptuando **31** y **35**. Una tendencia similar fue observada en NALM-6, puesto que la mayoría de los compuestos presentaron valores similares de IC_{50}.

La relación estructura-actividad revela que la introducción del grupo guanidina potencia la citotoxicidad del esqueleto chalcona en comparación con la azidochalcona **24**, y los resultados de los ensayos de citotoxicidad de los *p*-tosilsulfonil derivados revelaron que el compuesto más potente contiene un anillo de *N*-metilpiperazina.

Para determinar la potencial selectividad de los compuestos híbridos **30** y **33** frente a las células de leucemia, se comparó el efecto con las células mononucleares humanas obtenidas de donantes sanos. Los linfocitos quiescentes y proliferantes mostraron menor citotoxicidad incluso a 10 µM de los compuestos híbridos.

Los efectos de los compuestos híbridos sobre el ciclo celular de las células leucémicas U-937 se llevaron a cabo con una selección de ellos (**27**, **29, 30, 32, 33 y 34)**. Solo **29** indujo una parada del ciclo celular en la fase G_2-M. Además, los compuestos **30** y **33** indujeron un aumento de 11-veces y 10-veces el porcentaje de células anexina V positivas, respectivamente, confirmando que estos compuestos son potentes inductores de apoptosis. Es destacable que los experimentos dosis respuesta revelaron que las células mononucleares de sangre periférica fueron más resistentes a los compuestos **30** y **33**, ya que los aumentos en los porcentajes de células anexina V positivas fueron solo 3-veces y 1.4-veces con respecto al control después del tratamiento con 10 µM de los compuestos mencionados.

Los estudios de activación enzimática de las cisteín proteasas (caspasas-3/7, 8 y 9) revelaron un aumento de aproximadamente tres veces y dos veces de las caspasas-3/7 y de la caspasa-9, respectivamente, después del tratamiento con las guanidinas **30** y **33**. Los experimentos de transferencia Western confirmaron el procesamiento de estas caspasas así como del enzima de reparación del DNA poli(ADP-ribosa) polimerasa, un sustrato de caspasa-3.

Puesto que la activación de la caspasa-9 depende de la liberación de citocromo *c* del espacio intermembrana mitocondrial al citosol, se investigó si la muerte

celular inducida por las guanidinas seleccionadas implica la liberación de esta proteína. Los experimentos dosis-respuesta revelaron que el nivel de citocromo *c* aumentó en las fracciones citosólicas de las células tratadas, resultados concordantes con el procesamiento y activación de la caspasa-9. Estos resultados sugieren que la inducción de muerte celular por estos compuestos específicos tiene lugar a través de la vía intrínseca.

3.3.3. Tercera serie. Conclusiones

En esta serie se investigaron los efectos de once guanidinas sintéticas conteniendo un núcleo 1,3-difenilpropenona sobre la viabilidad de seis líneas de cáncer humanas. El compuesto más citotóxico frente a las células de cáncer humanas de esta serie contiene un grupo *N*-tosil y una *N*-metilpiperazina (Figura 10). Las relaciones estructura-actividad revelaron que: (i) la presencia de un anillo de piperazina en *p*-toluensulfonil guanidinas indujo una mayor respuesta citotóxica que los derivados isopropilamino, diisopropilamino, piperidina, morfolina o fenilamino correspondientes y (ii) la presencia de un anillo de piperidina en *N*-fenilguanidinas potenció la citotoxicidad en comparación con los derivados diisopropilamino, morfolino y *N*-metilpiperazina correspondientes. Los compuestos más citotóxicos en células leucémicas humanas fueron la *p*-toluensulfonilguanidina conteniendo una *N*-metilpiperazina **30** y la *N*-metil-*N*-fenilguanidina conteniendo un anillo de

piperidina **33**. Ambos compuestos mostraron menor toxicidad en células mononucleares de sangre periférica humanas, sugiriendo que estos pueden tener valor terapéutico potencial. Estos compuestos inducen muerte celular regulada en células de leucemia, asociada a la liberación de citocromo *c*, activación de caspasas e hidrólisis de PARP y la expresión de niveles elevados de la proteína anti-apoptótica Bcl-2 no bloqueó la inhibición de la viabilidad celular.

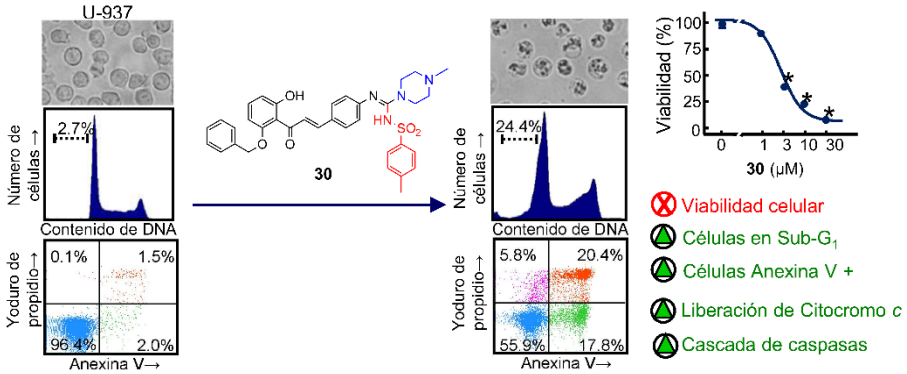

Figura 10. La *p*-toluensulfonilguanidina conteniendo una *N*-metilpiperazina **30** inhibe la viabilidad de células de cáncer humanas y es un potente inductor de apoptosis en la línea de leucemia humana U-937.

Los resultados de los estudios de la tercera serie se han publicado en la revista *International Journal of Molecular Sciences* en el año 2022 [55].

Autores (p.o. de firma): Estévez-Sarmiento F, Saavedra E, Brouard I, Peyrac J, Hernández-Garcés J, García C, Quintana J, Estévez F.

Título: Guanidine Derivatives Containing the Chalcone Skeleton Are Potent Antiproliferative Compounds against Human Leukemia Cells.

Revista: *International Journal of Molecular Sciences* 2022 Dec 8;23(24):15518.

https://doi.org/10.3390/ijms232415518

Indicios de calidad:

(A) Base de datos de indexación: *Journal Citation Reports*

(B) Año: 2021

(C) Índice de impacto: 6,208

(D) Posición que ocupa en la categoría: 69/297, Q1

(E) Categoría: *Biochemistry & Molecular Biology*

4. Material y métodos

4.1. Reactivos, procedimientos sintéticos, purificación y elucidación estructural.

Los reactivos empleados para la purificación de compuestos y los productos de partida para la síntesis se obtuvieron de Aldrich Chemical Co., o de otras compañías químicas sin purificación adicional. Todos estos procedimientos, así como la elucidación estructural de los compuestos a través de espectrometría RMN protónica y de ^{13}C y espectrometría de masas se llevaron a cabo en el Instituto de Productos Naturales y Agrobiología del Consejo Superior de Investigaciones Científicas (La Laguna, Tenerife) y en el Instituto de Bio-Orgánica "Antonio González" bajo la dirección del Dr. Ignacio Brouard Martín y la Dra. Celina García González, respectivamente.

El medio de cultivo RPMI 1640 fue de Biowest (#L0495-500 RPMI 1640 C/L-Glutamina, Nuaillé, Francia). El suero bovino fetal de Gibco (#10270-106, Life Technologies, Paisley, Reino Unido). Los antibióticos penicilina y estreptomicina fueron de Biowest (#BWSTL0018-1). Los sustratos colorimétricos de caspasas (caspasa-8, #368057; caspasa-9, #218805 y de caspasa-3/7, #235400) fueron de Calbiochem (Darmstadt, Alemania). La

acrilamida y bisacrilamida (#1610147 40% disolución acrilamida/Bis 29:1), el persulfato amónico (#161-0700), la *N*,*N*,*N´*,*N´*-tetrametiletilendiamina (TEMED, #161-0800) y el marcador de masas moleculares relativas Dual Color (#1610374) fueron de Bio-Rad (Hercules, CA, EE. UU.). Las membranas de transferencia Immobilon (#IPVH00010) y el sustrato quimioluminiscente HRP (#WBKLS) fueron de Millipore (Temecula, CA, EE. UU.). La glicina de grado Biología Molecular (#A1067), Tris grado tampón (#A1379), el metanol grado HPLC (#A1635), el etanol absoluto (#A3693), el SDS (dodecil sulfato sódico) grado Biología Molecular (#A2263), NaCl (#A2942), NaOH (#A3910), el dimetil sulfóxido (#A3672), la sacarosa (#A2211), el bromuro de tiazolil azul de tetrazolio (#A2231, Biochemica), EDTA grado Biología Molecular (#A2937), HEPES grado Biología Molecular (#A3724), Ponceau S (#A1405), KCl, grado Biología Molecular (#A2939), yoduro de propidio (#A2261), Nonidet® P40 (#A1694, Biochemica), CHAPS (#A1099, Biochemica), DTT (ditiotreitol, grado Biología Molecular, #32948) fueron de Applichem (Darmstadt, Alemania). La RNasa A (libre de DNAsa) fue de Sigma (#R6513) y de Applichem (#A3832). El 2-mercaptoetanol (#M3148), el Tween 20 (#P7949), MTT (#M5655); la disolución de azul de Tripán (#T8154), el etopósido (#E1383) y el hidrocloruro de doxorrubicina (# D1515) fueron de Sigma (St. Louis, MO, EE.UU.). El kit de detección de apoptosis Annexin V-FITC (#556547) fue de

Becton y Dickinson (BD Pharmingen, San Diego, CA, EE. UU.). El Ficoll-Paque™ PLUS (#17-1440-02, Cytiva, Uppsala, Suecia) y los anticuerpos secundarios (#GEHENA9310 anticuerpo policlonal anti-ratón conjugado con peroxidasa de rábano y #GEHENA9340 anticuerpo policlonal anti-conejo conjugado con peroxidasa) fueron de General Electric (Little Chalfont, Reino Unido).

4.2. Cultivos celulares y ensayos de citotoxicidad

Las células humanas HL-60 (DSMZ Nº ACC 3) de leucemia mieloide aguda, U-937 (DSMZ Nº ACC 5) de linfoma histiocítico, MOLT-3 (DSMZ Nº ACC 84) de leucemia linfoblástica aguda, NALM-6 (DSMZ Nº ACC 128) de leucemia precursora de célula B y SK-MEL-1 (DSMZ Nº ACC 303) de melanoma se obtuvieron de la Colección Alemana de Microorganismos y Cultivos Celulares (Braunschweig, Alemania). Las células se propagaron en suspensión en medio RPMI 1640 conteniendo 2 mM L-glutamina y 10% (v/v) suero bovino fetal y 100 unidades/mL penicilina y 100 µg/mL estreptomicina a 37 °C en una atmósfera húmeda conteniendo 5% CO_2, y se mantuvieron a una densidad de 0.5-1.0 x 10^6 células/mL, excepto las células SK-MEL-1 que se mantuvieron entre 0.1-0.3 x 10^6 células/mL. La línea celular U-937 que expresa niveles elevados de Bcl-2 humano (designadas como U-937/Bcl-2)

fueron donadas por la Dra. Jacqueline Bréard (Faculté de Pharmacie Paris-Sud, Chatenay-Malabry, Francia) y cultivadas en medio RPMI 1640 conteniendo 10% (v/v) suero bovino fetal a 37 ºC en una atmósfera húmeda conteniendo 5% CO_2. La viabilidad celular se determinó por el método de exclusión del azul de tripán contando las células en un hemocitómetro. La viabilidad celular fue superior al 95% en todos los experimentos. Las células se resuspendieron en medio fresco 24 h antes de los tratamientos para asegurar el crecimiento exponencial. Las células HL-60 y U-937 exhibían tiempos de doblaje característicos de aproximadamente 25 h y 30-35 h, respectivamente, las MOLT-3 y NALM-6 de 40 h, mientras que las células SK-MEL-1 exhibían un tiempo de doblaje de varios días (alrededor de 48-72 h). Las disoluciones stock de 50 mM de todos los compuestos ensayados se hicieron en dimetilsulfóxido (DMSO) y las alícuotas se congelaron a −20ºC. Las diluciones posteriores se hicieron en medio de cultivo inmediatamente antes de su uso. En todos los experimentos, la concentración final de DMSO no excedió del 0.3% (v/v), una concentración que no fue tóxica para las células.

Las células mononucleares humanas de sangre periférica (PBMCs) se aislaron de sangre tratada con heparina de voluntarios sanos por centrifugación con Ficoll-Paque Plus (GE Healthcare Bio-Sciences AB; Uppsala, Suecia). Las PBMCs también se estimularon con fitohemaglutinina (PHA, 2 µg/mL,

#L1668, Sigma-Aldrich) durante 48 h antes de los tratamientos. Todos los donantes dieron el consentimiento informado y se obtuvo la correspondiente autorización del Comité Ético de Investigación Clínica del Complejo Hospitalario Universitario Insular-Materno Infantil de Gran Canaria (CEIC-CHUIMI-2015/780, 13 de agosto de 2015).

Los efectos sobre la viabilidad celular de los compuestos se evaluaron con el ensayo colorimétrico del bromuro del 3-(4,5-dimetil-2-tiazolil)-2,5-difenil-2*H*-tetrazolio (MTT). Brevemente, 4.000 (HL-60 y U-937), 6.000 (NALM-6, SK-MEL-1), o 10.000 (MOLT-3) células creciendo exponencialmente se sembraron en microplacas de 96 pocillos con concentraciones crecientes de los compuestos. Después de la adición de MTT (0.5 mg/mL), las células se incubaron a 37 °C durante 4 h. Se añadió dodecil sulfato sódico (SDS, 10% p/v) en 0.05 M HCl y se incubó durante toda la noche a temperatura de laboratorio en oscuridad. La absorbancia se midió a 570 nm en un lector de microplacas (Modelo 680 de Bio-Rad, Hercules, CA, EE.UU.). Las concentraciones induciendo un 50% de inhibición del crecimiento celular (IC_{50}) se determinaron gráficamente para cada experimento utilizando el programa Prism 5.0 (GraphPad, La Jolla, CA, EE.UU.). Los valores son medias ± error estándar de al menos tres experimentos independientes, realizados por triplicado.

4.3. Evaluación y cuantificación de apoptosis y análisis del ciclo celular

La microscopía fluorescente se utilizó para identificar cambios nucleares asociados con la apoptosis como se ha descrito previamente. Las células se trataron con el correspondiente compuesto por un determinado período de tiempo y se fijaron con 3% paraformaldehído durante 10 min a temperatura de laboratorio. Las células se tiñeron con bisbencimida (Hoechst 33258) durante 15 min y se visualizaron con un microscopio Zeiss de fluorescencia [56]. La apoptosis se cuantificó con un kit de detección de apoptosis utilizando Anexina V-FITC (BD Pharmingen, San Diego, CA, EE. UU.), y llevado a cabo de acuerdo con el protocolo del fabricante.

Para estudiar cambios en el contenido de DNA celular, se llevó a cabo un análisis de citometría de flujo de células teñidas con yoduro de propidio usando un citómetro BD FACSVerse™ (BD Biosciences, San Jose, CA, EE. UU.) como se ha descrito [20]. Brevemente, las células se recogieron y se centrifugaron a 500 ×*g*, se lavaron con PBS y se resuspendieron en 50 µL de PBS. Después de la adición de 1 mL de etanol al 75% frío (−20 °C), las células fijadas se almacenaron a −20 °C durante toda la noche. Las muestras se centrifugaron a 500 ×*g* y se lavaron con PBS y finalmente se resuspendieron en 1 mL de PBS conteniendo 50 µg/mL de yoduro de propidio y 100 µg/mL de RNasa A y se incubaron durante 1 h a 37 °C en la oscuridad. El porcentaje

de células con menor tinción de DNA, compuesto de células apoptóticas resultantes de las fragmentación o disminución de la cantidad de cromatina, se cuantificó de un mínimo de 10.000 células por condición experimental. Los restos celulares se excluyeron del análisis.

4.4. Transferencia Western

El análisis de transferencia Western de proteínas se llevó a cabo como se ha descrito previamente [57]. Las transferencias Western para el análisis de caspasas y PARP se llevó a cabo como se describe a continuación. Las células tratadas con los compuestos a estudiar durante los tiempos especificados se lavaron dos veces con PBS y después se lisaron en un tampón conteniendo 50 mM Tris-HCl, pH 8.0, 150 mM NaCl, 1.0% Triton X-100, 0.1 mM fluoruro de fenilmetilsulfonilo (inhibidor general de serín proteasas, #P7626, Sigma), y 1 μg/mL de los inhibidores de proteasas leupeptina (inhibidor reversible competitivo de cisteín proteasas y de serín proteasas, #L2023, Sigma), pepstatina A (inhibidor de proteasas ácidas /aspartil peptidasas; #P5318, Sigma, stock 1 mg/mL, EtOH:HOAc, 9:1) y aprotinina (inhibidor competitivo de serín proteasas, #A1153, Sigma, stock 5 mg/mL H_2O). Cantidades iguales de proteínas se desnaturalizaron en tampón Laemli 2x (0.125 M Tris-HCl, pH

6.8, 4% SDS (dodecilsulfato sódico), 10% mercaptoetanol, 20% glicerol y 0.004% azul de bromofenol) a 95 ºC durante 5 min. Las muestras se separaron en un gel de poliacrilamida en SDS al 7.5% (PARP) o 12.5% (caspasas), y electrotransferidas a una membrana de PVDF (fluoruro de polivinilideno, membrana de transferencia Immobilon-P de Millipore). Después de bloquear la membrana con 5% leche desnatada en Tris-salino tamponado conteniendo 0.1% Tween-20 durante 1 h, se incubó con los correspondientes anticuerpos primarios seguidos por los correspondientes anticuerpos secundarios. Los complejos antígenos-anticuerpos se visualizaron por quimioluminiscencia utilizando el equipo ChemiDoc (Bio-Rad, Hercules, CA, EE. UU.).

Para la determinación de la liberación de citocromo *c* mitocondrial al citosol, las células se lavaron dos veces con PBS y se resuspendieron en tampón 20 mM HEPES (pH 7.5) conteniendo 250 mM sacarosa, 1.5 mM $MgCl_2$, 10 mM KCl, 1 mM EDTA, 1 mM EGTA, 1 mM ditiotreitol, 0.1 mM fluoruro de fenilmetilsulfonilo, y 5 μg/mL leupeptina, aprotinina, y pepstatina A. Después de 15 min en hielo, las células se lisaron pasándolas varias veces a través de una aguja 22-G, y el lisado se centrifugó a 1.000 x*g* durante 5 min a 4 °C para eliminar núcleos y células no rotas. El sobrenadante se centrifugó a 105.000x*g* durante 45 min a 4 °C, y el sobrenadante resultante se usó como la fracción soluble citosólica.

Los anticuerpos primarios usados en las transferencias Western se adquirieron de las siguientes compañías: anti-caspasa-3 (#ADI-AAP-113, dilución 1:2.000), -8 (#ADI-AAM-118, dilución 1:1.000) y -9 (#ADI-AAM-139, dilución 1:1.000) de Enzo (Plymouth Meeting, PA, EE. UU.); anti-caspasa-9 (#9502, dilución 1:1.000) fue adquirido también de Cell Signaling Technology (Beverly, MA, EE. UU.); anti-poli(ADP-ribosa) polimerasa (PARP, #551024, dilución 1:5.000) y anti-citocromo *c* (#556433, dilución 1:1.000) de BD Pharmingen (San Diego, CA, EE. UU.). Anti-β-actina (clon AC-74, #A2228, dilución 1:3.000) y anti-tubulina (#2125, dilución 1:1.000) fueron de Sigma-Aldrich (Saint Louis, MO, EE. UU.) y Cell Signaling Technology (Beverly, MA, EE. UU.), respectivamente. Los anticuerpos secundarios (#NA9310 y #NA9340) fueron de GE Healthcare (Little Chalfont, Reino Unido). Las membranas de PVDF fueron de Millipore (Temecula, CA, EE. UU.).

4.5. Ensayo de la actividad caspasa

Después de los tratamientos, las células se recolectaron por centrifugación a 1.000x*g* durante 5 min a 4 ºC y se lavaron con PBS, y los precipitados celulares se mantuvieron en hielo. Las células se resuspendieron en tampón de lisis (50 mM HEPES, pH 7.4, 1 mM ditiotreitol, 0.1 mM EDTA, 0.1% Chaps), se mantuvieron en hielo durante 5 min y se lisaron pasándolas varias

veces a través de una aguja 22-G. Después de la centrifugación durante 10 min a 17.000×*g* a 4 °C, se determinó la concentración de proteínas de los sobrenadantes por el método de Bradford y se almacenaron a −20 °C hasta la determinación de la actividad enzimática caspasa por un método colorimétrico. Se usaron cantidades iguales de proteínas de los diferentes tratamientos, y los ensayos se mantuvieron en hielo. La actividad enzimática se determinó midiendo el aumento de la absorbancia a 405 nm después de la incubación a 37 °C. Los sustratos colorimétricos específicos para las actividades de la caspasa-3, -8 y -9 fueron *N*-acetil-Asp-Glu-Val-Asp-*p*-nitroanilina (DEVD-*p*NA), *N*-acetil-Ile-Glu-Thr-Asp-*p*-nitroanilina (IETD-*p*NA) y *N*-acetil-Leu-Glu-His-Asp-*p*-nitroanilina (LEHD-*p*NA), respectivamente.

4.6. Ensayo de polimerización de tubulina in vitro

Los ensayos de polimerización de tubulina *in vitro* se llevaron a cabo con reactivos de un kit de acuerdo con las especificaciones del fabricante (Cytoskeleton Inc., Denver, CO, EE. UU.). Brevemente, concentraciones diferentes del compuesto a ensayar se incubaron con tubulina bovina purificada en tampón 80 mM PIPES (pH 7.0) conteniendo 1 mM GTP, 1 mM EGTA, 1 mM $MgCl_2$ y 10% glicerol, y el aumento de la absorbancia se midió a 340 nm en un lector de microplacas Beckman Coulter DTX880 a 37 ºC y se

registró cada 30 s durante 50 min. El taxol (10 μM) y la colchicina (5 μM) se usaron como controles positivos de promoción e inhibición de la polimerización de tubulina, respectivamente.

4.7. Análisis estadístico

La comparación entre los distintos tratamientos se realizó por el método de la t de Student o análisis de la varianza, considerando significativos los valores de $P < 0.05$.

5. Conclusiones

1. Se ha evaluado el efecto de quince flavonoides sintéticos sobre la viabilidad de células de melanoma humano SK-MEL-1. La 3´-hidroxi-3,4´-dimetoxiflavona es el inhibidor de la viabilidad celular más potente: (i) detiene el ciclo celular en la fase G_2-M, (ii) induce la liberación de citocromo *c* y la activación de las caspasas iniciadoras implicadas en las vías extrínseca e intrínseca de apoptosis e (iii) inhibe la polimerización de tubulina.

2. Se ha explorado las relaciones estructura-citotoxicidad de ocho guayanolidas cloradas, siete de ellas obtenidas de fuentes naturales y un derivado semisintético, usando como modelos líneas celulares de leucemia y de melanoma humanas. Las relaciones estructura-actividad ponen de manifiesto que la introducción de un grupo alquilante en C8 potencia la citotoxicidad y que el grupo α-metilén-γ-lactona es esencial. La liniclorina A fue una de las inhibidoras de la viabilidad más potentes en células de cáncer humanas e inductora de apoptosis. El mecanismo de muerte celular implica la liberación de citocromo *c* mitocondrial, la activación de las caspasas involucradas en las vías intrínseca y extrínseca y la proteolisis del enzima de reparación del DNA poli(ADP-ribosa)polimerasa.

3. Se ha investigado los efectos de once guanidinas sintéticas conteniendo un núcleo 1,3-difenilpropenona sobre la viabilidad de seis líneas de cáncer humanas. El inhibidor de la viabilidad más potente en las células de cáncer humanas contiene un grupo *N*-tosil y una *N*-metilpiperazina. Los compuestos más citotóxicos en células leucémicas humanas fueron la *p*-toluensulfonilguanidina conteniendo una *N*-metilpiperazina y la *N*-metil-*N*-fenilguanidina conteniendo un anillo de piperidina. Ambos compuestos mostraron menor toxicidad en células mononucleares de sangre periférica humanas, sugiriendo que estos pueden tener valor terapéutico potencial. Estos compuestos inducen muerte celular regulada en células de leucemia, asociada a la liberación de citocromo *c*, activación de caspasas e hidrólisis de PARP y la expresión de niveles elevados de la proteína anti-apoptótica Bcl-2 no bloqueó la inhibición de la viabilidad celular.

Referencias

1. Newman DJ, Cragg GM. Natural products as sources of new drugs from 1981 to 2014. *J Nat Prod.* **2016**; *79*:629–661. https://doi.org/10.1021/acs.jnatprod.5b01055

2. Harvey AL, Edrada-Ebel R, Quinn RJ. The re-emergence of natural products for drug discovery in the genomics era. *Nat Rev Drug Discov.* **2015**; *14*:111–29. https://doi.org/10.1038/nrd4510

3. Armando RG, Mengual Gómez DL, Gomez DE. New drugs are not enough-drug repositioning in oncology: An update. *Int J Oncol.* **2020**; *56*:651–684. https://doi.org/10.3892/ijo.2020.4966

4. Hamed AR, Abdel-Azim NS, Shams KA, Hammouda FM. Targeting multidrug resistance in cancer by natural chemosensitizers. *Bull Natl Res Cent*. **2019**; *43*:8 https://doi.org/10.1186/s42269-019-0043-8

5. Nikolaou M, Pavlopoulou A, Georgakilas AG, Kyrodimos E. The challenge of drug resistance in cancer treatment: a current overview. *Clin Exp Metastasis*. **2018**; *35*:309–318. https://doi.org/10.1007/s10585-018-9903-0

6. Sarkar S, Horn G, Moulton K, Oza A, Byler S, Kokolus S, Longacre M. Cancer development, progression, and therapy: an epigenetic overview. *Int J Mol Sci*. **2013**; *14*:21087–113. https://doi.org/10.3390/ijms141021087

7. Byler S, Goldgar S, Heerboth S, Leary M, Housman G, Moulton K, Sarkar S. Genetic and epigenetic aspects of breast cancer progression and therapy. *Anticancer Res.* **2014**; *34*(3):1071–1078.

8. Heerboth S, Lapinska K, Snyder N, Leary M, Rollinson S, Sarkar S. Use of epigenetic drugs in disease: an overview. *Genet Epigenet.* **2014**; *6*:9–19. https://doi.org/10.4137/GEG.S12270

9. Cheng S, Gao N, Zhang Z, Chen G, Budhraja A, Ke Z, Son YO, Wang X, Luo J, Shi X. Quercetin induces tumor-selective apoptosis through downregulation of Mcl-1 and activation of Bax. *Clin Cancer Res.* **2010**; *16*:5679–5691. https://doi.org/10.1158/1078-0432.CCR-10-1565

10. Ravishankar D, Rajora AK, Greco F, Osborn HM. Flavonoids as prospective compounds for anti-cancer therapy. *Int J Biochem Cell Biol.* **2013**; *45*:2821–2831. https://doi.org/10.1016/j.biocel.2013.10.004

11. Galluzzi L, Vitale I, Aaronson SA et al. Molecular mechanisms of cell death: recommendations of the Nomenclature Committee on Cell Death 2018. *Cell Death Differ*. **2018**; *25*:486–541. https://doi.org/10.1038/s41418-017-0012-4

12. Ashkenazi A. Targeting the extrinsic apoptotic pathway in cancer: lessons learned and future directions. *J Clin Invest.* **2015**; *125*:487–489. https://doi.org/10.1172/JCI80420

13. Fulda S, Galluzzi L, Kroemer G. Targeting mitochondria for cancer therapy. *Nat Rev Drug Discov.* **2010**; *9*:447–464. https://doi.org/10.1038/nrd3137

14. Delbridge AR, Strasser A. The BCL-2 protein family, BH3-mimetics and cancer therapy. *Cell Death Differ.* **2015**; *22*:1071–1080. https://doi.org/10.1038/cdd.2015.50

15. Tummers B, Green DR. Caspase-8: regulating life and death. *Immunol Rev.* **2017**; *277*:76–89. https://doi.org/10.1111/imr.12541

16. Julien O, Wells JA. Caspases and their substrates. *Cell Death Differ.* **2017**; *24*:1380–1389. https://doi.org/10.1038/cdd.2017.44

17. Cohen GM. Caspases: the executioners of apoptosis. *Biochem J.* **1997**; *326*:1–16. https://doi.org/10.1042/bj3260001

18. Hsiang CY, Wu SL, Ho TY. Morin inhibits 12-O-tetradecanoylphorbol-13-acetate-induced hepatocellular transformation via activator protein 1 signaling pathway and cell cycle progression. *Biochem Pharmacol.* **2005**; *69*:1603–1611. https://doi.org/10.1016/j.bcp.2005.03.008

19. Rubio S, Quintana J, López M, Eiroa JL, Triana J, Estévez F. Phenylbenzopyrones structure-activity studies identify betuletol derivatives as potential antitumoral agents. *Eur J Pharmacol.* **2006**; *548*:9–20. https://doi.org/10.1016/j.ejphar.2006.07.020

20. Rubio S, Quintana J, Eiroa JL, Triana J, Estévez, F. Acetyl derivative of quercetin 3-methyl ether-induced cell death in human leukemia cells is amplified by the inhibition of ERK. *Carcinogenesis* **2007**; *28*:2105–2113. https://doi.org/10.1093/carcin/bgm131

21. Beutler JA, Cardellina JHII, Lin CM, Hamel E, Cragg GM, Boyd MR. Centaureidin, a cytotoxic flavone from *Polymnia fruticosa*, inhibits tubulin polymerization. *Bioorg Med Chem Lett.* **1993**; *3*:581–584. https://doi.org/10.1016/S0960-894X(01)81233-6

22. Lichius JJ, Thoison O, Montagnac A, Païs M, Guéritte-Voegelein F, Sévenet T, Cosson JP, Hadi AH. Antimitotic and cytotoxic flavonols from *Zieridium pseudobtusifolium* and *Acronychia porteri*. *J Nat Prod.* **1994**; *57*:1012–1016. https://doi.org/10.1021/np50109a024

23. Shobeiri N, Rashedi M, Mosaffa F, Zarghi A, Ghandadi M, Ghasemi A, Ghodsi R. Synthesis and biological evaluation of quinoline analogues of flavones as potential anticancer agents and tubulin polymerization inhibitors. *Eur J Med Chem.* **2016**; *114*:14–23. https://doi.org/10.1016/j.ejmech.2016.02.069

24. Beutler JA, Hamel E, Vlietinck AJ, Haemers A, Rajan P, Roitman JN, Cardellina JH 2nd, Boyd MR. Structure-activity requirements for flavone cytotoxicity and binding to tubulin. *J Med Chem.* **1998**; *41*:2333–2338. https://doi.org/10.1021/jm970842h

25. Torres F, Quintana J, Estévez F. 5,7,3'-Trihydroxy-3,4'-dimethoxyflavone inhibits the tubulin polymerization and activates the sphingomyelin pathway. *Mol Carcinog.* **2011**; *50*:113–122. https://doi.org/10.1002/mc.20693

26. Ren Y, Yu J, Kinghorn AD. Development of Anticancer Agents from Plant-Derived Sesquiterpene Lactones. *Curr Med Chem.* **2016**; *23*:2397–2420. https://doi.org/10.2174/0929867323666160510123255

27. Quintana J, Estévez F. Recent Advances on Cytotoxic Sesquiterpene Lactones. *Curr Pharm Des.* **2018**; *24*:4355–4361. https://doi.org/10.2174/1381612825666190119114323

28. Merfort I. Perspectives on sesquiterpene lactones in inflammation and cancer. *Curr Drug Targets* **2011**; *12*:1560–1573. https://doi.org/10.2174/138945011798109437

29. Ghantous A, Gali-Muhtasib H, Vuorela H, Saliba NA, Darwiche N. What made sesquiter-pene lactones reach cancer clinical trials?. *Drug Discov. Today* **2010**; *15*:668–678. https://doi.org/10.1016/j.drudis.2010.06.002

30. González AG, Bermejo J, Breton JL, Massanet GM, Domínguez B, Amaro JM. The chemistry of the *Compositae*. Part XXXI. Absolute configuration of the sesquiterpene lactones centaurepensin (chlorohyssopifolin A), acroptilin

(chlorohyssopifolin C), and repin. *J Chem Soc., Perkin Trans I* **1976**; 1663–1666. https://doi.org/10.1039/P19760001663

31. Chen C, Yu J, Fleck BA, Hoare SR, Saunders J, Foster AC. Phenylguanidines as selective nonpeptide melanocortin-5 receptor antagonists. *J Med Chem.* **2004**; *47*:4083–4088. https://doi.org/10.1021/jm0400496

32. Shukla S, Sood AK, Goyal K, Singh A, Sharma V, Guliya N, Gulati S, Kumar S. Chalcone Scaffolds as Anticancer Drugs: A Review on Molecular Insight in Action of Mechanisms and Anticancer Properties. *Anticancer Agents Med Chem.* **2021**; *21*: 1650–1670. https://doi.org/10.2174/1871520620999201124212840

33. Ashour HF, Abou-Zeid LA, El-Sayed MA, Selim KB. 1,2,3-Triazole-Chalcone hybrids: Synthesis, in vitro cytotoxic activity and mechanistic investigation of apoptosis induction in multiple myeloma RPMI-8226. *Eur J Med Chem.* **2020**; *189*:112062. https://doi.org/10.1016/j.ejmech.2020.112062

34. Rodríguez I, Saavedra E, del Rosario H, Perdomo J, Quintana J, Prencipe F, Oliva P, Romagnoli R, Estévez F. Apoptosis pathways triggered by a potent antiproliferative hybrid chalcone on human melanoma cells. *Int J Mol Sci.* **2021**; *22*:13462. https://doi.org/10.3390/ijms222413462

35. Estévez-Sarmiento F, Said M, Brouard I, León F, García C, Quintana J, Estévez F. 3'-Hydroxy-3,4'-dimethoxyflavone blocks tubulin polymerization

and is a potent apoptotic inducer in human SK-MEL-1 melanoma cells. *Bioorg Med Chem.* **2017**; *25*:6060–6070. https://doi.org/10.1016/j.bmc.2017.09.043

36. Nicolini F, Burmistrova O, Marrero MT, Torres F, Hernández C, Quintana J, Estévez F. Induction of G_2-M phase arrest and apoptosis by the flavonoid tamarixetin on human leukemia cells. *Mol Carcinog.* **2014**; *53*:939–950. https://doi.org/10.1002/mc.22055

37. Zeng G, Liu J, Chen H, Liu B, Zhang Q, Li M, Zhu R. Dihydromyricetin induces cell cycle arrest and apoptosis in melanoma SK-MEL-28 cells. *Oncol Rep*. **2014**; *31*:2713–2719. https://doi.org/10.3892/or.2014.3160

38. Ma G, Chen K, Zhang L, Li Y. Advance in biological activities of natural guaiane-type sesquiterpenes. *Med Chem Res.* **2019**; *28*:1339–1358. https://doi.org/10.1007/s00044-019-02385-7

39. Li J, Yoshida Y, Kurita M, Usuki T. Cynaropicrin and inhibition of NF-κB activation: A structure activity relationship study. *Bioorg Med Chem Lett.* **2019**; *29*:1518–1521. https://doi.org/10.1016/j.bmcl.2019.04.004

40. Zeng J, Zhan J. Chlorinated natural products and related halogenases. *Isr J Chem.* **2019**; *59*: 387–402. https://doi.org/10.1002/ijch.201800175

41. Engvild K. Chlorine-containing natural compounds in higher plants. *Phytochemistry* **1986**; *25*:781–791. https://doi.org/10.1016/0031-9422(86)80002-4

42. Bruno M, Rosselli S, Maggio A, Raccuglia RA, Bastow KF, Lee KH. Cytotoxic activity of some natural and synthetic guaianolides. *J Nat Prod.* **2005**; *68*:1042–1046. https://doi.org/10.1021/np0500575

43. Scotti MT, Fernandes MB, Ferreira MJ, Emerenciano VP. Quantitative structure-activity relationship of sesquiterpene lactones with cytotoxic activity. *Bioorg Med Chem.* **2007**; *15*:2927–2934. https://doi.org/10.1016/j.bmc.2007.02.005

44. González AG, Bermejo J, Bretón JL, Massanet GM, Triana J. Chlorohyssopifolin C, D, E and vahlenin, four new sesquiterpene lactones from *Centaurea hyssopifolia*. *Phytochemistry* **1974**; *13*:1193–1l97. https://doi.org/10.1016/0031-9422(74)80099-3

45. González AG, Bermejo J, Amaro JM, Massanet GM, Galindo A, Cabrera I. Sesquiterpene lactones from *Centaurea linifolia* Vahl. *Can J Chem.* **1978**; *56*: 491–494. https://doi.org/10.1139/v78-079

46. González AG, Bermejo J, Massanet GM, Amaro JM. Action of silver nitrate on chlorinated sesquiterpene lactones. *An Quim.* **1978** (1968–1979), *74* (11):1443–1445.

47. Harris P, Ralph P. Human leukemic models of myelomonocytic development: a review of the HL-60 and U937 cell lines. *J Leukoc Biol.* **1985**; *37*:407–422. https://doi.org/10.1002/jlb.37.4.407

48. Chanput W, Peters V, Wichers H. THP-1 and U937 Cells, in: Verhoeckx K, Cotter P, López-Expósito I, Kleiveland C, Lea T, Mackie A, Requena T, Swiatecka D, Wichers H. (Eds.), The Impact of Food Bioactives on Health: in vitro and ex vivo models, Springer, **2015**; 147–159.

49. Tukov FF, Anand S, Gadepalli RS, Gunatilaka AA, Matthews JC, Rimoldi JM. Inactivation of the cytotoxic activity of repin, a sesquiterpene lactone from *Centaurea repens*. *Chem Res Toxicol.* **2004**; *17*:1170–1176. https://doi.org/10.1021/tx049864e

50. Amundson SA, Myers TG, Scudiero D, Kitada S, Reed JC, Fornace AJ Jr. An informatics approach identifying markers of chemosensitivity in human cancer cell lines. *Cancer Res.* **2000**; *60*:6101–6110. http://cancerres.aacrjournals.org/content/60/21/6101

51. Ooi LC, Watanabe N, Futamura Y, Sulaiman SF, Darah I, Osada H. Identification of small molecule inhibitors of p27(Kip1) ubiquitination by high-throughput screening. *Cancer Sci.* **2013**; *104*:1461–1467. https://doi.org/10.1111/cas.12246

52. Estévez-Sarmiento F, Saavedra E, Ruiz-Estévez M, León F, Quintana J, Brouard I, Estévez F. Chlorinated Guaiane-Type Sesquiterpene Lactones as Cytotoxic Agents against Human Tumor Cells. *Int J Mol Sci.* **2020**; *21*(24):9767. https://doi.org/10.3390/ijms21249767

53. Berlinck RGS, Bernardi DI, Fill T, Fernandes AAG, Jurberg ID. The chemistry and biology of guanidine secondary metabolites. *Nat Prod Rep.* **2021**; *38*:586–667. https://doi.org/10.1039/d0np00051e

54. Berlinck RG, Burtoloso AC, Kossuga MH. The chemistry and biology of organic guanidine derivatives. *Nat Prod Rep.* **2008**; *25*:919–954. https://doi.org/10.1039/b507874c

55. Estévez-Sarmiento F, Saavedra E, Brouard I, Peyrac J, Hernández-Garcés J, García C, Quintana J, Estévez F. Guanidine Derivatives Containing the Chalcone Skeleton Are Potent Antiproliferative Compounds against Human Leukemia Cells. *Int J Mol Sci.* **2022**; *23*(24):15518. https://doi.org/10.3390/ijms232415518

56. Said M, Brouard I, Quintana J, Estévez F. Antiproliferative activity and apoptosis induction by 3',4'-dibenzyloxyflavonol on human leukemia cells. *Chem Biol Interact.* **2017**; *268*: 13–23. https://doi.org/10.1016/j.cbi.2017.02.010

57. Negrín G, Rubio S, Marrero MT, Quintana J, Eiroa JL, Triana J, Estévez F. The eudesmanolide tanapsin from *Tanacetum oshanahanii* and its acetate induce cell death in human tumor cells through a mechanism dependent on reactive oxygen species. *Phytomedicine* **2015**; 22:385–393. https://doi.org/10.1016/j.phymed.2015.01.008

Bioorganic & Medicinal Chemistry 25 (2017) 6060–6070

Contents lists available at ScienceDirect

Bioorganic & Medicinal Chemistry

journal homepage: www.elsevier.com/locate/bmc

3′-Hydroxy-3,4′-dimethoxyflavone blocks tubulin polymerization and is a potent apoptotic inducer in human SK-MEL-1 melanoma cells

Francisco Estévez-Sarmiento [a], Mercedes Said [a], Ignacio Brouard [b], Francisco León [b], Celina García [c], José Quintana [a], Francisco Estévez [a,*]

[a] Departamento de Bioquímica y Biología Molecular, Unidad Asociada al Consejo Superior de Investigaciones Científicas (CSIC), Instituto Universitario de Investigaciones Biomédicas y Sanitarias, Universidad de las Palmas de Gran Canaria, Paseo Blas Cabrera Felipe s/n, 35016 Las Palmas de Gran Canaria, Spain
[b] Instituto de Productos Naturales y Agrobiología, CSIC, Avenida Astrofísico Francisco Sánchez 3, 38206 La Laguna, Tenerife, Spain
[c] Instituto Universitario de Bio-Orgánica "Antonio González" (IUBO-AG), Departamento de Química Orgánica, Universidad de La Laguna, Avda. Astrofísico Francisco Sánchez 2, 38206 La Laguna, Tenerife, Spain

ARTICLE INFO

Article history:
Received 27 July 2017
Revised 26 September 2017
Accepted 30 September 2017
Available online 3 October 2017

Keywords:
Apoptosis
Caspases
Cytotoxicity
Flavonoids
Melanoma

ABSTRACT

Flavonoids are naturally occurring polyphenolic compounds and are among the most promising anticancer agents. A series of flavonols and their 3-methyl ether derivatives were synthesized and assessed for cytotoxicity. It was found that 3′-hydroxy-3,4′-dimethoxyflavone (flavonoid **7a**) displayed strong cytotoxicity against human SK-MEL-1 melanoma cells and blocked tubulin polymerization, but had no significant cytotoxic effects against quiescent or proliferating human peripheral blood mononuclear cells. Our analyses showed that flavonoid **7a** induces G_2-M cell cycle arrest and apoptosis in melanoma cells which is associated with cytochrome *c* release and activation of both extrinsic and intrinsic apoptotic pathways of cell death.

1. Introduction

Natural products are important sources of potential new anticancer agents. Approximately 63% of anticancer drugs introduced over the last 25 years are natural products or can be traced back to a natural products source.[1] Flavonoids are secondary metabolites with low molecular weight and phenolic structure, occurring ubiquitously in food plants, and being a common component in the human diet. Many flavonoids display a vast array of biological activities including antitumor properties.[2,3] These properties of flavonoids are mediated by different types of cell cycle arrest and induction of apoptosis. This kind of cell death is characterized by DNA fragmentation, chromatin condensation, and formation of apoptotic bodies. It is mediated by the activation of a class of cysteine proteases, known as caspases, by two main pathways.[4,5] In the intrinsic pathway, diverse pro-apoptotic signals induce mitochondrial cytochrome *c* release to the cytosol, and promote apoptosome assembly and caspase-9 activation. In the extrinsic pathway, apoptosis is mediated by death receptors and involves caspase-8 activation. Both caspase-8 and caspase-9 activate caspase-3, which is responsible for cleaving specific cellular proteins during apoptosis.

Previous research has shown that flavonoids with a hydroxy group at position 3 are potential anticancer agents and that methylation of these compounds increases their antiproliferative activity against human tumor cells.[6–8] Knowledge of the effects of flavonoid substitution profiles on their antitumoral and tubulin polymerization inhibitory activity has witnessed much progress in recent years. Casticin and centaureidin (Fig. 1), are two important members of the family of flavones which show two methoxy groups at the C4′ and C3 positions and one hydroxy at the C3′ position and are promising anticancer agents due to their high cytotoxicity against a variety of cancer cells.

Centaureidin was the first cytotoxic flavone described as a tubulin interactive agent and this was followed by the identification of a flavone which incorporated the same substitution profile as centaureidin and that inhibited the incorporation of tubulin into microtubules.[9,10] Recently, methoxylated flavones have been used as the lead compounds in the design of new analogues as tubulin inhibitors.[11] Analyses of structure and activity showed that i) compounds that contain the previously indicated substitution profile

Abbreviations: MTT, 3-(4,5-dimethyl-2-thiazolyl)-2,5-diphenyl-2*H*-tetrazolium bromide; PI, propidium iodide.

* Corresponding author.
E-mail address: francisco.estevez@ulpgc.es (F. Estévez).

https://doi.org/10.1016/j.bmc.2017.09.043
0968-0896/

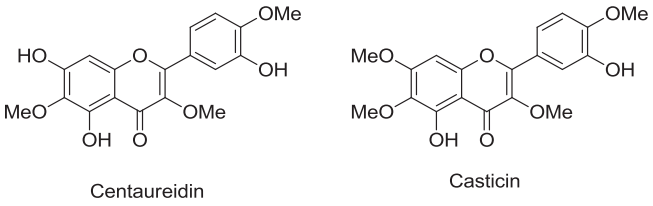

Fig. 1. Chemical structure of anticancer 3-methoxyflavones.

were more active as inhibitors of tubulin polymerization than those that did not, ii) the substitution of a methoxy in C3 for a hydroxy group dramatically decreased the activity of the compound, and iii) substitutions in the A ring do not seem to be relevant at all.[12] Studies in our research group confirmed that the substitution profile (methoxy on C3, C4′ and hydroxy on C3′) leads to compounds with antileukemic activity and significant capacity to inhibit tubulin polymerization.[13]

The potential significance of flavonoids containing this substitution pattern in antimelanoma therapy is largely unexplored to date. The main aim of this work was to investigate the cytotoxic effects of 15 synthetic flavonoids against SK-MEL-1 melanoma cells and elucidate the mechanism of cell death for the most effective compounds. The results show 3′-hydroxy-3,4′-dimethoxyflavone, **7a** to be the most cytotoxic compound against this cell line. We provide new evidence that shows for the first time that this flavonoid induces apoptotic cell death which is mediated by caspase activation and tubulin polymerization inhibition.

2. Results and discussion

2.1. Chemistry

In this manuscript, the design and synthesis of 15 flavonoids was developed with the purpose of determining the minimum structural requirements for a flavone to induce cell death in the human melanoma cell line SK-MEL-1. We focused mainly on the B ring substituents and the C-3 position (C ring). Four compounds were designed to contain the same pair of 3′-hydroxy-4′-methoxy substituents (B ring) and all four possible combinations of methoxy/hydrogen groups at position C-7 (**5a**, **5b**) and hydroxy/methoxy groups at C-3 (**7a**, **7b**). Additionally, the same compounds were prepared with a 4′-hydroxy-3′-methoxy pair of substituents in the B ring (**5c**, **5d** and **7c**, **7d**). Finally, the collection was completed with similar examples containing just one hydroxy group in the B ring (positions 4′ and 2′). Two acetophenones and four aldehydes were used as starting material for this collection of flavones (Scheme 1).

The synthetic route did not differ from the traditional one. An aldol condensation reaction in basic media was used to generate eight compounds with a chalcone skeleton (**3a-h**) which were subsequently subjected to the Algar-Flynn-Oyamada cyclization under oxidative conditions to produce eight benzylated flavonols.[14] These compounds were submitted to hydrogenation reaction conditions to obtain the free alcohols (**5a-h**).[15] The methylation reaction employing MeI provided methyl ethers (**6a-g**) which were then deprotected in order to obtain the free alcohols (**7a-g**).[16]

2.2. Biological evaluation

2.2.1. A synthetic phenylbenzopyrone derivative, 3′-hydroxy-3,4′-dimethoxyflavone, inhibits the growth and cell viability of human SK-MEL-1 melanoma cells

Previous studies have demonstrated that the methoxyflavones have higher antiproliferative activity than the corresponding hydroxylated derivatives and that the presence of 3′-hydroxy-4′-methoxy groups on the B ring of the flavonoid skeleton enhances the cytotoxicity.[7,12,13,17]

In the present study, the potential cytotoxic properties of a series of 15 flavonoids, including flavonols and 3-methyl ether

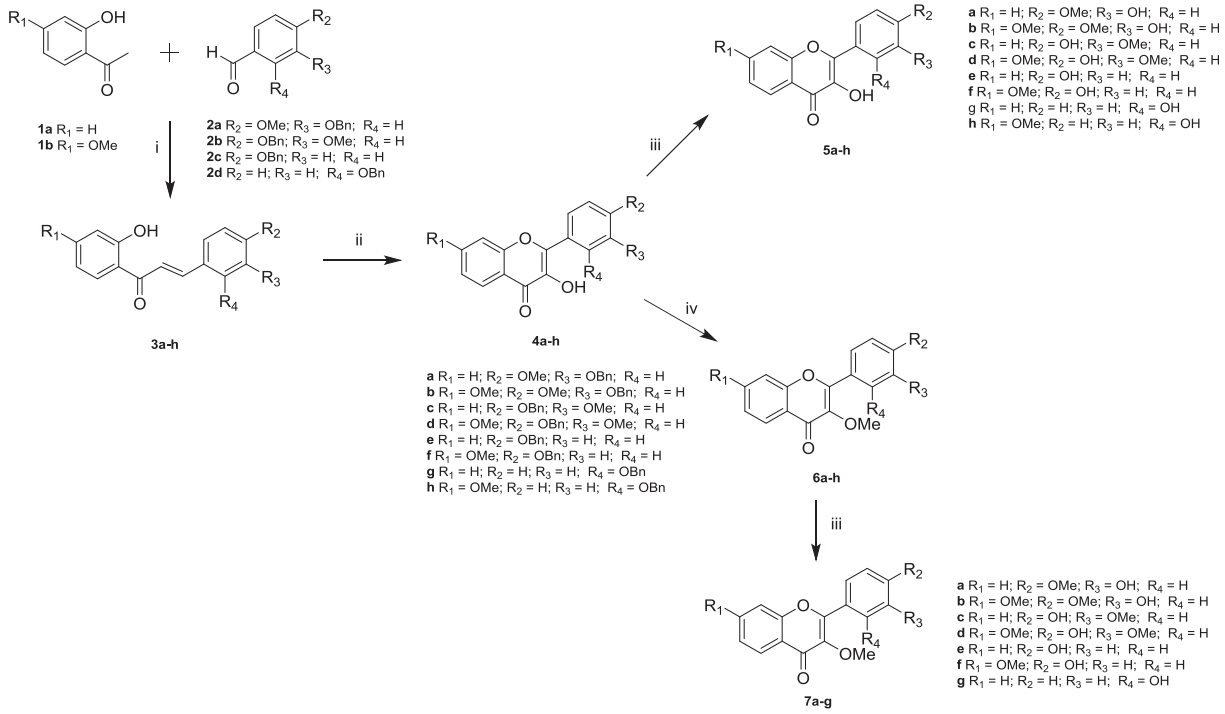

i) NaOHaq (50%), EtOH; ii) KOH/H_2O_2, MeOH; iii) H_2, Pd/C (10%), THF; iv) MeI, K_2CO_3, Acetone.

Scheme 1. Synthesis of the intermediate chalcones and methyl ethers.

derivatives with one or two substituents on the B ring (2-phenyl group) and an additional substituent on the A ring were evaluated using the human melanoma cell line SK-MEL-1 (Scheme 1, Table 1). We tested antiproliferative activity with an MTT [3-(4,5-dimethylthiazol-2-yl)-2,5-diphenyl tetrazolium bromide] assay. The compounds containing two substituents on the B ring were found to show significant differences in their cytotoxicity between the flavonols and their corresponding 3-methoxy derivatives (**5c** vs **7c** and **5a** vs **7a**). The 3-methylether derivative **7a** is more cytotoxic than the corresponding flavonol **5a**. The IC_{50} values (the concentrations that induce a 50% inhibition of cell growth) for **7a** against SK-MEL-1 cells was 6.9 ± 1.1 μM, while the IC_{50} value for **5a** was 32.6 ± 7.1 μM. The effects of the flavonoid **7a** on SK-MEL-1 cells viability were visualized by phase contrast microscopy. While control cells appeared perfectly round and healthy, there was a clear reduction in the number of cells and they appeared unhealthy after treatment with increasing concentrations of **7a** (Fig. 2A).

Although there were no differences between the flavonols **5c** and **5a**, the position of the hydroxy and methoxy groups on the B ring seems to play a key role in determining the potency of 3-methoxyflavonols on cell viability (**7a** vs **7c**).

For the flavonols containing one substituent at the C7 position on the A ring and one hydroxy group on the B ring (**5f** and **5h**), the position of the hydroxy group on the B ring does not seem to be important, since the 4′-hydroxy derivative was inactive as well as the 2′-hydroxy derivative (**5f** vs **5h**) and methylation of the hydroxy group located at the C3 position did not affect antiproliferative activity either (**5f** vs **7f**). The presence of a methoxy at the C7 position on the A ring apparently is not a major determinant of cytotoxicity (**5g** vs **5h** and **7e** vs **7f**).

In the case of flavonols (**5b** vs **5d**) and their corresponding 3-methylethers (**7b** and **7d**) that contained one substituent in C7 on the A ring and two substituents on the B ring, there were significant differences in cytotoxicity against melanoma cells between the position of the hydroxy and methoxy groups on the B ring (**5d** vs **5b**). In the case of 3-methylether derivatives (**7b** vs **7d**), the substitution pattern of the latter groups on the B ring seems to play a key role in conferring cytotoxicity since the 3′-hydroxy-4′-methoxy derivative (**7b**) exhibited a higher potency than 4′-hydroxy-3′-methoxy derivative **7d**.

In the case of flavonoids containing 3′-hydroxy-4′-methoxy substituents on the B ring, the 3-hydroxy-7-methoxy flavonoid (**5b**) was more potent than the 3,7-dimethoxy derivative (**7b**). In all cytotoxicity assays the chemotherapeutic etoposide was used as a positive control (Table 1).

The cytotoxicity experiments revealed that 3′-hydroxy-3,4′-dimethoxyflavone (**7a**) displays strong cytotoxic activity against the human melanoma cell line SK-MEL-1 with an IC_{50} value as low as 6.9 μM (Table 1, Fig. 2B). Moreover, we also assayed the effects of **7a** on the growth of the human lymphocytes and found that it did not significantly affect cell viability of quiescent and proliferating cells (Fig. 2C). Since **7a** was the most cytotoxic compound we decided to investigate whether this flavonoid displays its cytotoxic action on SK-MEL-1 cells through activation of the apoptotic pathway.

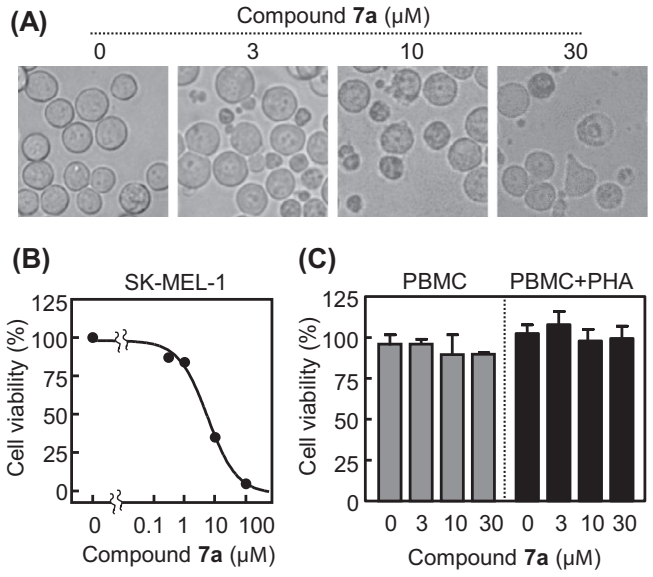

Fig. 2. Effects of **7a** on SK-MEL-1 melanoma cells viability. (A) Cells were incubated with vehicle or the described concentrations of **7a** for 24 h and images were obtained with an inverted phase-contrast microscope. (B) Cells were cultured in the presence of the described concentrations of **7a** for 72 h, and thereafter cell viability was determined by the MTT reduction assay. The results are representative of those obtained in at least three independent experiments. (C) Effect of **7a** on cell viability of peripheral blood mononuclear cells (PBMCs). Quiescent and phytohemagglutinine-activated PBMC cells from healthy human origin were cultured in the presence of the specified concentrations of **7a** for 24 h. Values represent means ± SE of three independent experiments each performed in triplicate. $^{*}P < 0.05$, significantly different from the untreated control.

*2.2.2. **7a** induces G_2-M arrest and apoptosis on human SK-MEL-1 melanoma cells*

To determine whether **7a**-induced cytotoxicity involves changes in cell cycle progression, we evaluated the effect of **7a** on cell-cycle phase distribution by flow cytometry. As shown in Table 2 and Fig. 3A, **7a** caused a significant G_2–M arrest at the expense of G_1 phase cell population in SK-MEL-1 cell line at all concentrations analysed (3–30 μM) and an increase in the percentage of sub-G_1 cells (apoptotic cells) as determined by flow cytometry after propidium iodide labeling. Flavonoid **7a** increased apoptosis and this effect is concentration-dependent. The percentage of sub-G_1 increased up to 22% after 24 h of treatment with 30 μM **7a** (Fig. 3A). The morphological changes characteristic of apoptotic cells (condensed and fragmented chromatin) after treatment with **7a** were also visualized by fluorescent microscopy (Fig. 3B). Taken together, these results indicate that **7a** induces cell-cycle arrest in the G_2–M phase and apoptosis on human melanoma cells.

*2.2.3. **7a** induces cell death by a caspase-dependent pathway in SK-MEL-1 cells*

To analyze whether the effect of **7a** is mediated by caspases, we examined whether this flavonoid induces the enzymatic activities of caspase-3-like proteases (caspase-3/7) and of caspase-8 and -9. To

Table 1
Effects of flavonoids on the growth of human SK-MEL-1 melanoma cells.

Compound	**5a**	**5b**	**5c**	**5d**	**5e**	**5f**	**5g**	**5h**
IC_{50} (μM)	32.6 ± 7.1	15.5 ± 2.8	22.0 ± 5.8	37.0 ± 5.0	>100	>100	>100	>100
Compound	**7a**	**7b**	**7c**	**7d**	**7e**	**7f**	**7g**	**Etoposide**
IC_{50} (μM)	6.9 ± 1.1	26.2 ± 1.9	79.0 ± 13.1	52.0 ± 8.2	91.0 ± 11.1	>100	>100	8.0 ± 4.1

Cells were cultured for 72 h in presence of the indicated compounds and the IC_{50} values were calculated using a colorimetric MTT assay. The data shown represent the mean ± SEM of 2–3 independent experiments with three determinations in each.

Table 2
Effect of different durations of treatment with **7a** on cell cycle phase distribution of human SK-MEL-1 melanoma cells.

	% Sub-G_1	% G_1	% S	% G_2-M
Control	4.5 ± 1.6	61.5 ± 1.7	17.7 ± 0.4	16.1 ± 0.2
3 μM **7a**	15.9 ± 1.1*	24.4 ± 0.5*	21.4 ± 1.2*	37.9 ± 2.6*
10 μM **7a**	9.2 ± 1.7*	14.4 ± 1.6*	23.7 ± 0.4	52.2 ± 3.9*
30 μM **7a**	21.9 ± 7.5*	30.7 ± 0.9*	26.8 ± 1.8*	20.2 ± 10.1*

Cells were cultured with increasing concentrations of **7a** for 24 h and the cell cycle phase distribution was determined by flow cytometry. The values are means ± SE of three independent experiments with three determinations in each. Asterisks indicate a significant difference ($P < 0.05$) compared with the corresponding controls.

this end, cells were treated with increasing concentrations of **7a** and cell lysates were assayed for the cleavage of the tetrapeptides DEVD-*p*NA, IETD-*p*NA and LEHD-*p*NA as specific substrates for caspase-3/7, caspase-8 and caspase-9, respectively. All these caspase activities were significantly detectable after 24 h of treatment with **7a** (Fig. 3C). Dose-response experiments show that a low concentration (3 μM) of **7a** was sufficient to induce caspase-3/7 activation, while caspase-8 and -9 caused lower levels of activation.

To determine whether **7a**-triggered apoptosis involves the processing of caspase-3, cells were treated with increasing concentrations of the flavonoid for 24 h and this caspase was analysed by Western blot. As shown in Fig. 3D, **7a** stimulated the cleavage of the main executioner caspase. It was also studied whether this apoptotic effect of **7a** involves the release of mitochondrial cytochrome *c*. The results showed a significant increase in the amount of this proapoptotic protein in the cytosol after treatment with **7a** in a concentration-dependent manner (Fig. 3D). Taken together these data show that both the intrinsic and the extrinsic pathways play an important role in cell death induced by **7a** in SK-MEL-1 melanoma cells.

2.2.4. Effect of *7a* on tubulin polymerization

As shown before, concentrations of flavonoid **7a** that inhibited SK-MEL-1 proliferation caused an increase in the number of cells in the G_2–M phase at 24 h, taking into account that these cells have

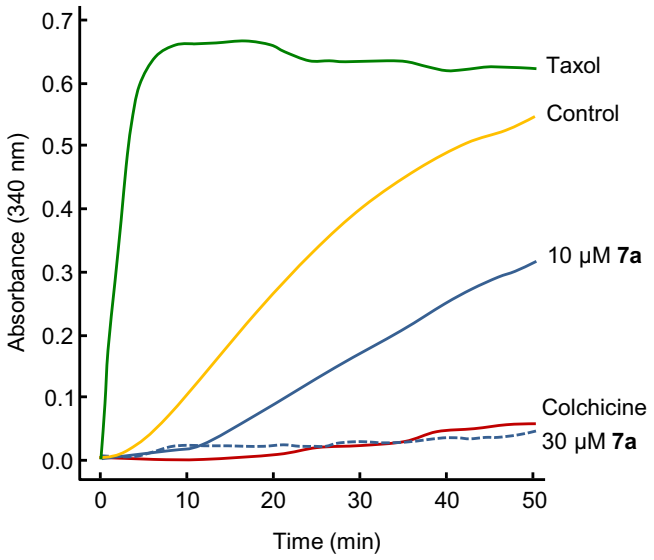

Fig. 4. Flavonoid **7a** blocks the tubulin polymerization *in vitro*. Purified tubulin protein in a reaction buffer was incubated at 37 °C in the absence (control) or in the presence of taxol (10 μM), colchicine (5 μM) or the indicated concentrations of **7a** and the absorbance at 340 nm was measured using a microplate reader.

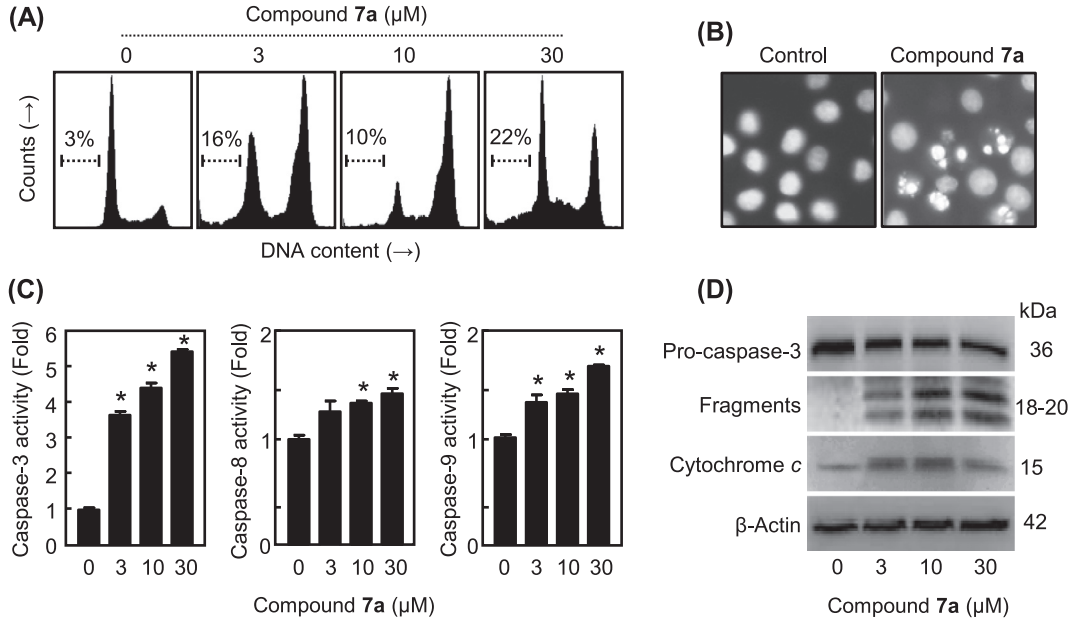

Fig. 3. Effects of **7a** on apoptosis induction in SK-MEL-1 melanoma cells. (A) Cells were incubated with increasing concentrations of **7a** for 24 h, subjected to flow cytometry using propidium iodide labeling and the percentage of cells in the sub-G_1 region (apoptotic cells) determined. (B) Photomicrographs of representative fields of SK-MEL-1 cells stained with bisbenzimide trihydrochloride to evaluate nuclear chromatin condensation (i.e. apoptosis) after treatment for 24 h with 30 μM of **7a**. (C) Activation of caspases in response to **7a**. The cells were treated with the described concentrations of **7a** and cell lysates were assayed for caspase 3/7, -8 and -9 activities. Results are expressed as factorial increases in caspase activity relative to the control. Values represent the means ± SEs of three independent experiments each performed in triplicate. *$P < 0.05$, significantly different from untreated control. (D) Effects of **7a** on processing of pro-caspase-3 and mitochondrial cytochrome *c* release. Cells were incubated in the presence of the described concentrations of **7a**, and whole cell lysates or cytosolic fractions (in the case of cytochrome *c*) were probed with antibodies raised against the indicated proteins by immunoblotting. β-Actin was used as a loading control.

long doubling times of approximately 72 h. Several flavonoids have been reported to exert their antiproliferative activity by targeting microtubules through tubulin binding.[12] One of the structural requirements usually found in flavones for tubulin interaction is the presence of a methoxy group at C-3. Since **7a** contains a methoxy group at C-3, G_2–M arrest induced by this flavonoid might be explained by the inhibition of microtubule formation or by changes in the expression and/or activity of G_2–M cell-cycle regulators. The flavonoid quercetin has been shown to inhibit cancer cell proliferation by depleting cellular microtubules and inhibiting microtubule polymerization through tubulin binding.[18] To confirm this hypothesis we used purified tubulin (containing no microtubule-associated proteins) in our assay and found that **7a** led to a concentration-dependent inhibition of tubulin assembly. Colchicine and taxol were used as positive controls of inhibition and promotion of tubulin polymerization, respectively (Fig. 4). Further studies are needed to determine the effect of this compound on these regulators such as the cyclin-dependent kinase-1, cyclin-dependent kinase inhibitor $p21^{Cip1}$, B-type cyclin isoforms, and cdc25C.

3. Conclusions

We have synthesized 15 flavonoids, including eight flavonols and seven 3-methyl ethers, with one or two substituents on the B ring and an additional substituent on the A ring, and evaluated their effects on cell viability of the malignant cell line SK-MEL-1. The B ring substituents included the pairs of 3′-hydroxy-4′-methoxy or 4′-hydroxy-3′-methoxy or just one hydroxy group. The 3-methoxyflavone **7a**, containing a 3′-hydroxy-4′-methoxy pair of substituents in the B ring, was the most cytotoxic compound against melanoma cells but had low cytotoxicity against human lymphocytes. The fact that human melanoma SK-MEL-1 cells were sensitive to **7a** is extremely interesting given that melanoma is the most aggressive and lethal skin cancer and frequently resists chemotherapy.

Relatively few studies have analysed the potential of flavonoids in antimelanoma therapy. Tamarixetin (3,5,7,3′-tetrahydroxy-4′-methoxyflavone) and dihydromyricetin are two known flavonoids that have been reported to display antiproliferative capacity against melanoma cells.[19,20] Tamarixetin exhibits cytotoxic properties on SK-MEL-1 cells but the pathways involved in cell death remain to be explored,[19] and comparative studies indicate that its cytotoxic capacity is three times lower than **7a** (IC_{50} = 23.1 ± 2.1 μM vs. 6.9 ± 1.1 μM). Dihydromyricetin suppress cell proliferation of SK-MEL-28 melanoma cells by inducing cell cycle arrest at the G_1 phase and apoptosis, although this occurs at higher concentrations than were used for flavonoid **7a**.

In summary, the present study on the human melanoma cells SK-MEL-1 demonstrates that the flavonoid **7a** arrested the cell cycle at the G_2-M phase, induced apoptotic cell death and blocked tubulin polymerization. Apoptosis was confirmed by i) fluorescent microscopy, ii) the appearance of a subdiploid DNA content and iii) caspase-3 activation. The antiproliferative effect of **7a** is associated with cytochrome *c* release and with the activation of the initiator caspases involved in the extrinsic and the intrinsic pathways of cell death.

4. Experimental

4.1. General information

Compounds used as starting materials and reagents were obtained from Aldrich Chemical Co., or other chemical companies and utilized without further purification. Melting points are uncorrected. ^{1}H NMR and ^{13}C NMR spectra were recorded at 400 and 500 MHz for ^{1}H and 100 and 125 MHz for ^{13}C, respectively. Chemical shifts (δ) are reported in parts per million relative to the residual solvent signals, and coupling constants (J) are reported in hertz. High resolution ESI mass spectra were obtained from a Fourier transform ion cyclotron resonance (FT-ICR) mass spectrometer, an RF-only hexapole ion guide, and an external electrospray ion source. Flash column chromatography was carried out using silica gel 60 (230–400 mesh), and analytical thin layer chromatography (TLC) was performed using silica gel aluminum sheets. All commercially available chemicals were used without further purification.

4.1.1. General procedure for the synthesis of chalcones (**3a**-**3h**)

A mixture of the acetophenone (5–10 mmol, 1 equiv) and the corresponding aldehyde (1 equiv) in EtOH (20–40 mL) was stirred at room temperature and a 50% aqueous solution of NaOH (5–8 mL) was added. The reaction mixture was stirred at room temperature until aldehyde consumption. After that, HCl (10%) was added until neutrality. Precipitated chalcones were generally filtered and crystallized from MeOH, although in some cases the product was purified using column chromatography. Chalcones **3a**, **3c**, **3e** and **3f** have been previously described.[21–25]

4.1.1.1. 3-Benzyloxy-2′-hydroxy-4,4′-dimethoxychalcone (**3b**).

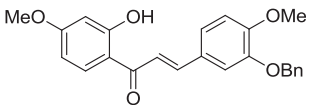

Orange solid, mp 145–146 °C (65%). IR (KBr, cm^{-1}) ν_{max}: 2956, 1716, 1683, 1635, 1607, 1558, 1540, 1508, 1456, 1436, 1374, 1260, 1236, 1156, 1130, 1020, 846. ^{1}H NMR (500 MHz, $CDCl_3$) δ = 13.44 (s, 1H, OH); 7.69 (d, 1H, J = 15.6 Hz, H-β); 7.67 (d, 1H, J = 8.3 Hz, H-6′); 7.40 (d, 2H, J = 7.5 Hz, 2xH-Ph); 7.31 (tt, 2H, J = 7.2, 1.5 Hz, 2xH-Ph); 7.26–7.22 (m, 2H, H-Ph and H-α); 7.15 (dd, 1H, J = 8.3, 1.9 Hz, H-6); 7.10 (d, 1H, J = 2.0 Hz, H-2); 6.83 (d, 1H, J = 8.3 Hz, H-5); 6.41–6.37 (m, 2H, H-5′ and H-3′); 5.12 (s, 2H, C$\underline{H}_2$-Ph); 3.85 (s, 3H, C$\underline{H}_3$O-C-4); 3.77 (s, 3H, C$\underline{H}_3$O-C-4′). ^{13}C NMR (125 MHz, $CDCl_3$) δ = 191.7 (C=O), 166.6 (C-2′), 166.0 (C-4′), 152.3 (C-4), 148.4 (C-3), 144.4 (C-β), 136.8 (C-Ph), 131.1 (C-6′), 128.7 (C-Ph), 128.1 (C-Ph), 127.7 (C-1), 127.4 (C-Ph), 123.6 (C-6), 118.1 (C-α), 114.1 (C-1′), 113.4 (C-2), 111.6 (C-5), 107.6 (C-5′), 101.0 (C-3′), 71.3 (C$\underline{H}_2$-Ph), 56.0 (C$\underline{H}_3$O-C-4), 55.6 (C$\underline{H}_3$O-C-4′). HRMS (ESI-FT-ICR) m/z: 413.1371 $[M+Na]^+$; calcd. for $C_{24}H_{22}O_5Na$: 413.1365.

4.1.1.2. 4-Benzyloxy-2′-hydroxy-3,4′-dimethoxychalcone (**3d**).

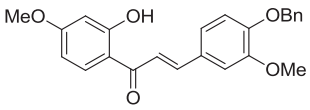

Orange solid, mp 153–155 °C (70%). IR (KBr, cm^{-1}) ν_{max}: 2936, 1633, 1571, 1508, 1454, 1443, 1420, 1370, 1338, 1297, 1259, 1213, 1128, 1019, 959, 846. ^{1}H NMR (500 MHz, $CDCl_3$) δ = 13.58 (s, 1H, OH); 7.87 (d, 1H, J = 15.3 Hz, H-β); 7.85 (d, 1H, J = 8.8 Hz, H-6′); 7.49–7.47 (m, 2H, 2xH-Ph); 7.44–7.42 (m, 3H, H-α and 2xH-Ph); 7.36 (t, 1H, J = 7.5 Hz, Ph); 7.22–7.21 (m, 2H, H-2 and H-6); 6.95 (d, 1H, J = 8.8 Hz, H-5); 6.53–6.51 (m, 2H, H-5′ and H-3′); 5.24 (s, 2H, C$\underline{H}_2$-Ph); 4.00 (s, 3H, C$\underline{H}_3$O-C-3); 3.88 (s, 3H,

$\underline{C}H_3O$-C-4′). ^{13}C NMR (125 MHz, $CDCl_3$) δ = 191.7 (C=O), 166.6 (C-2′), 166.1 (C-3 or C-4′), 150.7 (C-4), 149.8 (C-3 or C-4′), 144.5 (C-β), 136.5 (Ph), 131.1 (C-6′), 128.6 (Ph), 128.1 (C-1), 128.1 (Ph), 127.2 (Ph), 123.0 (C-2 or C-6), 118.1 (C-α), 114.1 (C-1′), 113.5 (C-5), 110.9 (C-2 or C-6), 107.6 (C-5′), 101.0 (C-3′), 70.9 ($\underline{C}H_2$-Ph), 56.1 ($\underline{C}H_3O$-C-3), 55.6 ($\underline{C}H_3O$-C-4′). HRMS (ESI-FT-ICR) *m*/*z*: 413.1370 $[M+Na]^+$; calcd. for $C_{24}H_{22}O_5Na$: 413.1365.

4.1.2. General procedure for the synthesis of flavonols

A solution of the corresponding 2-hydroxychalcone (2–4 mmol) in 3.0 M KOH in MeOH (20–30 mL) was cooled at 0 °C. An aqueous solution of H_2O_2 (30%) (5–8 mL) was added to the chalcone solution. The resulting mixture was stirred at room temperature, until the starting material was totally consumed, as evidenced by TLC. The reaction mixture was cooled in an ice bath and distilled water (2–4 mL) was added. HCl (2M) was added until pH 2 and the precipitate was filtered and washed with distilled water and extracted with EtOAc. The organic layer was washed with brine until neutrality and dried with anhydrous $MgSO_4$. The solvent was evaporated in vacuo and the residue was purified using a chromatographic column [SiO_2, petroleum ether:EtOAc (1:0–7:3)]. Flavonols **4c** and **4e** have been previously described.[26,27]

*4.1.2.1. 2-[3-(Benzyloxy)-4-methoxyphenyl]-3-hydroxy-4H-chromen-4-one (**4a**).*

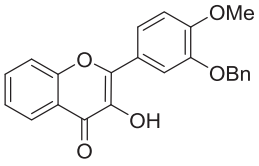

Yellow pale solid, mp 202–203 °C (79%). IR (KBr, cm^{-1}) ν_{max}:3249, 2929, 1612, 1560, 1515, 1480, 1438, 1413, 1336, 1267, 1204, 1176, 1144, 1124, 1017. ^1H NMR (500 MHz, $CDCl_3$) δ = 8.27 (dd, 1H, *J* = 8.0, 1.4 Hz, H-5); 7.95–7.93 (m, 2H, H-2′ and H-6′); 7.73 (ddd, 1H, *J* = 8.5, 7.1, 1.5 Hz, H-7); 7.58–7.55 (m, 3H, H-8 and 2xH-Ph); 7.46–7.42 (m, 3H, H-6 and 2xH-Ph); 7.36 (tt, 1H, *J* = 7.4, 1.9 Hz, Ph); 7.08 (d, 1H, *J* = 9.1 Hz, H-5′); 7.02 (s, 1H OH); 5.30 (s, 2H, $C\underline{H}_2$-Ph); 4.01 (s, 3H $C\underline{H}_3O$-C-4′). ^{13}C NMR (125 MHz, $CDCl_3$) δ = 173.1 (C-4), 155.2 (C-9), 151.5 (C-4′), 148.0 (C-3′), 145.1 (C-2), 137.7 (C-3), 136.9 (C-7), 133.4 (Ph), 128.6 (Ph), 128.0 (Ph), 127.5 (Ph), 125.4 (C-5), 124.4 (C-6), 123.6 (C-1′), 122.0 (C-6′), 120.6 (C-10), 118.1 (C-8), 113.6 (C-2′), 111.4 (C-5′), 71.3 ($\underline{C}H_2$-Ph), 56.0 ($\underline{C}H_3O$-C-4‴‴). HRMS (ESI-FT-ICR) *m*/*z*: 397.1048 $[M+Na]^+$; calcd. for $C_{23}H_{18}O_5Na$: 397.1052.

*4.1.2.2. 2-[3-(Benzyloxy)-4-methoxyphenyl]-3-hydroxy-4H-chromen-4-one (**4b**).*

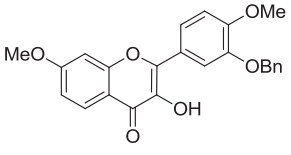

Yellow pale solid, mp 192–193 °C (71%). IR (KBr, cm^{-1}) ν_{max}: 3243, 1608, 1560, 1505, 1453, 1403, 1261, 1210, 1176, 1165, 1144, 1122, 1019, 841. ^1H NMR (500 MHz, $CDCl_3$) δ = 8.15 (d, 1H, *J* = 8.9 Hz, H-5); 7.90–7.78 (m, 2H, H-2′ and H-6′); 7.56 (d, 2H, *J* = 8.4 Hz, 2xH-Ph); 7.45–7.42 (m, 2xH-Ph); 7.39–7.34 (m, 1H, Ph); 7.05 (d, 1H, *J* = 8.6 Hz, H-5′); 7.01 (dd, 1H, *J* = 8.9, 2.2 Hz, H-6); 6.92 (d, 1H, *J* = 2.3 Hz, H-8); 5.29 (s, 2H, $C\underline{H}_2$-Ph); 4.00 (s, 3H, $C\underline{H}_3O$-C-4′); 3.97 (s, 3H, $C\underline{H}_3O$-C-7). ^{13}C NMR (125 MHz, $CDCl_3$) δ = 172.4 (C-4), 164.1 (C-7), 157.1 (C-9), 151.2 (C-4′), 147.9 (C-3′), 144.4 (C-2), 137.3 (C-3), 136.9 (Ph), 128.6 (Ph), 128.0 (Ph), 127.6 (Ph), 126.7 (C-5), 123.7 (C-1′), 121.6 (C-6′), 114.6 (C-6), 114.6 (C-10), 113.7 (C-2′), 111.4 (C-5′), 99.8 (C-8), 71.3 ($\underline{C}H_2$-Ph), 56.0 ($\underline{C}H_3O$-C-4′), 55.8 ($\underline{C}H_3O$-C-7). HRMS (ESI-FT-ICR) *m*/*z*: 427.1162 $[M+Na]^+$; calcd. for $C_{24}H_{20}O_6Na$: 427.1158.

*4.1.2.3. 2-[4-(Benzyloxy)-3-methoxyphenyl]-3-hydroxy-7-methoxy-4H-chromen-4-one (**4d**).*

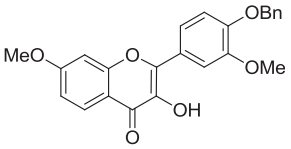

Yellow pale solid, mp 160–162 °C (55%). IR (KBr, cm^{-1}) ν_{max}: 3422, 2923, 2851, 2009, 1651, 1616, 1506, 1455, 1401, 1262, 1213, 1012. ^1H NMR (500 MHz, $CDCl_3$) δ = 8.11 (d, 1H, *J* = 8.8 Hz, H-5); 7.84 (d, 1H, *J* = 2.0 Hz, H-2′); 7.77 (dd, 1H, *J* = 8.6, 2.1 Hz, H-6′); 7.46 (d, 2H, *J* = 7.2 Hz, 2xH-Ph); 7.38 (t, 2H, *J* = 7.4 Hz, 2xH-Ph); 7.35–7.29 (m, 1H, Ph); 7.00 (d, 1H, *J* = 8.6 Hz, H-5′); 6.98 (dd, 1H, *J* = 8.9, 2.3 Hz, H-6); 6.92 (d, 1H, *J* = 2.4 Hz, H-8); 5.24 (s, 2H, $C\underline{H}_2$-Ph); 3.99 (s, 3H, $C\underline{H}_3O$-C-3′); 3.92 (s, 3H, $C\underline{H}_3O$-C-7). ^{13}C NMR (125 MHz, $CDCl_3$) δ = 172.6 (C-4), 164.1 (C-7), 157.1 (C-9), 149.6 (C-4′), 149.4 (C-3′), 144.5 (C-2), 137.4 (C-3), 136.6 (Ph), 128.6 (Ph), 128.0 (Ph), 127.2 (Ph), 126.7 (C-5), 124.2 (C-1′), 120.9 (C-6′), 114.7 (C-6), 114.6 (C-10), 113.3 (C-5′), 111.1 (C-1′), 99.8 (C-8), 70.8 ($\underline{C}H_2$-Ph), 56.2 ($\underline{C}H_3O$-C-3′), 55.8 ($\underline{C}H_3O$-C-7). HRMS (ESI-FT-ICR) *m*/*z*: 427.1153 $[M+Na]^+$; calcd. for $C_{24}H_{20}O_6Na$: 427.1158.

*4.1.2.4. 2-[4-(Benzyloxy)phenyl]-3-hydroxy-7-methoxy-4H-chromen-4-one (**4f**).*

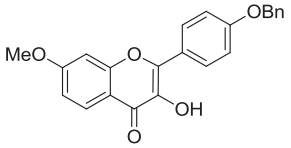

Yellow pale solid, mp 163–164 °C (52%). IR (KBr, cm^{-1}) ν_{max}: 3274, 1603, 1560, 1508, 1452, 1423, 1401, 1378, 1315, 1257, 1209, 1179, 1170, 1119, 1027, 1015, 953, 882, 832. ^1H NMR (500 MHz, $CDCl_3$) δ = 8.24 (d, 2H, *J* = 8.9 Hz, H-2′ and H-6′); 8.16 (d, 1H, *J* = 8.9 Hz, H-5); 7.50 (d, 2H, *J* = 7.2 Hz, 2xH-Ph); 7.46–7.43 (m, 2H, 2xH-Ph); 7.39 (tt, 1H, *J* = 6.2, 1.2 Hz, Ph); 7.15 (d, 2H, *J* = 9.0 Hz, H-3′ and H-5′); 7.02 (dd, 1H, *J* = 8.9, 2.3 Hz, H-6); 6.97 (d, 1H, *J* = 2.3 Hz, H-8); 5.19 (s, 2H, $C\underline{H}_2$-Ph); 3.96 (s, 3H, $C\underline{H}_3O$-C-7). ^{13}C NMR (125 MHz, $CDCl_3$) δ = 172.5 (C-4), 164.1 (C-7), 160.0 (C-4′), 157.2 (C-9), 144.6 (C-2), 137.3 (C-3), 136.5 (Ph), 129.2 (C-2′ and C-6′), 128.7 (Ph), 128.1 (Ph), 127.5 (Ph), 126.7 (C-5), 123.9 (C-1′), 114.9 (C-3′ and C-5′), 114.7 (C-6 and C-10), 99.8 (C-8), 70.1 ($\underline{C}H_2$-Ph), 55.8 ($\underline{C}H_3O$-C-4′). HRMS (ESI-FT-ICR) *m*/*z*: 397.1059 $[M+Na]^+$; calcd. for $C_{23}H_{18}O_5Na$: 397.1052.

*4.1.2.5. 2-[2-(Benzyloxy)phenyl]-3-hydroxy-4H-chromen-4-one (**4g**).*

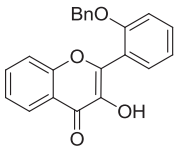

Yellow pale solid, mp 138–139 °C (64%). IR (KBr, cm^{-1}) ν_{max}: 3289, 3066, 3029, 2929, 2872, 1949, 1910, 1815, 1633, 1614, 1606, 1567, 1486, 1469, 1417, 1382, 1347, 1287, 1211, 1135, 1102, 1050, 1024, 900, 859. ^{1}H NMR (500 MHz, $CDCl_3$) δ = 8.18 (dd, 1H, *J* = 8.1, 1.1 Hz, H-5); 7.57–7.54 (m, 2H, H-4′ or H-6′ and H-7); 7.37 (d, 1H, *J* = 8.4 Hz, H-8); 7.36 (dt, 1H, *J* = 9.0, 1.5 Hz, H-6′ or H-4′); 7.31 (t, 1H, *J* = 7.4 Hz, H-6); 7.27 (d, 2H, *J* = 7.1 Hz, Ph); 7.20–7.13 (m, 3H, 3xH-Ph); 7.03–7.00 (m, 2H, H-3 and H-5′); 6.52 (s, 1H, OH); 5.08 (s, 2H, C<u>H</u>$_2$-Ph). ^{13}C NMR (125 MHz, $CDCl_3$) δ = 173.3 (C-4), 156.6 (C-2′), 156.0 (C-9), 145.9 (C-2), 138.9 (C-3), 136.7 (Ph), 133.3 (C-7), 132.0 (C-4′ or C-6′), 131.1 (C-6′ or C-4′), 128.5 (Ph), 127.8 (Ph), 126.9 (Ph), 125.5 (C-5), 124.3 (C-6), 121.4 (C-10), 120.9 (C-5′), 120.2 (C-1′), 118.4 (C-8), 113.4 (C-3′), 70.5 (<u>C</u>H$_2$-Ph). HRMS (ESI-FT-ICR) *m*/*z*: 367.0944 $[M+Na]^+$; calcd. for $C_{22}H_{16}O_4Na$: 367.0946.

*4.1.2.6. 2-[2-(Benzyloxy)phenyl]-3-hydroxy-7-methoxy-4H-chromen-4-one (**4h**).*

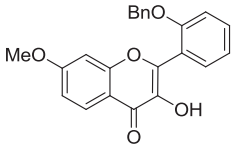

White solid, mp 161–162 °C (60%). IR (KBr, cm^{-1}) ν_{max}: 3275, 3032, 2936, 2841, 1608, 1567, 1505, 1454, 1408, 1318, 1276, 1257, 1230, 1204, 1168, 1130, 1112, 1048, 1026, 995, 954, 885, 835. ^{1}H NMR (500 MHz, $CDCl_3$) δ = 8.20 (d, 1H, *J* = 8.9 Hz, H-5); 7.68 (dd, 1H, *J* = 7.5, 1.6 Hz, H-6′); 7.49 (dt, 1H, *J* = 7.7, 1.7 Hz, H-4′); 7.42 (d, 2H, *J* = 6.9 Hz, 2xH-Ph); 7.35–7.28 (m, 3H, 3xH-Ph); 7.18–7.14 (m, 2H, H-3′ and H-5′); 7.03 (dd, 1H, *J* = 8.9, 2.3 Hz, H-6); 6.87 (d, 1H, *J* = 2.3 Hz, H-8); 6.62 (s, 1H, OH); 5.22 (s, 2H, C<u>H</u>$_2$-Ph); 3.90 (s, 3H, C<u>H</u>$_3$O-C-7). ^{13}C NMR (125 MHz, $CDCl_3$) δ = 172.7 (C-4), 164.0 (C-7), 157.9 (C-9), 156.5 (C-2′), 145.1 (C-2), 138.5 (C-3), 136.8 (Ph), 131.8 (C-4′), 131.1 (C-6′), 128.4 (Ph), 127.8 (Ph), 126.9 (Ph), 126.8 (C-5), 120.9 (C-3′ or C-5′), 120.3 (C-1′), 115.3 (C-10), 114.7 (C-6), 113.5 (C-5′ or C-3′), 99.8 (C-8), 70.5 (<u>C</u>H$_2$-Ph), 55.8 (<u>Me</u>O-C-7). HRMS (ESI-FT-ICR) *m*/*z*: 397.1059 $[M+Na]^+$; calcd. for $C_{23}H_{18}O_5Na$: 397.1052.

4.1.3. General procedure for the 3-methylation of flavonols

Methyl iodide (1.2 equiv.) and potassium carbonate (2 equiv.) were added to a solution of the flavonols (1 equiv.) in acetone (0.1 M) under argon atmosphere and stirred. After standing overnight, the resulting mixture was filtered and the solvent was removed under vacuum to leave a yellow pale solid, which was purified by flash column chromatography or recrystallized from EtOH. 3-Methoxyflavones **6d-f** have been previously described.[28]

*4.1.3.1. 3′-Benzyloxy-3,4′-dimethoxyflavone (**6a**).*

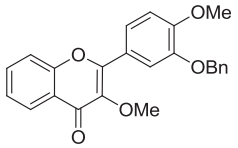

Yellow pale solid, mp 104–106 °C (65%). IR (KBr, cm^{-1}) ν_{max}: 2931, 2839, 1637, 1615, 1601, 1560, 1511, 1468, 1438, 1378, 1329, 1267, 1243, 1212, 1171, 1134, 1020, 974, 891, 812. ^{1}H NMR (500 MHz, $CDCl_3$) δ = 8.24 (dd, 1H, *J* = 7.9, 1.7 Hz, H-5); 7.79–7.76 (m, 2H, H-2′ and H-6′); 7.65 (ddd, 1H, *J* = 8.6, 7.1, 1.7 Hz, H-7); 7.50–7.46 (m, 3H, H-8 and 2xH-Ph); 7.41–7.35 (m, 3H, H-6 and 2xH-Ph); 7.32 (t, 1H. *J* = 7.4 Hz, Ph); 7.02 (d, 1H, *J* = 8.4 Hz, H-5′); 5.26 (s, 2H, C<u>H</u>$_2$-Ph); 3.98 (s, 3H, C<u>H</u>$_3$O-C-4′); 3.73 (s, 3H, C<u>H</u>$_3$O-C-3). ^{13}C NMR (125 MHz, $CDCl_3$) δ = 174.9 (C-4), 155.3 (C-2), 155.1 (C-9), 151.8 (C-4′), 147.7 (C-3′), 140.9 (C-3), 136.8 (Ph), 133.2 (C-7), 128.6 (Ph), 128.0 (Ph), 127.2 (Ph), 125.8 (C-5), 124.5 (C-6), 124.1 (C-10), 123.3 (C-1′), 122.5 (C-6′), 117.8 (C-8), 114.3 (C-2′), 111.3 (C-5′), 71.1 (<u>C</u>H$_2$-Ph), 59.8 (<u>C</u>H$_3$O-C-3), 56.0 (<u>C</u>H$_3$O-C-4′). HRMS (ESI-FT-ICR) *m*/*z*: 411.1219 $[M+Na]^+$; calcd. for $C_{24}H_{20}O_5Na$: 411.1208.

*4.1.3.2. 3′-Benzyloxy-3,7,4′-trimethoxyflavone (**6b**).*

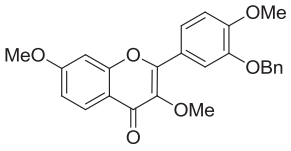

Yellow pale solid, mp 154–155 °C (68%). IR (KBr, cm^{-1}) ν_{max}: 3014, 2931, 2847, 1611, 1513, 1445, 1382, 1364, 1327, 1266, 1256, 1215, 1170, 1133, 1103, 1022, 953, 836. ^{1}H NMR (500 MHz, $CDCl_3$) δ = 8.06 (d, 1H, *J* = 8.9 Hz, H-5); 7.68–7.65 (m, 2H, H-2′ and H-6′); 7.41 (d, 2H, *J* = 7.2 Hz, 2xH-Ph); 7.31 (t, 2H, *J* = 7.5 Hz, 2xH-Ph); 7.24 (t, 1H, *J* = 7.3 Hz, Ph); 6.94 (d, 1H, *J* = 8.5 Hz, H-5′); 6.88 (dd, 1H, *J* = 8.9, 2.2 Hz, H-6); 6.77 (d, 1H, *J* = 2.3 Hz, H-8); 5.18 (s, 2H, C<u>H</u>$_2$-Ph); 3.90 (s, 3H, C<u>H</u>$_3$O-C-4′); 3.84 (s, 3H, C<u>H</u>$_3$O-C-7); 3.64 (s, 3H, C<u>H</u>$_3$O-C-3). ^{13}C NMR (125 MHz, $CDCl_3$) δ = 174.4 (C-4), 163.9 (C-7), 156.8 (C-9), 154.8 (C-2), 151.7 (C-4′), 147.7 (C-3′), 140.7 (C-3), 136.9 (Ph), 128.6 (Ph), 127.9 (Ph), 127.2 (Ph), 127.1 (C-5), 123.4 (C-1′), 122.3 (C-6′), 118.0 (C-10), 114.2 (C-6 or C-2′), 114.2 (C-2′ or C-6), 111.2 (C-5′), 99.9 (C-8), 71.1 (<u>C</u>H$_2$-Ph), 59.9 (<u>C</u>H$_3$O-C-4′), 56.0 (<u>C</u>H$_3$O-C-7), 55.8 (<u>C</u>H$_3$O-C-3). HRMS (ESI-FT-ICR) *m*/*z*: 419.1483 $[M+H]^+$; calcd. for $C_{25}H_{23}O_6$: 419.1495.

*4.1.3.3. 4′-Benzyloxy-3,3′-dimethoxyflavone (**6c**).*

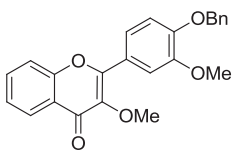

White solid, mp 128–129 °C (80%). IR (KBr, cm^{-1}) ν_{max}: 3064, 3005, 2931, 2849, 1733, 1638, 1615, 1601, 1561, 1511, 1469, 1438, 1419, 1379, 1330, 1270, 1241, 1212, 1170, 1135, 1012,

972, 915, 889, 879. ^{1}H NMR (500 MHz, $CDCl_3$) δ = 8.30 (dd, 1H, J = 7.9,1.5 Hz, H-5); 7.81 (d, 1H, J = 1.9 Hz, H-2′); 7.74 (dd, 1H, J = 8.5, 1.9 Hz, H-6′); 7.70 (ddd, 1H, J = 8.5, 7.2, 1.5 Hz, H-7); 7.56 (d, 1H, J = 8.3 Hz, H-8); 7.51 (d, 2H, J = 7.2 Hz, 2xH-Ph); 7.45–7.42 (m, 3H, H-6 and 2xH-Ph); 7.36 (t, 1H, J = 7.4 Hz, Ph); 7.05 (d, 1H, J = 8.6 Hz, H-5′); 5.30 (s, 2H, C$\underline{H}_2$-Ph); 4.02 (s, 3H, C$\underline{H}_3$O-C-3′); 3.93 (s, 3H, C$\underline{H}_3$O-C-3). ^{13}C NMR (125 MHz, $CDCl_3$) δ = 174.9 (C-4), 155.4 (C-2), 155.1 (C-9), 150.4 (C-4′), 149.2 (C-3′), 141.0 (C-3), 136.5 (C-Ph), 133.3 (C-7), 128.7 (C-Ph), 128.1 (C-Ph), 127.2 (C-Ph), 125.8 (C-5), 124.6 (C-6), 124.2 (C-10), 123.7 (C-1′), 122.0 (C-6′), 117.8 (C-8), 113.1 (C-5′), 112.1 (C-2′), 70.8 (C$\underline{H}_2$-Ph), 60.0 (C$\underline{H}_3$O-C-3), 56.2 (C$\underline{H}_3$O-C-3′). HRMS (ESI-FT-ICR) m/z: 389.1385 $[M+H]^+$; calcd. for $C_{24}H_{21}O_5$: 389.1389.

*4.1.3.4. 2′-Benzyloxy-3-methoxyflavone (**6g**).*

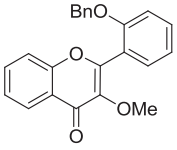

White solid, mp 115 °C (59%). IR (KBr, cm^{-1}) ν_{max}: 3064, 3033, 3005, 2936, 1643, 1622, 1610, 1581, 1570, 1489, 1466, 1450, 1385, 1278, 1254, 1230, 1212, 1171, 1148, 1111, 1048, 1008, 955, 900. ^{1}H NMR (500 MHz, $CDCl_3$) δ = 8.34 (dd, 1H, J = 8.0, 1.6 Hz, H-5); 7.69 (ddd, 1H, J = 8.6, 7.1, 1.6 Hz, H-7); 7.55 (dd, 1H, J = 7.4, 1.5 Hz, H-6′); 7.51–7.48 (m, 2H, H-8 and H-4′); 7.44 (ddd, 1H, J = 8.7, 7.9, 0.9, Hz, H-6); 7.38 (d, 2H, J = 7.1 Hz, 2xH-Ph); 7.33–7.27 (m, 3H, 3xH-Ph); 7.15–7.12 (m, 2H, H-3′ and H-5′); 5.21 (s, 2H, C$\underline{H}_2$-Ph); 3.83 (s, 3H, C$\underline{H}_3$O-C-2′). ^{13}C NMR (125 MHz, $CDCl_3$) δ = 174.9 (C-4), 156.5 (C-2′), 156.2 (C-2), 155.7 (C-9), 142.0 (C-3), 136.6 (Ph), 133.2 (C-7), 131.9 (C-4′), 131.0 (C-6′), 128.5 (Ph), 127.8 (Ph), 126.9 (Ph), 125.9 (C-5), 124.6 (C-10), 124.5 (C-6), 120.7 (C-3′ or C-5′), 120.7 (C-1′), 118.1 (C-8), 113.1 (C-5′ or C-3′), 70.4 (C$\underline{H}_2$-Ph), 60.5 (C$\underline{H}_3$O-C2′). HRMS (ESI-FT-ICR) m/z: 381.1107 $[M+Na]^+$; calcd. for $C_{23}H_{18}O_4Na$: 381.1103.

4.1.4. General procedure for debenzylation

20 mg of 10% Pd/C was added to a solution of the required compound in THF (0.1 M). The reaction mixture was stirred at room temperature for 1 h under an atmosphere of 1.5 atm H_2(g) after replacement of the air by nitrogen. The Pd/C was filtered through Celite and the solvent was evaporated under reduced pressure. The crude was purified by flash column chromatography or recrystallized from EtOH. Flavonoids **5b**, **5c**, **5d**, **5e**, **5f**, **5g**, **7c**, **7d** and **7f** have been previously described.[26,29–32]

*4.1.4.1. 3-Hydroxy-2-(3-hydroxy-4-methoxyphenyl)-4H-chromen-4-one (**5a**).*

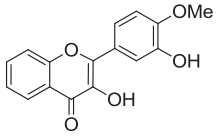

White solid, mp 201–203 °C (80%). IR (KBr, cm^{-1}) ν_{max}: 3296, 3028, 3205, 3028, 1584, 1537, 1523, 1487, 1464, 1417, 1369, 1350, 1329, 1291, 1257, 1207, 1182, 1142, 1121, 1111, 1041, 1026, 883, 811. ^{1}H NMR (500 MHz, DMSO d_6) δ = 9.38 (s, 1H, OH-C-3); 9.34 (s, 1H, OH-C-3′); 8.10 (dd, 1H, J = 8.0, 1.5 Hz, H-5); 7.79–7.75 (m, 2H, H-7 and H-2′); 7.72–7.70 (m, 2H, H-8 and H-6′); 7.44 (dt, 1H, J = 7.9, 0.9 Hz, H-6); 7.10 (d, 1H, J = 8.7 Hz, H-5′); 3.85 (s, 3H, C$\underline{H}_3$O-C-4′). ^{13}C NMR (125 MHz, DMSO d_6) δ =172.5 (C-4), 154.3 (C-9), 149.2 (C-4′), 146.1 (C-3′), 145.6 (C-2), 138.1 (C-3), 133.4 (C-7), 124.6 (C-5), 124.3 (C-6), 123.7 (C-1′), 121.2 (C-10), 119.7 (C-6′), 118.1 (C-8), 114.7 (C-2′), 111.7 (C-5′), 55.5 (C$\underline{H}_3$O-C4′). HRMS (ESI-FT-ICR) m/z: 285.0768 $[M+H]^+$; calcd. for $C_{16}H_{13}O_5$: 285.0763.

*4.1.4.2. 3-Hydroxy-2-(3-hydroxy-4-methoxyphenyl)-7-methoxy-4H-chromen-4-one (**5b**).*

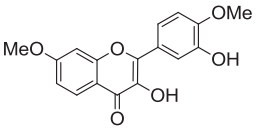

White solid, mp 179–181 °C (82%). IR (KBr, cm^{-1}) ν_{max}: 3389, 3013, 2936, 2842, 1614, 1563, 1557, 1506, 1455, 1407, 1335, 1261, 1212, 1167, 1138, 1121, 1027, 1010, 960, 836. ^{1}H NMR (500 MHz, DMSO d_6) δ = 9.27 (s, 1H, OH-C-3′); 9.23 (s, 1H, OH-C-3); 7.98 (d, 1H, J = 8.9 Hz, H-5); 7.74 (d, 1H, J = 2.2 Hz, H-2′); 7.70 (dd, 1H, J = 8.6, 2.2 Hz, H-6′); 7.23 (d, 1H, J = 2.3 Hz, H-8); 7.09 (d, 1H, J = 8.7 Hz, H-5′); 7.03 (dd, 1H, J = 8.85, 2.3 Hz, H-6); 3.91 (s, 3H, C$\underline{H}_3$O-C-7), 3.85 (s, 3H, C$\underline{H}_3$O-C4′). ^{13}C NMR (125 MHz, DMSO d_6) δ = 172.0 (C-4), 163.4 (C-7), 156.2 (C-9), 149.0 (C-4′), 146.1 (C-3′), 144.9 (C-2), 137.8 (C-3), 126.0 (C-5), 123.8 (C-1′), 119.4 (C-6′), 115.0 (C-10), 114.6 (C-2′), 114.4 (C-6), 111.7 (C-5′), 100.1 (C-8), 56.0 (C$\underline{H}_3$O-C-7), 55.6 (C$\underline{H}_3$O-C-4′). HRMS (ESI-FT-ICR) m/z: 337.0680 $[M+Na]^+$; calcd. for $C_{17}H_{14}O_6Na$: 337.0688.

*4.1.4.3. 3-Hydroxy-2-(2-hydroxyphenyl)-7-methoxy-4H-chromen-4-one (**5h**).*

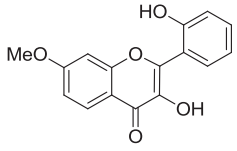

White solid, mp 165–166 °C (75%). IR (KBr, cm^{-1}) ν_{max}: 3233, 2929, 1618, 1610, 1507, 1450, 1406, 1260, 1206, 1169, 1131, 1111, 1026, 996, 954, 885, 834. ^{1}H NMR (500 MHz, DMSO d_6) δ = 9.32 (brs, 1H, OH); 8.02 (d, 1H, J = 8.9 Hz, H-5); 7.43 (dd, 1H, J = 7.6, 1.5 Hz, H-6′); 7.34 (dt, 1H, J = 8.3, 1.6 Hz, H-4′); 7.10 (d, 1H, J = 2.2 Hz, H-8); 7.04 (dd, 1H, J = 8.9, 2.2 Hz, H-6); 6.98 (d, 1H, J = 7.9 Hz, H-3′); 6.94 (t, 1H, J = 7.4 Hz, H-5′); 3.88 (s, 3H, C$\underline{H}_3$O-C-7); 3.35 (brs, 1H, OH). ^{13}C NMR (125 MHz, DMSO d_6) δ = 172.1 (C-4), 163.3 (C-7), 156.9 (C-9), 155.3 (C-2′), 146.7 (C-2), 138.5 (C-3), 131.2 (C-4′), 130.8 (C-6′), 126.1 (C-5), 118.6 (C-5′), 118.3 (C-1′), 116.3 (C-3′), 115.8 (C-10), 114.3 (C-6), 100.1 (C-8), 55.9 (C$\underline{H}_3$O-C-7). HRMS (ESI-FT-ICR) m/z: 285.0766 $[M+H]^+$; calcd. for $C_{16}H_{13}O_5$: 285.0763.Anal. Calcd for $C_{16}H_{12}O_5$: C 67.60; H 4.25. Found: C 67.58; H 4.50.

*4.1.4.4. 2-(3-Hydroxy-4-methoxyphenyl)-3-methoxy-4H-chromen-4-one (**7a**).*

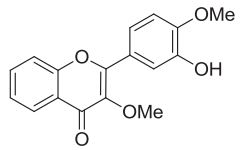

White solid, mp 138–139 °C (78%). IR (KBr, cm^{-1}) ν_{max}: 3358, 2933, 2840, 1613, 1557, 1509, 1469, 1438, 1385, 1337, 1275, 1253, 1213, 1172, 1126, 1035, 1023, 1011, 979, 892. ^{1}H NMR (400 MHz, $CDCl_3$) δ = 8.24 (dd, 1H, *J* = 8.0, 1.8 Hz, H-5); 7.76–7.74 (m, 2H, 2′ and H-6′); 7.65 (ddd, 1H, *J* = 8.5, 7.2, 1.4 Hz, H-7); 7.51 (d, 1H, *J* = 8.2 Hz, H-8); 7.37 (t, 1H, *J* = 7.8 Hz, H-6); 6.96 (d, 1H, *J* = 9.2 Hz, H-5″); 5.88 (s, 1H, OH); 3.97 (s, 3H, C<u>H</u>$_3$O-C-3); 3.89 (s, 3H, C<u>H</u>$_3$O-C-4′). ^{13}C NMR (100 MHz, $CDCl_3$) δ = 175.3 (C-4), 155.2 (C-2 or C-9), 155.1 (C-9 or C-2), 148.9 (C-3), 145.6 (C-3′), 141.3 (C-4′), 133.2 (C-7), 125.7 (C-5), 124.5 (C-6), 124.2 (C-1′ or C-10), 124.1 (C-10 or C-1′), 121.6 (C-6′), 117.8 (C-8), 114.6 (C-2′), 110.4 (C-5′), 59.8 (<u>C</u>H$_3$O-C-4′), 56.0 (<u>C</u>H$_3$O-C-3). HRMS (ESI-FT-ICR) *m*/*z*: 321.0725 $[M+Na]^+$; calcd. for $C_{17}H_{14}O_5Na$: 321.0739. Anal. Calcd for $C_{17}H_{14}O_5$: C 68.45; H 4.73. Found: C 68.41; H 5.09.

*4.1.4.5. 2-(3-Hydroxy-4-methoxyphenyl)-3,7-dimethoxy-4H-chromen-4-one (**7b**).*

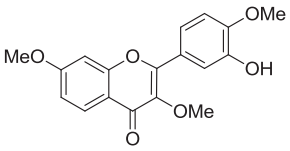

White solid, mp 174–175 °C (75%).IR (KBr, cm^{-1}) ν_{max}: 3234, 2932, 2840, 1605, 1560, 1508, 1438, 1386, 1367, 1274, 1255, 1213, 1169, 1128, 1103, 1017, 982, 952, 836. ^{1}H NMR (400 MHz, $CDCl_3$) δ = 8.06 (d, 1H, *J* = 8.8 Hz, H-5); 7.65 (dd, 1H, *J* = 6.8, 3.5 Hz, H-6′); 7.63 (brs, 1H, H-2′); 6.97 (d, 1H, J = Hz, H-5′); 6.96 (d, 1H, J = Hz, H-6); 6.81 (d, 1H, *J* = 2.3 Hz, H-8); 5.86 (s, 1H, OH); 3.89 (s, 3H, C<u>H</u>$_3$O-C-4′); 3.83 (s, 3H, C<u>H</u>$_3$O-C-7); 3.80 (s, 3H, C<u>H</u>$_3$O-C-3). ^{13}C NMR (100 MHz, $CDCl_3$) δ = 174.5 (C-4), 163.9 (C-7), 156.8 (C-9), 154.8 (C-2), 148.5 (C-4′), 145.5 (C-3′), 140.9 (C-3), 127.0 (C-5), 124.1 (C-1′), 121.3 (C-6′), 118.0 (C-10), 114.4 (C-2′), 114.2 (C-6), 110.3 (C-5′), 99.9 (C-8), 59.9 (<u>C</u>H$_3$O-C-3), 56.0 (<u>C</u>H$_3$O-C-4′), 55.7 (<u>C</u>H$_3$O-C-7). HRMS (ESI-FT-ICR) *m*/*z*: 351.0844 $[M]^+$; calcd. for $C_{18}H_{16}O_6$: 351.0845. Anal. Calcd for $C_{18}H_{16}O_6$: C 65.85; H 4.91. Found: C 65.85; H 5.09.

*4.1.4.6. 2-(4-Hydroxyphenyl)-3-methoxy-4H-chromen-4-one (**7e**).*

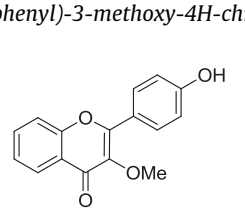

White solid, mp 220 °C (80%). IR (KBr, cm^{-1}) ν_{max}: 3217, 2917, 2849, 1603, 1555, 1509, 1469, 1385, 1283, 1242, 1213, 1177, 1149, 1110, 1034, 1007, 953, 898, 811. ^{1}H NMR (500 MHz, DMSO d_6) δ = 10.2 (brs, 1H, OH); 8.07 (dd, 1H, *J* = 7.9, 1.6 Hz, H-5); 7.98 (d, 2H, *J* = 8.9 Hz, H-2′ and H-6′); 7.79 (ddd, 1H, *J* = 8.5, 7.0, 1.6 Hz, H-7); 7.71 (dd, 1H, *J* = 8.4, 0.6 Hz, H-8); 7.46 (ddd, 1H, *J* = 8.0, 7.0, 1.0 Hz, H-6); 6.96 (d, 2H. *J* = 8.9 Hz, H3′ and H-5′); 3.80 (s, 3H, C<u>H</u>$_3$O-C-3). ^{13}C NMR (125 MHz, DMSO d_6) δ =173.5 (C-4), 159.9(C-2), 155.2 (C-4′), 154.5 (C-9), 139.7 (C-3), 133.7 (C-7), 130.1 (C-2′ and C-6′), 124.8 (C-5 or C-6), 124.8 (C-6 or C-5), 123.4 (C-10), 120.9 (C-1′), 118.2 (C-8), 115.5 (C-3′ and C-5′), 59.3 (<u>C</u>H$_3$O-C-3). HRMS (ESI-FT-ICR) *m*/*z*: 269.0818 $[M+H]^+$; calcd. for $C_{16}H_{13}O_4$: 269.0814. Anal. Calcd for $C_{16}H_{12}O_4$: C 71.64; H 4.51. Found: C 71.91; H 4.76.

*4.1.4.7. 2-(2-Hydroxyphenyl)-3-methoxy-4H-chromen-4-one (**7g**).*

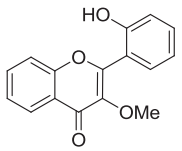

White solid, mp 191–192 °C (77%). IR (KBr, cm^{-1}) ν_{max}: 3235, 3007, 2940, 1612, 1560, 1466, 1454, 1388, 1293, 1252, 1212, 1147, 1111, 1037, 1007, 955, 901. ^{1}H NMR (500 MHz, DMSO d_6) δ = 9.96 (s, 1H, OH); 8.13 (dd, 1H, *J* = 8.1, 1.6 Hz, H-5); 7.80 (ddd, 1H, *J* = 8.6, 7.1, 1.6 Hz, H-7); 7.63 (d, 1H, *J* = 8.4 Hz, H-8); 7.50 (ddd, 1H, *J* = 8.0, 7.3, 0.9 Hz, H-6); 7.41 (dd, 1H, *J* = 7.6, 1.6 Hz, H-6′); 7.37 (ddd, 1H, *J* = 8.2, 7.5, 1.6 Hz, H-4′); 7.00 (d, 1H, *J* = 8.2 Hz, H-3′); 6.94 (dt, 1H, *J* = 7.5, 0.8 Hz, H-5′); 3.73 (s, 3H, C<u>H</u>$_3$O-C-3). ^{13}C NMR (125 MHz, DMSO d_6) δ = 173.6 (C-4), 156.4 (C-2), 155.3 (C-2′), 155.1 (C-9), 141.1 (C-3), 133.8 (C-7), 131.7 (C-4′), 130.4 (C-6′), 124.9 (C-5), 124.8 (C-6), 123.9 (C-10), 118.7 (C-5′), 118.3 (C-8), 118.0 (C-1′), 116.1 (C-3′), 59.5 (<u>C</u>H$_3$O-C-3). HRMS (ESI-FT-ICR) *m*/*z*: 269. $[M+H]^+$; calcd. for $C_{16}H_{13}O_4$: 269.0814. Anal. Calcd for $C_{16}H_{12}O_4$: C 71.67; H 4.51. Found: C 71.30; H 4.44.

4.2. Biological assays

4.2.1. Cell culture and cytotoxicity assays

SK-MEL-1 melanoma cells were obtained from the German Collection of Microorganisms and Cell Cultures (Braunschweig, Germany) and grown in RPMI 1640 containing 2 mM L-glutamine supplemented with 10% (v/v) heat-inactivated fetal bovine serum and 100 units/mL penicillin and 100 μg/mL streptomycin at 37 °C in a humidified atmosphere containing 5% CO_2. Human peripheral blood mononuclear cells (PBMCs) were isolated from heparin-anticoagulated blood of healthy volunteers by centrifugation with Ficoll-Paque Plus (GE Healthcare Bio-Sciences AB; Uppsala, Sweden). PBMCs were also stimulated with phytohemagglutinine (PHA, 2 μg/mL) for 48 h before experimental treatment.

The cytotoxicity of compounds was evaluated by using a colorimetric 3-(4,5-dimethyl-2-thiazolyl)-2,5-diphenyl-2*H*-tetrazolium bromide (MTT) assay. Briefly, 1×10^4 exponentially growing cells were seeded in 96-well microculture plates with various compounds concentrations. After the addition of MTT (0.5 mg/mL), cells were incubated at 37 °C for 4 h. Sodium dodecyl sulfate (10% w/v) in 0.05 M HCl was added to the wells and then incubated at room temperature overnight under dark conditions. The absorbance was measured at 570 nm. Concentrations inducing a 50% inhibition of cell growth (IC_{50}) were determined graphically for each experiment by a nonlinear regression using the curve-fitting routine implemented within the software Prism 4.0 (GraphPad). Values are means ± SE from at least three independent experiments, with each performed in triplicate.

4.2.2. Evaluation and quantification of apoptosis and analysis of the cell cycle

Fluorescent microscopy was used to identify nuclear changes associated with apoptosis as previously described.[33] To study changes in the cell DNA content, flow cytometric analysis of propidium iodide-stained nuclei was carried out using a BD FACSVerse™ cytometer (BD Biosciences, San Jose, CA, USA) as described.[8] Briefly, cells were collected and centrifuged at 500×*g*, washed with PBS and resuspended in 50 μL of PBS. Following dropwise addition of 1 mL of ice-cold 75% ethanol, fixed cells were stored at −20 °C for 1 h. Samples were then centrifuged at 500×*g* and washed with PBS and finally resuspended in 1 mL of PBS containing 50 μg/mL propidium iodide and 100 μg/mL RNase A and incubated for 1 h at 37 °C in the dark. The percentage of cells with decreased DNA staining, composed of apoptotic cells resulting from either fragmentation or decreased chromatin, was counted (minimum of 10,000 cells per experimental condition). Cell debris was excluded from analysis by selective gating based on anterior and right angle scattering.

4.2.3. Western blot analysis

Immunoblot analysis of caspase-3 and cytochrome *c* was performed as previously described.[34] Briefly, after treatments, cells were washed twice with PBS and then resuspended in ice-cold buffer [20 mM HEPES (pH 7.5), 1.5 mM $MgCl_2$, 10 mM KCl, 1 mM EDTA, 1 mM EGTA, 1 mM dithiothreitol, 0.1 mM phenylmethylsulfonyl fluoride, and 5 μg/mL leupeptin, aprotinin, and pepstatin A] containing 250 mM sucrose. After 15 min on ice, cells were lysed by pushing them several times through a 22-gauge needle, and the lysate was spun down at 1000×*g* for 5 min at 4 °C to eliminate nuclei and unbroken cells. The supernatant fraction was centrifuged at 105,000×*g* for 45 min at 4 °C, and the resulting supernatant was used as the soluble cytosolic fraction.

4.2.4. Assay of caspase activity

After treatments, cells were harvested by centrifugation at 1000×*g* for 5 min at 4 °C and washed with PBS, and the cell pellets were kept on ice. The cells were resuspended in cell lysis buffer (50 mM HEPES, pH 7.4, 1 mM dithiothreitol, 0.1 mM EDTA, 0.1% Chaps) and held on ice for 5 min. After centrifugation for 10 min at 17,000×*g* at 4 °C, the supernatants were analysed for protein concentration by the Bradford dye binding assay and stored at −20 °C until used to study caspase colorimetric enzymatic activity. Equal amounts of protein from different treatments were used, and the assays were set up on ice. The net increase of absorbance at 405 nm after incubation at 37 °C was indicative of enzyme activity. Specific colorimetric substrates for caspase-3, -8 and -9 activities were *N*-acetyl-Asp-Glu-Val-Asp-*p*-nitroaniline (DEVD-*p*NA), *N*-acetyl-Ile-Glu-Thr-Asp-*p*-nitroaniline (IETD-*p*NA) and *N*-acetyl-Leu-Glu-His-Asp-*p*-nitroaniline (LEHD-*p*NA), respectively.

4.2.5. In vitro tubulin polymerization assay

In vitro tubulin polymerization assays were performed with reagents as described by the manufacturer (Cytoskeleton Inc., Denver, CO, USA). Briefly, different concentrations of **7a** were incubated with purified bovine tubulin in 80 mM PIPES buffer (pH 7.0) containing 1 mM GTP, 1 mM EGTA, 1 mM $MgCl_2$, and 10% glycerol, and the increase in absorbance was measured at 340 nm in a Beckman Coulter DTX880 microplate reader at 37 °C and recorded every 30 s for 50 min. Taxol (10 μM) and colchicine (5 μM) were used as positive controls of promotion and inhibition of tubulin polymerization, respectively.

4.2.6. Statistical analysis

Student's *t* test was used to determine the statistical significance of differences between means of control and treated samples, with p values of <0.05 considered significant.

Acknowledgments

Funding: This research was supported in part by the Spanish Ministerio de Economía y Competitividad (MINECO) and the European Regional Development Fund (CTQ2015-63894-P).

Conflicts of interest

None.

A. Supplementary data

Supplementary data associated with this article can be found, in the online version, at https://doi.org/10.1016/j.bmc.2017.09.043.

References

1. Newman DJ, Cragg GM. Natural products as sources of new drugs from 1981 to 2014. *J Nat Prod*. 2016;79:629–661.
2. Cheng S, Gao N, Zhang Z, et al. Quercetin induces tumor-selective apoptosis through downregulation of Mcl-1 and activation of Bax. *Clin Cancer Res*. 2010;16:5679–5691.
3. Ravishankar D, Rajora AK, Greco F, Osborn HM. Flavonoids as prospective compounds for anti-cancer therapy. *Int J Biochem Cell Biol*. 2013;45:2821–2831.
4. Ashkenazi A. Targeting the extrinsic apoptotic pathway in cancer: lessons learned and future directions. *J Clin Invest*. 2015;125:487–489.
5. Fulda S, Galluzzi L, Kroemer G. Targeting mitochondria for cancer therapy. *Nat Rev Drug Discov*. 2010;9:447–464.
6. Hsiang CY, Wu SL, Ho TY. Morin inhibits 12-O-tetradecanoylphorbol-13-acetate-induced hepatocellular transformation via activator protein 1 signaling pathway and cell cycle progression. *Biochem Pharmacol*. 2005;69:1603–1611.
7. Rubio S, Quintana J, López M, Eiroa JL, Triana J, Estévez F. Phenylbenzopyrones structure-activity studies identify betuletol derivatives as potential antitumoral agents. *Eur J Pharmacol*. 2006;548:9–20.
8. Rubio S, Quintana J, Eiroa JL, Triana J, Estévez F. Acetyl derivative of quercetin 3-methyl ether-induced cell death in human leukemia cells is amplified by the inhibition of ERK. *Carcinogenesis*. 2007;28:2105–2113.
9. Beutler JA, Cardellina JHII, Lin CM, Hamel E, Cragg GM, Boyd MR. Centaureidin, a cytotoxic flavone from *Polymnia fruticosa*, inhibits tubulin polymerization. *Bioorg Med Chem Lett*. 1993;3:581–584.
10. Lichius JJ, Thoison O, Montagnac A, et al. Antimitotic and cytotoxic flavonols from *Zieridium pseudobtusifolium* and *Acronychia porteri*. *J Nat Prod*. 1994;57:1012–1016.
11. Shobeiri N, Rashedi M, Mosaffa F, et al. Synthesis and biological evaluation of quinoline analogues of flavones as potential anticancer agents and tubulin polymerization inhibitors. *Eur J Med Chem*. 2016;114:14–23.
12. Beutler JA, Hamel E, Vlietinck AJ, et al. Structure-activity requirements for flavone cytotoxicity and binding to tubulin. *J Med Chem*. 1998;41:2333–2338.
13. Torres F, Quintana J, Estévez F. 5,7,3′-Trihydroxy-3,4′-dimethoxyflavone inhibits the tubulin polymerization and activates the sphingomyelin pathway. *Mol Carcinog*. 2011;50:113–122.
14. De Meyer N, Haemers A, Mishra L, et al. 4′-Hydroxy-3-methoxyflavones with potent antipicornavirus activity. *J Med Chem*. 1991;34:736–746.
15. Kim MK, Choo H, Chong Y. Water-soluble and cleavable quercetin–amino acid conjugates as safe modulators for P-glycoprotein-based multidrug resistance. *J Med Chem*. 2014;57:7216–7233.
16. Juvale K, Stefan K, Wiese M. Synthesis and biological evaluation of flavones and benzoflavones as inhibitors of BCRP/ABCG2. *Eur J Med Chem*. 2013;67:115–126.
17. Walle T. Methoxylated flavones, a superior cancer chemopreventive flavonoid subclass? *Semin Cancer Biol*. 2007;17:354–362.
18. Gupta K, Panda D. Perturbation of microtubule polymerization by quercetin through tubulin binding: a novel mechanism of its antiproliferative activity. *Biochemistry*. 2002;41:13029–13038.
19. Nicolini F, Burmistrova O, Marrero MT, et al. Induction of G_2-M phase arrest and apoptosis by the flavonoid tamarixetin on human leukemia cells. *Mol Carcinog*. 2014;53:939–950.
20. Zeng G, Liu J, Chen H, et al. Dihydromyricetin induces cell cycle arrest and apoptosis in melanoma SK-MEL-28 cells. *Oncol Rep*. 2014;31:2713–2719.
21. Cabrera M, Simoens M, Falchi G, et al. Synthetic chalcones, flavanones, and flavones as antitumoral agents: biological evaluation and structure-activity relationships. *Bioorg Med Chem*. 2007;15:3356–3367.

22. Bhatti HA, Uddin N, Ayub K, et al. Synthesis, characterization of flavone, isoflavone, and 2,3-dihydrobenzofuran-3-carboxylate and density functional theory studies. *Eur J Chem*. 2015;6:305–313.
23. Hsieh CT, Hsieh TJ, El-Shazly M, et al. Synthesis of chalcone derivatives as potential anti-diabetic agents. *Bioorg Med Chem Lett*. 2012;22:3912–3915.
24. Chen YP, Zhang ZY, Li YP, et al. Syntheses and evaluation of novel isoliquiritigenin derivatives as potential dual inhibitors for amyloid-beta aggregation and 5-lipoxygenase. *Eur J Med Chem*. 2013;66:22–31.
25. Chang CY, Huang LJ, Wang JP, Teng CM, Chen SC, Kuo SC. Synthesis and anti-platelet, anti-inflammatory and anti-allergic activities of methoxyisoflavanquinone and related compounds. *Chem Pharm Bull (Tokyo)*. 2000;48:964–973.
26. Qin CX, Chen X, Hughes RA, Williams SJ, Woodman OL. Understanding the cardioprotective effects of flavonols: discovery of relaxant flavonols without antioxidant activity. *J Med Chem*. 2008;51:1874–1884.
27. Singh SK, Gaur R, Kumar A, Fatima R, Mishra L, Srikrishna S. The flavonoid derivative 2-(4′-Benzyloxyphenyl)-3-hydroxy-chromen-4-one protects against Aβ42-induced neurodegeneration in transgenic Drosophila: insights from in silico and in vivo studies. *Neurotox Res*. 2014;26:331–350.
28. Rao MLN, Kumar A. Pd-catalyzed atom-economic couplings of triarylbismuth reagents with 2-bromo- and 2,6-dibromochromones and synthesis of medicinally important fisetin. *Tetrahedron Lett*. 2014;55:5764–5770.
29. Cimanga K, Ying L, De Bruyne T, et al. Radical scavenging and xanthine oxidase inhibitory activity of phenolic compounds from *Bridelia ferruginea* stem bark. *J Pharm Pharmacol*. 2001;53:757–761.
30. Venkateswararao E, Son MJ, Sharma N, et al. Exploration of pharmacophore in chrysosplenol C as activator in ventricular myocyte contraction. *ACS Med Chem Lett*. 2015;6:758–763.
31. Gunduz S, Goren AC, Ozturk T. Facile syntheses of 3-hydroxyflavones. *Org Lett*. 2012;14:1576–1579.
32. Moon BH, Lee Y, Ahn JH, Lim Y. Complete assignment of ^{1}H and ^{13}C NMR data of some flavonol derivatives. *Magn Reson Chem*. 2005;43:858–860.
33. Said M, Brouard I, Quintana J, Estévez F. Antiproliferative activity and apoptosis induction by 3′,4′-dibenzyloxyflavonol on human leukemia cells. *Chem Biol Interact*. 2017;268:13–23.
34. Negrín G, Rubio S, Marrero MT, et al. The eudesmanolide tanapsin from *Tanacetum oshanahanii* and its acetate induce cell death in human tumor cells through a mechanism dependent on reactive oxygen species. *Phytomedicine*. 2015;22:385–393.

3´-Hydroxy- 3,4´-dimethoxyflavone Blocks Tubulin Polymerization and is a Potent Apoptotic Inducer in Human SK-MEL-1 Melanoma Cells

Francisco Estévez-Sarmiento[a], Mercedes Said[a], Ignacio Brouard[b], Francisco León[b], Celina García[c], José Quintana[a], Francisco Estévez[a,*]

[a] Departamento de Bioquímica y Biología Molecular, Unidad Asociada al Consejo Superior de Investigaciones Científicas (CSIC), Instituto Universitario de Investigaciones Biomédicas y Sanitarias, Universidad de las Palmas de Gran Canaria, Paseo Blas Cabrera Felipe s/n, 35016 Las Palmas de Gran Canaria, Spain

[b]Instituto de Productos Naturales y Agrobiología, CSIC, Avenida Astrofísico Francisco Sánchez 3, 38206 La Laguna, Tenerife, Spain

[c]Instituto Universitario de Bio-Orgánica "Antonio González" (IUBO-AG), Departamento de Química Orgánica, Universidad de La Laguna, Avda. Astrofísico Francisco Sánchez 2, 38206 La Laguna, Tenerife, Spain

[*]Corresponding author. Tel.: +34 928 451443; fax: +34 928 451441

E-mail address: francisco.estevez@ulpgc.es (F.Estévez)

Supplementary data

Content:

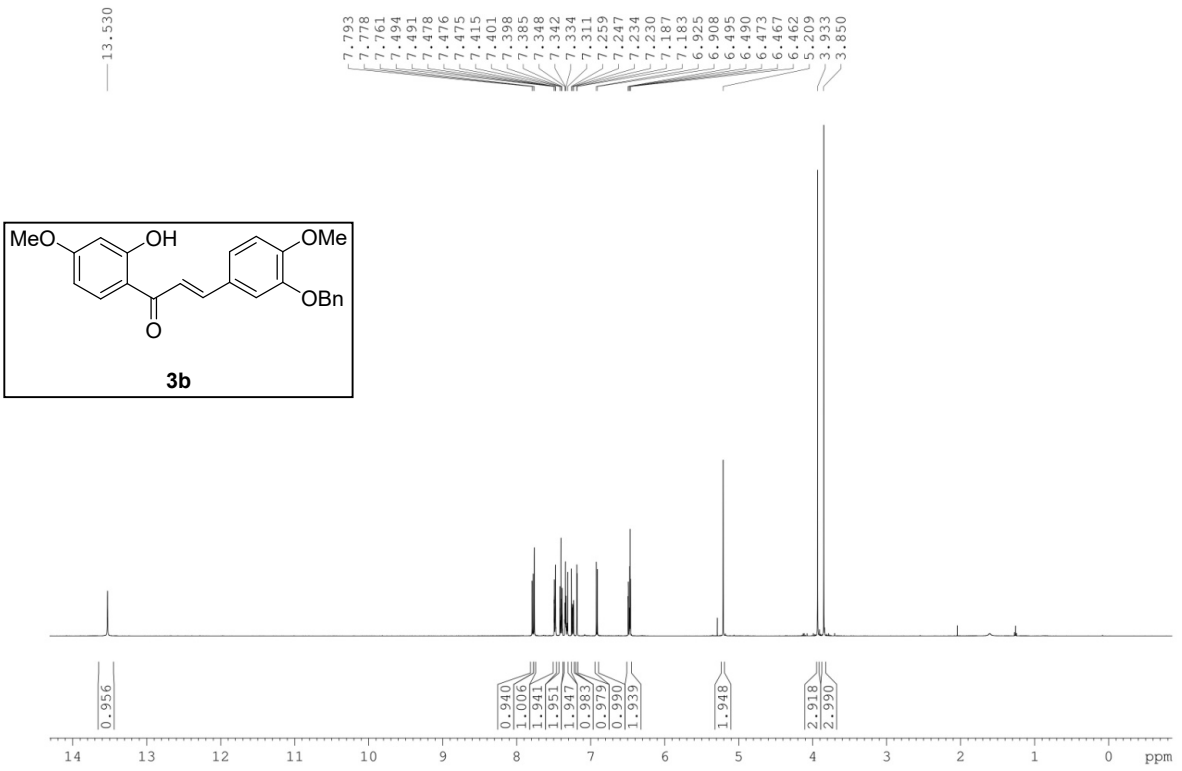

Figure 1.500 MHz ^{1}H NMR spectrum in $CDCl_3$ of compound **3b**

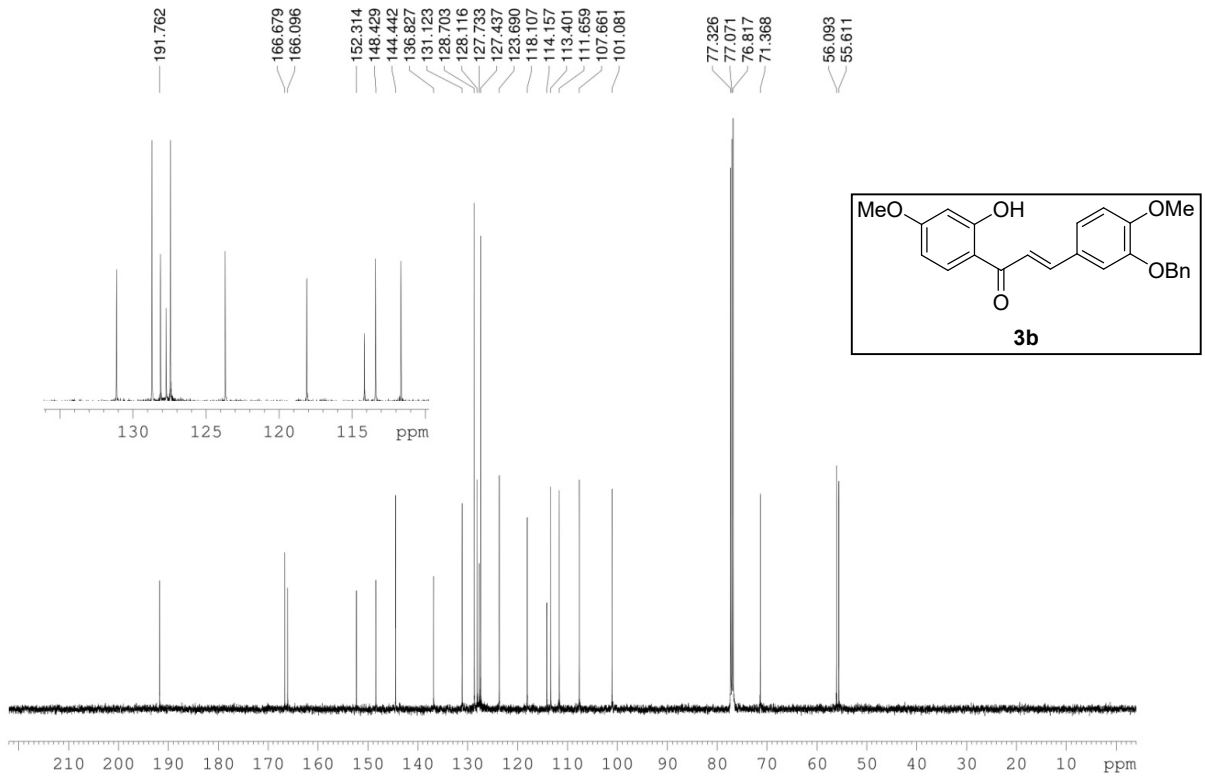

Figure 2.125 MHz ^{13}C NMR spectrum in $CDCl_3$ of compound **3b**

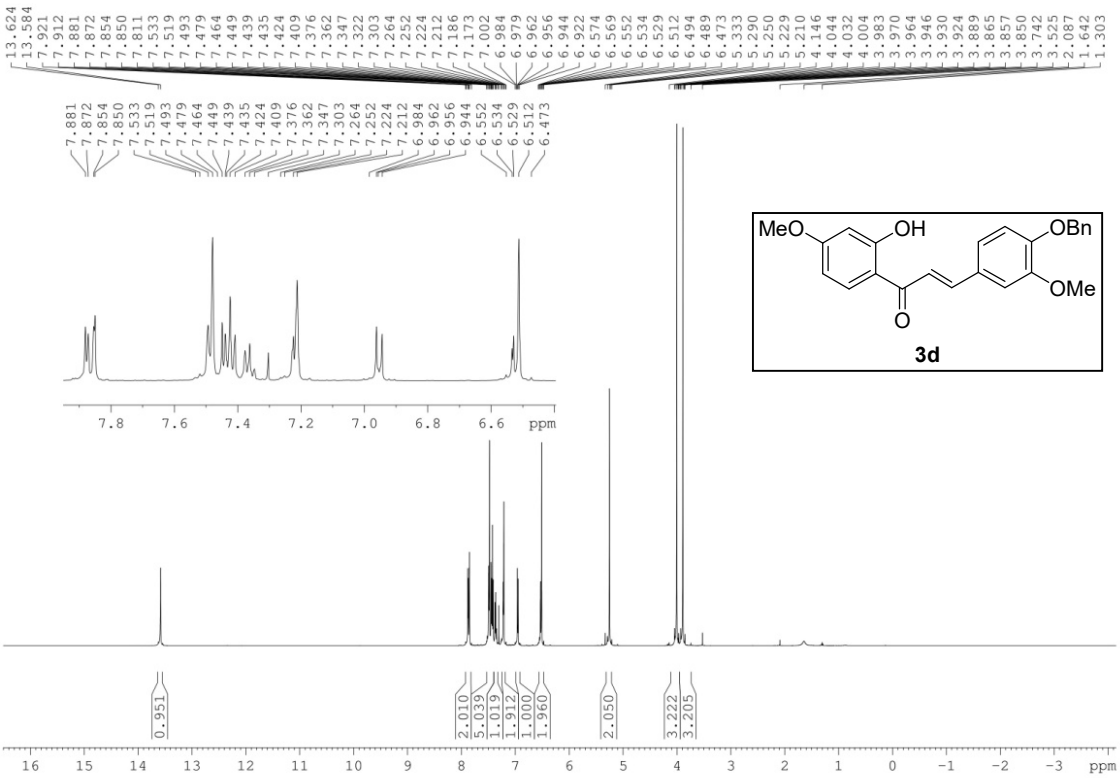

Figure 3.500 MHz ^{1}H NMR spectrum in $CDCl_3$ of compound **3d**

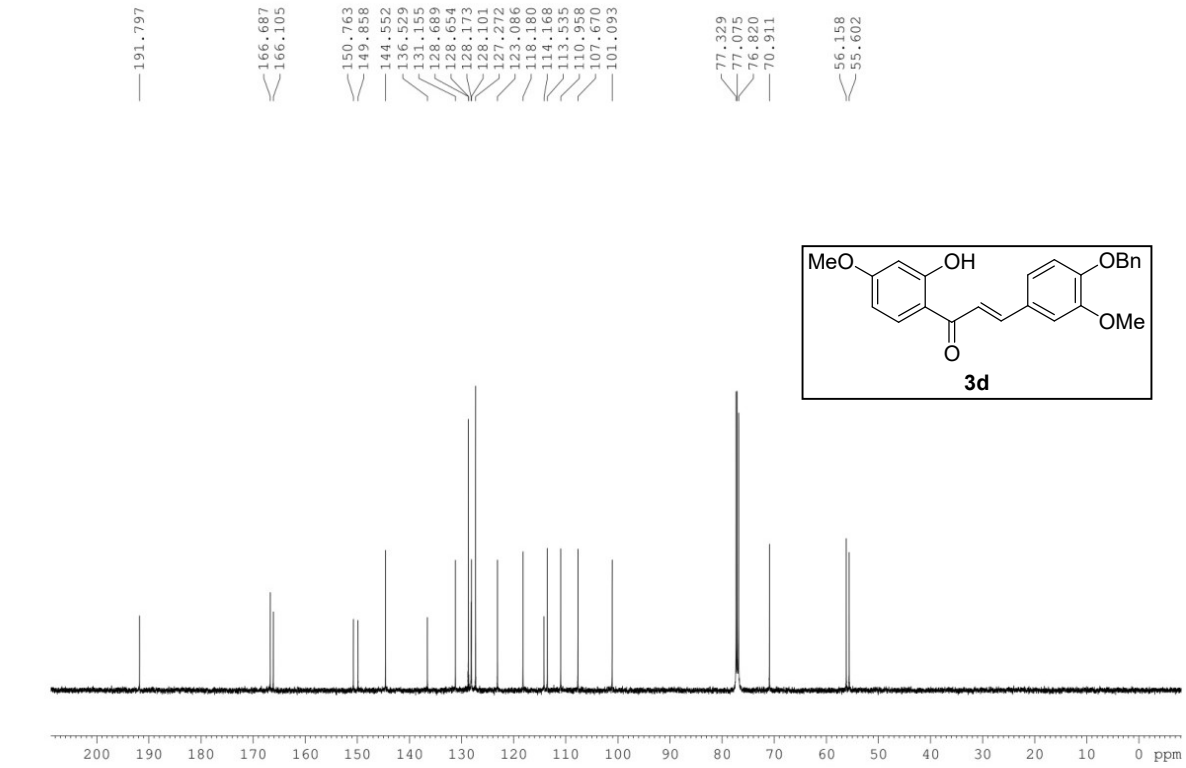

Figure 4.125 MHz ^{13}C NMR spectrum in $CDCl_3$ of compound **3d**

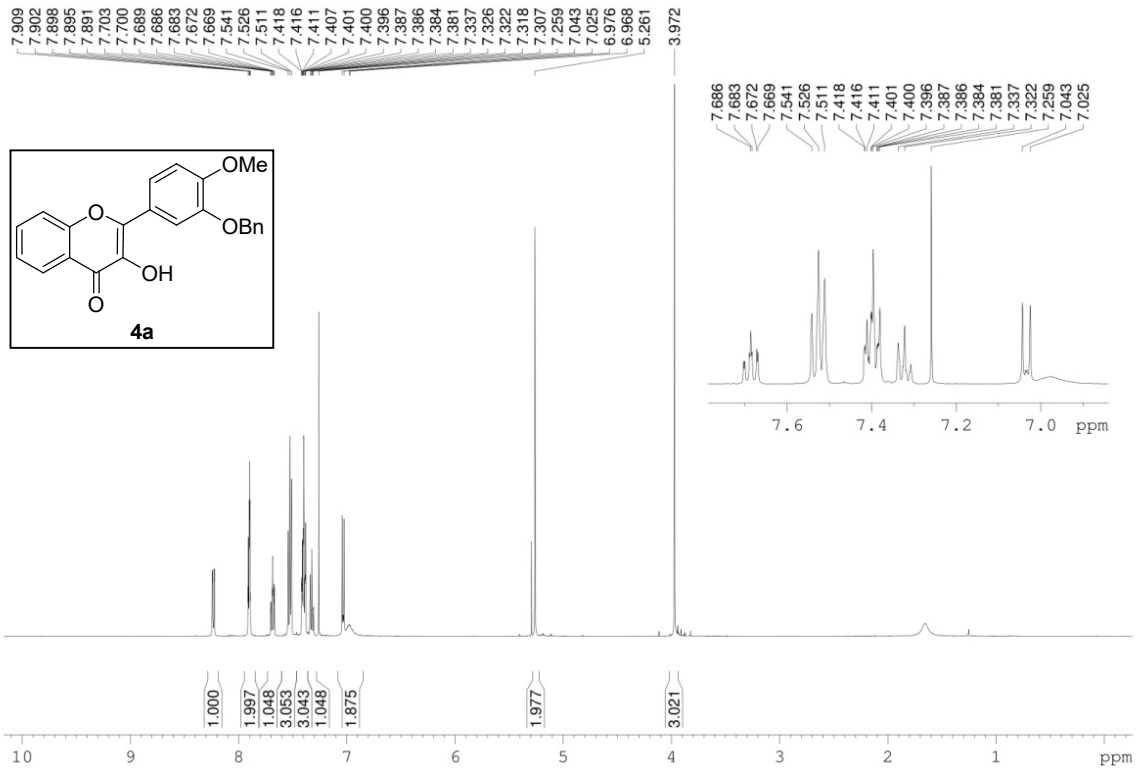

Figure 5.500 MHz ^{1}H NMR spectrum in $CDCl_3$ of compound **4a**

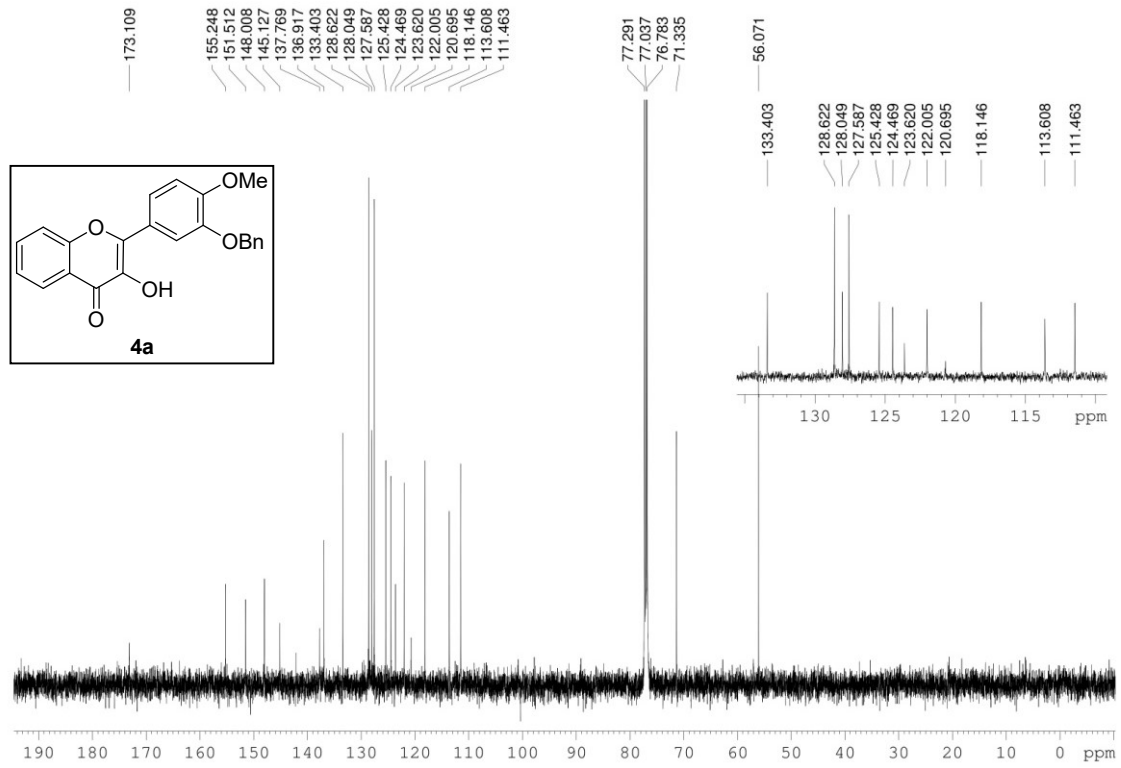

Figure 6.125 MHz ^{13}C NMR spectrum in $CDCl_3$ of compound **4a**

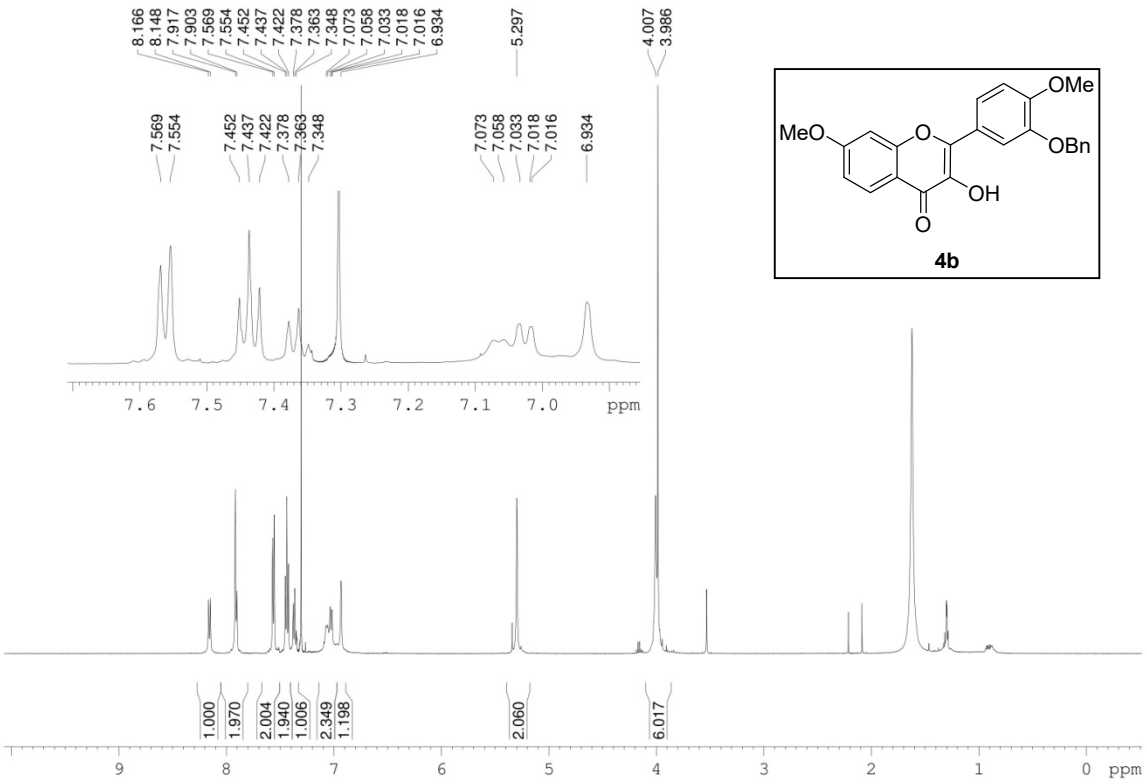

Figure 7.500 MHz ^{1}H NMR spectrum in $CDCl_3$ of compound **4b**

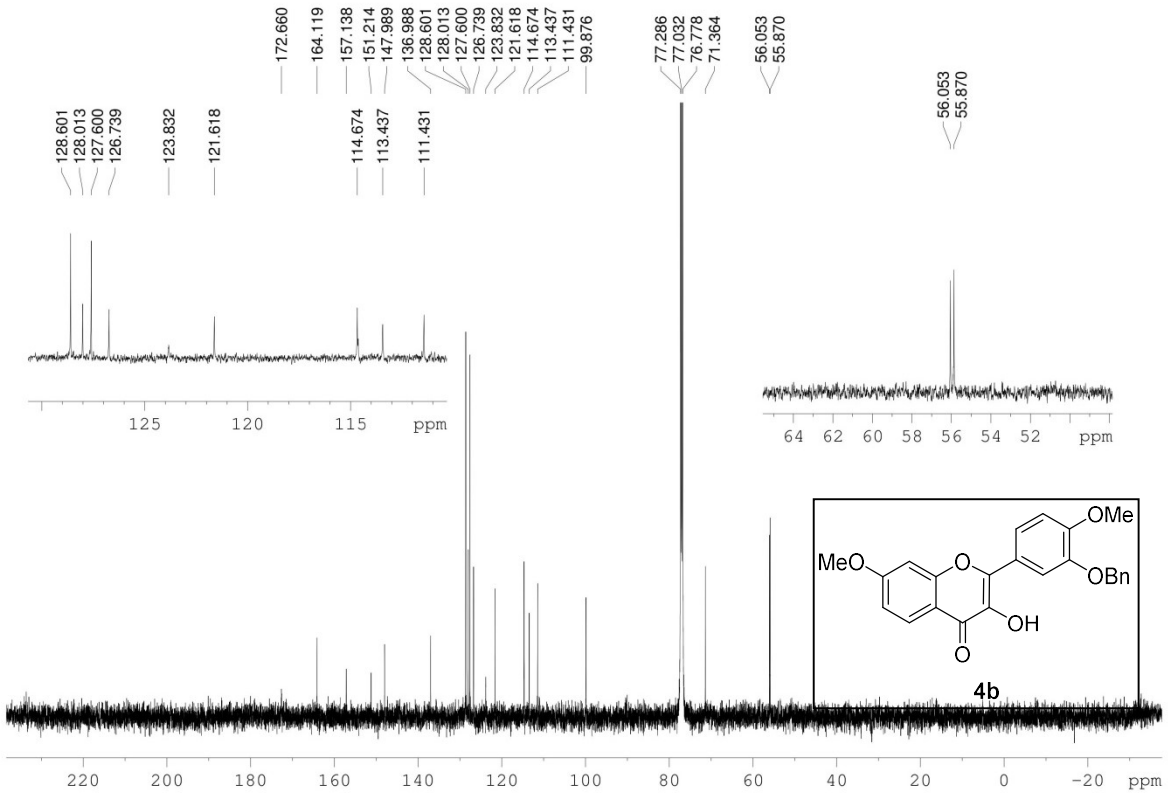

Figure 8.125 MHz ^{13}C NMR spectrum in $CDCl_3$ of compound **4b**

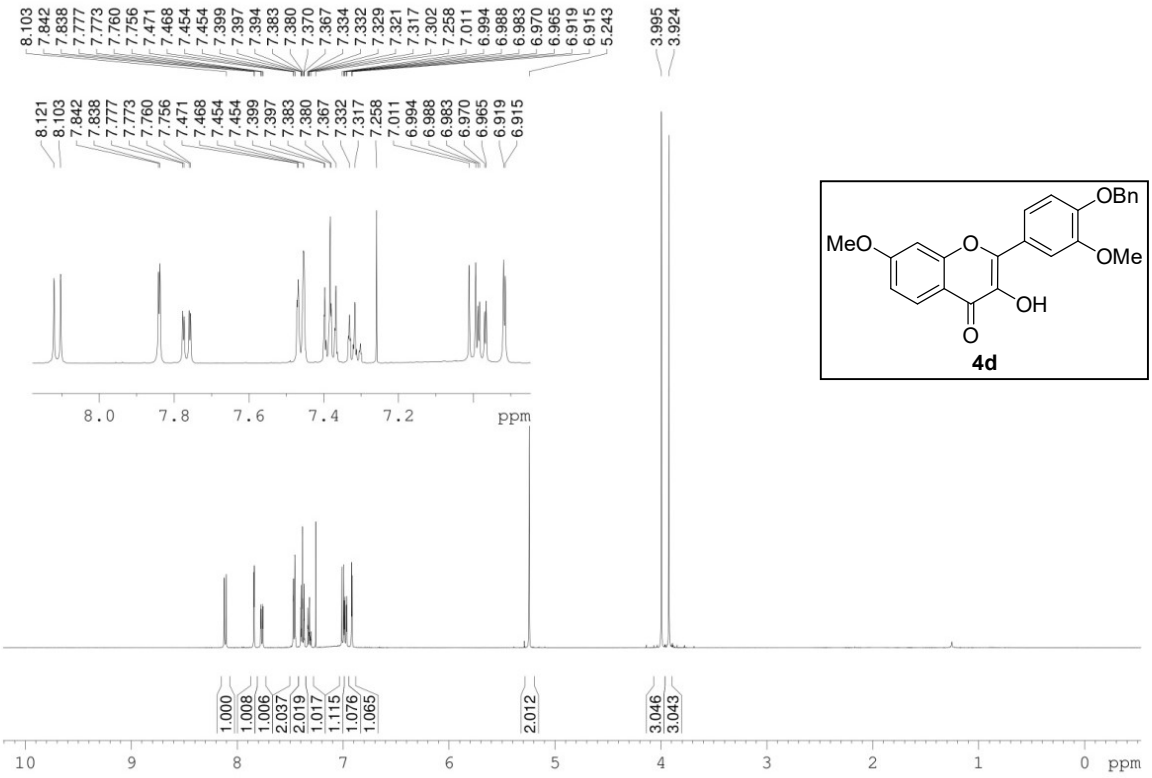

Figure 9.500 MHz ^{1}H NMR spectrum in $CDCl_3$ of compound **4d**

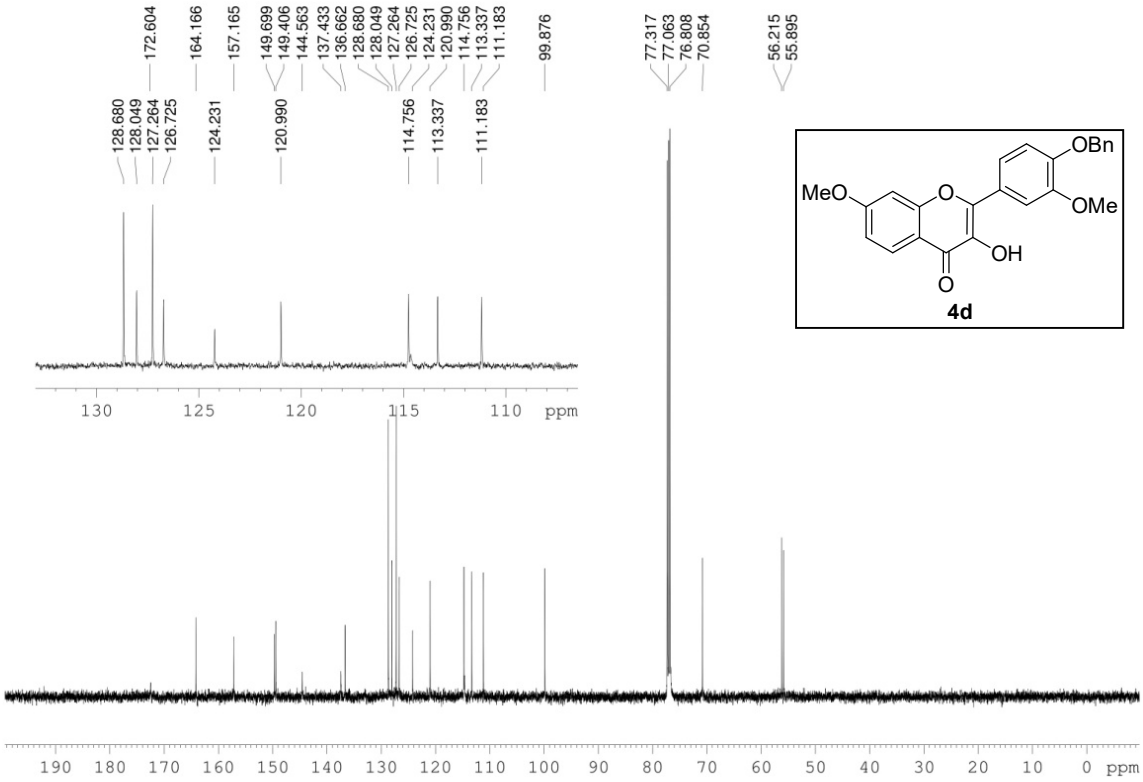

Figure 10.125 MHz ^{13}C NMR spectrum in $CDCl_3$ of compound **4d**

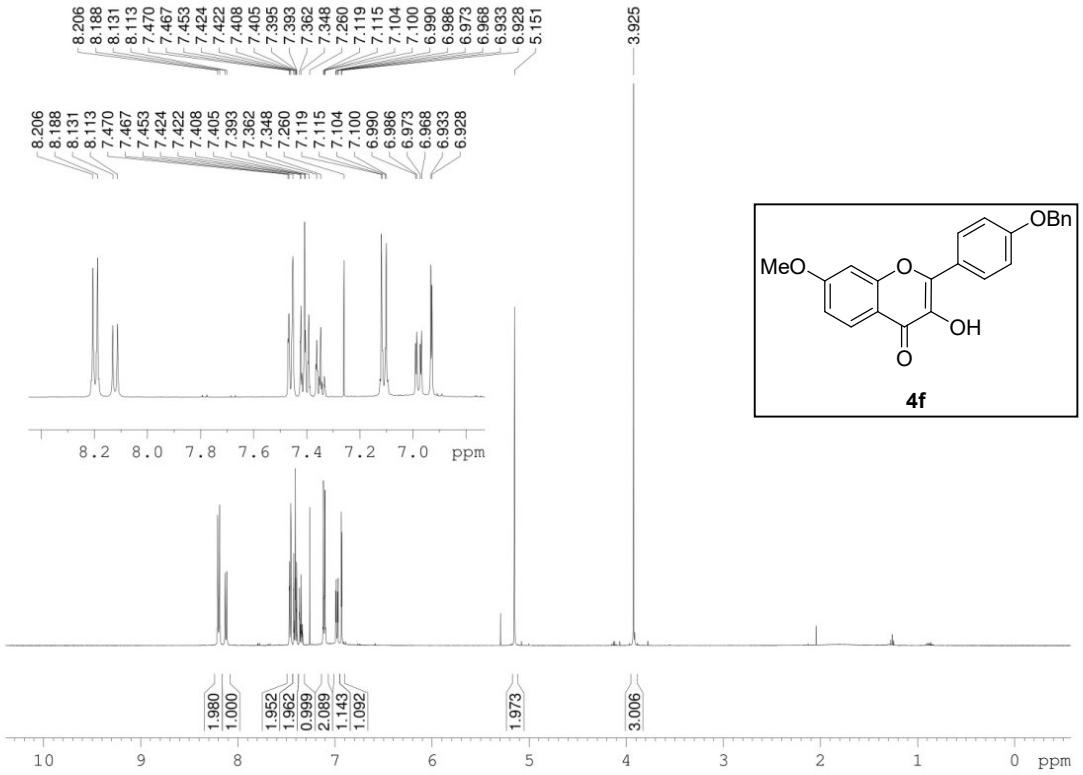

Figure 11.500 MHz ^{1}H NMR spectrum in $CDCl_3$ of compound **4f**

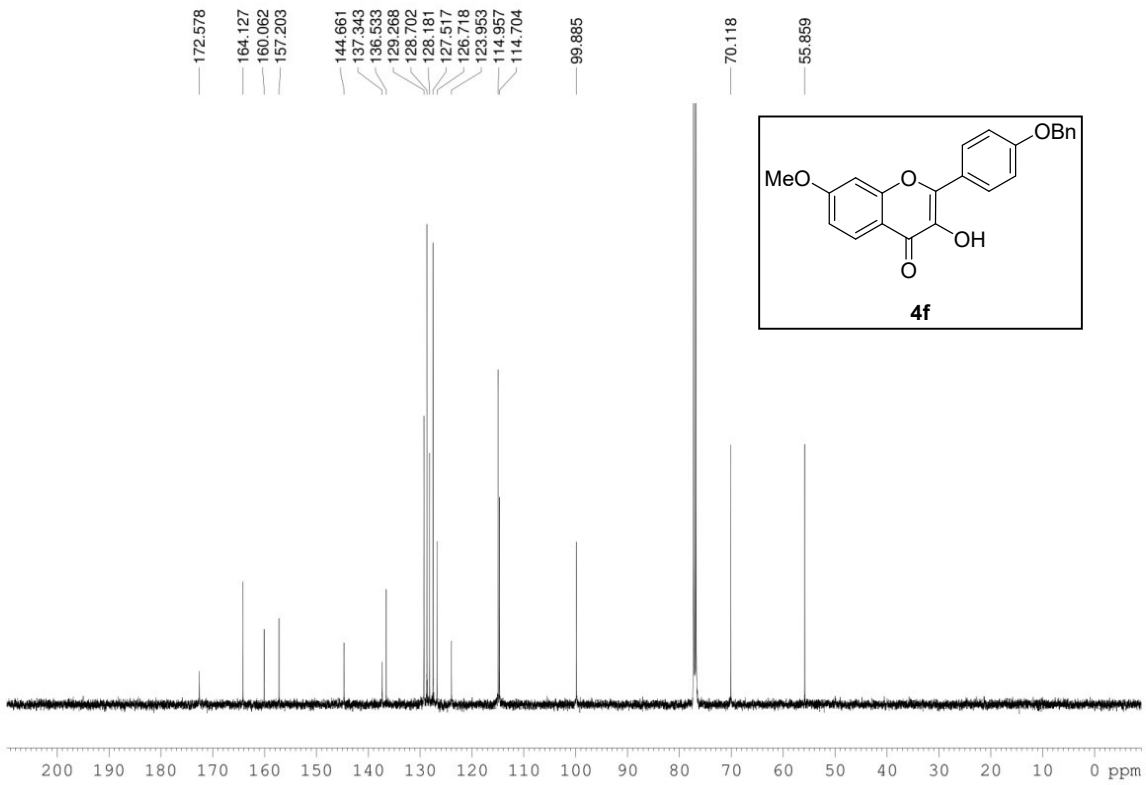

Figure 12.125 MHz ^{13}C NMR spectrum in $CDCl_3$ of compound **4f**

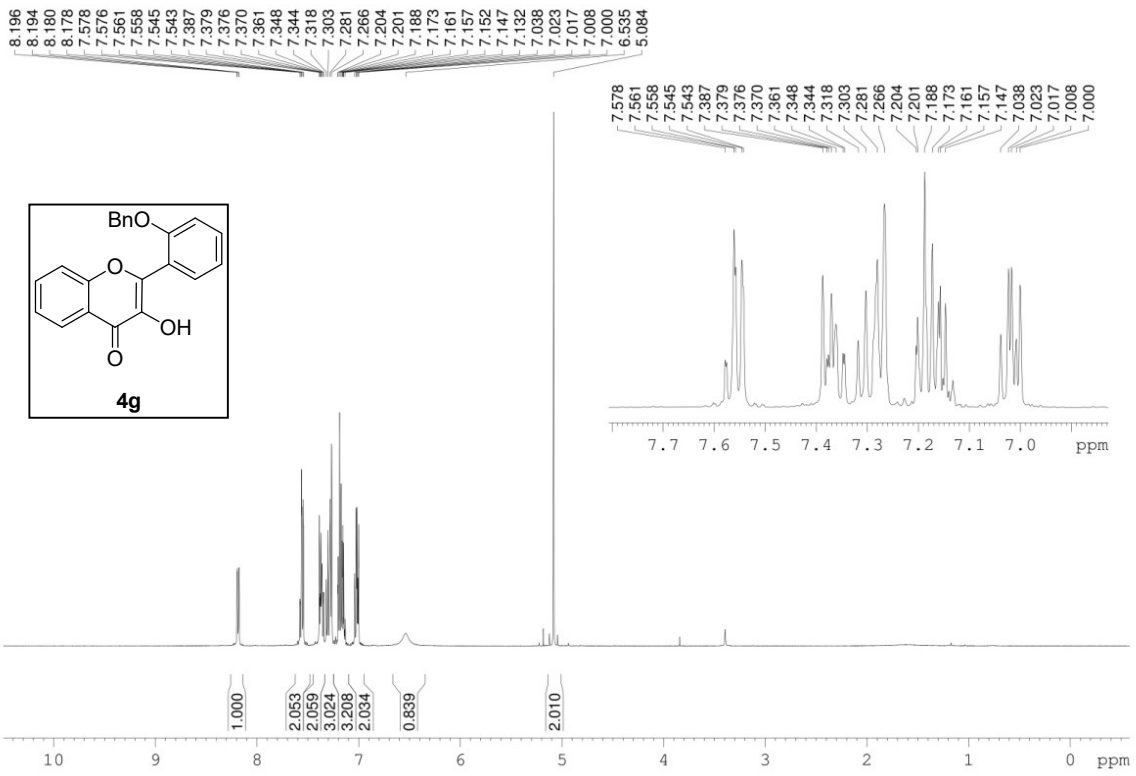

Figure 13.500 MHz ^{1}H NMR spectrum in $CDCl_3$ of compound **4g**

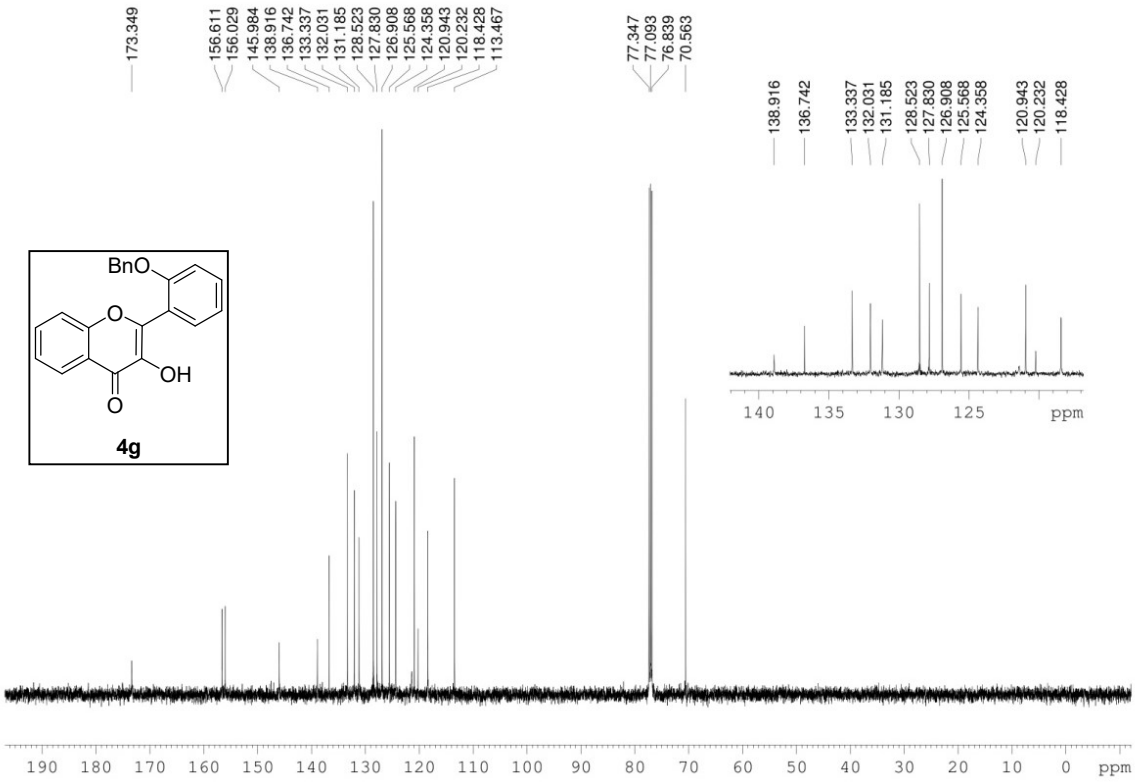

Figure 14.125 MHz ^{13}C NMR spectrum in $CDCl_3$ of compound **4g**

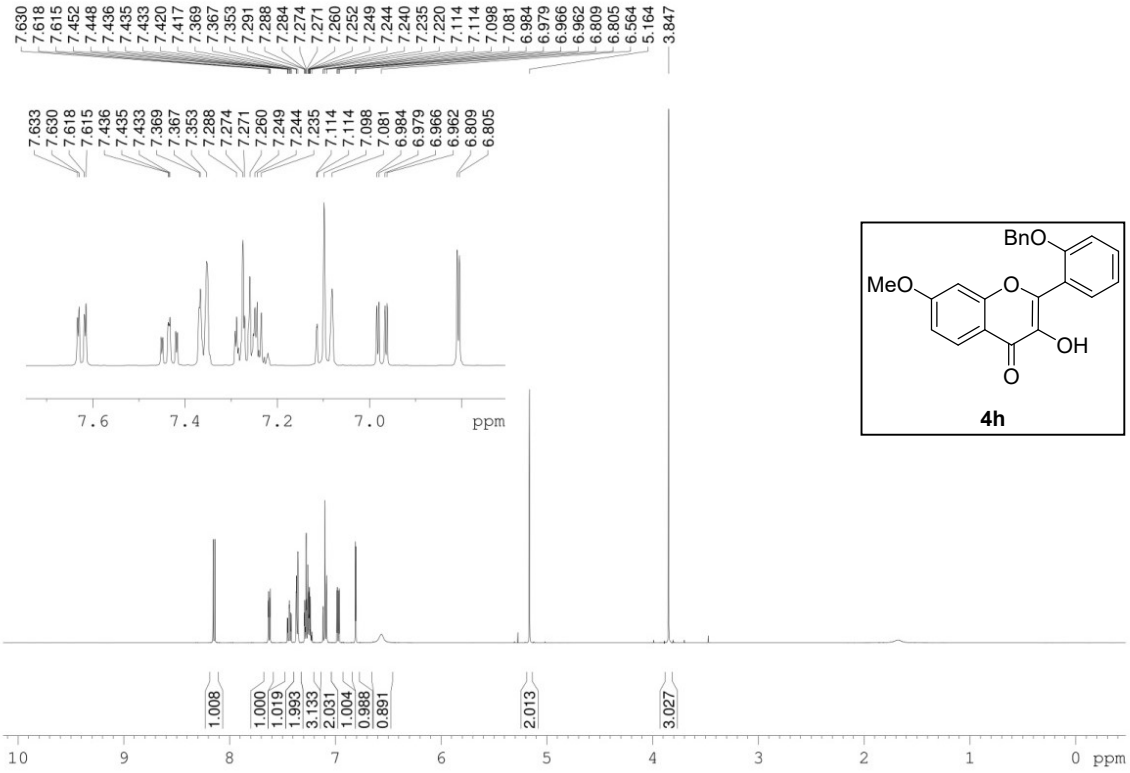

Figure 15.500 MHz ^{1}H NMR spectrum in $CDCl_3$ of compound **4h**

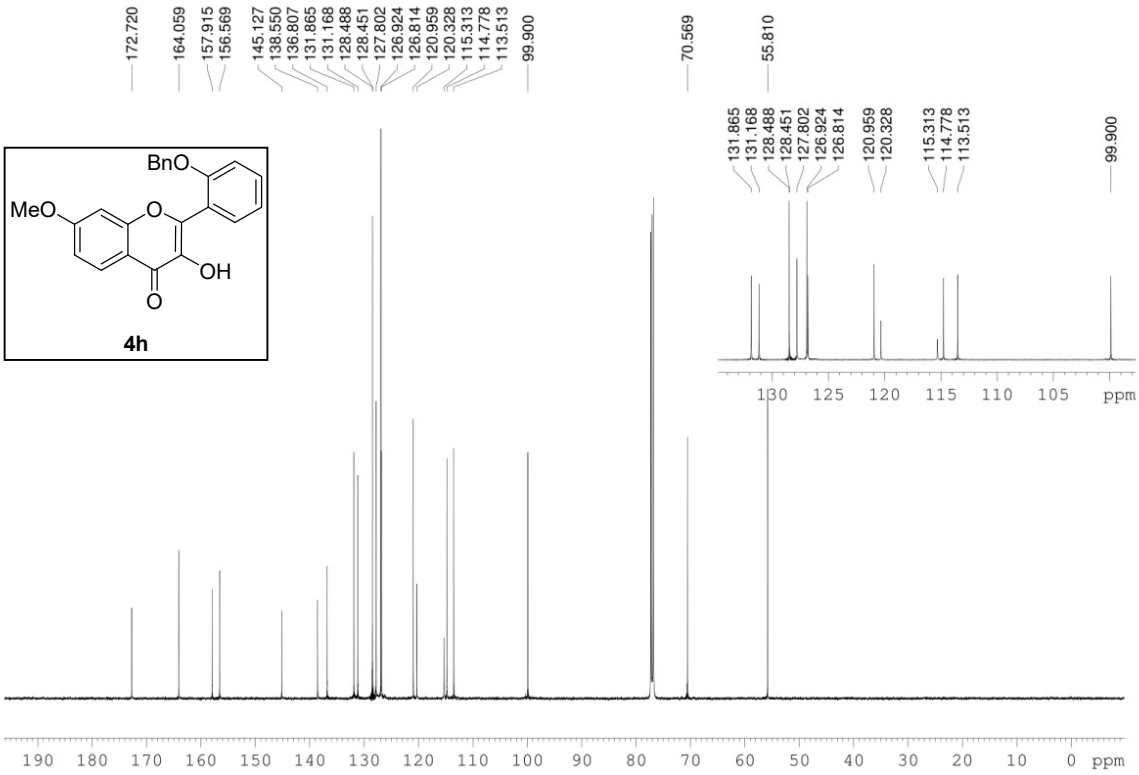

Figure 16.125 MHz ^{13}C NMR spectrum in $CDCl_3$ of compound **4h**

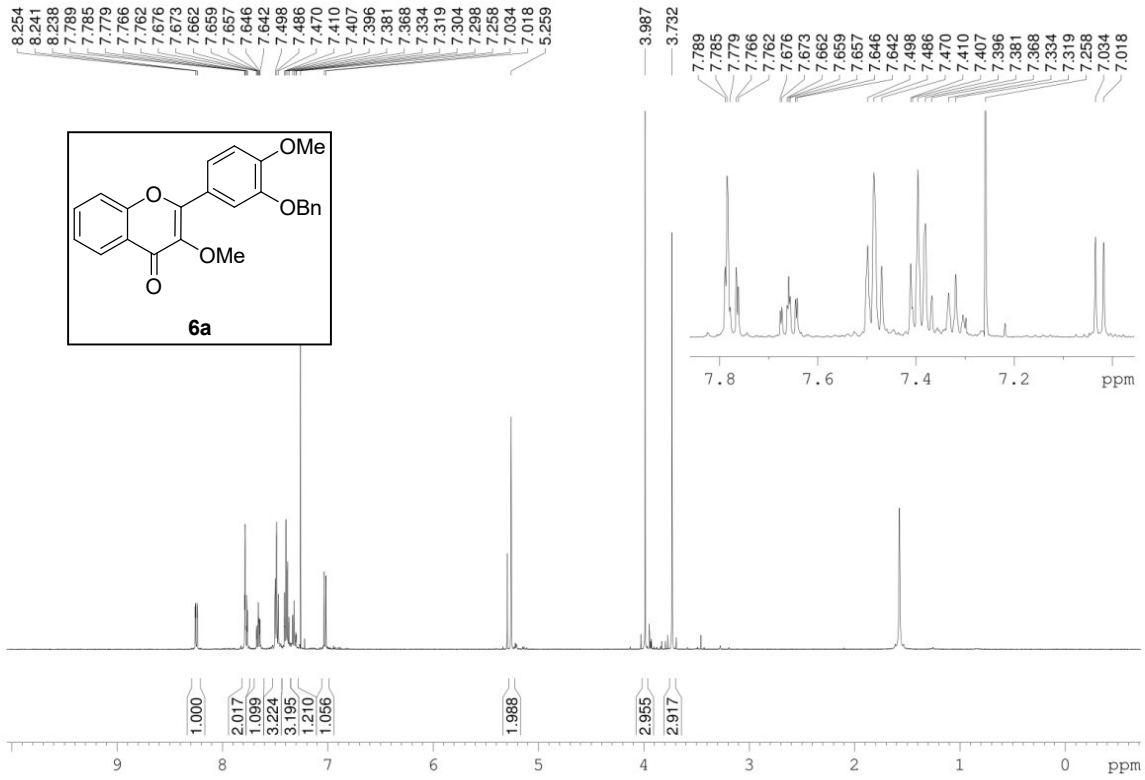

Figure 17.500 MHz ^{1}H NMR spectrum in $CDCl_3$ of compound **6a**

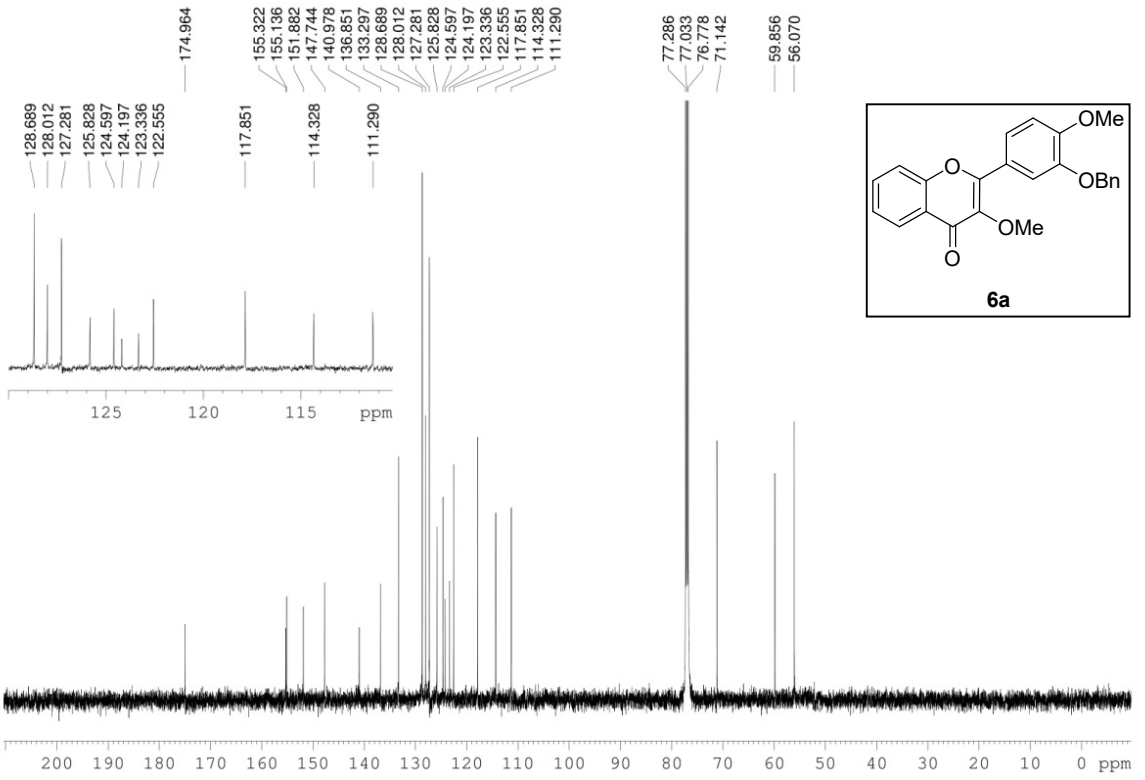

Figure 18.125 MHz ^{13}C NMR spectrum in $CDCl_3$ of compound **6a**

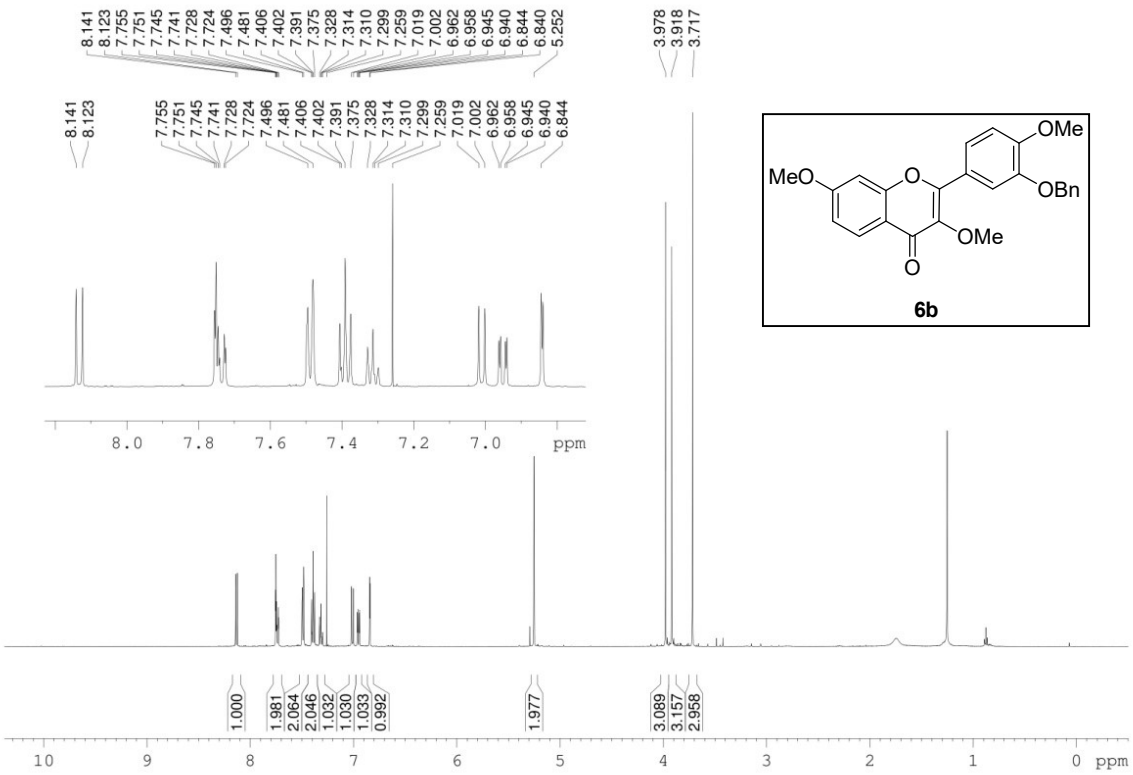

Figure 19.500 MHz ^{1}H NMR spectrum in $CDCl_3$ of compound **6b**

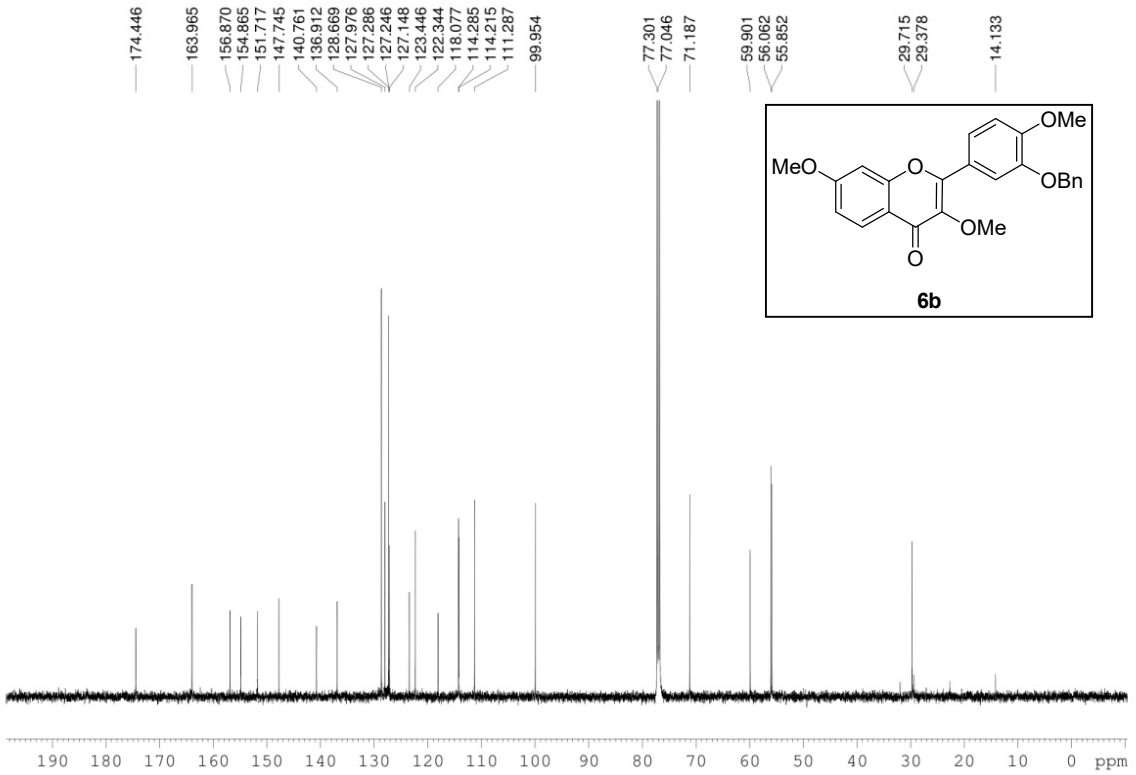

Figure 20.125 MHz ^{13}C NMR spectrum in $CDCl_3$ of compound **6b**

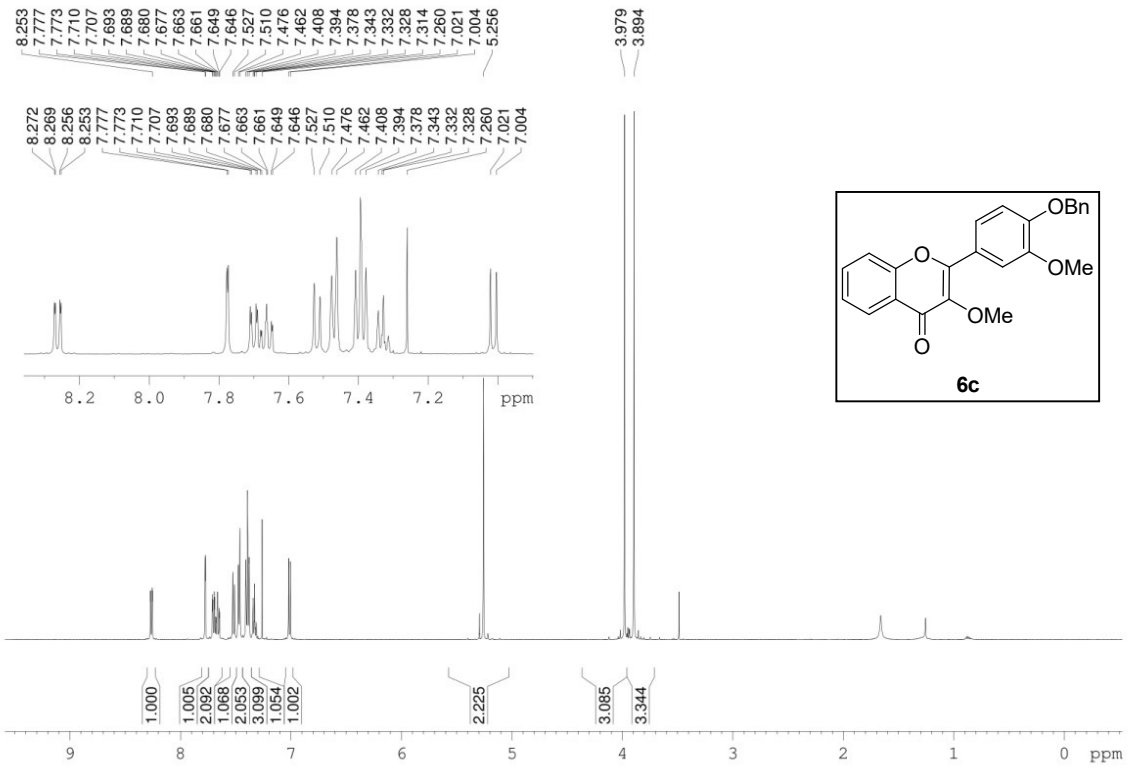

Figure 21.500 MHz ^{1}H NMR spectrum in $CDCl_3$ of compound **6c**

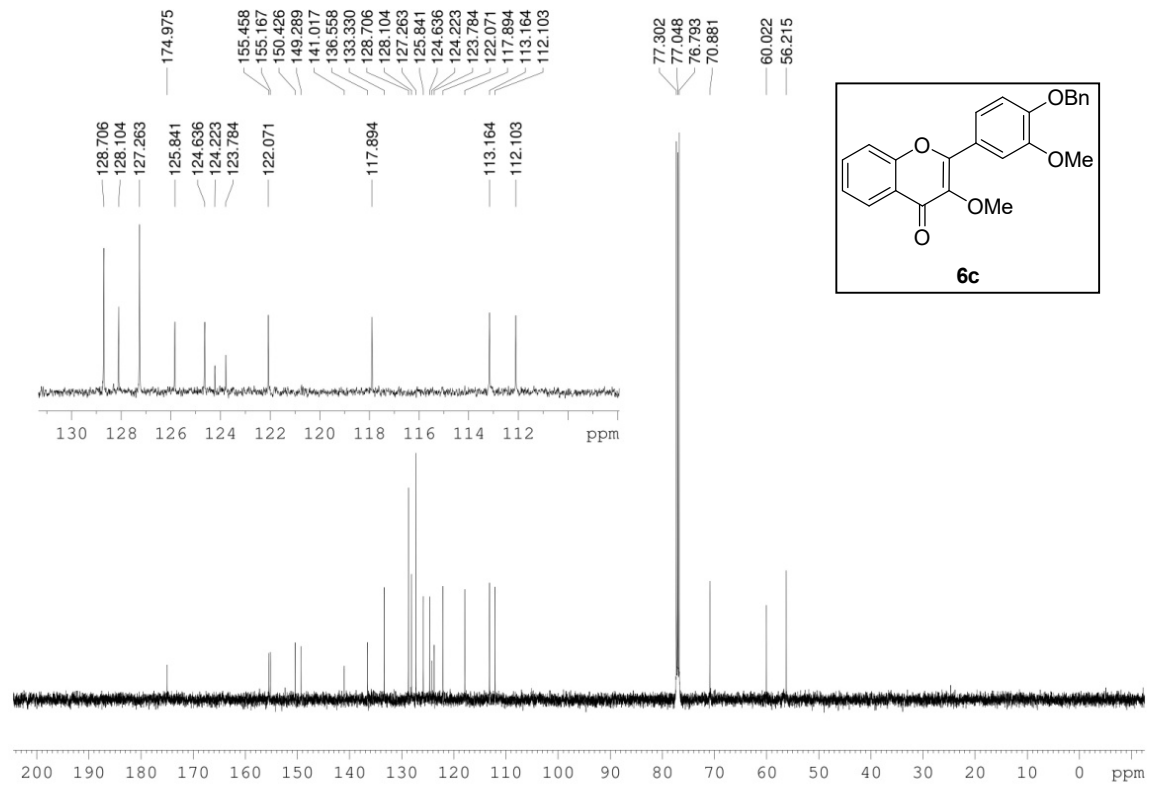

Figure 22.125 MHz ^{13}C NMR spectrum in $CDCl_3$ of compound **6c**

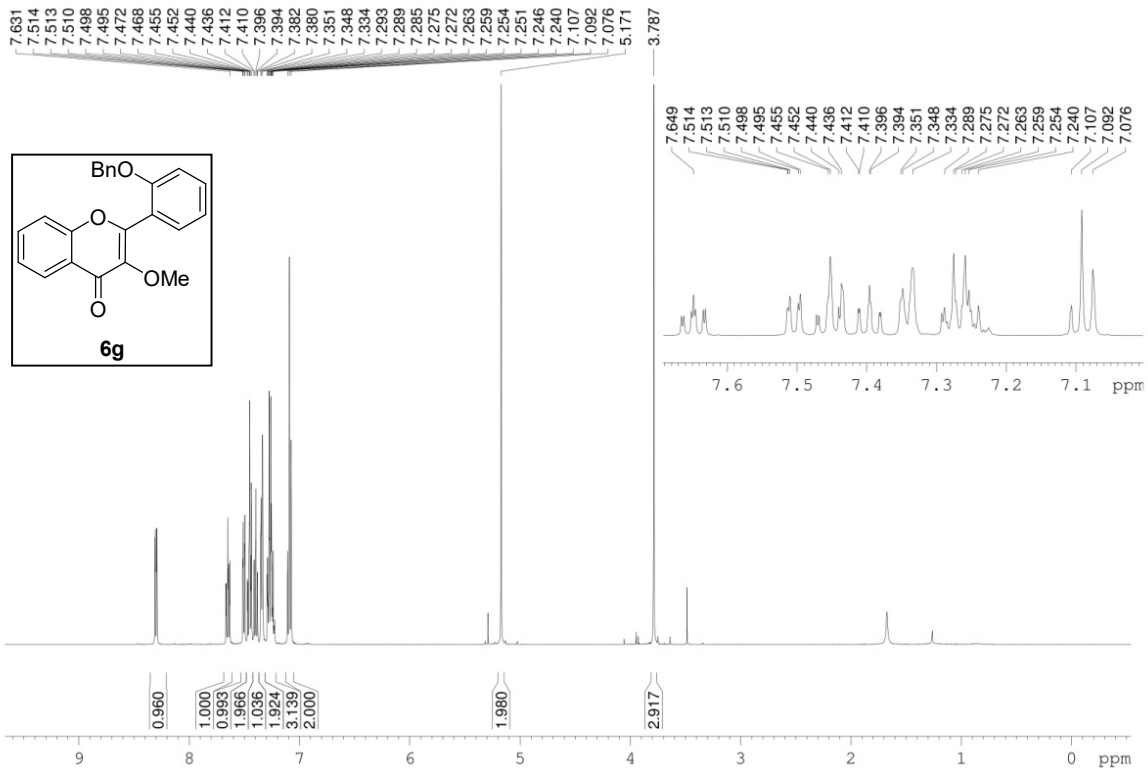

Figure 23.500 MHz ^{1}H NMR spectrum in $CDCl_3$ of compound **6g**

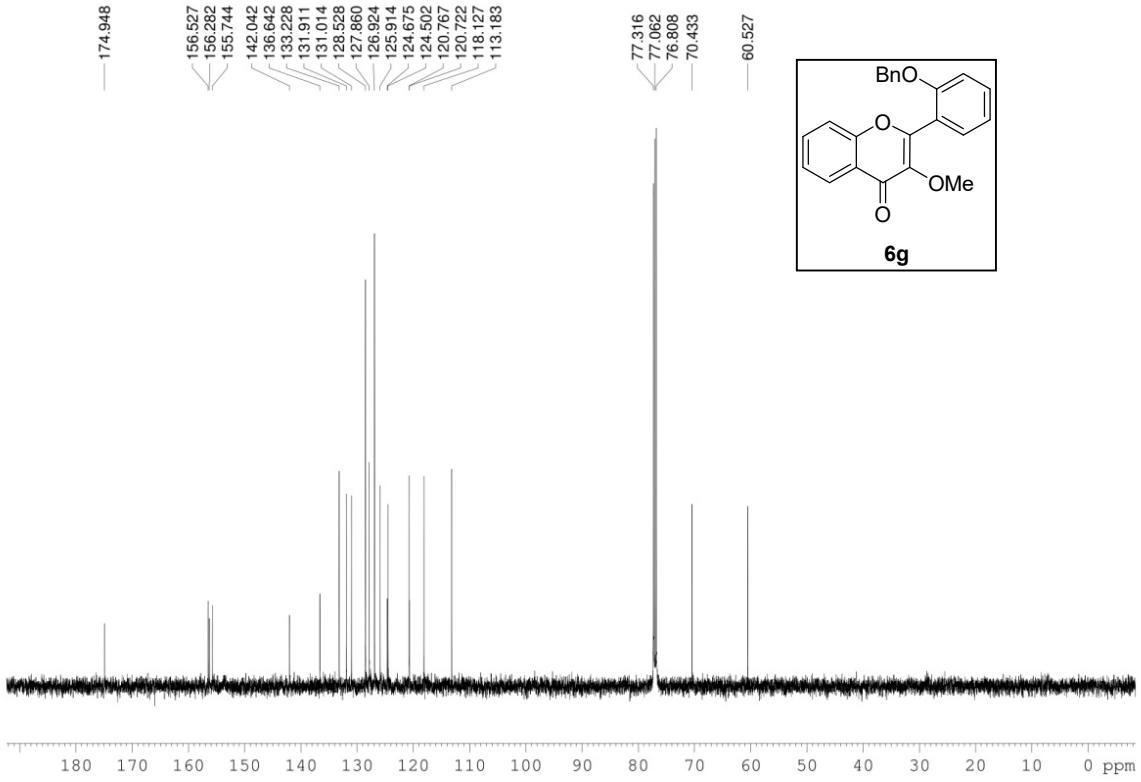

Figure 24.125 MHz ^{13}C NMR spectrum in $CDCl_3$ of compound **6g**

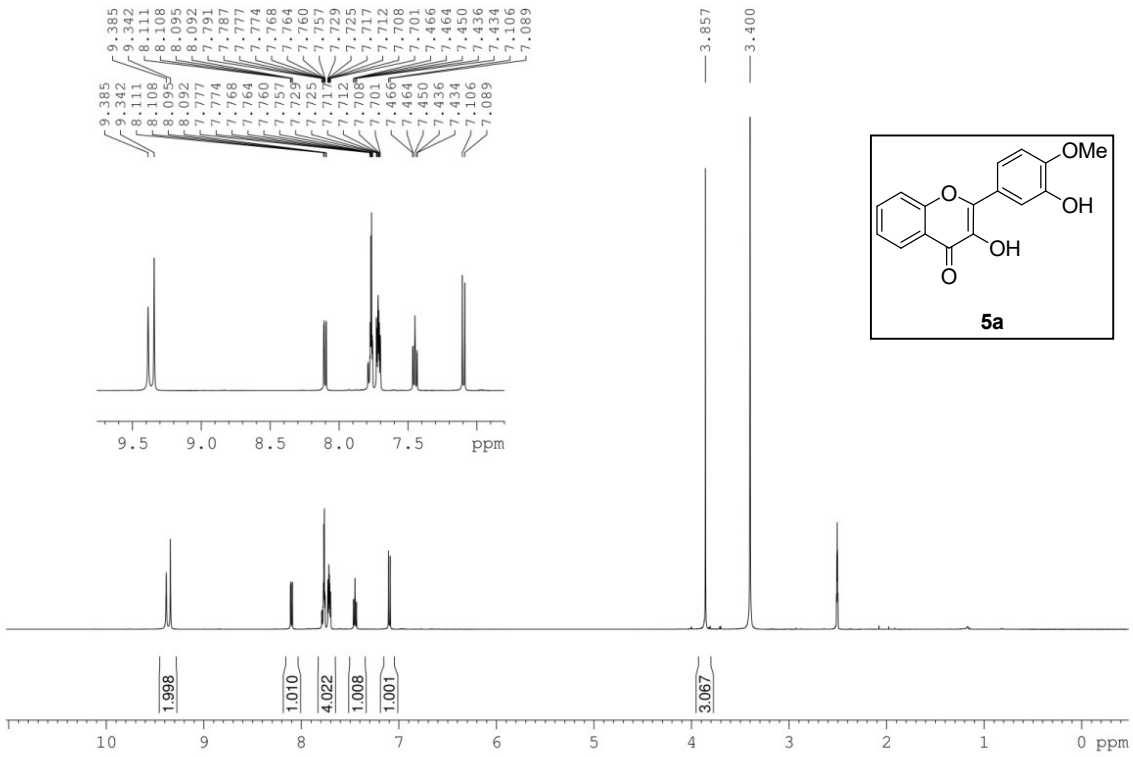

Figure 25.500 MHz ^{1}H NMR spectrum in DMSO of compound **5a**

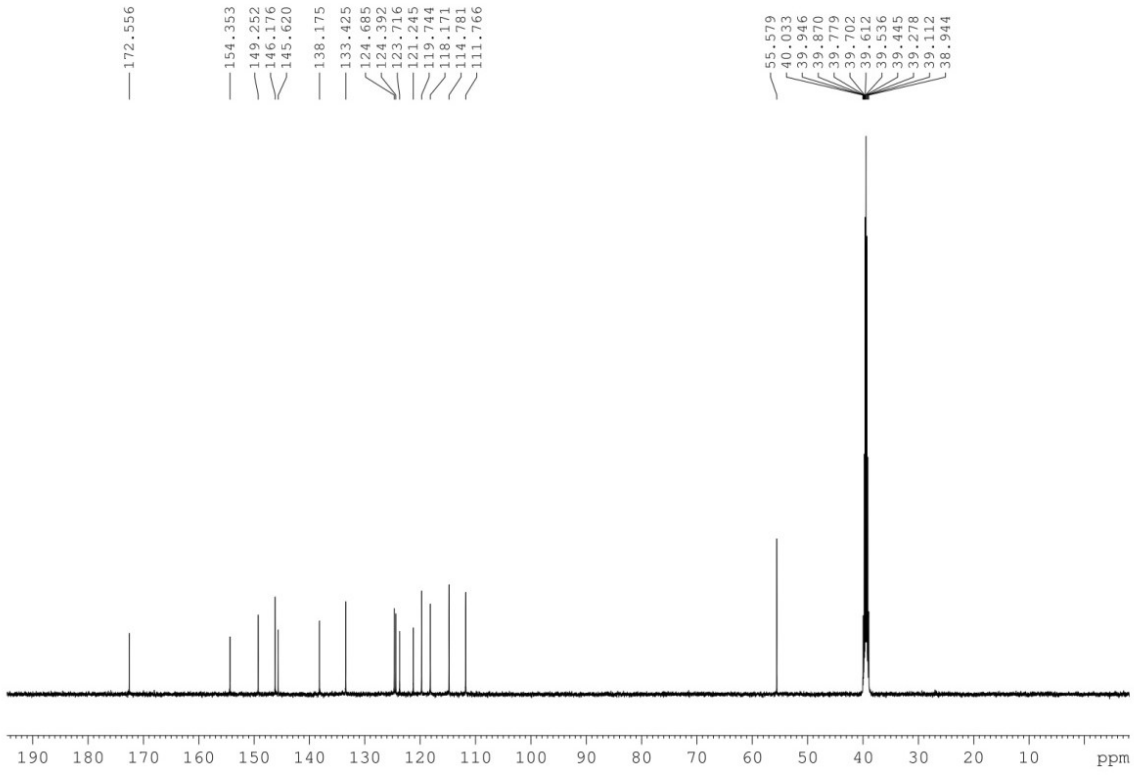

Figure 26.125 MHz ^{13}C NMR spectrum in DMSO of compound **5a**

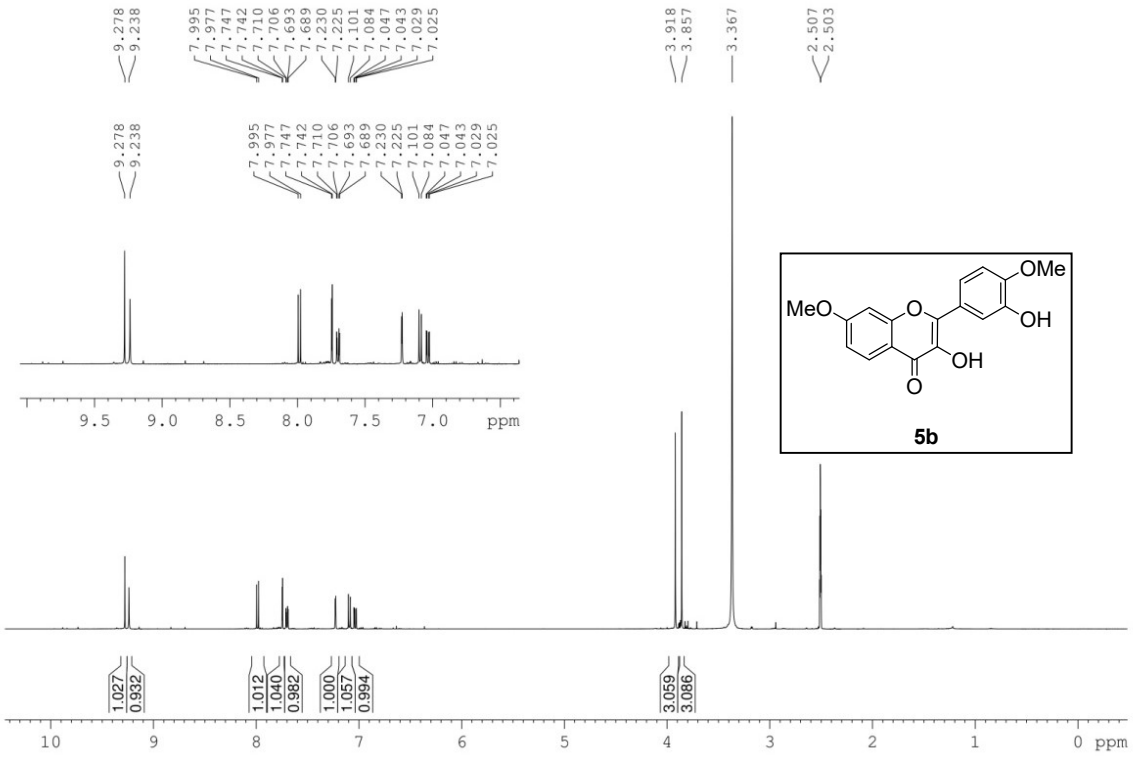

Figure 27.500 MHz ^{1}H NMR spectrum in DMSO of compound **5b**

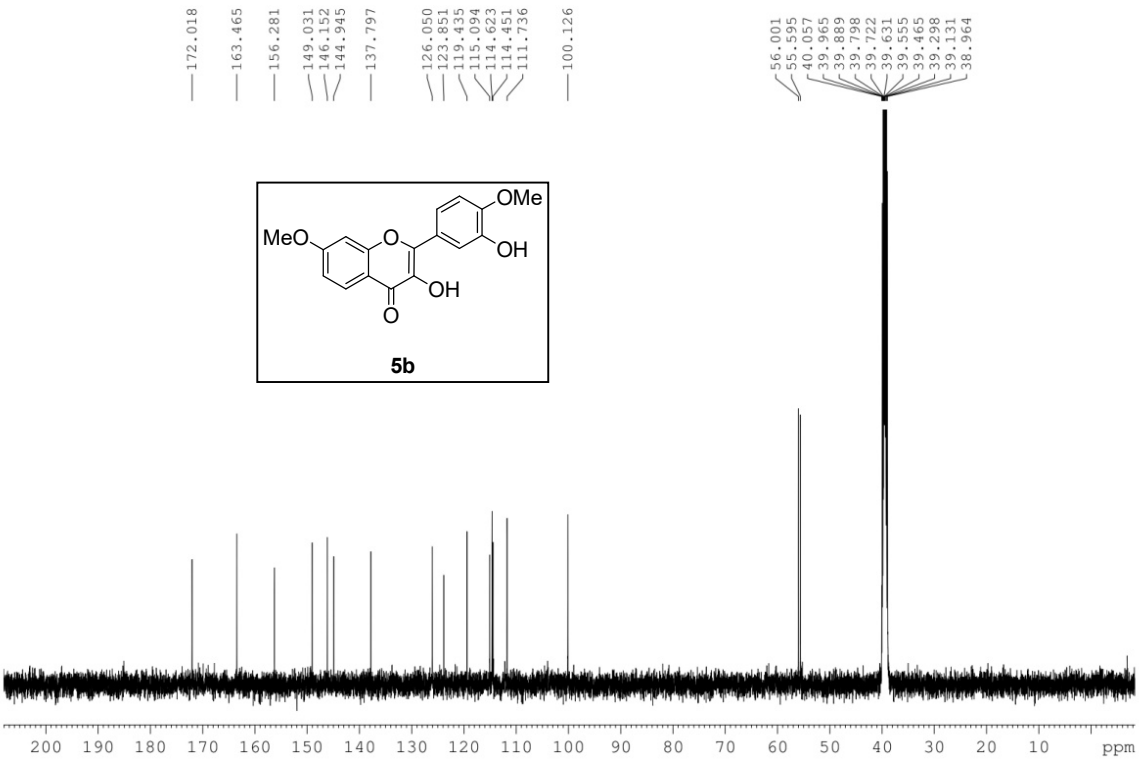

Figure 28.125 MHz ^{13}C NMR spectrum in DMSO of compound **5b**

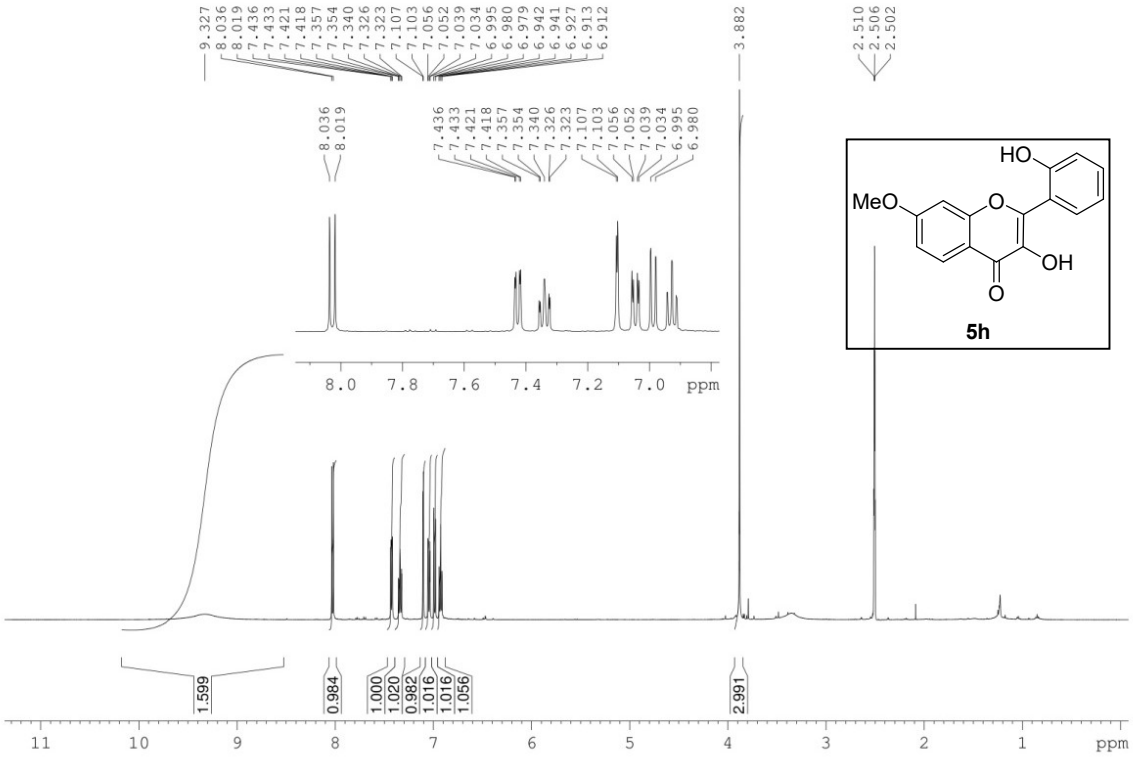

Figure 29.500 MHz ^{1}H NMR spectrum in DMSO of compound **5h**

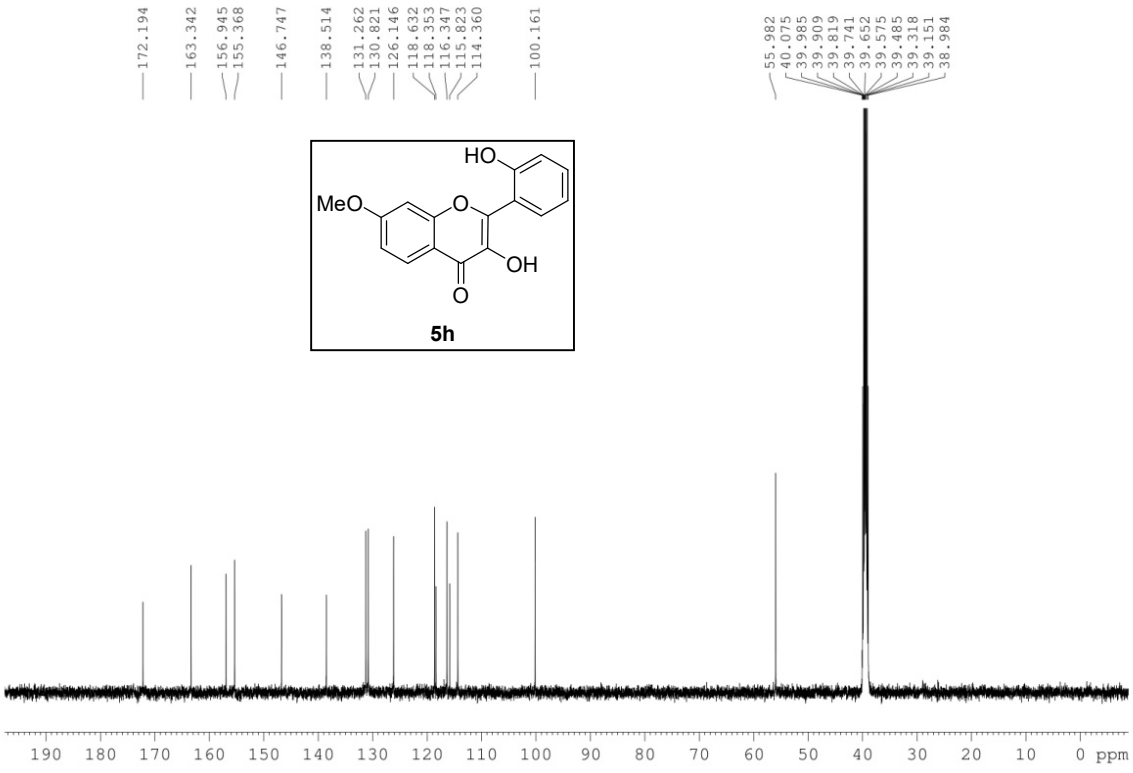

Figure 30.125 MHz ^{13}C NMR spectrum in DMSO of compound **5h**

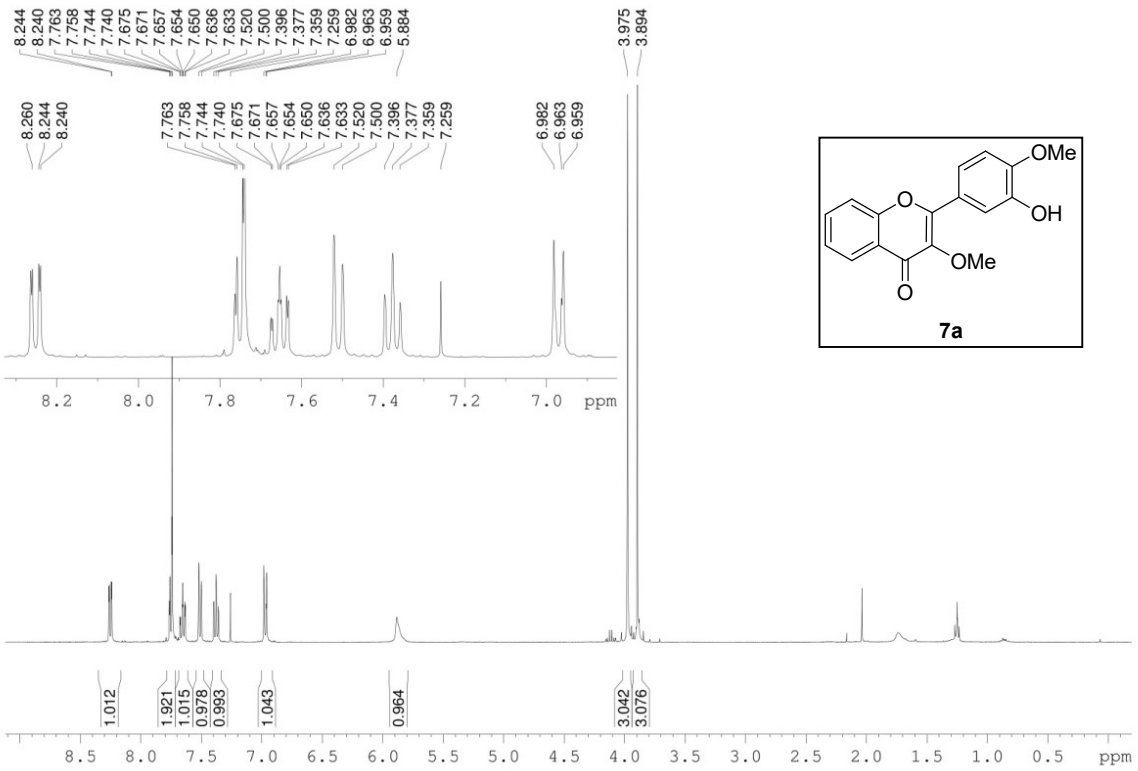

Figure 31.400 MHz ^{1}H NMR spectrum in $CDCl_3$ of compound **7a**

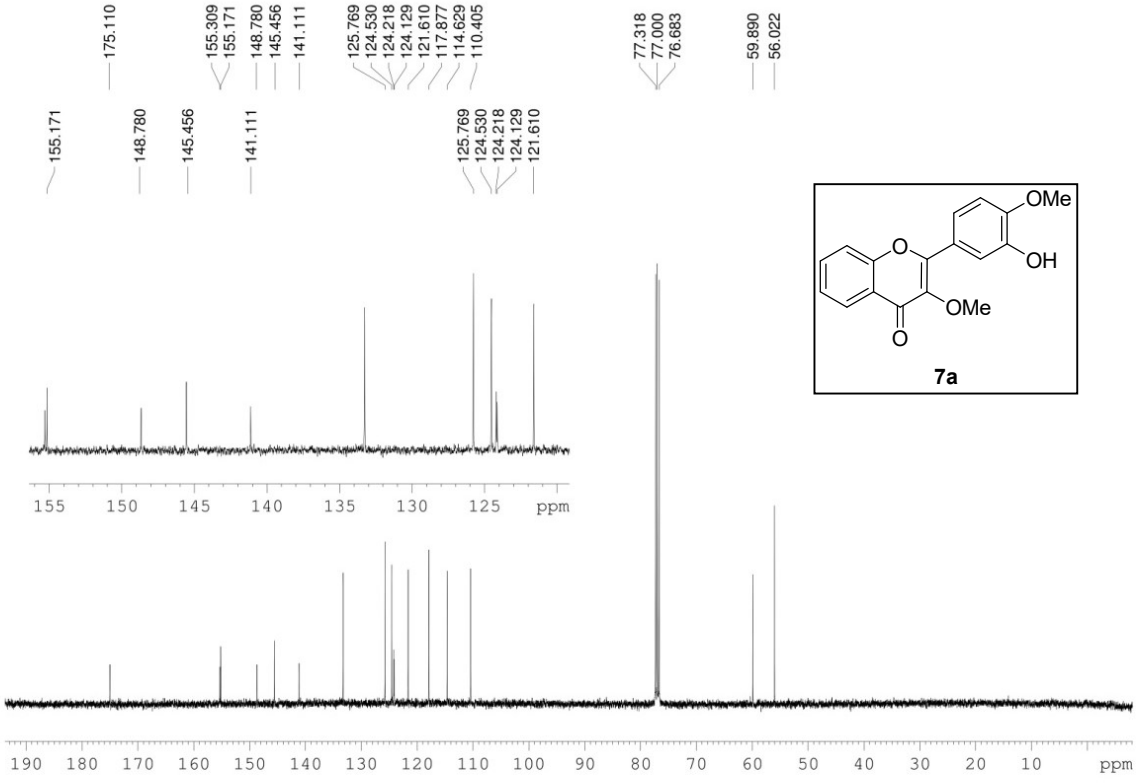

Figure 32.100 MHz ^{13}C NMR spectrum in $CDCl_3$ of compound **7a**

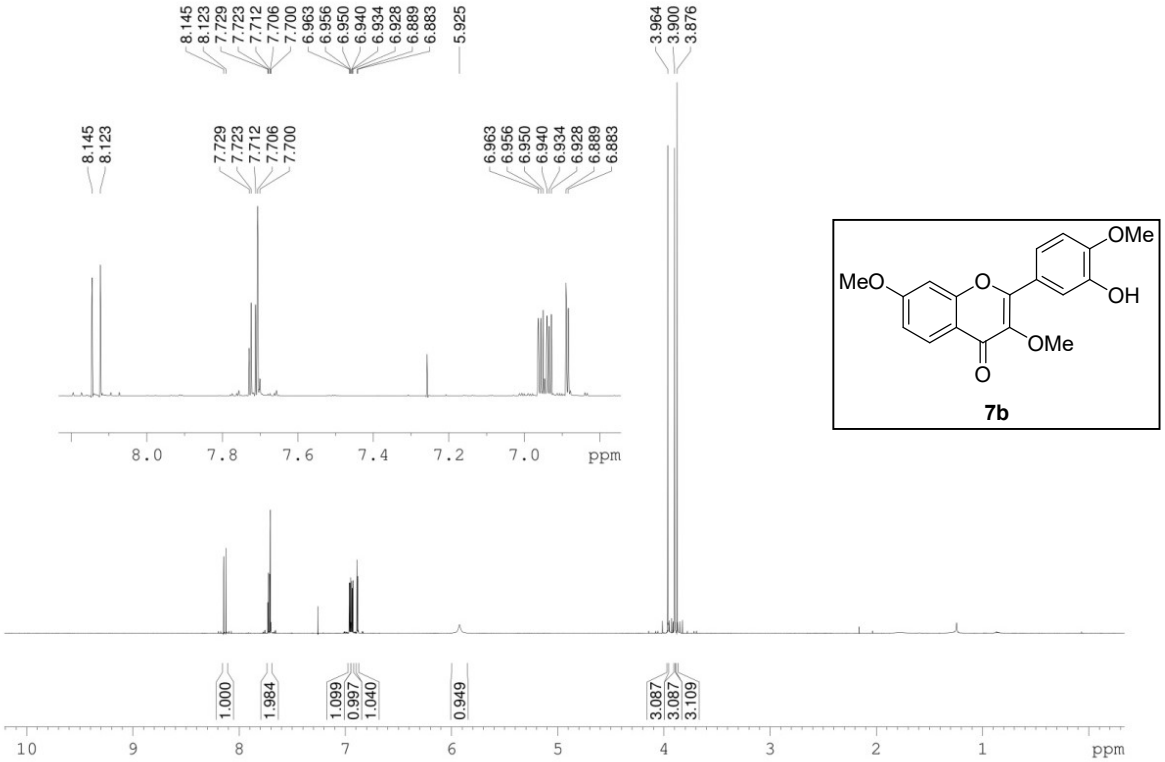

Figure 33.400 MHz ^{1}H NMR spectrum in $CDCl_3$ of compound **7b**

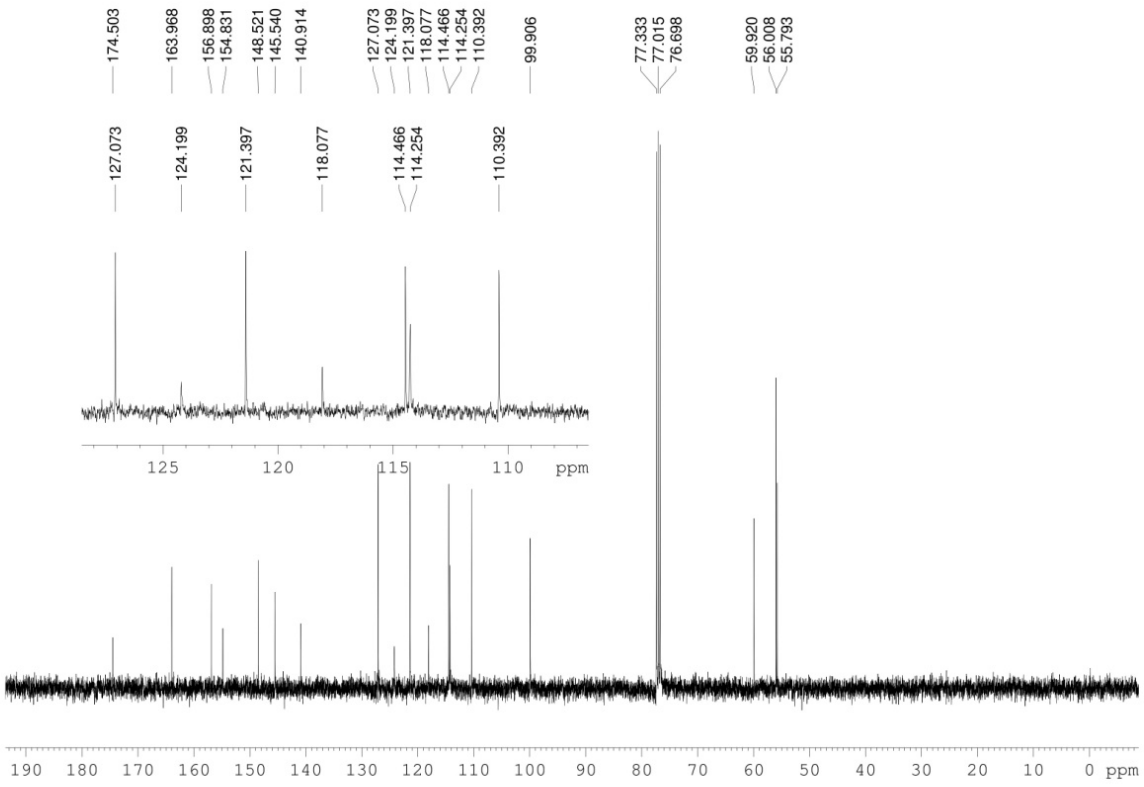

Figure 34.100 MHz ^{13}C NMR spectrum in $CDCl_3$ of compound **7b**

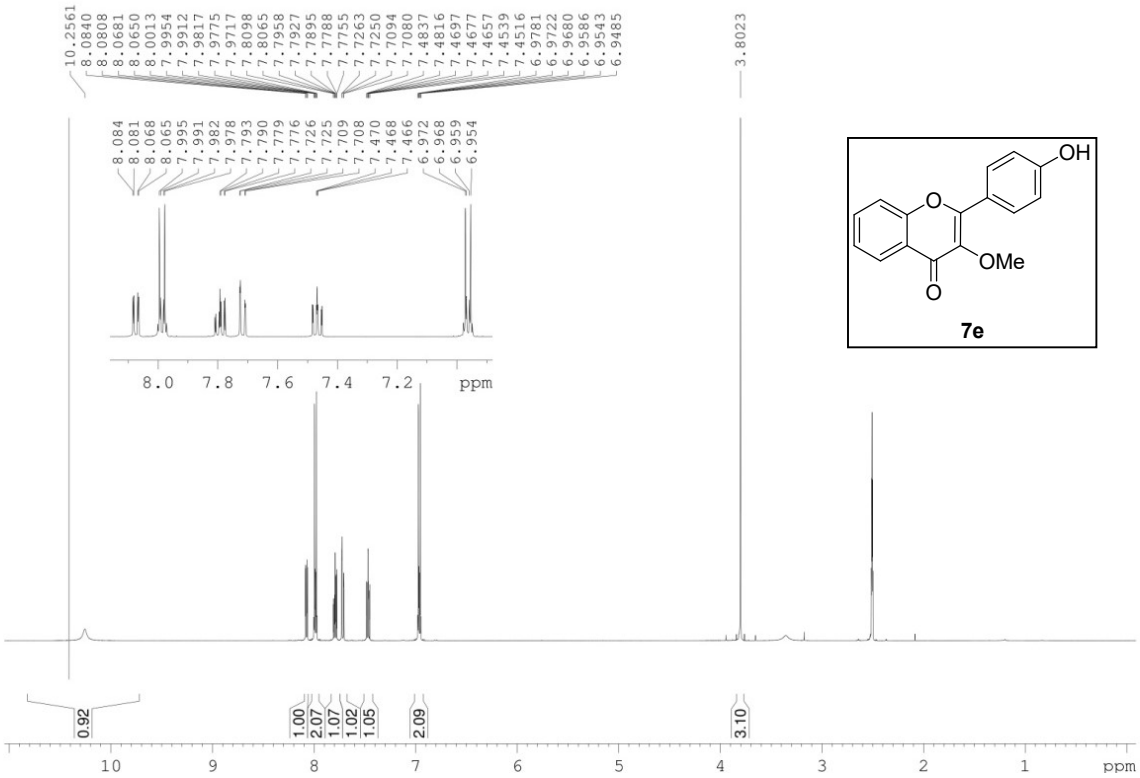

Figure 35.500 MHz ^{1}H NMR spectrum in DMSO of compound **7e**

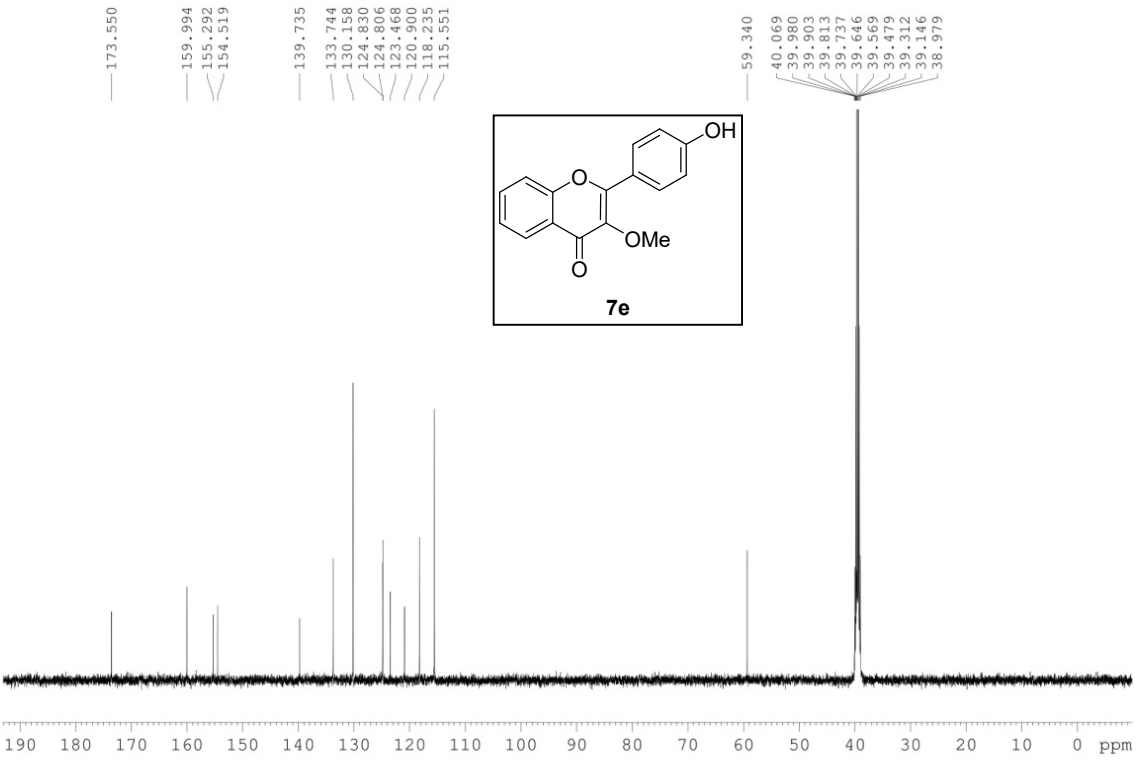

Figure 36.125 MHz ^{13}C NMR spectrum in DMSO of compound **7e**

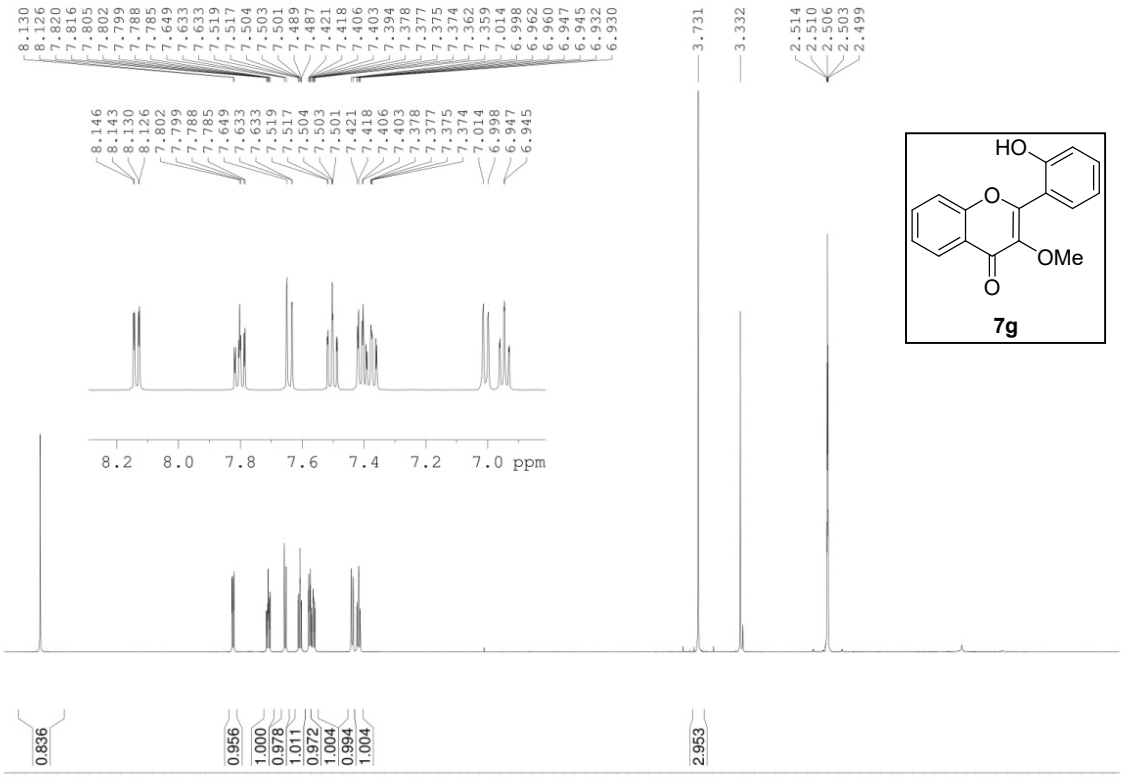

Figure 37.500 MHz ^{1}H NMR spectrum in DMSO of compound **7g**

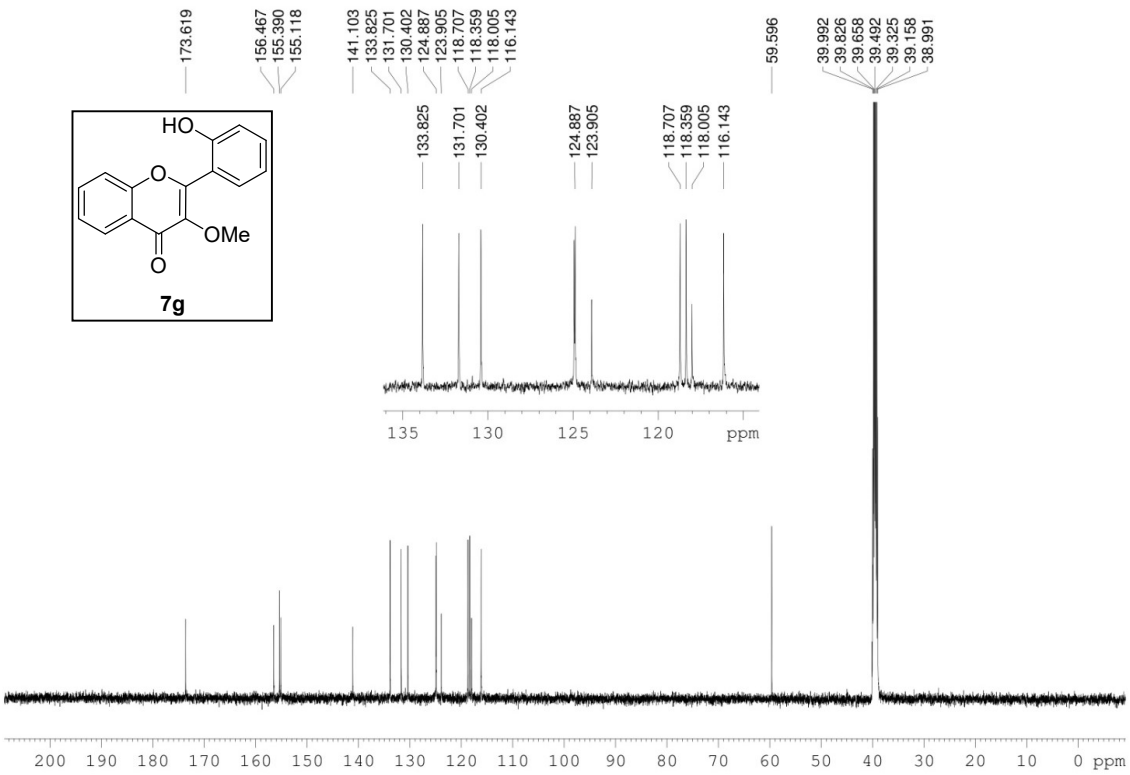

Figure 38.125 MHz ^{13}C NMR spectrum in DMSO of compound **7g**

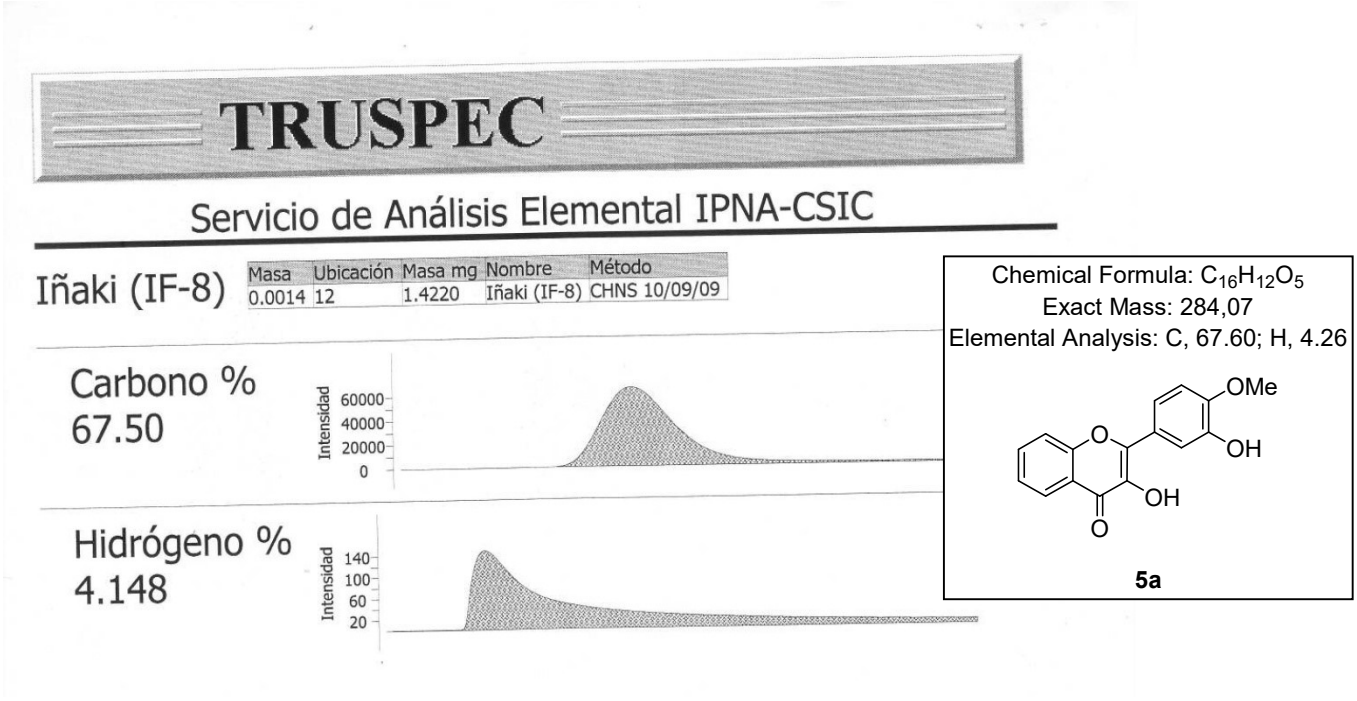

Figure 39. Elemental analysis of compound **5a**

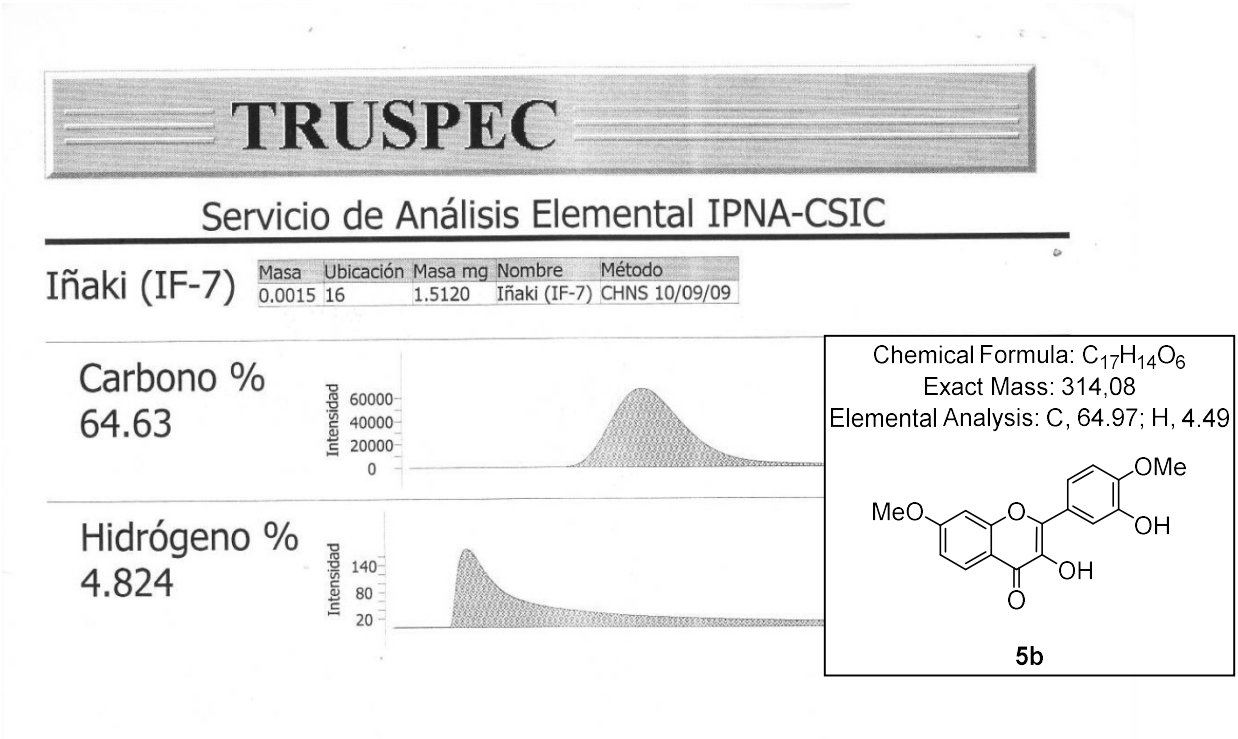

Figure 40. Elemental analysis of compound **5b**

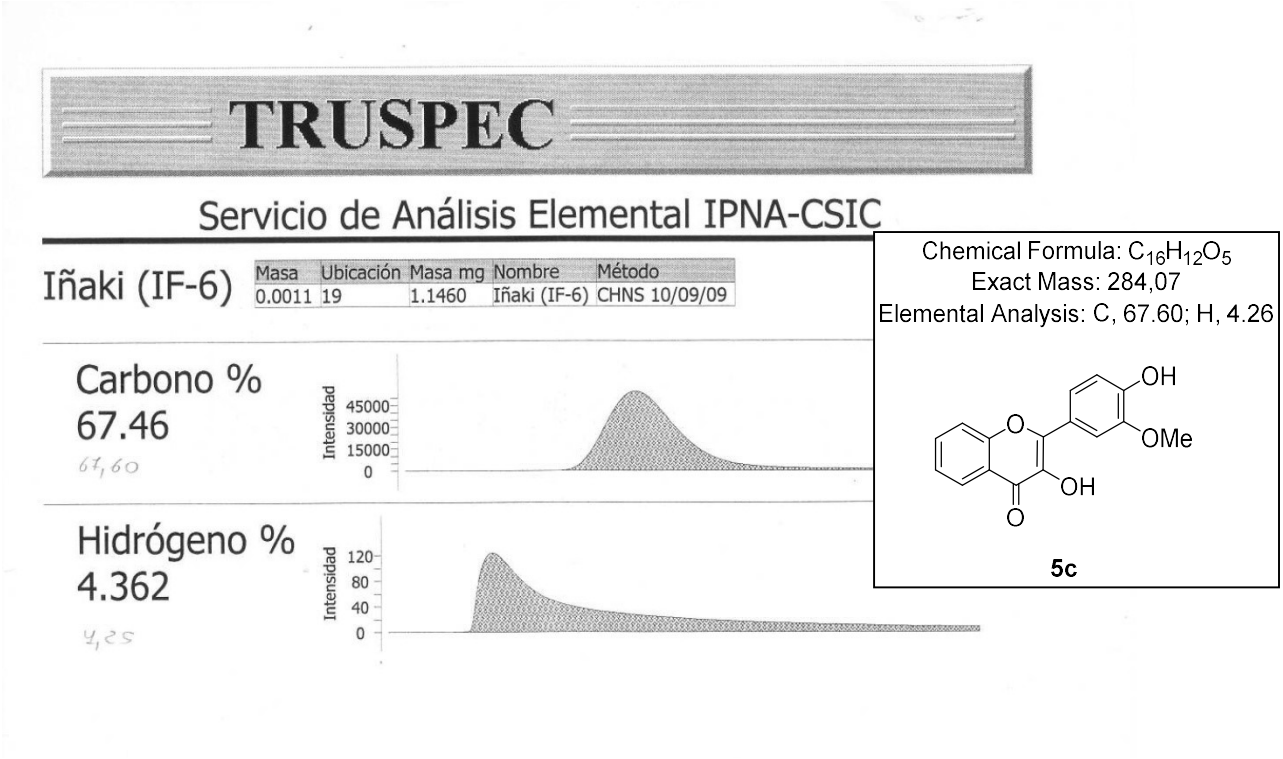

Figure 41. Elemental analysis of compound **5c**

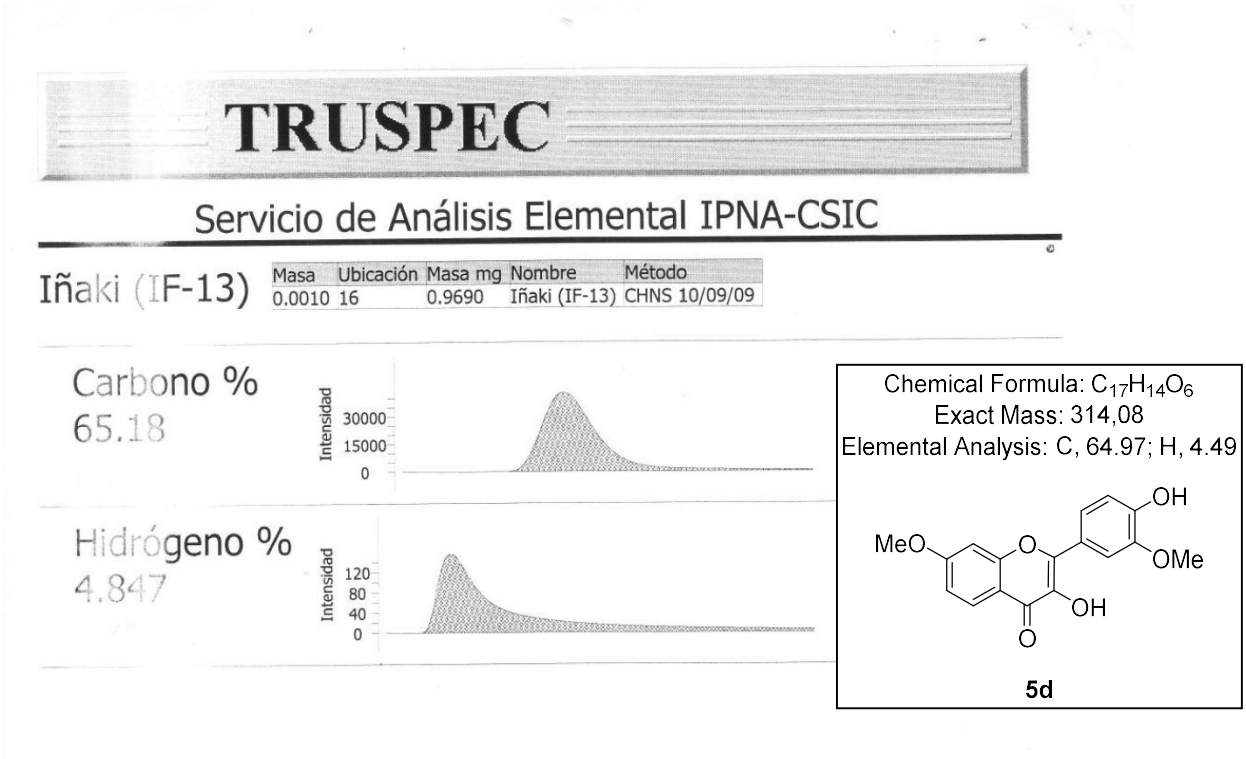

Figure 42. Elemental analysis of compound **5d**

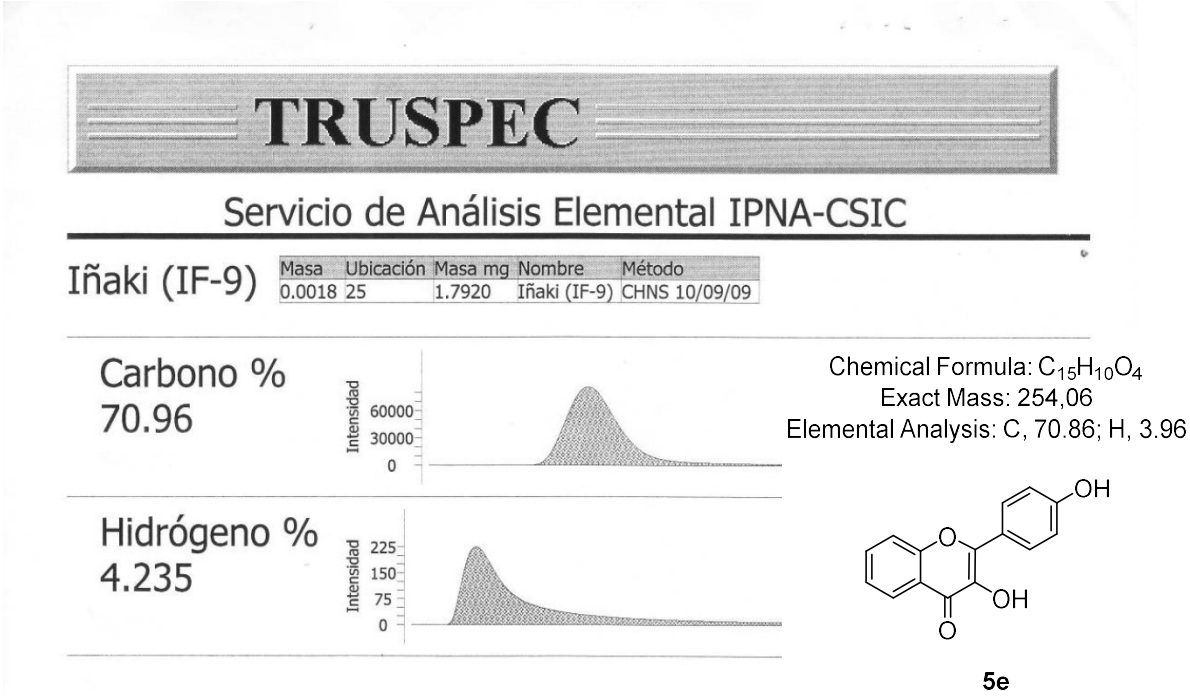

Figure 43. Elemental analysis of compound **5b**

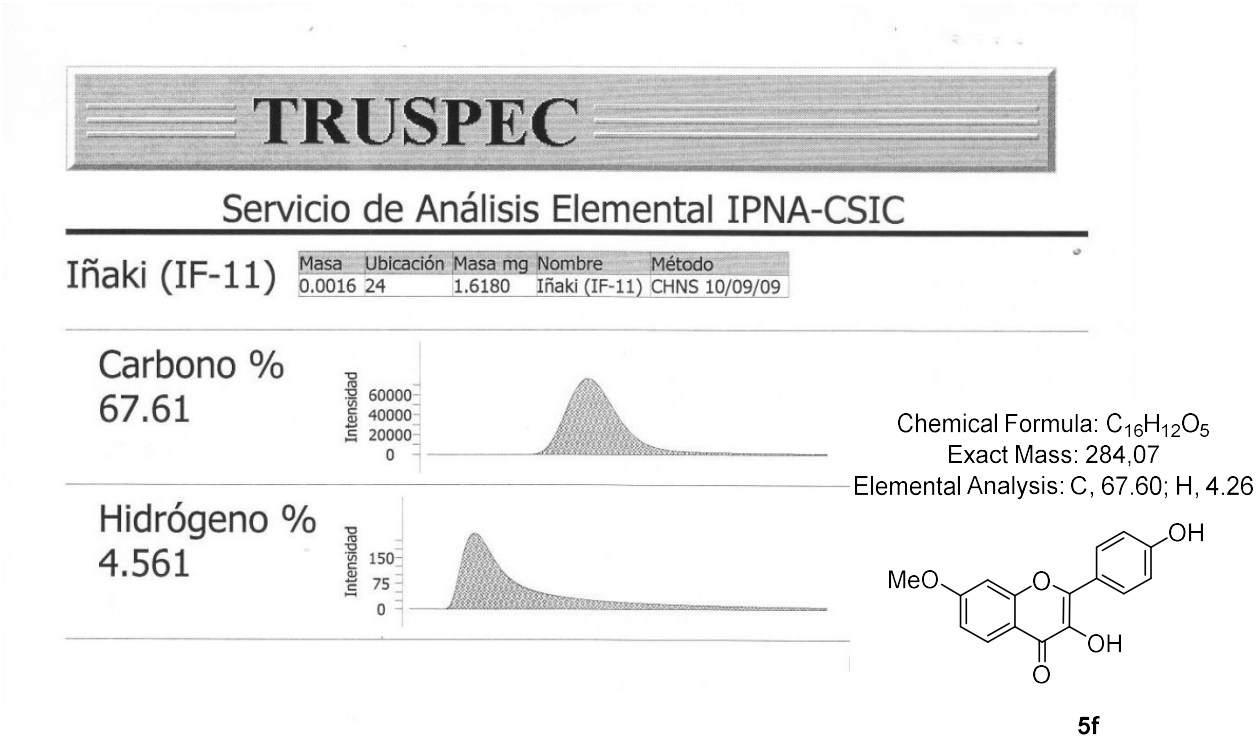

Figure 44. Elemental analysis of compound **5f**

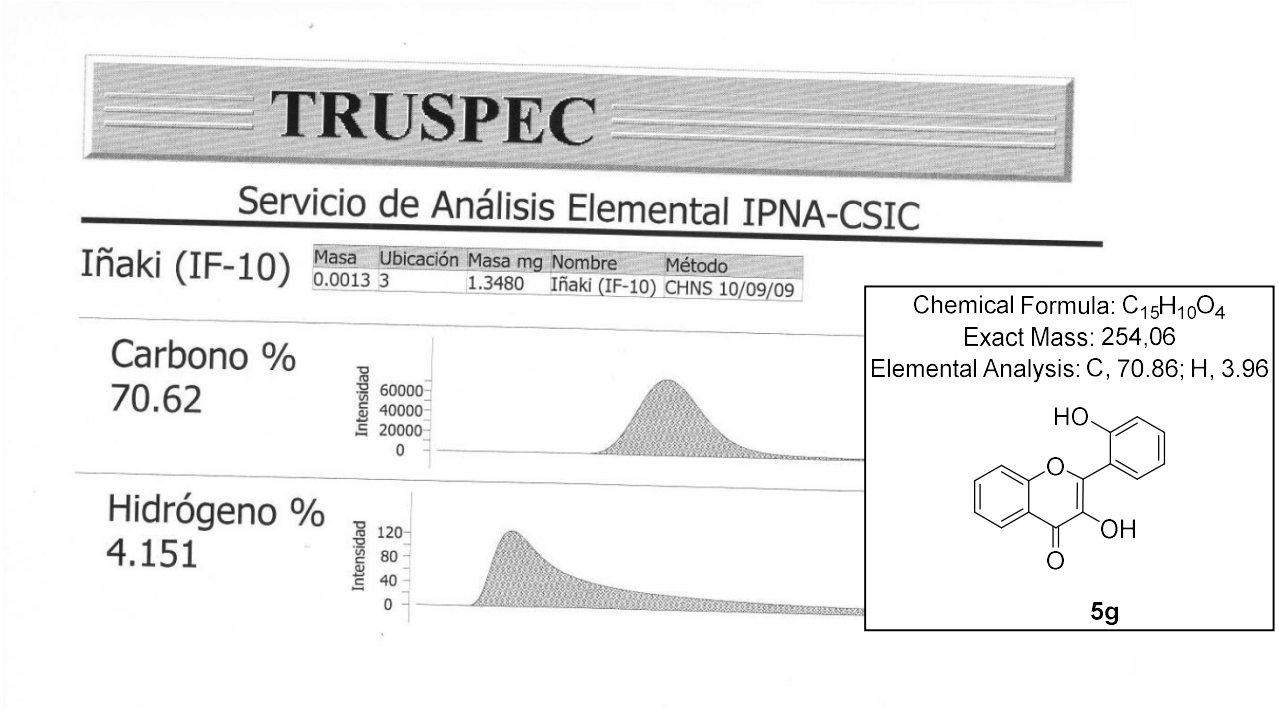

Figure 45. Elemental analysis of compound **5g**

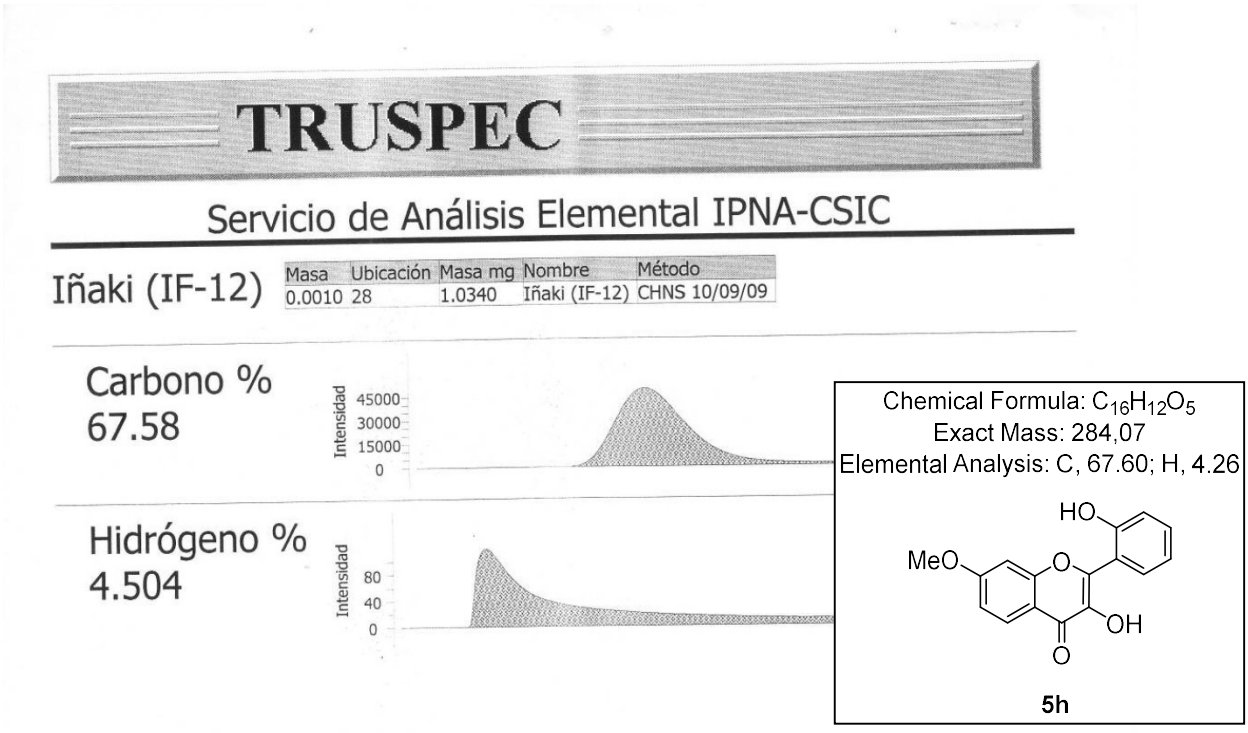

Figure 46. Elemental analysis of compound **5h**

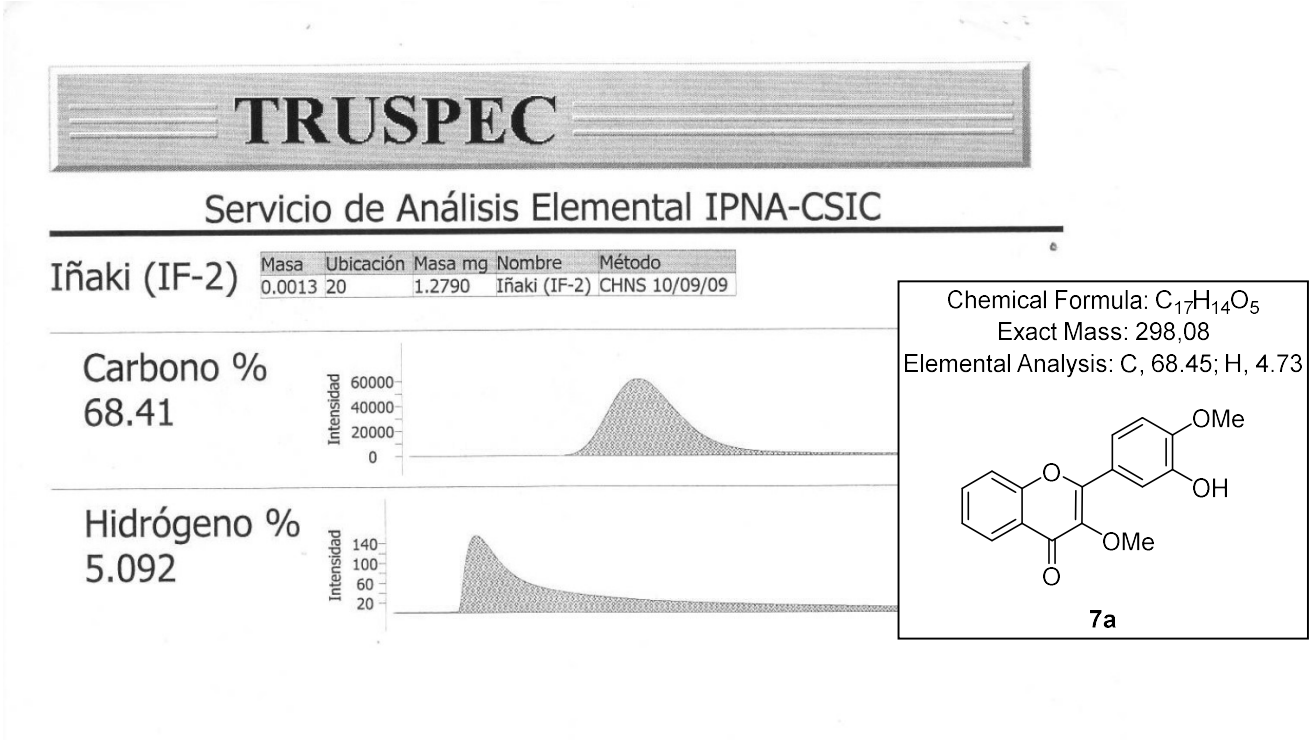

Figure 47. Elemental analysis of compound **7a**

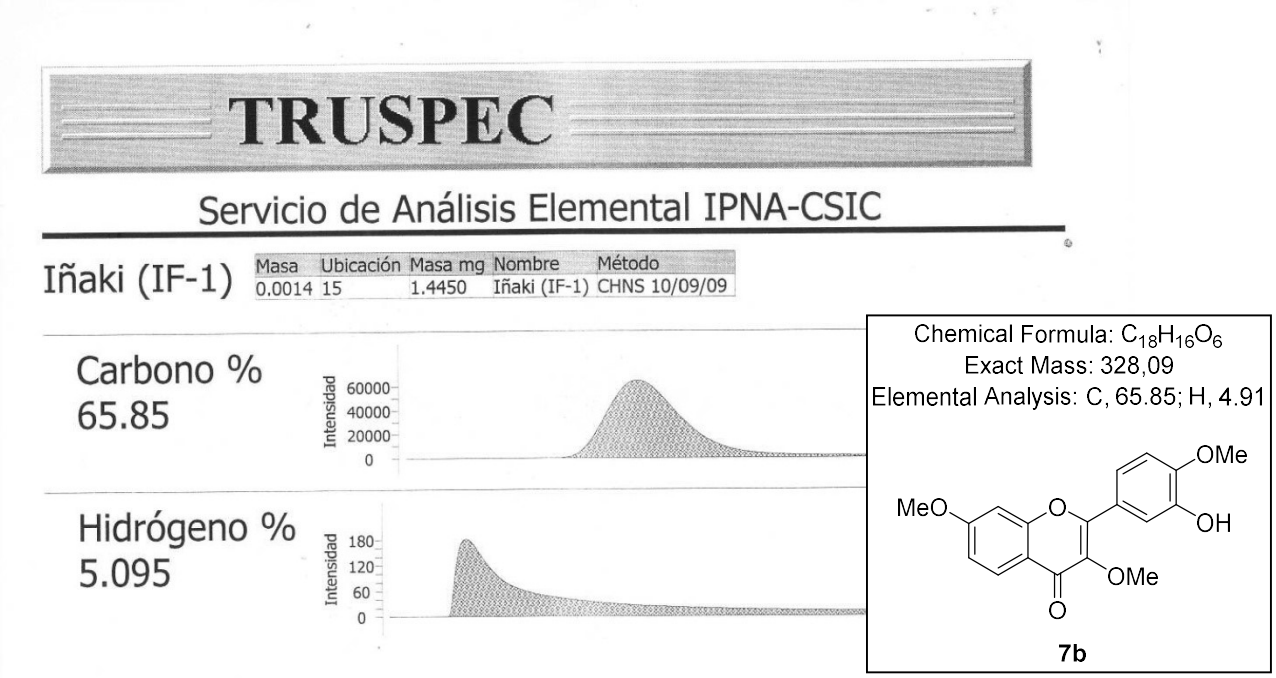

Figure 48. Elemental analysis of compound **7b**

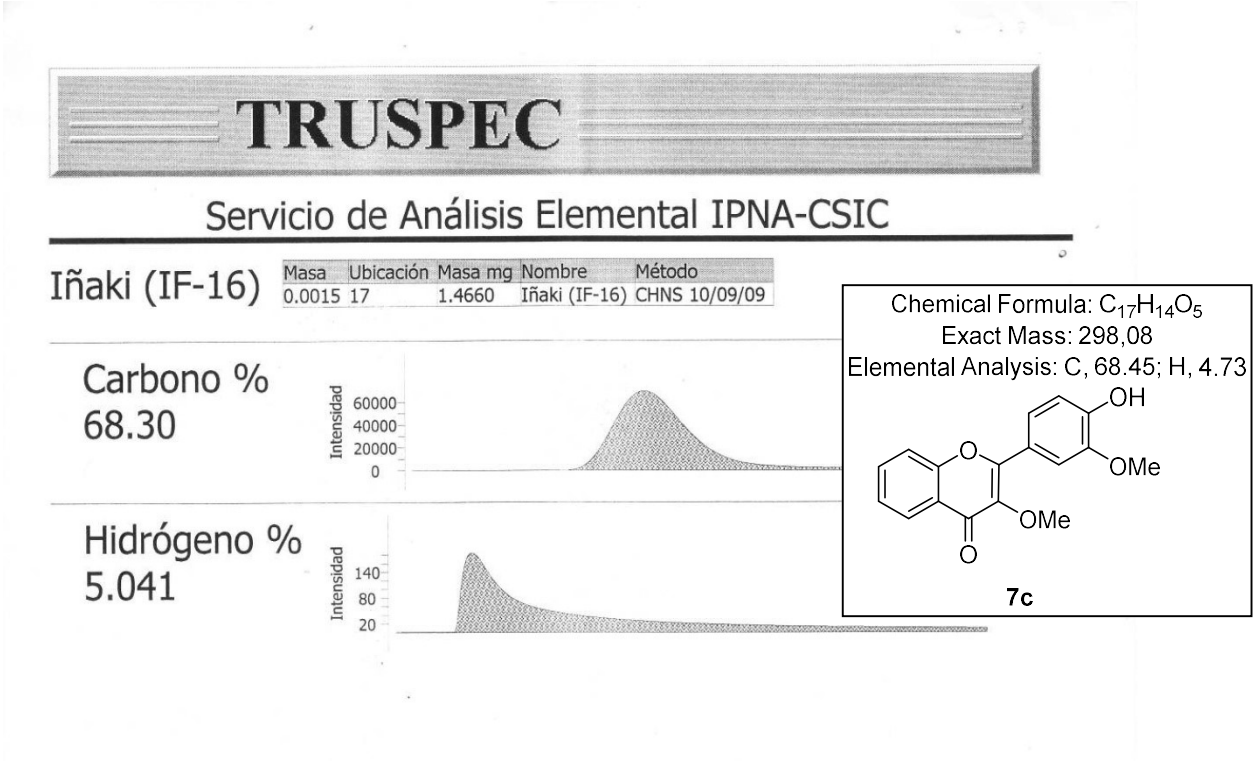

Figure 49. Elemental analysis of compound **7c**

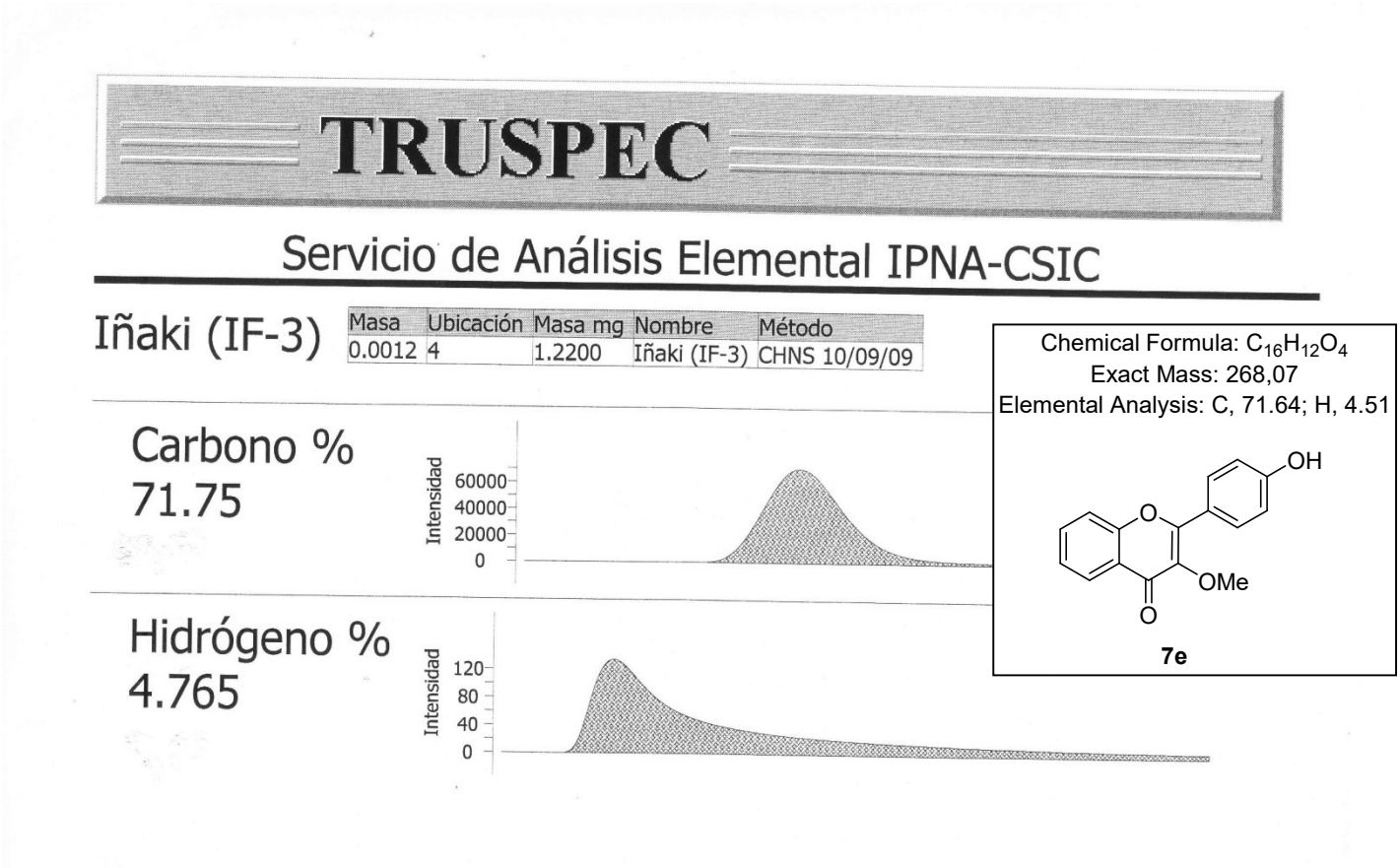

Figure 50. Elemental analysis of compound **7e**

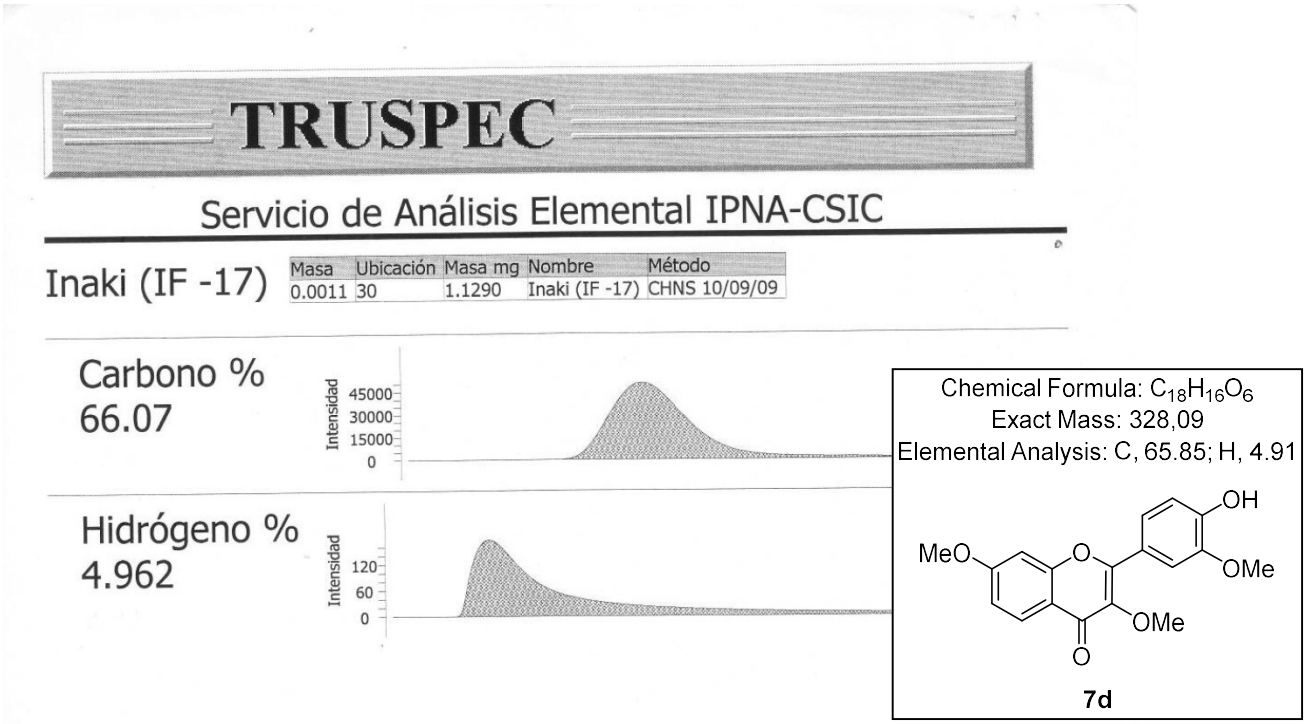

Figure 51. Elemental analysis of compound **7d**

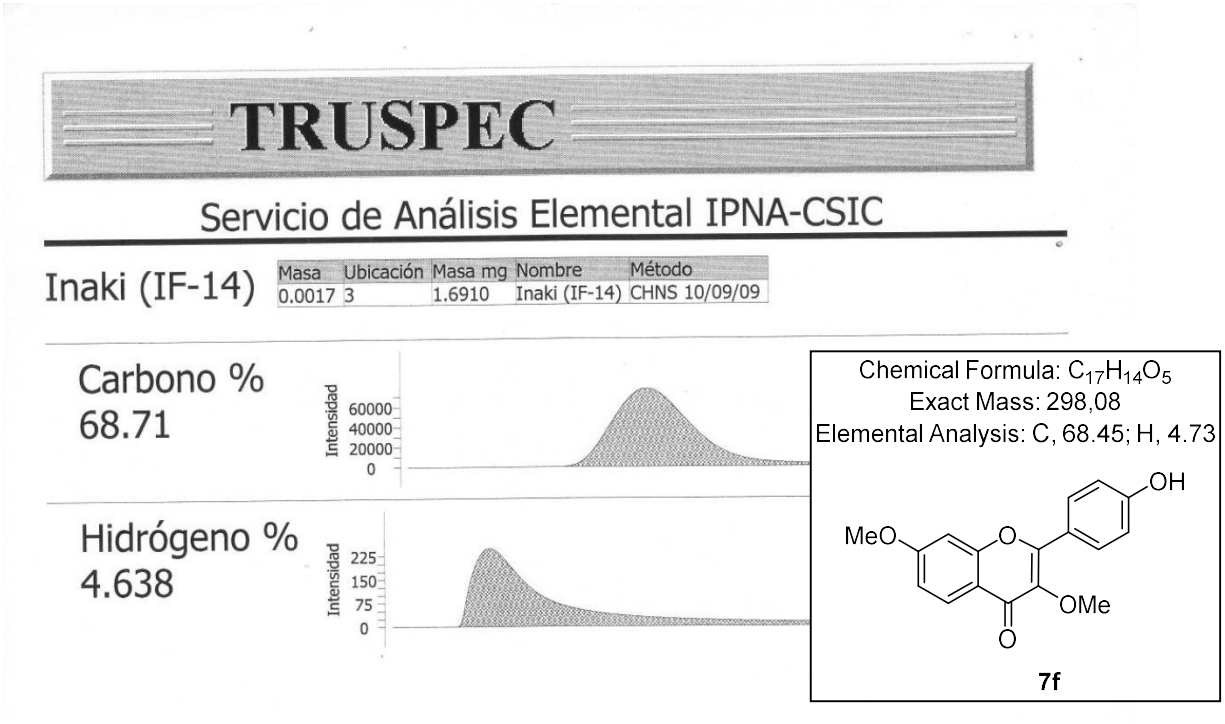

Figure 52. Elemental analysis of compound **7f**

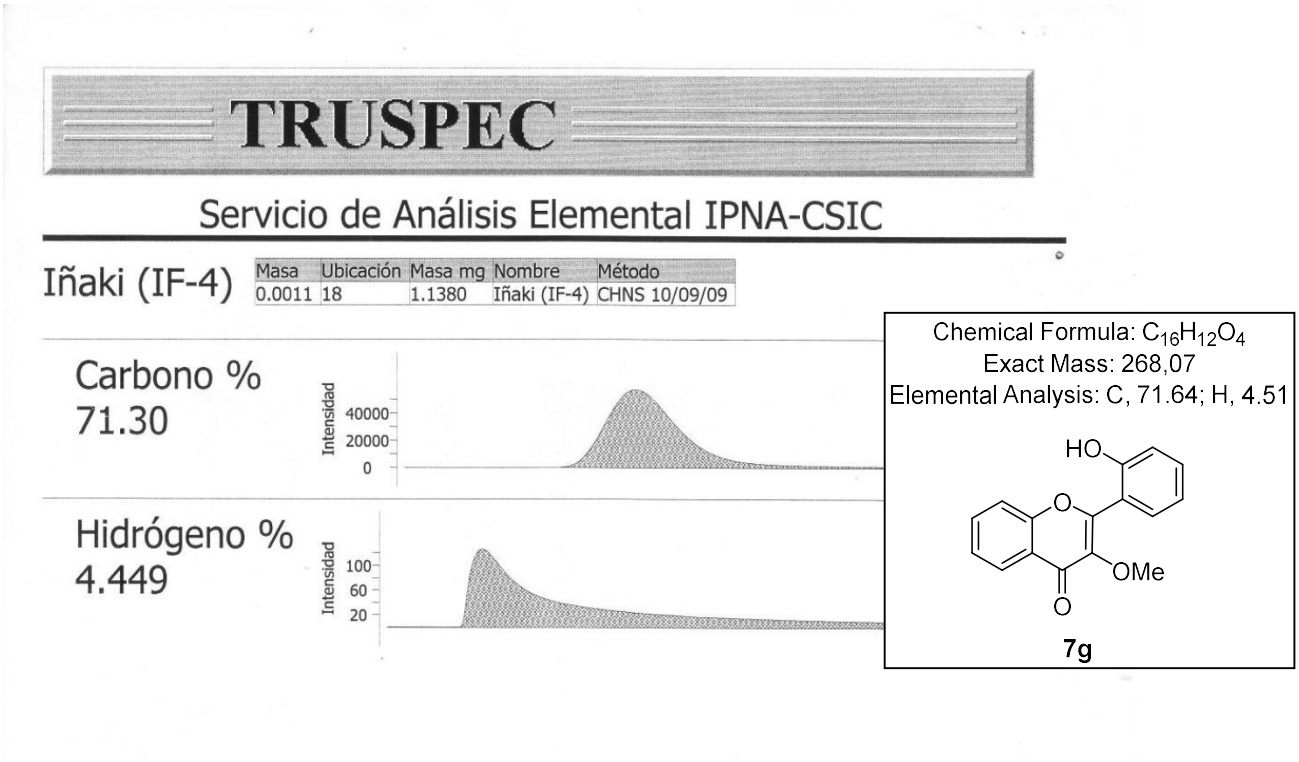

Figure 53. Elemental analysis of compound **7g**

International Journal of
Molecular Sciences

IMPACT FACTOR 6.208

Indexed in: PubMed

Article

Chlorinated Guaiane-Type Sesquiterpene Lactones as Cytotoxic Agents against Human Tumor Cells

Francisco Estévez-Sarmiento, Ester Saavedra, Mercedes Ruiz-Estévez, Francisco León, José Quintana, Ignacio Brouard and Francisco Estévez

MDPI

https://doi.org/10.3390/ijms21249767

International Journal of
Molecular Sciences

MDPI

Article

Chlorinated Guaiane-Type Sesquiterpene Lactones as Cytotoxic Agents against Human Tumor Cells

Francisco Estévez-Sarmiento [1], Ester Saavedra [1], Mercedes Ruiz-Estévez [2], Francisco León [3], José Quintana [1], Ignacio Brouard [4] and Francisco Estévez [1,*]

1 Departamento de Bioquímica y Biología Molecular, Instituto Universitario de Investigaciones Biomédicas y Sanitarias (IUIBS), Grupo de Química Orgánica y Bioquímica, Universidad de Las Palmas de Gran Canaria, Unidad Asociada al CSIC, 35016 Las Palmas de Gran Canaria, Spain; francisco.estevez103@alu.ulpgc.es (F.E.-S.); ester.saavedra102@alu.ulpgc.es (E.S.); jose.quintana@ulpgc.es (J.Q.)

2 Recombinetics, Inc., Eagan, MN 55121, USA; mercy.ruiz@recombinetics.com

3 Department of Drug Discovery and Biomedical Sciences, College of Pharmacy, University of South Carolina, Columbia, SC 29208, USA; jleon@mailbox.sc.edu

4 Instituto de Productos Naturales y Agrobiología, Consejo Superior de Investigaciones Científicas, 38206 La Laguna, Spain; ibrouard@ipna.csic.es

* Correspondence: francisco.estevez@ulpgc.es; Tel.: +34-928-451443

Received: 10 November 2020; Accepted: 16 December 2020; Published: 21 December 2020

Abstract: Guaiane-type sesquiterpene lactones are naturally occurring compounds which have attracted attention due to their array of biological activities. In this study, chlorinated guaianolides **1**–**8**, isolated from plants of the genus *Centaurea*, were evaluated against the human leukemia cell lines HL-60, U-937, a specific U-937 cell line that overexpresses the anti-apoptotic Bcl-2 protein and the human melanoma cell line SK-MEL-1. This established the relevant structure-growth inhibition relationships. Chlorohyssopifolins A (**1**), C (**3**) and D (**4**) and linichlorin A (**6**) were the most potent compounds in terms of inducing growth inhibition in the four cell lines. IC_{50} values were below 10 μM in all cases. Chlorohyssopifolins A (**1**) and D (**4**) and linichlorin A (**6**) were potent apoptotic inducers in human U-937 leukemia cells, as determined by fluorescent microscopy and flow cytometry, and their mechanism of action was associated with cytochrome *c* release, caspase activation and poly(ADP-ribose)polymerase cleavage. Overall this study shows that guaianolides induce cytotoxicity against human tumor cells and provides important insights into the cell death pathways that are involved.

Keywords: apoptosis; cytotoxicity; caspase; poly(ADP-ribose) polymerase; sesquiterpene lactone; guaianolide

1. Introduction

Natural products may be considered as starting points in the design and development of potential compounds of interest for human medicine. Sesquiterpene lactones are naturally occurring compounds that display a wide array of biological properties and are potential agents against cancer [1,2]. Guaianolides belong to a class of sesquiterpene lactones characterized by three fused rings, two five-membered rings and a seven-membered ring structure with a wide range of biological activities [3]. Some compounds of this class exhibit anti-inflammatory activity due to inhibition of the transcription factor NF-κB [4–6].

Halogenated compounds generally contain a chlorine atom and about 5000 of them have been isolated from natural sources. They have a wide range of beneficial bioactivities that have led to applications in the pharmaceutical industry. Currently, half of the molecules in high-performance

screening contain halogen atoms [6]. Many of these halogenated compounds are chlorohydrins isolated together with their corresponding epoxides [7]. Naturally occurring halogenated sesquiterpene lactones and synthetic derivatives exhibit antitumor and cytotoxic activities and have potential as anticancer agents [8,9].

Apoptosis induction is an important response to many chemotherapeutic agents. This is a mode of regulated cell death characterized by the translocation of phosphatidylserine to the outside of the plasma membrane, formation of apoptotic bodies, chromatin condensation and internucleosomal DNA fragmentation. There are at least two major apoptotic pathways, referred to as the intrinsic pathway and the extrinsic pathway, depending on the cell type [10]. The intrinsic pathway involves the translocation of cytochrome *c* from mitochondria to cytoplasm and caspase-9 activation, which cleaves and activates downstream effector caspases-3, -6 and -7, which in turn trigger the cleavage of key structural and regulatory proteins to effect cell death [11]. The extrinsic pathway involves cell surface death receptors, such as tumor necrosis factor, Fas and TRAIL receptors, and is dependent on the initiator caspase-8, which cleaves and activates the downstream effector caspases [12]. Both caspase-8 and caspase-9 activate caspase-3, which is responsible for breaking specific cellular proteins during apoptosis [13]. Caspase-3 is one of the key executioners of apoptosis, being responsible for the proteolytic cleavage of many key proteins, including the nuclear enzyme poly(ADP-ribose)polymerase which is normally involved in DNA repair [14].

In this study we analyzed the structure–cytotoxicity relationships of eight halogenated guaianolides (seven of them isolated from plants from the genus *Centaurea*, family *Asteraceae*) against human leukemia and melanoma cells. The compounds were selected from our sesquiterpene library, constructed during previous studies that had shown that guaianolides-type sesquiterpene lactones were the most cytotoxic compounds against different cancer cell lines [15]. The guaianolides assayed were isolated from natural sources as previously described [16–18]. The chlorinated guaianolides chlorohyssopifolins A (**1**), B (**2**), C (**3**), D (*4*) and E (**5**) were isolated from *Centaurea hyssopifolia* Vahl. Linichlorin A (**6**) and linichlorin C (**7**) were isolated from *Centaurea linifolia* Vahl. The compound 11,13-Dihydrochlorohyssopifolin C (**8**) was obtained from chlorohyssopifolin A through reduction with Zn-Cu followed by epoxide formation with $AgNO_3$ [18] (Figure 1). The evaluated guaianolides have the following properties in common: (i) the presence of a double bond as a methylene group at position ten (C-10); (ii) the presence of a hydroxy group and/or an acetyl group in position three of the cyclopentane ring; (iii) different substituents on C-8; and (iv) the presence of a chlorine atom either in position C-15, in the ester moiety or both. Some of the most potent compounds against human tumor cells, i.e., chlorohyssopifolins A (**1**) and D (**4**) and linichlorin A (**6**), were evaluated to determine whether the effects on cell viability were due to the activation of the apoptotic pathway. Specifically, we studied the effects on apoptosis induction and caspase activation. The aim of this study was to explore the structure–cytotoxicity relationships of eight selected sesquiterpene lactones belonging to the guaianolide class against human leukemia and melanoma cells, as well as the mechanism of action of the most potent compounds on apoptosis induction using the human leukemia cells U-937. These cells were chosen since they provided a useful model for the study of neoplasia and therapeutics [19,20]. So far, the potential use of these halogenated guaianolides in antileukemia therapy has been left largely unexplored. We evaluated whether caspase activation and the release of cytochrome *c* were involved in the mechanism of action.

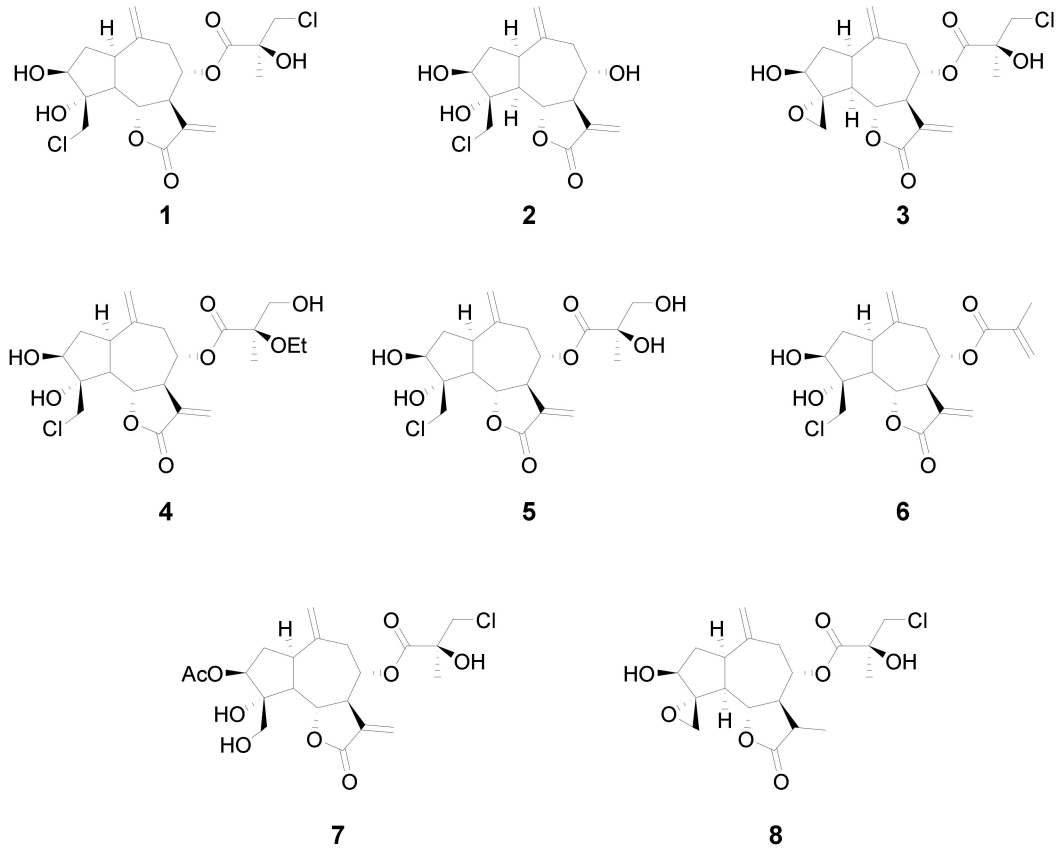

Figure 1. Chemical structures of the guaianolides assayed.

2. Results

2.1. Chlorinated Guaianolides Inhibit the Growth of Human Tumor Cells

Growth inhibition of human tumor cells in culture was determined by the 3-(4,5-dimethylthiazol-2-yl)-2,5-diphenyl-2*H*-tetrazolium bromide (MTT) dye-reduction assay. A representative microplate is shown in Figure S1. For this assay, cells were incubated with increasing concentrations of guaianolides for 72 h and concentrations inducing a 50% inhibition of cell growth (IC_{50}) values were determined by using nonlinear regression (Graph Pad 5.0 software). Guaianolides treatment resulted in a concentration-dependent inhibition of cellular proliferation, except for guaianolides **5** and **8,** which were not cytotoxic, since the IC_{50} values were greater than 30 μM (Supplementary Materials, Figure S2). Most compounds were cytotoxic against all assayed cell lines. In general, no significant differences in cytotoxicity were detected among the four cell lines (Table 1). The most potent compounds against HL-60 cells were chlorohyssopifolins A (**1**), B (**2**), C (**3**) and D (**4**) and linichlorins A (**6**) and C (**7**), with IC_{50} values between 1.2 μM and 7.5 μM, and the less potent compounds were chlorohyssopifolin E (**5**) and 11,13-dihydrochlorohyssopifolin C (**8**). Similar results were obtained for the histiocytic lymphoma U-937 cells. To explore whether the survival protein Bcl-2 is able to protect cells from guaianolides cytotoxicity, the effect against U-937 cell overexpressing Bcl-2 was compared with the parental U-937 cells. As shown in Table 1, the overexpression of Bcl-2 did not protect cells against cytotoxicity. The effects of these guaianolides were also assessed in a melanoma cell line. Melanoma is the most aggressive type of skin cancer and is resistant to most novel therapies. The results revealed that the SK-MEL-1 melanoma cells were also sensitive to the cytotoxic effects of the guaianolides assayed, with chlorohyssopifolin A (**1**) and linichlorin A (**6**) being the most potent compounds, although chlorohyssopifolins C (**3**) and D (**4**) yielded IC_{50} values below 10 μM (Table 1).

Table 1. Effects of guaianolides on cell viability of human tumor cell lines.

	IC_{50} (μM)			
	HL-60	**U-937**	**U-937/Bcl-2**	**SK-MEL-1**
Chlorohyssopifolin A (**1**)	5.9 ± 0.9	2.9 ± 1.2	1.7 ± 1.5	3.4 ± 0.6
Chlorohyssopifolin B (**2**)	7.5 ± 1.5	9.2 ± 2.7	13.4 ± 3.7	11.5 ± 2.0
Chlorohyssopifolin C (**3**)	4.1 ± 2.1	5.2 ± 2.5	1.2 ± 0.8	6.9 ± 0.9
Chlorohyssopifolin D (**4**)	4.9 ± 1.8	3.9 ± 1.4	1.0 ± 0.6	7.6 ± 1.4
Chlorohyssopifolin E (**5**)	–	–	–	–
Linichlorin A (**6**)	1.2 ± 0.6	1.9 ± 0.5	2.9 ± 1.8	3.6 ± 1.3
Linichlorin C (**7**)	4.9 ± 1.7	5.0 ± 0.4	12.8 ± 1.9	10.5 ± 0.4
11,13-Dihydrochlorohyssopifolin C (**8**)	–	–	–	–

The IC_{50} values were calculated from cells treated for 72 h using the methodology described in the Materials and Methods section. The data shown represent the mean ± SD of 3–5 independent experiments with three determinations each. – means not active, IC_{50} values > 30 μM. HL-60, U-937, U-937/Bcl-2: acute myeloid leukemia; SK-MEL-1: melanoma.

The following structure–cytotoxicity relationships were established from the IC_{50} values in the cancer cells assayed: (i) the presence of the α-methylene-γ-lactone functional group is essential for cytotoxicity; (ii) the presence of an ester group on C-8 can both increase (**1** vs. **2**) (at least against U-937, U-937/Bcl-2 and SK-MEL-1) or decrease cytotoxicity (**2** vs. **5**) because it is dependent on the hydrophobicity of the radical; (iii) the introduction of an epoxide functional group on the C-4 of the cyclopentane ring has no effect on cytotoxicity; and (iv) the introduction of an additional alkylating group on the C-8 enhances cytotoxicity (**2** vs. **6**).

To compare the cytotoxic effects of the guaianolides analyzed in this report, we included etoposide as a positive control in all MTT experiments. The IC_{50} values for etoposide were 0.5 ± 0.2 μM, 1.5 ± 0.3 μM and 9.0 ± 3.5 μM in HL-60, U-937 and SK-MEL-1 cells, respectively.

The visualization of the human tumor cells after treatment with the selected guaianolides chlorohyssopifolins A (**1**) and D (**4**) and linichlorin A (**6**) revealed important morphological changes as well as an important reduction in the number of cells (Figure 2).

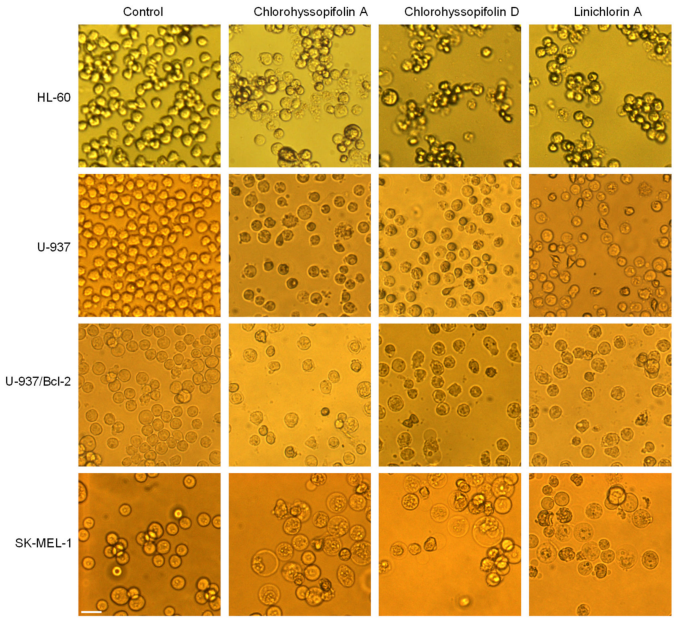

Figure 2. Cells were incubated with dimethylsulfoxide (DMSO) (control) or 10 μM of the compounds shown at the top of the figure for 24 h and images were obtained with an inverted phase-contrast microscope. Original magnification 20×. Bar represents 10 μm.

2.2. Chlorinated Guaianolides Induce Apoptotic Cell Death

In order to determine the mechanism involved in the cytotoxicity induced by chlorohyssopifolins A (**1**) and D (**4**) and linichlorin A (**6**), nuclear morphology was evaluated by fluorescent microscopy after DNA staining with Hoechst 33,258. Cells treated with these guaianolides showed fragmented and condensed chromatin characteristics of apoptotic cell death (Figure 3).

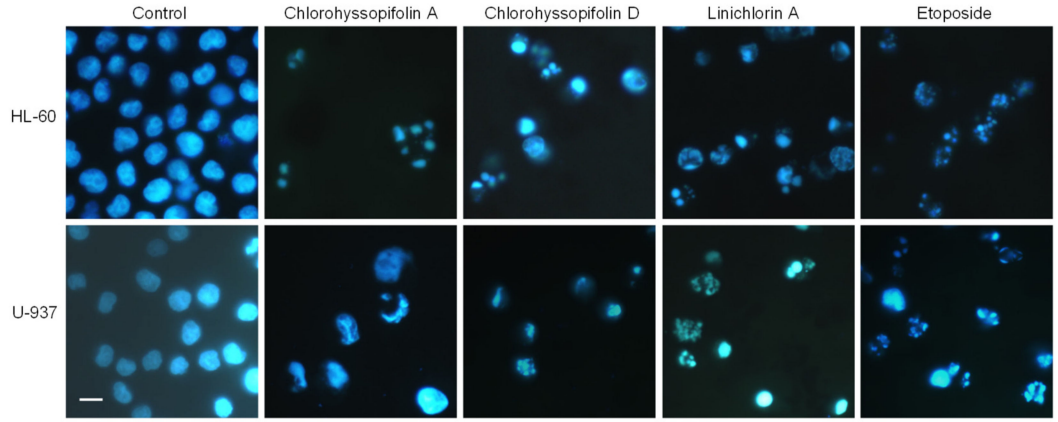

Figure 3. Cells were treated with the indicated guaianolides at a concentration of 10 μM for 24 h, stained with Hoechst 33,258 and visualized under a fluorescence microscope. Etoposide (3 μM) was included as a positive control. Original magnification 40×. Bar represents 10 μm.

To confirm that the specified guaianolides induce apoptotic cell death, HL-60 and U-937 cells were treated with the selected compounds, analyzed by flow cytometry after propidium iodide staining and the percentage of apoptotic cells (sub-G_1 fraction) was determined (Figure 4a). The results showed that the percentages of apoptotic cells increased approximately 16-fold (32.0 ± 9.5% vs. 2.0 ± 0.8%), 14-fold (27.5 ± 6.5% vs. 2.0 ± 0.8%), 13-fold (26.0 ± 5.5% vs. 2.0 ± 0.8%) and 13-fold (25.1 ± 3.5% vs. 2.0 ± 0.8%) in HL-60 cells after 24-h exposure of chlorohyssopifolins A (**1**), C (**3**) and D (**4**) and linichlorin A (**6**), respectively. In U-937 cells, the percentages of apoptotic cells increased approximately 10-fold (16.7 ± 5.2% vs. 1.7 ± 0.8%), 12-fold (21.0 ± 4.0% vs. 1.7 ± 0.8%), 19-fold (32 ± 5.7% vs. 1.7 ± 0.8%) and 12-fold (20.1 ± 3.5% vs. 1.7 ± 0.8%) after exposure to chlorohyssopifolins A (**1**), C (**3**) and D (**4**) and linichlorin A (**6**), respectively (Figure 4b). These results reveal that chlorohyssopifolins A (**1**), C (**3**) and D (**4**) and linichlorin A (**6**) were the most potent compounds in inducing apoptosis in U-937 and HL-60 cells. Due to limited availability of naturally occurring compounds, we selected chlorohyssopifolins A (**1**) and D (**4**) and linichlorin A (**6**) for additional experiments.

2.3. Chlorohyssopifolins A (1) and D (4) and Linichlorin A (6) Induce Externalization of Phosphatidylserine, Poly(ADP-ribose)Polymerase (PARP) Cleavage and Cytochrome c Release

Apoptosis induction in U-937 cells was also determined by double staining with annexin V-FITC and propidium iodide and analysis by flow cytometry. As shown in Figure 5a, chlorohyssopifolins A (**1**) and D (**4**) and linichlorin A (**6**) induce phosphatidylserine translocation to the cell surface. A hallmark of apoptosis that indicates caspase activation is cleavage of poly(ADP-ribose)polymerase (PARP), an enzyme involved in DNA repair and a known substrate for caspase-3. To determine whether these guaianolides induce PARP cleavage, U-937 cells were treated with 10 μM of compounds for 24 h and lysates were analyzed by immunoblotting. The results revealed that the guaianolides induced the hydrolysis of the 116 kDa full-length PARP protein to yield the 85 kDa fragment (Figure 5b).

The mitochondrial apoptotic pathway involves the release of cytochrome *c* from mitochondria. To investigate whether guaianolides promote cytochrome *c* release, cytosolic fractions were analyzed using Western blotting. As shown in Figure 5c, guaianolides treatment resulted in a concentration-dependent release of the mitochondrial protein cytochrome *c* into the cytosol.

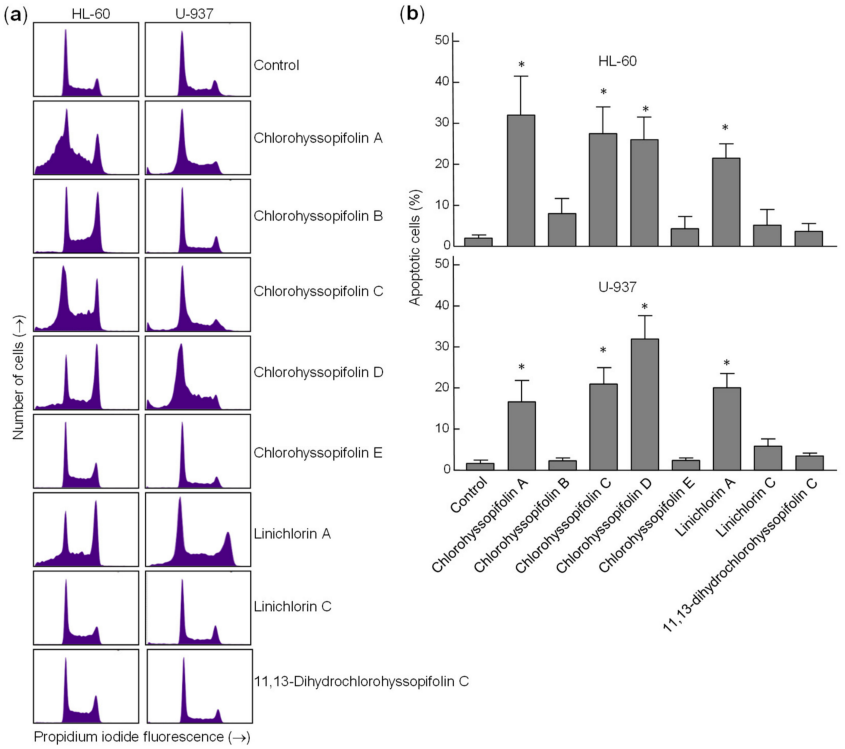

Figure 4. Increase in percentage of apoptotic cells (sub-G_1 fraction) due to guaianolides. (**a**) Representative histograms of flow cytometry experiments after propidium iodide staining of cells incubated in the presence 10 μM of the indicated guaianolides for 24 h. (**b**) Cells were treated as above and the percentages of apoptotic cells were determined by flow cytometric analysis after propidium iodide staining. Bars represent means ± S.D. of two independent experiments each performed in triplicate. * $p < 0.05$, significantly different from untreated control.

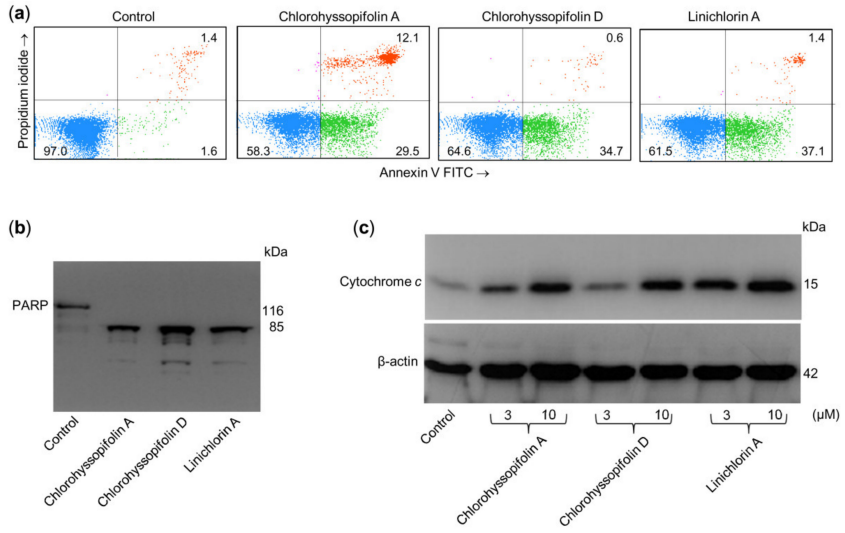

Figure 5. Chlorohyssopifolins A (**1**) and D (**4**) and linichlorin A (**6**) are potent apoptotic inducers in U-937 cells. (**a**) Cells were incubated in the presence of 10 μM of the indicated guaianolides and subjected to flow cytometric analysis after double staining with Annexin V-FITC and propidium iodide. (**b**) Cells were treated as above and Poly(ADP-ribose) polymerase cleavage was determined using Western blot analysis. (**c**) Cytochrome *c* release induced by the specified compounds at the indicated concentrations was analyzed using Western blotting.

2.4. Bcl-2 Over-Expression Did Not Block Apoptosis Induction by Chlorohyssopifolins A (**1**) *or D* (**4**) *or Linichlorin A* (**6**)

Human B-cell lymphoma-2 (Bcl-2) is a key protein involved in apoptosis inhibition through its regulation of mitochondrial membrane potential and cytochrome *c* release needed for the activation of caspase-9. Therefore, it should be interesting to clarify whether this protein is able to protect cells against the increase of apoptotic cells triggered by chlorohyssopifolins A (**1**) and D (**4**) and linichlorin A (**6**). To this end, we tested the cell line overexpressing Bcl-2 (U-937/Bcl-2) and observed that the overexpression of this survival factor did not block apoptosis triggered by chlorohyssopifolin A (**1**) or linichlorin A (**6**), but weakly decreased the percentage of apoptotic cells induced by chlorohyssopifolin D (**4**) (Figure 6a,b). As shown in Figure 6, the percentages of apoptotic cells increased approximately 8-fold (16.3 ± 1.0% vs. 2.0 ± 0.8%), 11-fold (21.8 ± 2.5% vs. 2.0 ± 0.8%) and 11-fold (22.2 ± 1.8% vs. 2.0 ± 0.8%) after 24 h of treatment with chlorohyssopifolins A (**1**) and D (**4**) and linichlorin A (**6**), respectively. These increases in the percentages of apoptotic cells were similar to those obtained in the parental U-937 cells indicated above except for those of chlorohyssopifolin D (**4**). For this compound the percentages of apoptotic cells increased to 30% and 22% for U-937 and U-937/Bcl-2, respectively. It is important to note that the flow cytometry experiments were carried out after 24 h of treatment. However, as indicated above, these guaianolides were able to induce cell death and showed similar IC_{50} values in both cell lines, i.e., the U-937 cell line overexpressing human Bcl-2 protein (U-937/Bcl-2) and the parental U-937 cell line, as determined by the MTT assay which was performed for 72 h (Table 1). These results indicate that, in addition to apoptosis, other mechanisms that induce cell growth inhibition in U-937/Bcl-2, such as cell cycle arrest, may be involved by these guaianolides.

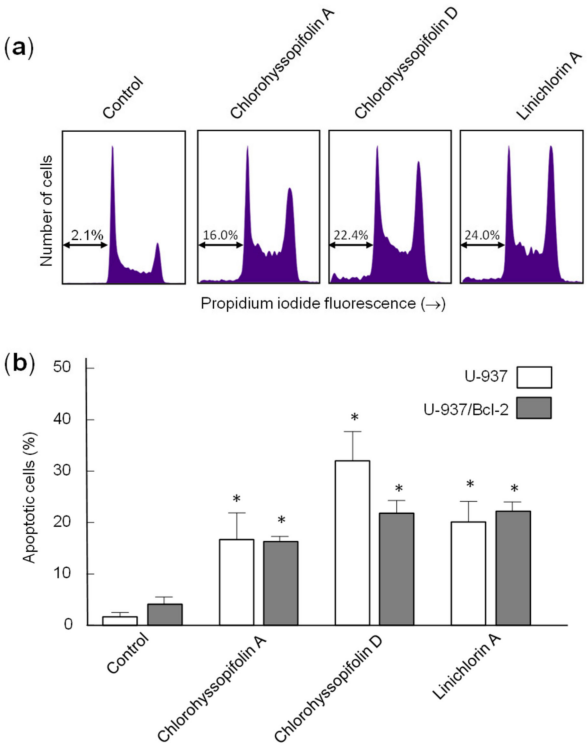

Figure 6. (**a**) Representative histograms obtained by flow cytometry after staining the U-937/Bcl-2 cells with propidium iodide. (**b**) Cells were incubated in the absence or presence of the indicated guaianolides at 10 μM concentration for 24 h and the percentages of apoptotic cells were determined by flow cytometric analysis after propidium iodide staining. Bars represent means ± S.D. of two independent experiments each performed in triplicate. * $p < 0.05$, significantly different from untreated control.

2.5. Chlorohyssopifolins A (**1**) *and D* (**4**) *and Linichlorin A* (**6**) *Stimulate Caspase Activity and Processing*

To define which caspases were involved during apoptosis induced by the selected guaianolides, the enzymatic activity of lysates on tetrapeptide substrates LEHD-*p*NA (for caspase-9), IETD-*p*NA (for caspase-8) and DEVD-*p*NA (for caspase-3/7) was analyzed after 24-h exposure to chlorohyssopifolins A (**1**) and D (**4**) and linichlorin A (**6**). As shown in Figure 7a, there was an approximately twofold increase in caspase-9 activity in response to chlorohyssopifolins A (**1**) and D (**4**) and a fourfold increase after treatment with linichlorin A (**6**). A similar activation of caspase-8 was also observed. The executioner caspase-3/7 activity increased approximately twofold, fivefold and sevenfold after treatment with chlorohyssopifolins A (**1**) and D (**4**) and linichlorin A (**6**), respectively. Processing of initiator caspases, caspase-8 and -9, as well as the main executioner caspase, caspase-3, was also investigated. To this end, cells were treated with chlorohyssopifolins A (**1**) and D (**4**) and linichlorin A (**6**) for 24 h and lysates were analyzed using Western blotting. The results showed processing of pro-caspase-3 by the three guaianolides in U-937 cells (Figure 7b). Processing of caspase-8 and -9 was also detected, linichlorin A (**6**) being the most potent compound in inducing procaspase processing, in accordance with enzymatic activities of caspase-3-like proteases (caspase-3/7) and of caspase-8 and -9.

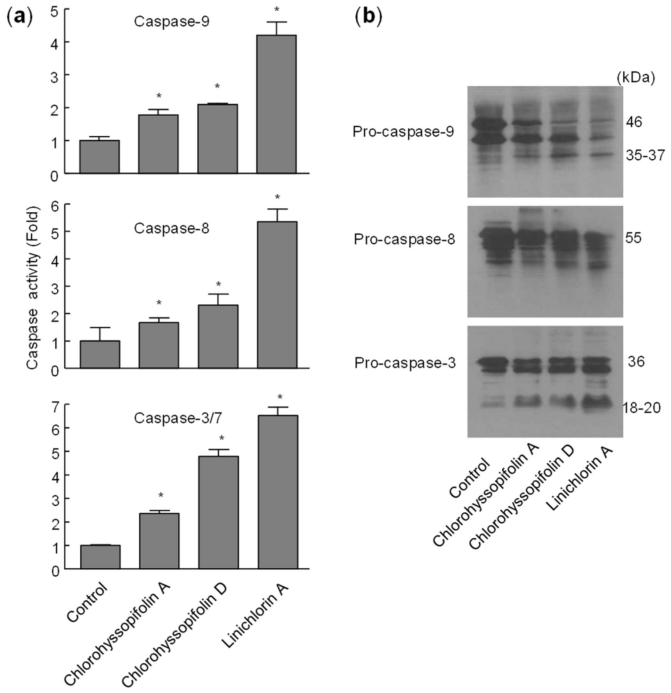

Figure 7. Chlorohyssopifolins A (**1**) and D (**4**) and linichlorin A (**6**) induce activation and processing of caspases in U-937 cells. (**a**) Cells were treated with 10 μM of the indicated guaianolide, harvested at 24 h and cell lysates were assayed for caspase-9, caspase-8 and caspase-3/7 activities using colorimetric substrates. Results are expressed as factorial increases in caspase activity compared with the control. Values represent means ± S.D. of two independent experiments each performed in triplicate. * $p < 0.05$, significantly different from untreated control. (**b**) Processing of caspases in response to chlorohyssopifolins A (**1**) and D (**4**) and linichlorin A (**6**). Cells were incubated with 10 μM of the indicated guaianolide for 24 h and the corresponding caspases were determined by Western blot analysis.

3. Discussion

In recent years there has been a renewed interest in naturally occurring compounds as potential chemopreventive and chemotherapeutic treatments against cancer. It is estimated that about 60% of compounds that are used in the fight against cancer may be considered as derived from natural products. Among these compounds, sesquiterpene lactones have received considerable attention

in the last 20 years [21]. Sesquiterpenes are compounds of fifteen carbon atoms with different skeletons, mainly (but not exclusively) germacrane, guaiano and eudesmane skeletons. Sesquiterpene lactones are characterized by an α-methylene-γ-lactone functional group which acts as an electrophile group able to react with specific nucleophiles functional groups in Michael-type addition reaction [4]. The germacranolide parthenolide is one of the most studied sesquiterpene lactones. It exhibits anti-inflammatory activity and promising potential anticancer activity [22,23]. The guaianolide-type sesquiterpene lactones have also attracted attention because, in general, they exhibit a higher cytotoxic activity compared with the other types of sesquiterpene lactones [15]. For example, arglabin and micheliolide can selectively inhibit acute myelogenous leukemia stem or progenitor cell growth and dehydroleucodine displayed antitumour activity in a preclinical melanoma model [24,25]. Interestingly, phase II clinical trials were recently completed [3] for mipsagargin, an analogue of the potent sarco-endoplasmic reticulum Ca^{2+}-ATPase inhibitor thapsigargin in several types of cancer.

Here we explored the structure–cytotoxicity relationships of eight chlorinated guaianolides, seven obtained from natural sources and one as a semisynthetic derivative, using human leukemia and melanoma cell lines as models. These compounds were characterized by the presence of exocyclic double bonds on carbons C-10 and C-11 and different substituents on carbons C-3, C-4 and C-8. The results of the studies of structure–cytotoxicity relationships revealed that: (i) the reduction of the double bond 11,13 blocked inhibitory activity in tumor cells, independent of the presence of an additional reactive electrophilic group; (ii) acetylation of hydroxy group on C-3 did not enhance cytotoxicity in comparison with the corresponding alcohol; (iii) the introduction of an ester group on C-8 amplified or decreased cytotoxicity; (iv) the increase in polarity of the hydrocarbon chain of the ester group on C-8 reduced cytotoxicity; (v) the introduction of an alkylating group such as an epoxide on C-4 did not enhance cytotoxicity but the introduction of an enone on C-8 did.

The importance of the α-methylene-γ-lactone in determining cytotoxicity in the presence of additional reactive electrophilic groups has been described for repin, a guaianolide isolated from *Centaurea repens* [26]. Previous studies have shown that chlorohyssopifolin A (**1**) inhibits cell viability of several cancer cell lines, including 1A9 (ovarian cancer), KB (nasopharyngeal cancer) and KB-V (vincristine-resistant KB subline), and that chlorohyssopifolin C (**3**) showed significant cytotoxicity against MCF-7 (estrogen receptor positive breast cancer). In that study the chlorohyssopifolins A (**1**) and C (**3**) were not assayed against human melanoma cells and the mechanism of cell death was not explored [8]. Similar to our results in human leukemia and melanoma cells, the study showed that the chlorohydrin on C-4 may be modified to an epoxide on the cyclic skeleton with no change in cytotoxicity, as demonstrated by the comparison of the IC_{50} values of chlorohyssopifolin A (**1**) and chlorohyssopifolin C (**3**). In addition, the presence of a diol in the side chain on C-8 (chlorohyssopifolin E (**5**)) rather than a chlorohydrin (chlorohyssopifolin A (**1**)) abolished activity. A similar observation has been described for the comparison between babylin A, which contains a diol in the side chain, and chlorohyssopifolin C (**3**) which contains a chlorohydrin in the side chain [8].

Interestingly, the guaianolides were able to inhibit cell viability in U-937/Bcl-2, a subline that overexpresses the survival protein Bcl-2, which has been involved in chemoresistance, especially in hematologic malignancies [27]. These results suggest that guaianolides seem capable of blocking the growth of human tumor cells by inactivation of the mitochondrial protection by Bcl-2. Moreover, SK-MEL-1 melanoma cells were sensitive to chlorohyssopifolins A (**1**), C (**3**) and D (**4**) and linichlorin A (**6**), emphasizing the potential of these compounds, given that melanoma is the most aggressive and lethal skin cancer.

The results of this work revealed that linichlorin A (**6**) was one of the most potent guaianolides in reducing the cell viability of the four human tumor cells assayed. Linichlorin A (**6**) has been reported as a negative regulator of the degradation of the cyclin-dependent kinases inhibitor $p27^{Kip1}$. This guaianolide inhibits the *in vitro* ubiquitination of $p27^{Kip1}$ by SCF^{Skp2}—the ubiquitin ligase (SCF) complex with S-phase kinase-associated protein 2- stabilizes $p27^{Kip1}$ levels in HeLa cells and inhibits the growth of human and mouse cancer cells [28]. Linichlorin A (**6**) has been shown to display

substantial, selective antiproliferative activity against cancer and transformed cells in the micromolar range. The IC_{50} values reported for linichlorin A (**6**) in HeLa (human cervix carcinoma), tsFT210 (mouse tumor cells) and NIH3T3 (mouse immortalized cells) were 3.2, 1.6 and 12.7 μM, respectively, as determined by WST-8 assay for 48 h. However, little is known about the mechanism of cell death induced by linichlorin A (**6**).

Flow cytometry experiments in the present study revealed that inhibition of cell viability by chlorohyssopifolins A (**1**), C (**3**) and D (**4**) and linichlorin A (**6**) was accompanied by an increase in the sub-G_1 fraction. The selected guaianolides chlorohyssopifolins A (**1**) and D (**4**) and linichlorin A (**6**) were able to induce nuclear morphological changes, such as fragmentation and condensation of chromatin, characteristic of apoptotic cell death. Experiments using U-937 cells as a model confirmed that these compounds are potent apoptotic inducers, as demonstrated by phosphatidylserine externalization and poly(ADP-ribose)polymerase cleavage. In addition, selected guaianolides induced a concentration-dependent release of mitochondrial apoptogenic cytochrome *c*, indicating that the intrinsic apoptotic pathway may play a key role in cell death. Enzymatic analysis revealed activation of caspase-9 and caspase-3, in accordance with the release of cytochrome *c*. Activation of caspase-8 was also detected in extracts of selected guaianolides-treated U-937 cells. In order to identify the primary targets and early mechanism of action of selected sesquiterpene lactones on U-937 cells, we used concentrations close to or threefold higher than the antiproliferative IC_{50} values, which were determined at 72 h of treatment, while flow cytometry and assays of caspase activity were analyzed after 24 h of treatment. Concentrations close to the IC_{50} values of selected sesquiterpene lactones were sufficient to trigger apoptosis. It is interesting to note that a low concentration (3 μM) of chlorohyssopifolins A (**1**) and D (**4**) and linichlorin A (**6**) was sufficient to induce cytochrome *c* release in U-937 cells. Taken together, these results indicate that both the extrinsic and the intrinsic pathways play an important role in cell death induced by chlorohyssopifolins A (**1**) and D (**4**) and linichlorin A (**6**).

In conclusion, chlorohyssopifolins A (**1**) and D (**4**) and linichlorin A (**6**) were shown to induce apoptosis via caspase activation. Although more research must be carried out to uncover the detailed pathway of cell death, these compounds are potentially interesting and should be considered for further preclinical and *in vivo* testing.

4. Materials and Methods

4.1. Drugs and Reagents

The guaianolides assayed were isolated from natural sources as previously described. Five sesquiterpene lactones containing chlorine, chlorohyssopifolins A (**1**), B (**2**), C (**3**), D (**4**) and E (**5**) were isolated from *Centaurea hyssopifolia* Vahl, which is an endemic dominant species on Iberian gypsum soils in central Spain [15,16]. Linichlorin A (**6**) is a sesquiterpene lactone that was first isolated from *Centaurea linifolia* Vahl, a native plant from the eastern part of Spain and Italy [17]. The chemical structures of sesquiterpene lactones were determined spectroscopically (proton nuclear magnetic resonance, infrared spectroscopy and mass spectrometry) as described previously. ^{1}H- NMR, ^{13}C-NMR and mass spectra of guaianolides are shown in Figures S3–S33 in Supplementary Materials.

4.2. Cell Culture

The human acute myeloid leukemia HL-60 (DSMZ N° ACC 3), the human histiocytic lymphoma U-937 (DSMZ N° ACC 5) and the human melanoma SK-MEL-1 (DSMZ N° ACC 303) were obtained from the German Collection of Microorganisms and Cell Cultures (Braunschweig, Germany), cultured in suspension in RPMI 1640 medium containing 10% (*v*/*v*) fetal bovine serum and maintained at 0.5–1.0 × 10^6 cells/mL, except SK-MEL-1 cells, which were maintained at 0.1–0.3 × 10^6 cells/mL. The U-937 cell line overexpressing human Bcl-2 (designated U-937/Bcl-2) was donated by Dr. Jacqueline Bréard (Faculté de Pharmacie Paris-Sud, Chatenay-Malabry, France) and cultured in RPMI 1640

medium containing 10% (*v*/*v*) fetal bovine serum at 37 °C in a humidified atmosphere containing 5% CO_2. Cell viability was determined by the trypan blue exclusion test. Cells were resuspended in fresh medium 24 h before treatments to ensure the exponential growth. HL-60 and U-937 cells exhibited characteristic doubling times of about 25 h and 35 h, respectively, while SK-MEL-1 cells exhibited a doubling time of several days (about 48–72 h). Stock solutions of 50 mM guaianolides were made in dimethylsulfoxide (DMSO) and aliquots were frozen at −20 °C. Further dilutions were made in culture medium immediately prior to use. In all experiments, the final concentration of DMSO did not exceed 0.2% (*v*/*v*), a concentration that was nontoxic to the cells.

4.3. Assay for Growth Inhibition

The effects of guaianolides on the cell viability of human tumor cells were assessed using the colorimetric 3-(4,5-dimethyl-2-thiazolyl)-2,5-diphenyl-2*H*-tetrazolium bromide (MTT) assay [29]. Exponentially growing cells (4000 for HL-60 and U-937; 6000 for SK-MEL-1) were seeded in 96-well microculture plates with increasing concentrations of guaianolides for 72 h at 37 °C. Surviving cells were detected based on their ability to metabolize MTT in formazan crystals, measuring the absorbance at 570 nm, and the IC_{50} (concentrations inducing a 50% inhibition of cell growth) values were calculated graphically using the curve-fitting algorithm of the computer software Prism 5.0 (GraphPad, La Jolla, CA, USA). Values were calculated as means ± SD from three to five independent experiments, each performed in triplicate.

4.4. Fluorescent Microscopy

Cells were treated with the corresponding compound for the specified time period and then fixed with 3% paraformaldehyde for 10 min at room temperature. Cells were then stained with bisbenzimide (Hoechst 33258) for 15 min and visualized under a fluorescence microscope.

4.5. Analysis by Flow Cytometry

After treatment with guaianolides, cells were fixed in 75% ethanol at −20 °C for at least 1 h, stained with propidium iodide and analyzed by flow cytometry using a BD FACS Verse cytometer. Apoptosis was quantified using an Annexin V-FITC apoptosis detection kit (BD Pharmingen, San Diego, CA, USA), performed according to the manufacturer's protocol.

4.6. Caspase Activity

Caspase activity was determined in cell lysates using specific colorimetric substrates for caspase-3/7, caspase-8 and caspase-9 [30]. Briefly, after treatments cells were washed twice in phosphate buffer saline, they were resuspended in 50 mM HEPES pH 7.4, 0.1 mM EDTA, 1 mM dithiothreitol, 0.1% Chaps, and lysed by pushing them several times through a 22-gauge needle. The cell lysates were centrifuged at 17,000× *g* at 4 °C for 10 min and the supernatants were analyzed for protein concentration and for caspase activity. Protein concentration was determined by the Bradford assay and caspase activity by the net increase of absorbance at 405 nm. The specific substrates for caspase-3/7, -8 and -9 were DEVD-*p*NA, IETD-*p*NA and LEHD-*p*NA, respectively.

4.7. Western Blot

Immunoblot analyses of caspases and PARP were performed as previously described [31]. Briefly, cells were treated with the specified compounds, washed twice with PBS and then lysed in a buffer containing 50 mM Tris-HCl, pH 8.0, 150 mM sodium chloride, 1.0% Triton X-100, 0.1 mM phenylmethylsulfonylfluoride and leupeptin, pepstatin A and aprotinin (1 µg/mL each). Equal amounts of proteins were denatured in 2x Laemli buffer (0.125 M Tris-HCl pH 6.8, 4% SDS, 10% mercaptoethanol, 20% glycerol and 0.004% bromophenol blue) at 95 °C for 5 min. The samples were separated on a 7.5% (PARP) or 12.5% (caspases) SDS-polyacrylamide gel and electrotransferred to a polyvinylidene

difluoride (PVDF) membrane. After blocking the membrane with 5% nonfat milk in Tris-buffered saline containing 0.1% Tween-20 for 1 h, it was incubated with the corresponding primary antibodies followed by the corresponding secondary antibodies. The antigen–antibodies complexes were visualized by enhanced chemiluminiscence.

For the cytosolic fractions, cells were washed twice with PBS, resuspended in 20 mM Hepes-KOH pH 7.5, 10 mM KCl, 1.5 mM $MgCl_2$, 1 mM EDTA, 1 mM EGTA, 0.1 mM phenylmethylsulfonylfluoride, 1 mM dithiothreitol, 250 mM sucrose and 1 µg/mL leupeptin, pepstatin A and aprotinin, and lysed by pushing them several times through a 22-gauge needle. Lysates were centrifuged at 1000× *g* for 5 min at 4 °C and the supernatants were spun down again at 105,000× *g* for 45 min at 4 °C. The resulting supernatants were used as the soluble cytosolic fraction.

The primary antibodies used for Western blots were purchased from the following companies: anti-caspase-3 (ADI-AAP-113), -8 (ADI-AAM-118) and -9 (ADI-AAM-139) from Enzo (Plymouth Meeting, PA, USA); anti-poly(ADP-ribose) polymerase (PARP) (551024) and anti-cytochrome *c* (556433) from BD Pharmingen (San Diego, CA, USA); anti-β-actin (clone AC-74, A2228) from Sigma-Aldrich (Saint Louis, MO, USA). Secondary antibodies (NA9310 and NA9340) were from GE Healthcare (Little Chalfont, UK). PVDF membranes were from Millipore (Temecula, CA, USA).

4.8. Statistical Analysis

Statistical differences between means of control and treated samples were tested using Student's *t*-test. *p*-values below 0.05 were considered as statistically significant.

Supplementary Materials: Supplementary materials can be found at http://www.mdpi.com/1422-0067/21/24/9767/s1. Representative MTT experiment of HL-60 cells treated with increasing concentrations of guaianolides for 72 h (Figure S1), dose-response curves of guaianolides **1–8** on human tumor cells viability (Figure S2) and ^{1}H-NMR and ^{13}C-NMR spectra, as well as high and low mass spectra (Figures S3–S33).

Author Contributions: F.E.-S., E.S. and M.R.-E. performed the biological experiments. I.B. and F.L. prepared and characterized the compounds. I.B., J.Q. and F.E. analyzed the data. F.E. designed the experiments and wrote the paper. All authors have read and agreed to the published version of the manuscript.

Funding: This research was funded by FEDER and AGENCIA CANARIA DE INVESTIGACIÓN, INNOVACIÓN Y SOCIEDAD DE LA INFORMACIÓN (PROID2017010095 FEDER/ACIISI) and in part by the Spanish Ministry of Science, Innovation and Universities and the European Regional Development Fund (PGC2018-094503-B-C21).

Acknowledgments: We thank J. Bréard for supplying U-937/Bcl-2 cells.

Conflicts of Interest: The authors declare no conflict of interest. The funders had no role in the design of the study; in the collection, analyses, or interpretation of data; in the writing of the manuscript, or in the decision to publish the results.

References

1. Ren, Y.; Yu, J.; Kinghorn, A.D. Development of Anticancer Agents from Plant-Derived Sesquiterpene Lactones. *Curr. Med. Chem.* **2016**, *23*, 2397–2420. [CrossRef]
2. Quintana, J.; Estévez, F. Recent Advances on Cytotoxic Sesquiterpene Lactones. *Curr. Pharm. Des.* **2018**, *24*, 4355–4361. [CrossRef]
3. Ma, G.; Chen, K.; Zhang, L.; Li, Y. Advance in biological activities of natural guaiane-type sesquiterpenes. *Med. Chem. Res.* **2019**, *28*, 1339–1358. [CrossRef]
4. Merfort, I. Perspectives on sesquiterpene lactones in inflammation and cancer. *Curr. Drug Targets* **2011**, *12*, 1560–1573. [CrossRef]
5. Li, J.; Yoshida, Y.; Kurita, M.; Usuki, T. Cynaropicrin and inhibition of NF-κB activation: A structure activity relationship study. *Bioorg. Med. Chem. Lett.* **2019**, *29*, 1518–1521. [CrossRef]
6. Zeng, J.; Zhan, J. Chlorinated natural products and related halogenases. *Isr. J. Chem.* **2019**, *59*, 387–402. [CrossRef]
7. Engvild, K. Chlorine-containing natural compounds in higher plants. *Phytochemistry* **1986**, *25*, 781–791. [CrossRef]

8. Bruno, M.; Rosselli, S.; Maggio, A.; Raccuglia, R.A.; Bastow, K.F.; Lee, K.H. Cytotoxic activity of some natural and synthetic guaianolides. *J. Nat. Prod.* **2005**, *68*, 1042–1046. [CrossRef]
9. Scotti, M.T.; Fernandes, M.B.; Ferreira, M.J.; Emerenciano, V.P. Quantitative structure-activity relationship of sesquiterpene lactones with cytotoxic activity. *Bioorg. Med. Chem.* **2007**, *15*, 2927–2934. [CrossRef]
10. Galluzzi, L.; Vitale, I.; Aaronson, S.A.; Abrams, J.M.; Adam, D.; Agostinis, P.; Alnemri, E.S.; Altucci, L.; Amelio, I.; Andrews, D.W.; et al. Molecular mechanisms of cell death: Recommendations of the Nomenclature Committee on Cell Death 2018. *Cell Death Differ.* **2018**, *25*, 486–541. [CrossRef]
11. Delbridge, A.R.; Strasser, A. The BCL-2 protein family, BH3-mimetics and cancer therapy. *Cell Death Differ.* **2015**, *22*, 1071–1080. [CrossRef]
12. Tummers, B.; Green, D.R. Caspase-8: Regulating life and death. *Immunol. Rev.* **2017**, *277*, 76–89. [CrossRef]
13. Julien, O.; Wells, J.A. Caspases and their substrates. *Cell Death Differ.* **2017**, *24*, 1380–1389. [CrossRef]
14. Cohen, G.M. Caspases: The executioners of apoptosis. *Biochem J.* **1997**, *326*, 1–16. [CrossRef]
15. González, A.G.; Bermejo, J.; Breton, J.L.; Massanet, G.M.; Domínguez, B.; Amaro, J.M. The chemistry of the Compositae. Part XXX1. Absolute configuration of the sesquiterpene lactones centaurepensin (chlorohyssopifolin A), acroptilin (chlorohyssopifolin C), and repin. *J. Chem. Soc. Perkin Trans. I* **1976**, 1663–1666. [CrossRef]
16. González, A.G.; Bermejo, J.; Bretón, J.L.; Massanet, G.M.; Triana, J. Chlorohyssopifolin C, D, E and vahlenin, four new sesquiterpene lactones from Centaurea hyssopifolia. *Phytochemistry* **1974**, *13*, 1193–1197. [CrossRef]
17. González, A.G.; Bermejo, J.; Amaro, J.M.; Massanet, G.M.; Galindo, A.; Cabrera, I. Sesquiterpene lactones from Centaurea linifolia Vahl. *Can. J. Chem.* **1978**, *56*, 491–494. [CrossRef]
18. González, A.G.; Bermejo, J.; Massanet, G.M.; Amaro, J.M. Action of silver nitrate on chlorinated sesquiterpene lactones. *An. Quim.* **1978**, *74*, 1443–1445.
19. Harris, P.; Ralph, P. Human leukemic models of myelomonocytic development: A review of the HL-60 and U937 cell lines. *J. Leukoc. Biol.* **1985**, *37*, 407–422. [CrossRef]
20. Chanput, W.; Peters, V.; Wichers, H. THP-1 and U937 Cells. In *The Impact of Food Bioactives on Health: In Vitro and Ex Vivo Models*; Verhoeckx, K., Cotter, P., López-Expósito, I., Kleiveland, C., Lea, T., Mackie, A., Requena, T., Swiatecka, D., Wichers, H., Eds.; Springer: Berlin/Heidelberg, Germany, 2015; pp. 147–159.
21. Ghantous, A.; Gali-Muhtasib, H.; Vuorela, H.; Saliba, N.A.; Darwiche, N. What made sesquiterpene lactones reach cancer clinical trials? *Drug Discov. Today* **2010**, *15*, 668–678. [CrossRef]
22. Guzman, M.L.; Rossi, R.M.; Karnischky, L.; Li, X.; Peterson, D.R.; Howard, D.S.; Jordan, C.T. The sesquiterpene lactone parthenolide induces apoptosis of human acute myelogenous leukemia stem and progenitor cells. *Blood* **2005**, *105*, 4163–4169. [CrossRef]
23. Ghantous, A.; Sinjab, A.; Herceg, Z.; Darwiche, N. Parthenolide: From plant shoots to cancer roots. *Drug Discov Today* **2013**, *18*, 894–905. [CrossRef]
24. Zhang, Q.; Lu, Y.; Ding, Y.; Zhai, J.; Ji, Q.; Ma, W.; Yang, M.; Fan, H.; Long, J.; Tong, Z.; et al. Guaianolide sesquiterpene lactones, a source to discover agents that selectively inhibit acute myelogenous leukemia stem and progenitor cells. *J. Med. Chem.* **2012**, *55*, 8757–8769. [CrossRef]
25. Costantino, V.V.; Lobos-Gonzalez, L.; Ibañez, J.; Fernandez, D.; Cuello-Carrión, F.D.; Valenzuela, M.A.; Barbieri, M.A.; Semino, S.N.; Jahn, G.A.; Quest, A.F.; et al. Dehydroleucodine inhibits tumor growth in a preclinical melanoma model by inducing cell cycle arrest, senescence and apoptosis. *Cancer Lett.* **2016**, *372*, 10–23. [CrossRef]
26. Tukov, F.F.; Anand, S.; Gadepalli, R.S.; Gunatilaka, A.A.; Matthews, J.C.; Rimoldi, J.M. Inactivation of the cytotoxic activity of repin, a sesquiterpene lactone from Centaurea repens. *Chem. Res. Toxicol.* **2004**, *17*, 1170–1176. [CrossRef]
27. Amundson, S.A.; Myers, T.G.; Scudiero, D.; Kitada, S.; Reed, J.C.; Fornace, A.J., Jr. An informatics approach identifying markers of chemosensitivity in human cancer cell lines. *Cancer Res.* **2000**, *60*, 6101–6110.
28. Ooi, L.C.; Watanabe, N.; Futamura, Y.; Sulaiman, S.F.; Darah, I.; Osada, H. Identification of small molecule inhibitors of p27(Kip1) ubiquitination by high-throughput screening. *Cancer Sci.* **2013**, *104*, 1461–1467. [CrossRef]
29. Mosmann, T. Rapid colorimetric assay for cellular growth and survival: Application to proliferation and cytotoxicity assays. *J. Immunol. Methods* **1983**, *65*, 55–63. [CrossRef]

30. Rubio, S.; Quintana, J.; Eiroa, J.L.; Triana, J.; Estévez, F. Acetyl derivative of quercetin 3-methyl ether-induced cell death in human leukemia cells is amplified by the inhibition of ERK. *Carcinogenesis* **2007**, *28*, 2105–2113. [CrossRef]
31. Estévez-Sarmiento, F.; Hernández, E.; Brouard, I.; León, F.; García, C.; Quintana, J.; Estévez, F. 3′-Hydroxy-3,4′-dimethoxyflavone-induced cell death in human leukaemia cells is dependent on caspases and reactive oxygen species and attenuated by the inhibition of JNK/SAPK. *Chem. Biol. Interact.* **2018**, *288*, 1–11. [CrossRef]

Supplementary Materials

Chlorinated guaiane-type sesquiterpene lactones as cytotoxic agents against human tumor cells

Francisco Estévez-Sarmiento[1], Ester Saavedra[1], Mercedes Ruiz-Estévez[2], Francisco León[3], José Quintana[1], Ignacio Brouard[4], and Francisco Estévez[1,*]

[1] Departamento de Bioquímica y Biología Molecular, Instituto Universitario de Investigaciones Biomédicas y Sanitarias (IUIBS), Grupo de Química Orgánica y Bioquímica, Universidad de Las Palmas de Gran Canaria, Unidad Asociada al CSIC, 35016 Las Palmas de Gran Canaria, Spain; francisco.estevez103@alu.ulpgc.es (F.E.-S.) ; ester.saavedra102@alu.ulpgc.es (E.S.) ; jose.quintana@ulpgc.es (J.Q.)

[2] Recombinetics, Inc., Eagan, MN 55121, USA; mercy.ruiz@recombinetics.com (M.R.-E.)

[3] Department of Drug Discovery and Biomedical Sciences. College of Pharmacy. University of South Carolina, Columbia, SC 29208, USA; jleon@mailbox.sc.edu (F.L.)

[4] Instituto de Productos Naturales y Agrobiología, Consejo Superior de Investigaciones Científicas, 38206 La Laguna, Spain; ibrouard@ipna.csic.es (I.B.)

***** Correspondence: francisco.estevez@ulpgc.es; Tel.: (+34 928 451443)

Table of Contents

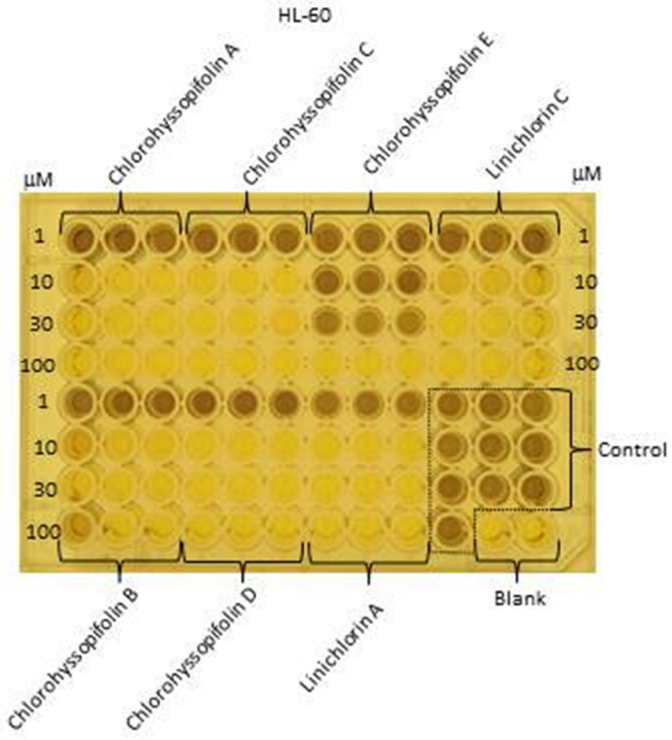

Figure S1. Representative MTT experiment of HL-60 cells treated with increasing concentrations of guaianolides for 72 h.

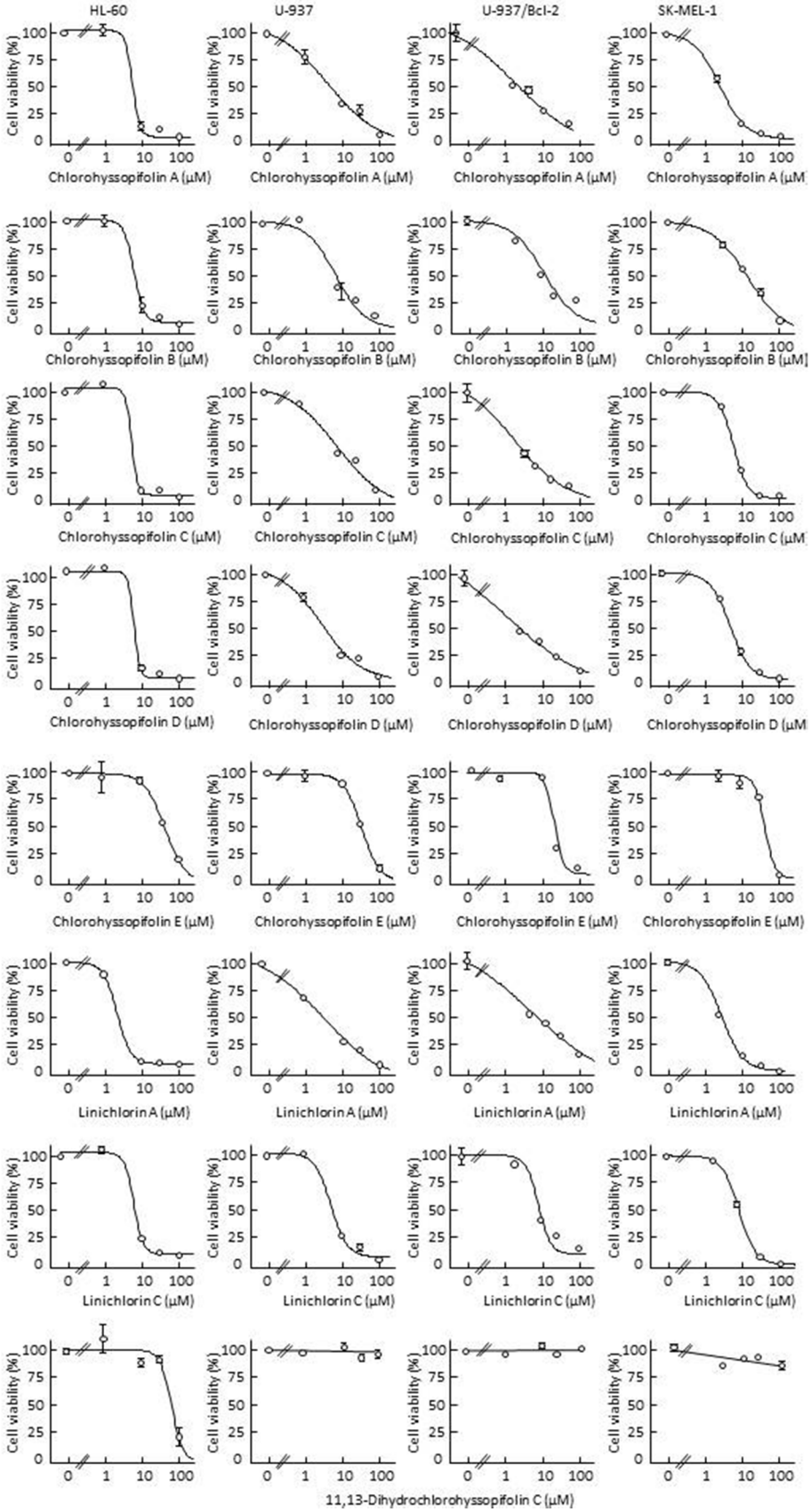

Figure S2. Dose-response curves of guaianolides **1**-**8** on human tumor cells viability. Cells were incubated in the presence of increasing concentrations of the indicated guaianolide for 72 h, and thereafter cell viability was determined by the MTT assay.

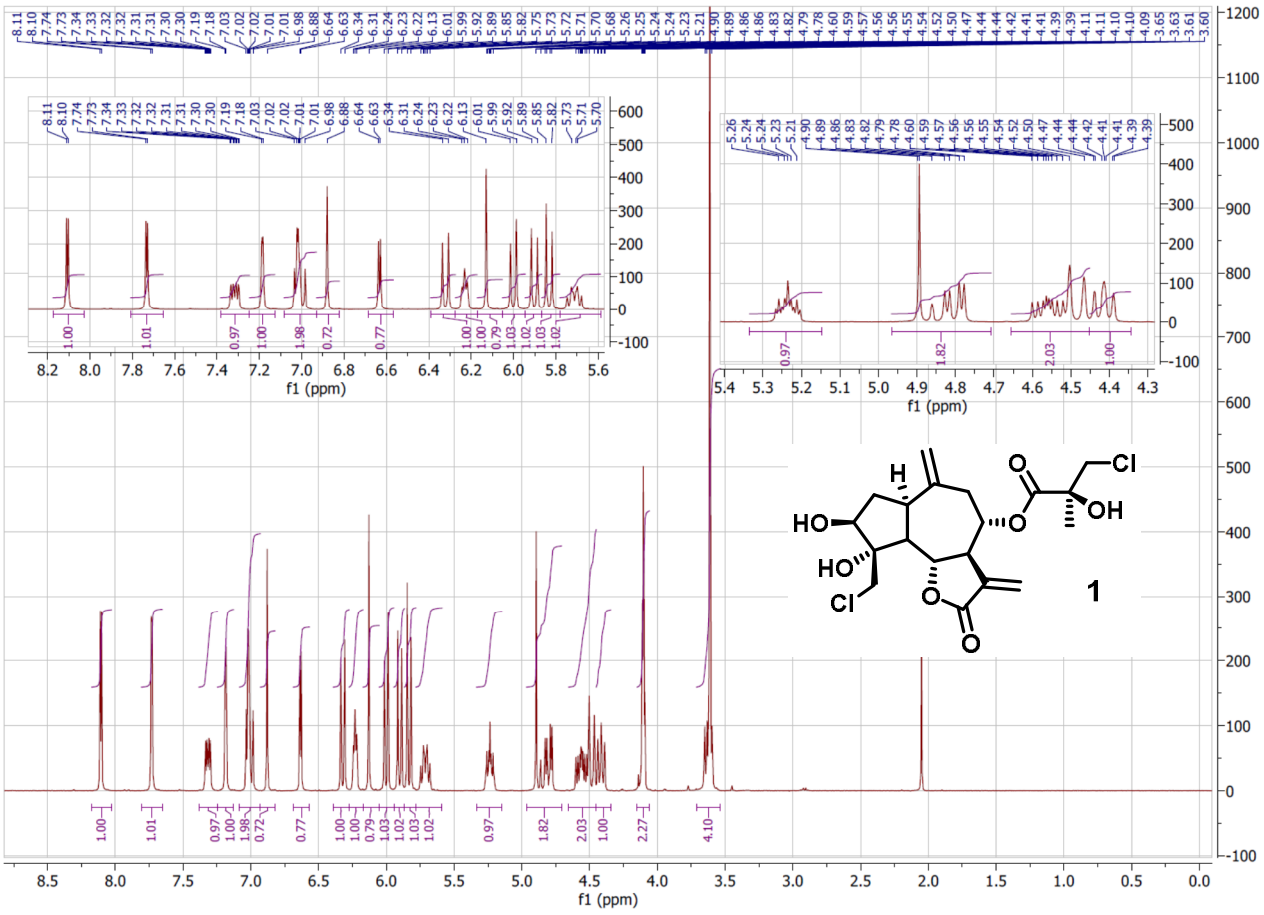

Figure S3: ^{1}H-NMR (500 MHz, Acetone-d6) Spectrum of Compound **1**

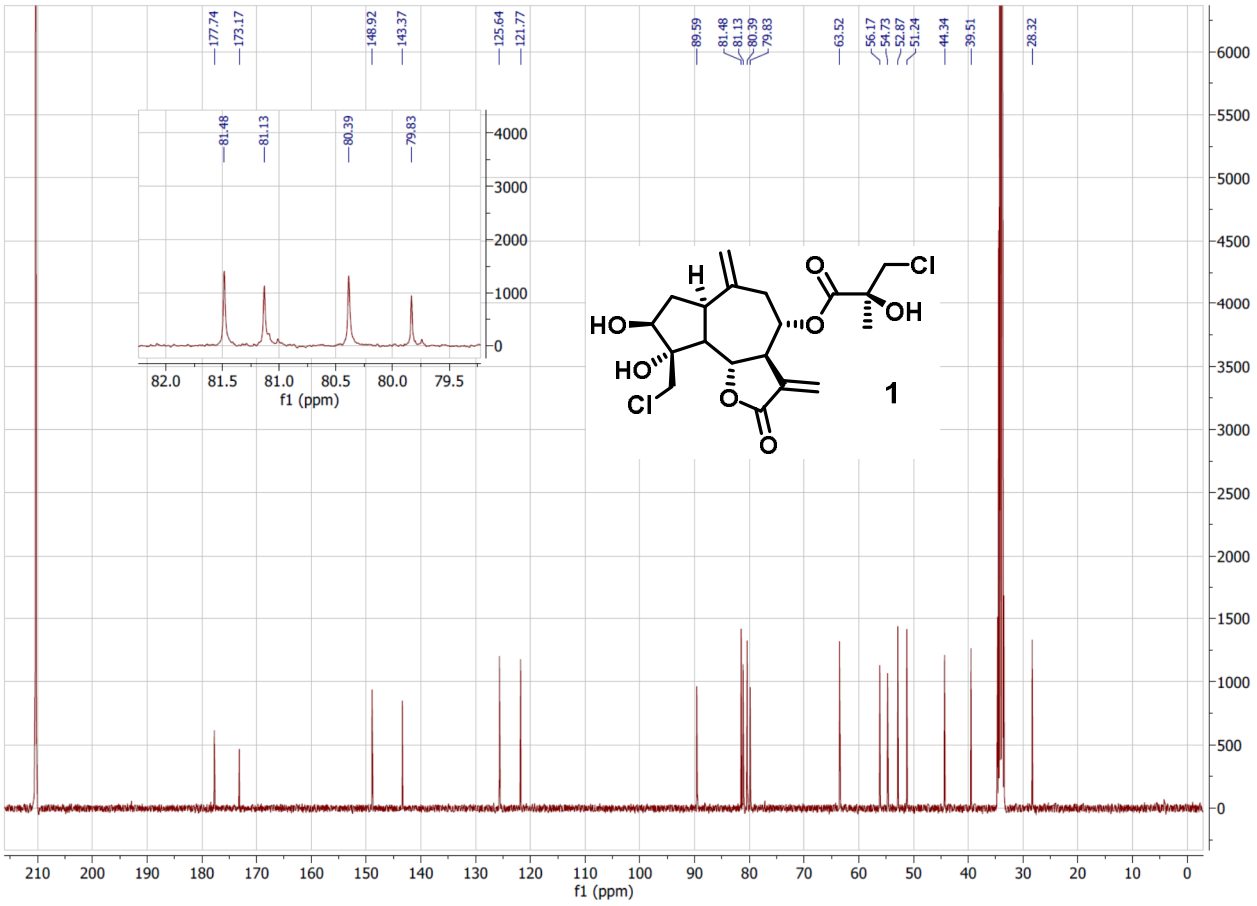

Figure S4: ^{13}C-NMR (125 MHz, Acetone-d6) Spectrum of Compound **1**

Elemental Composition Report **Page 1**

Multiple Mass Analysis: 5 mass(es) processed
Tolerance = 5.0 PPM / DBE: min = -3.0, max = 120.0
Element prediction: Off
Number of isotope peaks used for i-FIT = 3

Monoisotopic Mass, Even Electron Ions
770 formula(e) evaluated with 5 results within limits (all results (up to 1000) for each mass)
Elements Used:
C: 0-19 H: 0-30 O: 0-7 Na: 0-1 35Cl: 0-2 37Cl: 0-2

Ignacio B
(ESI-20-667) Ignacio B (IB-Cl-H-A) 12 (0.487)

1: TOF MS ES+
3.12e+003

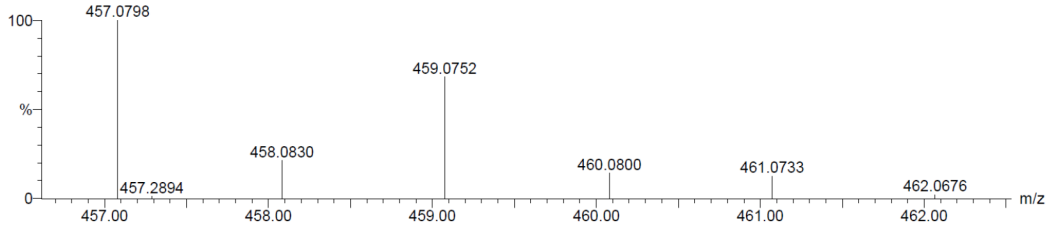

Minimum:	10.00				-3.0			
Maximum:	100.00		5.0	5.0	120.0			
Mass	RA	Calc. Mass	mDa	PPM	DBE	i-FIT	i-FIT (Norm)	Formula
457.0798	100.00	457.0797	0.1	0.2	6.5	35.4	0.0	C19 H24 O7 Na 35Cl2
458.0830	21.17	---						
459.0752	68.12	459.0767	-1.5	-3.3	6.5	20.8	0.9	C19 H24 O7 Na 35Cl 37Cl
		459.0736	1.6	3.5	5.5	20.4	0.5	C19 H26 O6 35Cl 37Cl2
460.0800	14.25	---						
461.0733	12.42	461.0738	-0.5	-1.1	6.5	18.7	1.0	C19 H24 O7 Na 37Cl2
		461.0715	1.8	3.9	4.5	18.2	0.5	C18 H26 O7 35Cl2 37Cl

Figure S5: HRESI-MS Spectrum of Compound **1**

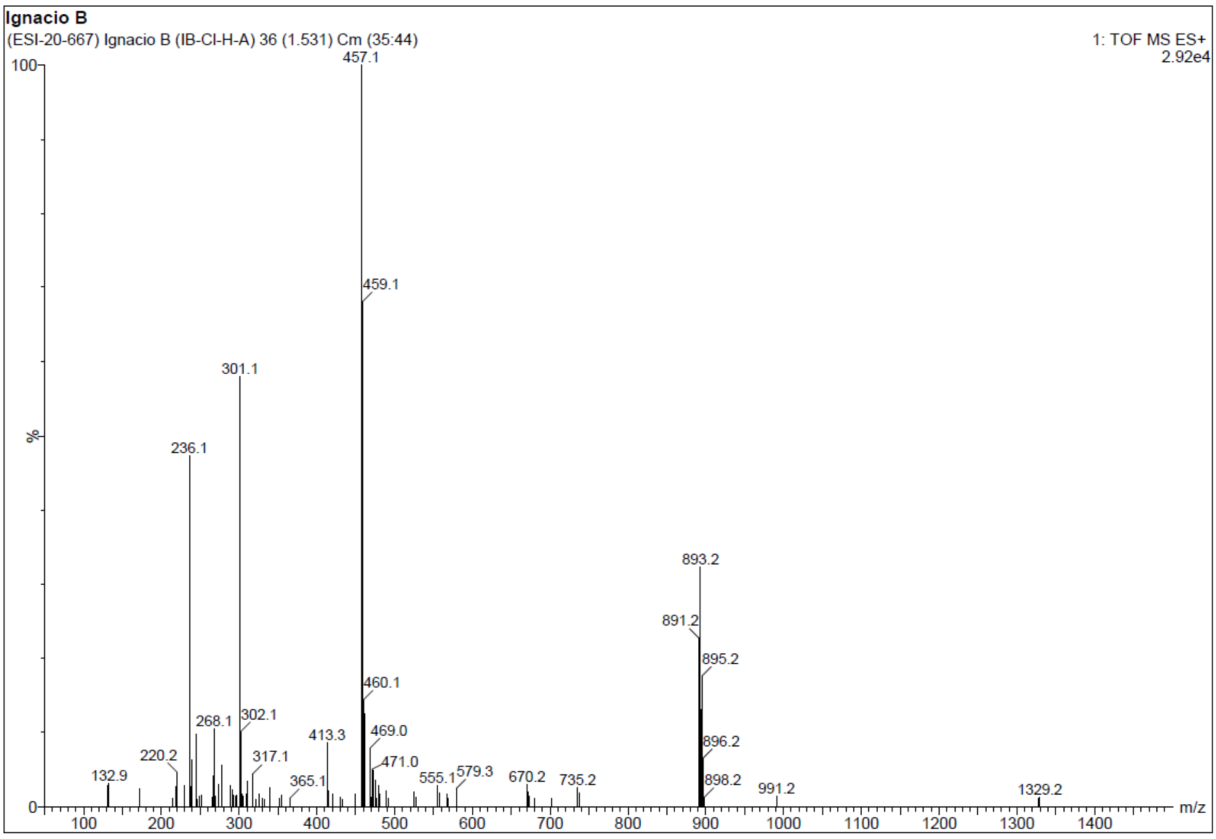

Figure S6: ESI-MS Spectrum of Compound **1**

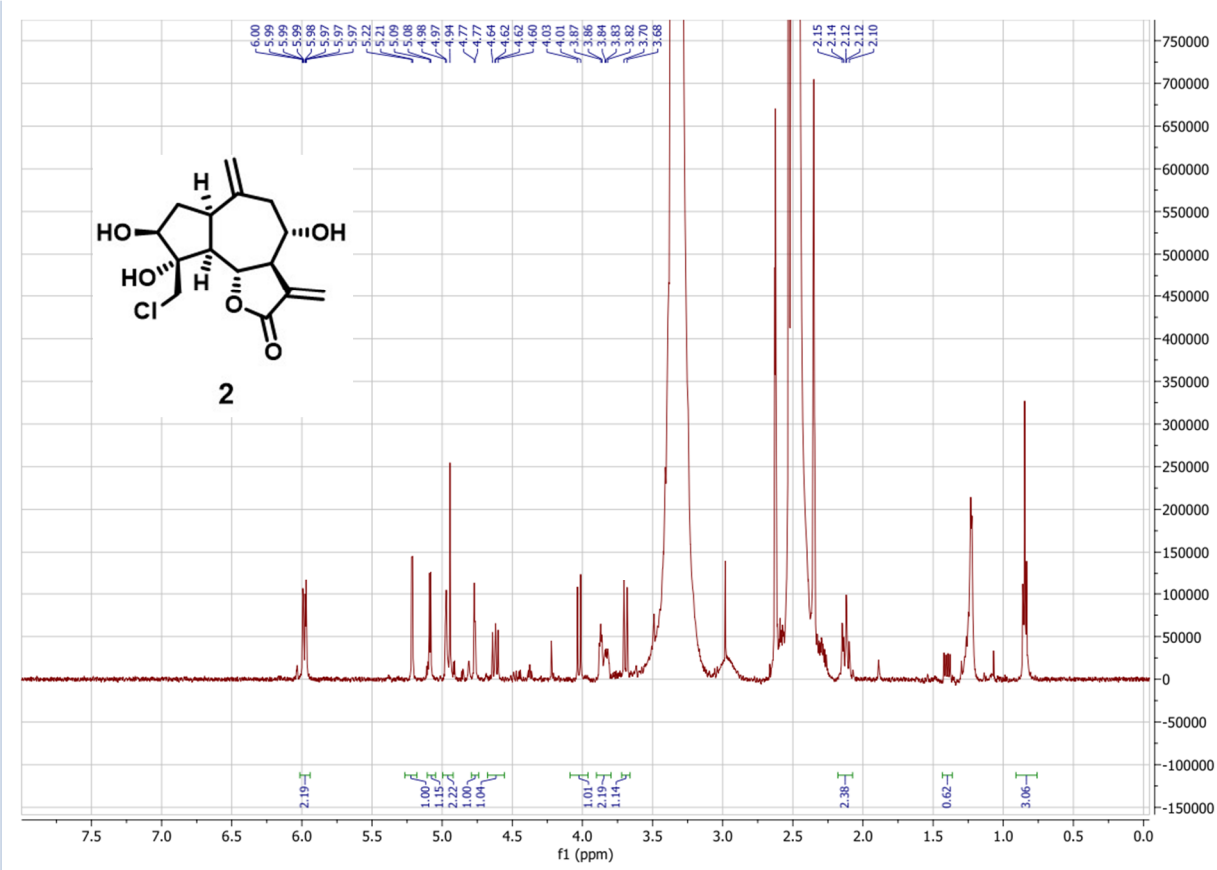

Figure S7: ^{1}H-NMR (500 MHz, DMSO-d6) Spectrum of Compound **2**

Elemental Composition Report **Page 1**

Multiple Mass Analysis: 2 mass(es) processed
Tolerance = 5.0 PPM / DBE: min = -3.0, max = 120.0
Element prediction: Off
Number of isotope peaks used for i-FIT = 3

Monoisotopic Mass, Even Electron Ions
1648 formula(e) evaluated with 7 results within limits (all results (up to 1000) for each mass)
Elements Used:
C: 0-60 H: 0-60 N: 0-1 O: 0-10 Na: 0-2 35Cl: 0-1 37Cl: 0-1

Ignacio B
(ESI-20-945) Igancio B (IB-CH- B) 11 (0.453)

1: TOF MS ES-
4.45e+003

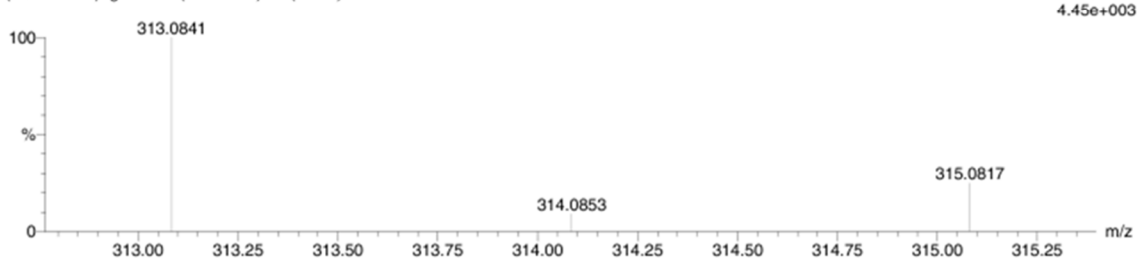

Minimum:	10.00				-3.0			
Maximum:	100.00		5.0	5.0	120.0			
Mass	RA	Calc. Mass	mDa	PPM	DBE	i-FIT	i-FIT (Norm)	Formula
313.0841	100.00	313.0841	0.0	0.0	12.5	26.2	1.9	C19 H14 O3 Na
		313.0843	-0.2	-0.6	6.5	25.6	1.3	C15 H18 O5 35Cl
		313.0844	-0.3	-1.0	-0.5	24.9	0.6	C10 H21 O7 Na 37Cl
315.0817	24.80	315.0821	-0.4	-1.3	4.5	23.9	1.3	C13 H17 O6 Na2
		315.0813	0.4	1.3	6.5	24.1	1.4	C15 H18 O5 37Cl
		315.0823	-0.6	-1.9	-1.5	23.7	1.1	C9 H21 O8 Na 35Cl
		315.0810	0.7	2.2	19.5	24.7	2.0	C24 H11 O

Figure S8: HRESI-MS Spectrum of Compound **2**

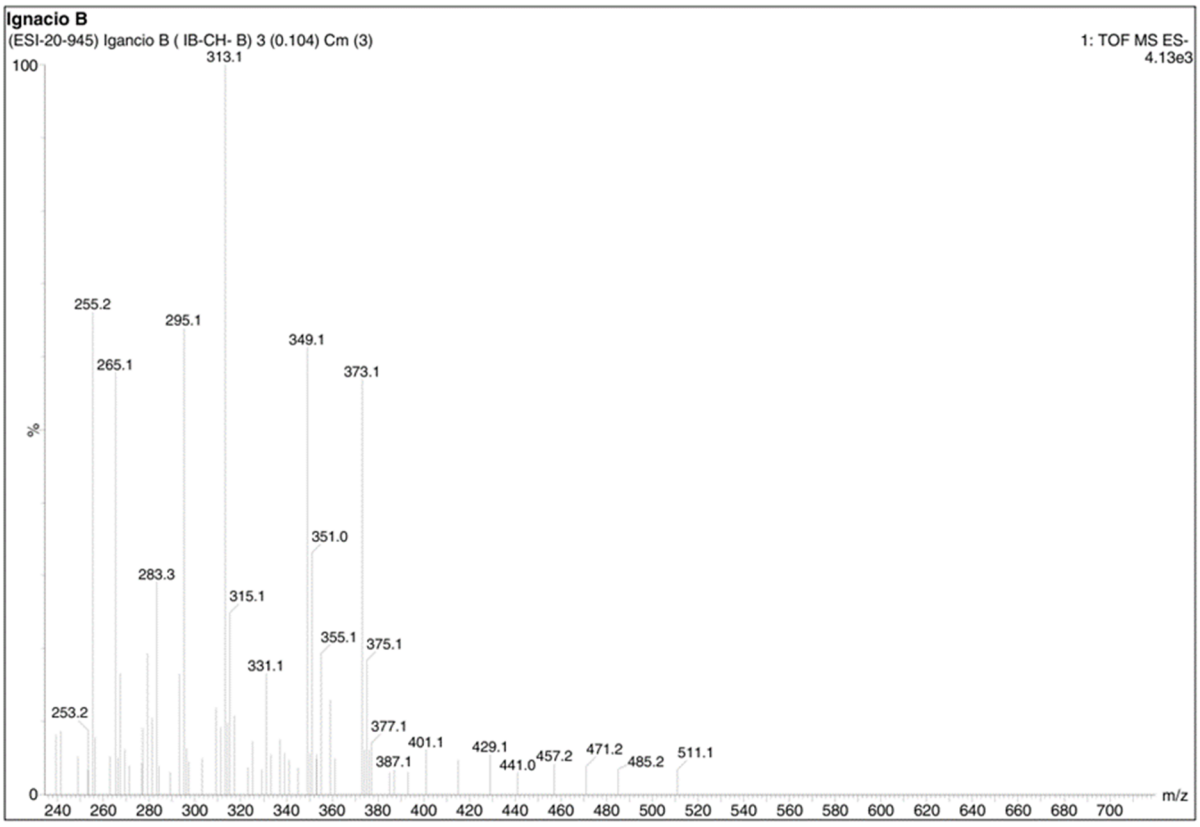

Figure S9: ESI-MS Spectrum of Compound **2**

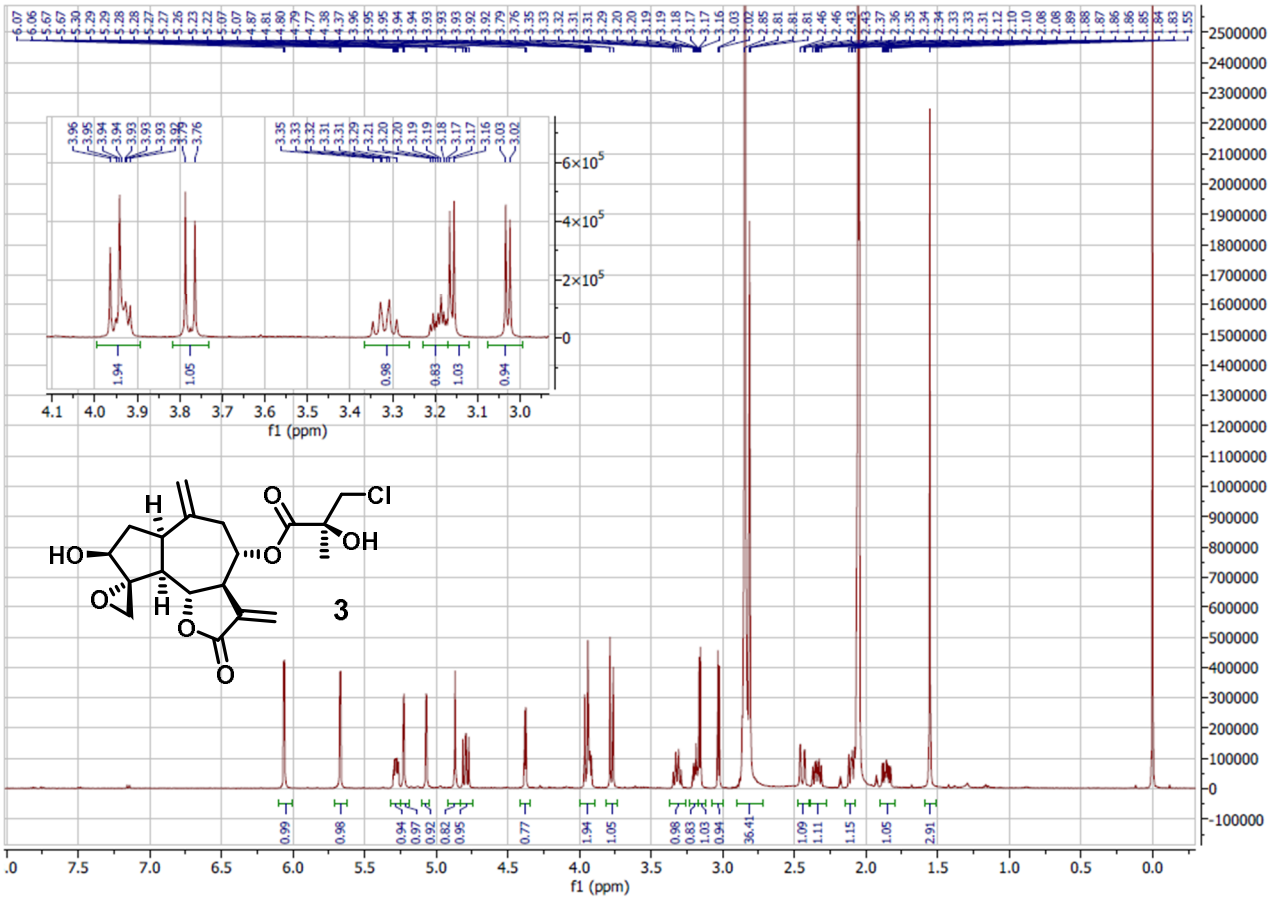

Figure S10: ^{1}H-NMR (500 MHz, Acetone-d6) Spectrum of Compound **3**

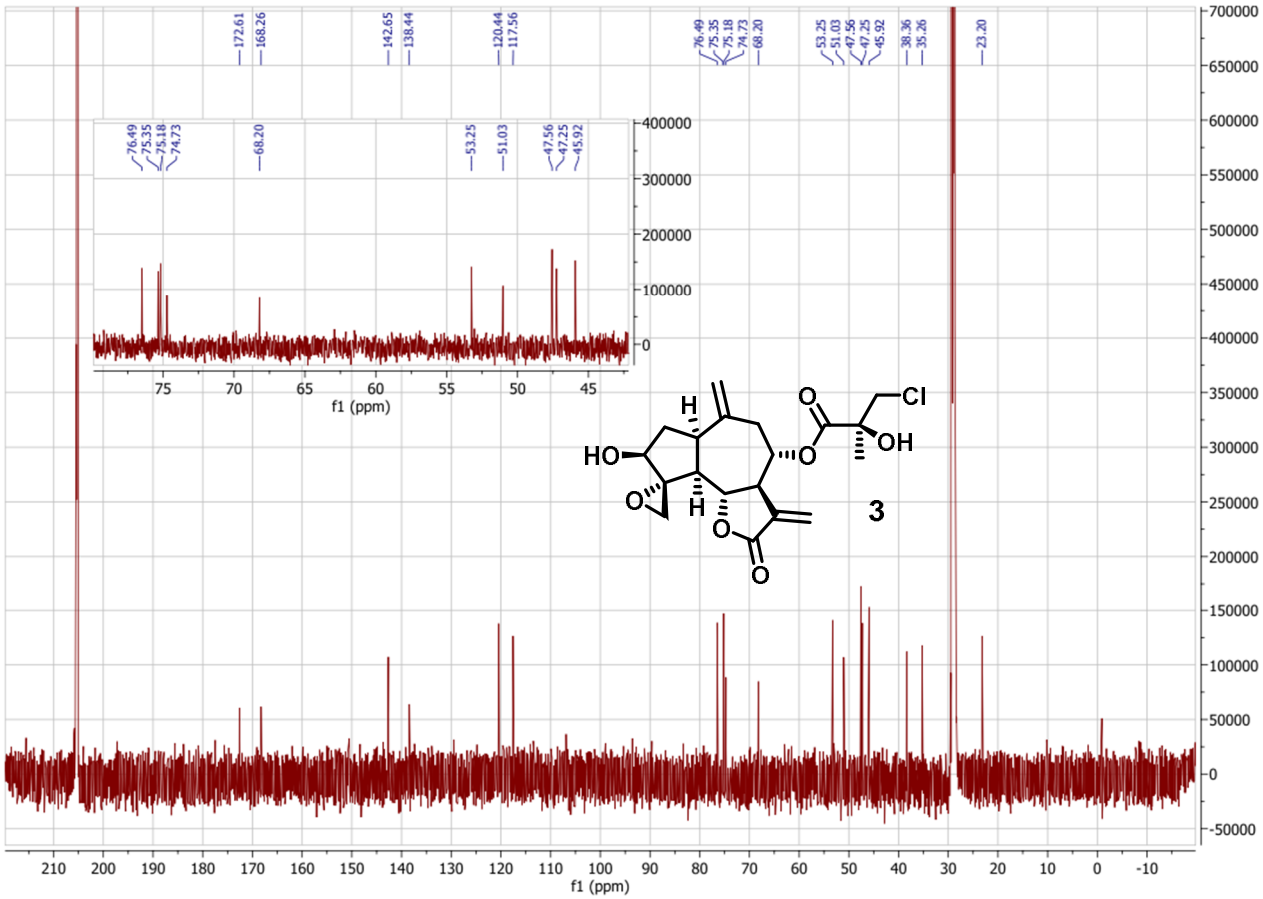

Figure S11: ^{13}C-NMR (125 MHz, Acetone-d6) Spectrum of Compound **3**

Elemental Composition Report **Page 1**

Multiple Mass Analysis: 3 mass(es) processed
Tolerance = 5.0 PPM / DBE: min = -3.0, max = 120.0
Element prediction: Off
Number of isotope peaks used for i-FIT = 3

Monoisotopic Mass, Even Electron Ions
443 formula(e) evaluated with 2 results within limits (all results (up to 1000) for each mass)
Elements Used:
C: 0-23 H: 0-100 O: 0-7 Na: 0-1 35Cl: 0-1 37Cl: 0-1

Ignacio B
(ESI-20-693) Ignacio B (IB CL-H-C) 21 (0.678)

2: TOF MS ES+
9.16e+002

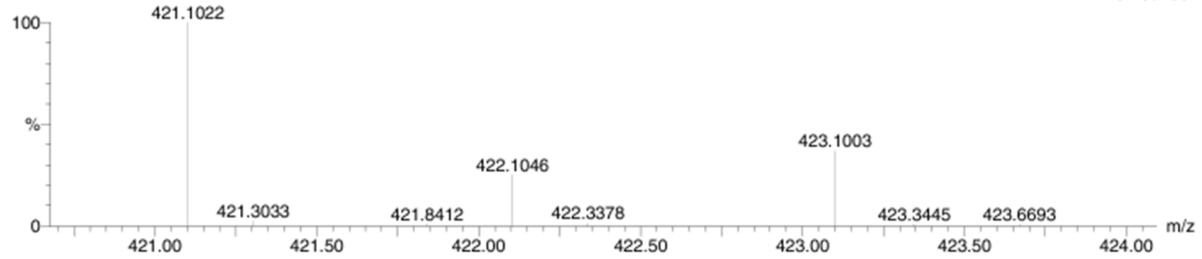

Minimum:	23.00				-3.0			
Maximum:	100.00		5.0	5.0	120.0			
Mass	RA	Calc. Mass	mDa	PPM	DBE	i-FIT	i-FIT (Norm)	Formula
421.1022	100.00	421.1030	-0.8	-1.9	7.5	41.3	0.0	C19 H23 O7 Na 35Cl
422.1046	25.15	---						
423.1003	36.78	423.1001	0.2	0.5	7.5	31.3	0.0	C19 H23 O7 Na 37Cl

Figure S12: HRESI-MS Spectrum of Compound **3**

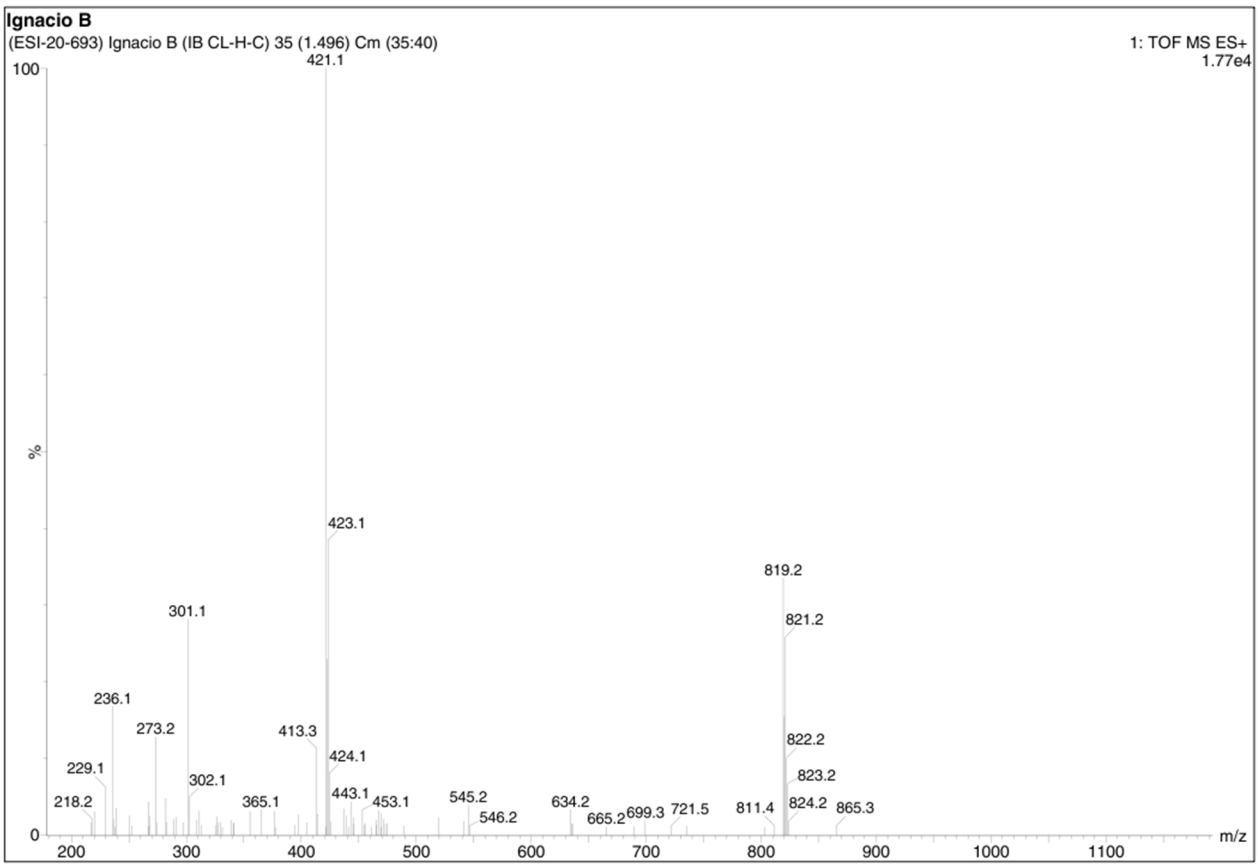

Figure S13: ESI-MS Spectrum of Compound **3**

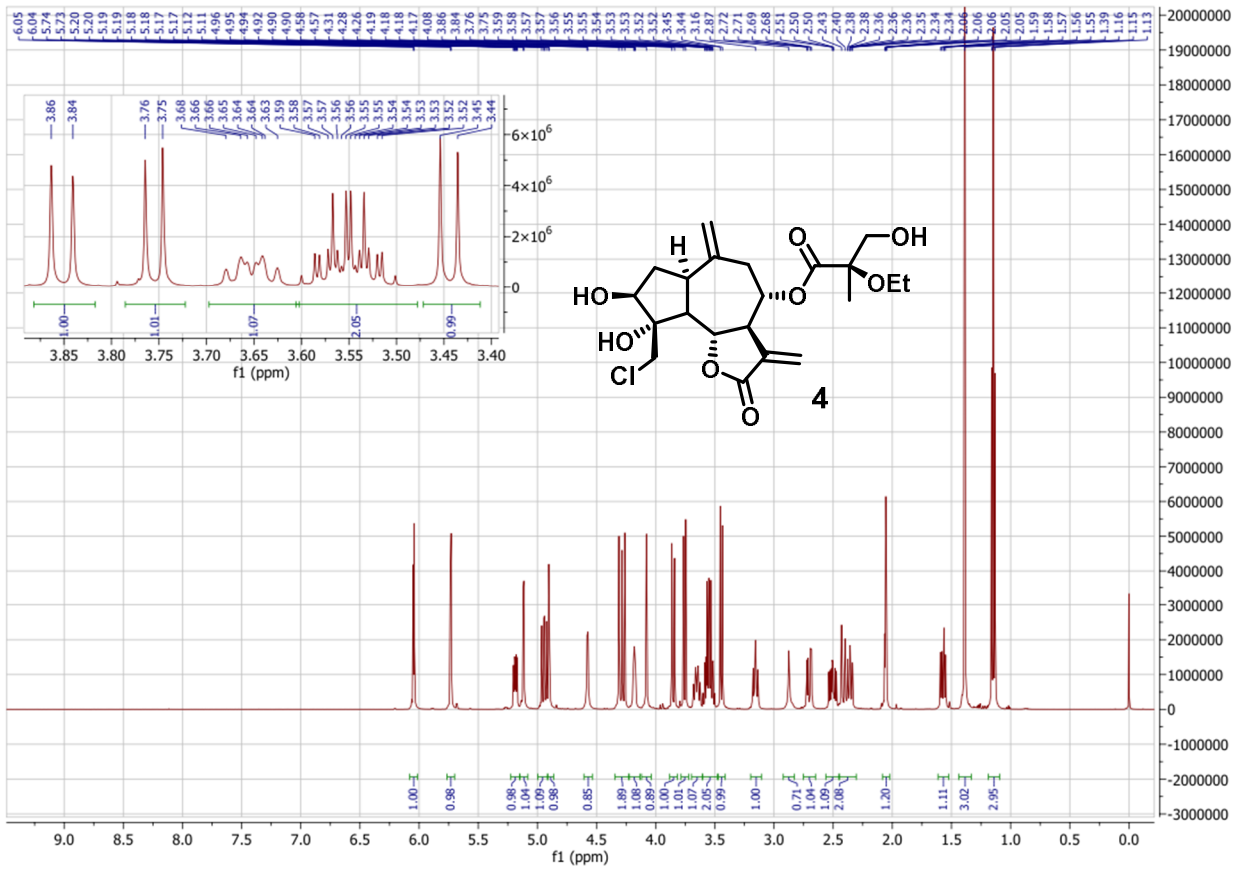

Figure S14: ^{1}H-NMR (500 MHz, Acetone-d6) Spectrum of Compound **4**

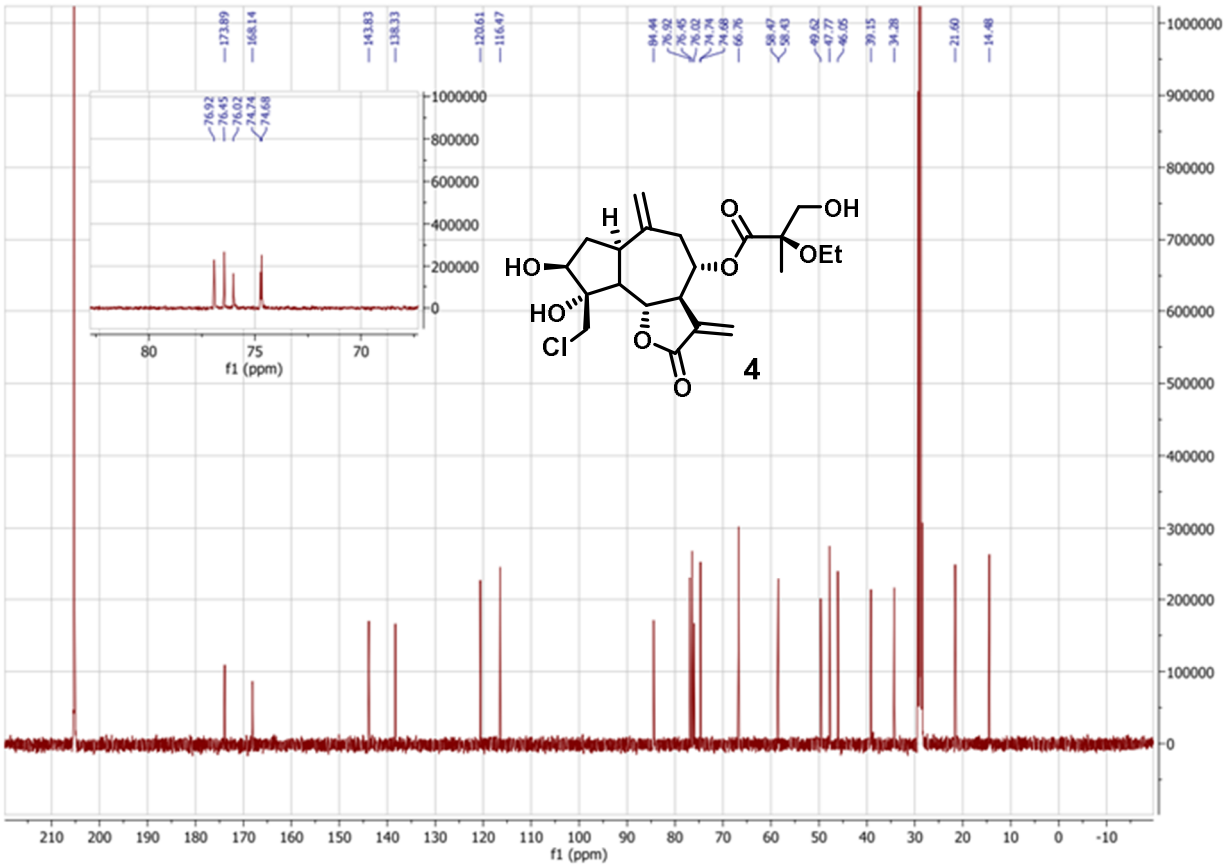

Figure S15: ^{13}C-NMR (125 MHz, Acetone-d6) Spectrum of Compound **4**

Elemental Composition Report **Page 1**

Multiple Mass Analysis: 3 mass(es) processed
Tolerance = 5.0 PPM / DBE: min = -3.0, max = 120.0
Element prediction: Off
Number of isotope peaks used for i-FIT = 3

Monoisotopic Mass, Even Electron Ions
460 formula(e) evaluated with 3 results within limits (all results (up to 1000) for each mass)
Elements Used:
C: 0-25 H: 0-60 O: 0-8 Na: 0-1 35Cl: 0-1 37Cl: 0-1
Ignacio B
(ESI-20-708) Ignacio B (IB Cl H D) 55 (1.861)

2: TOF MS ES+
5.36e+003

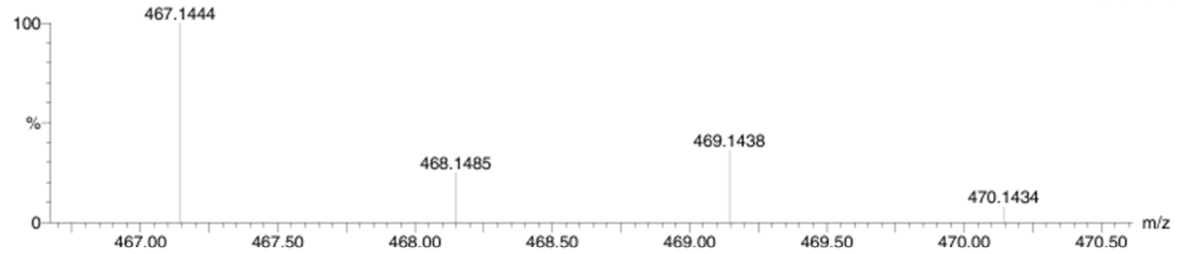

Minimum:	23.00				-3.0			
Maximum:	100.00		5.0	5.0	120.0			
Mass	RA	Calc. Mass	mDa	PPM	DBE	i-FIT	i-FIT (Norm)	Formula
467.1444	100.00	467.1449	-0.5	-1.1	6.5	25.9	0.0	C21 H29 O8 Na 35Cl
468.1485	24.89	---						
469.1438	36.19	469.1443	-0.5	-1.1	9.5	24.5	0.9	C23 H28 O8 37Cl
		469.1419	1.9	4.0	6.5	24.2	0.6	C21 H29 O8 Na 37Cl

Figure S16: HRESI-MS Spectrum of Compound **4**

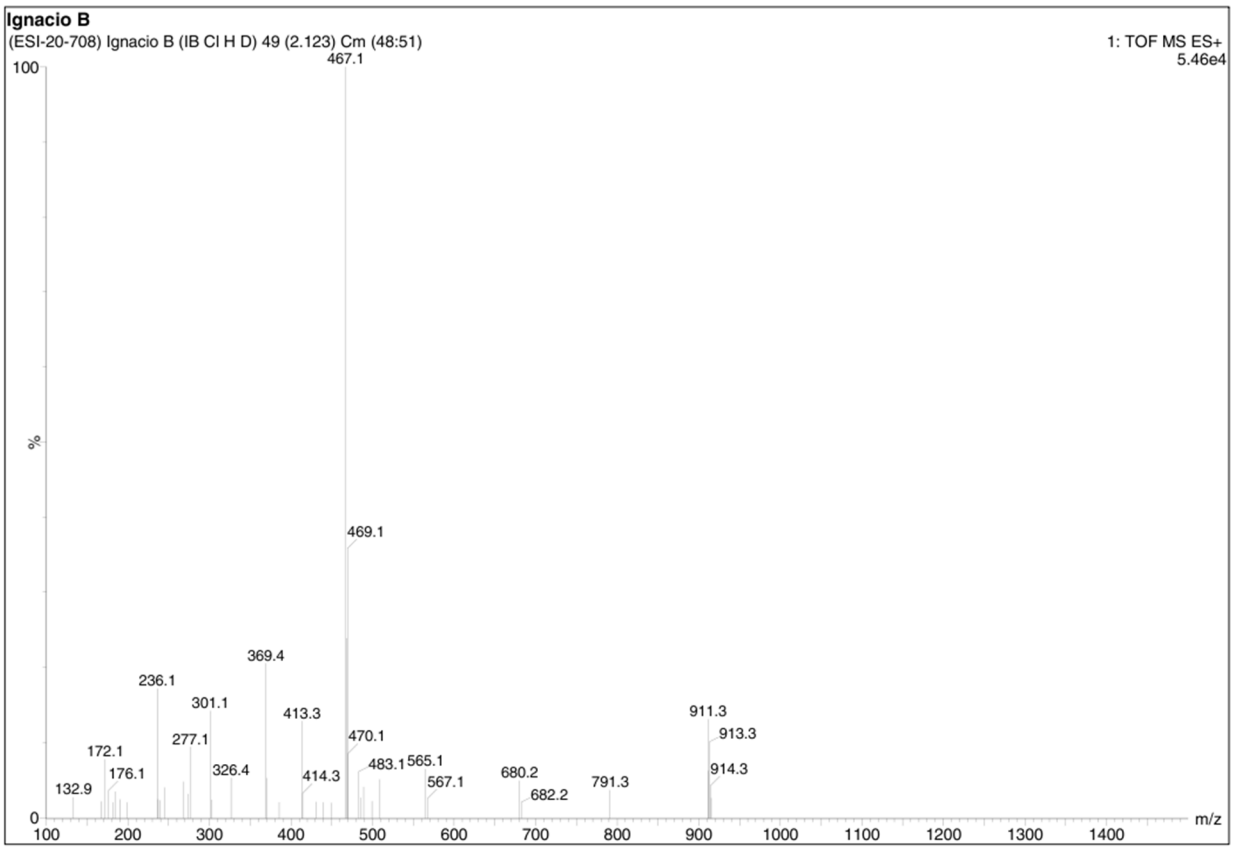

Figure S17: ESI-MS Spectrum of Compound **4**

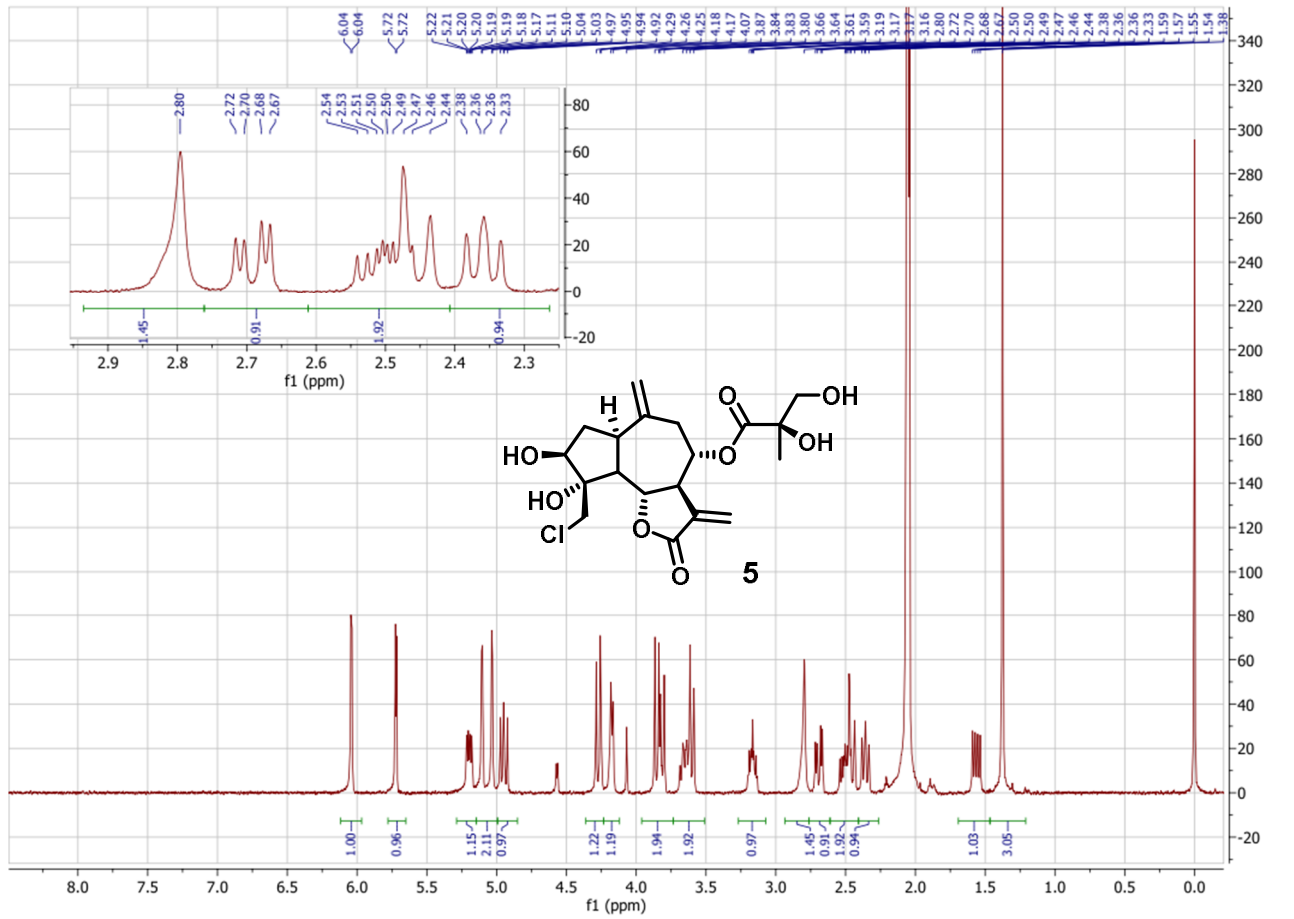

Figure S18: ^{1}H-NMR (500 MHz, Acetone-d6) Spectrum of Compound **5**

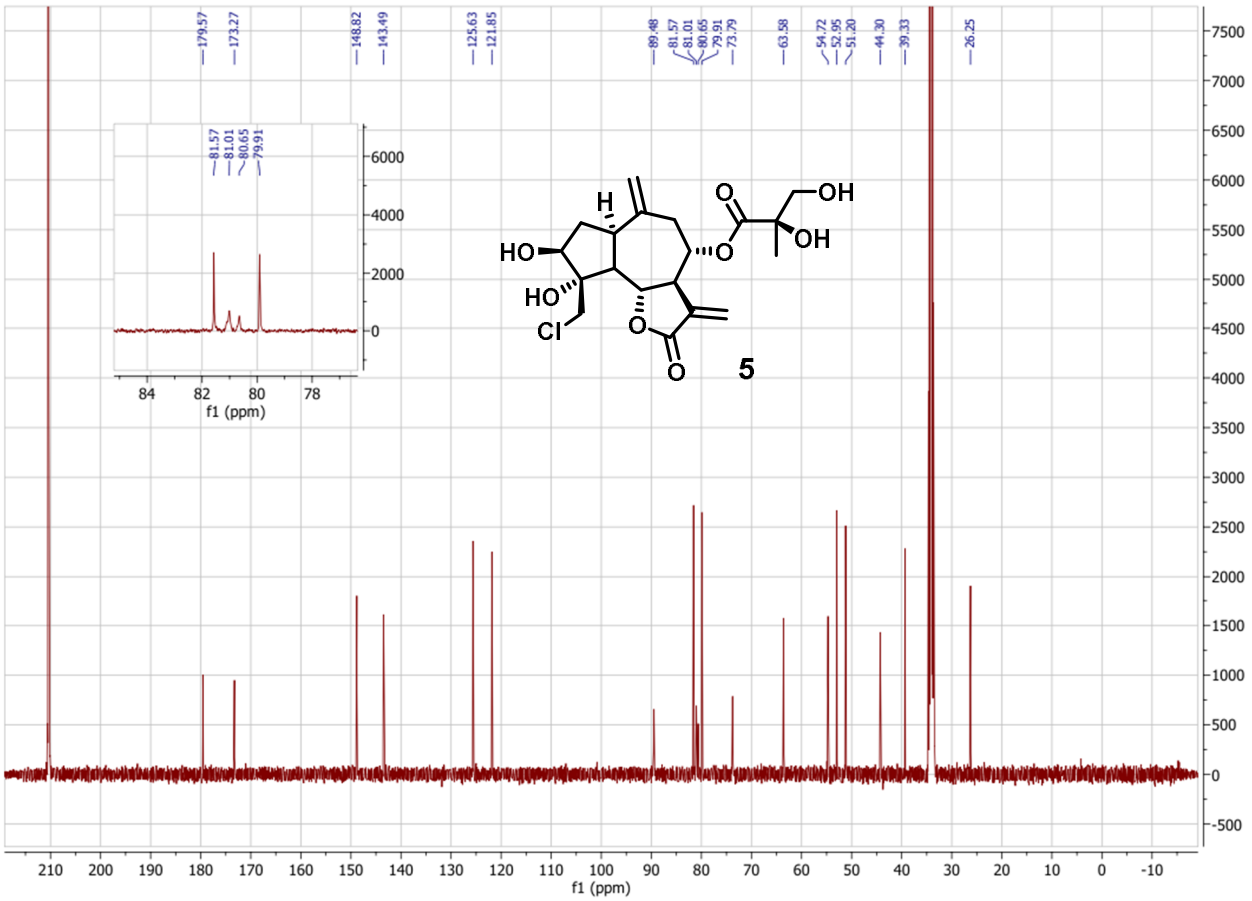

Figure S19: ^{13}C-NMR (125 MHz, Acetone-d6) Spectrum of Compound **5**

Elemental Composition Report **Page 1**

Multiple Mass Analysis: 4 mass(es) processed
Tolerance = 5.0 PPM / DBE: min = -3.0, max = 120.0
Element prediction: Off
Number of isotope peaks used for i-FIT = 3

Monoisotopic Mass, Even Electron Ions
803 formula(e) evaluated with 3 results within limits (all results (up to 1000) for each mass)
Elements Used:
C: 0-20 H: 0-52 O: 0-12 Na: 0-1 35Cl: 0-1 37Cl: 0-1

Ignacio B
(ESI-20-678) Ignacio B (IB CL H E) 20 (0.834)

1: TOF MS ES+
4.67e+003

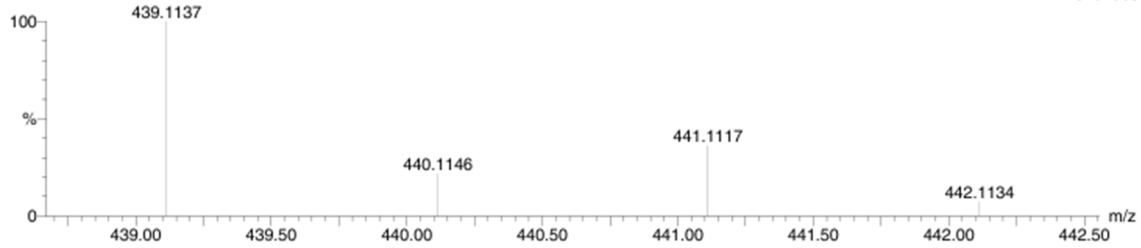

Minimum:	5.00				-3.0			
Maximum:	100.00		5.0	5.0	120.0			
Mass	RA	Calc. Mass	mDa	PPM	DBE	i-FIT	i-FIT (Norm)	Formula
439.1137	100.00	439.1136	0.1	0.2	6.5	25.9	0.0	C19 H25 O8 Na 35Cl
440.1146	21.61	---						
441.1117	36.01	441.1108	0.9	2.0	0.5	21.5	0.6	C15 H29 O10 35Cl 37Cl
		441.1106	1.1	2.5	6.5	21.8	0.8	C19 H25 O8 Na 37Cl
442.1134	7.28	---						

Figure S20: HRESI-MS Spectrum of Compound **5**

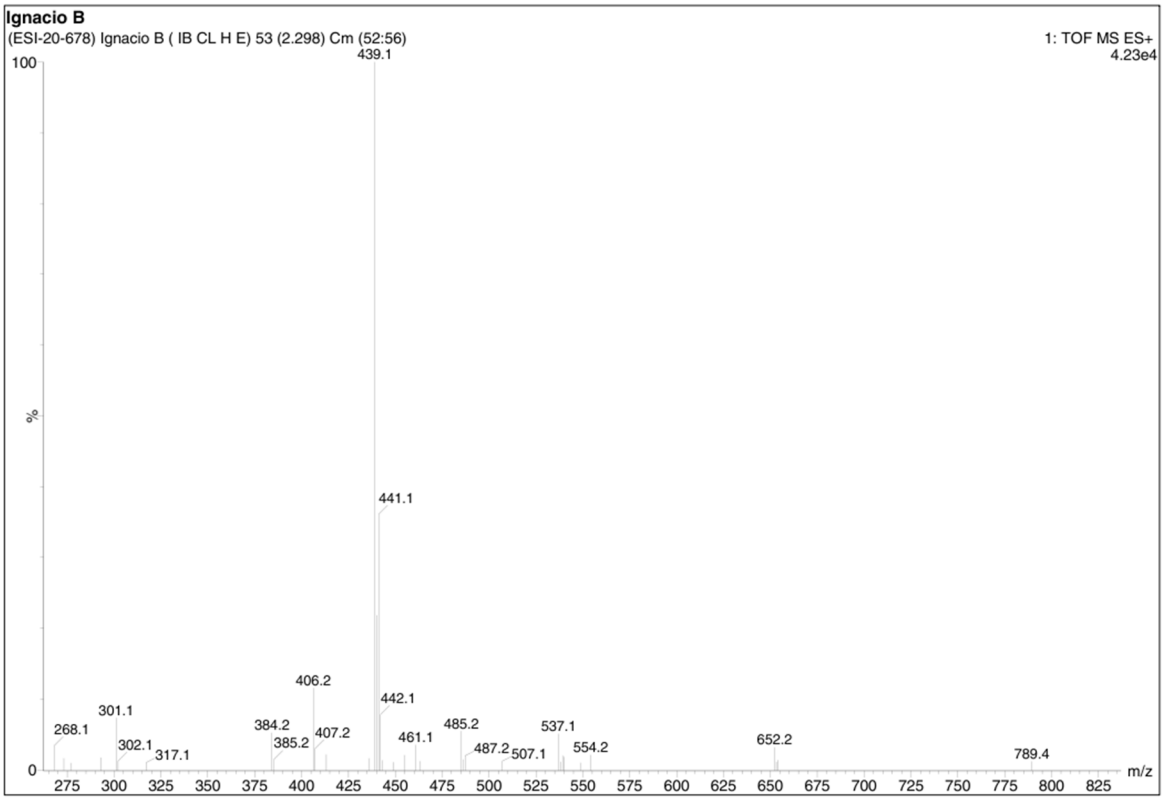

Figure S21: ESI-MS Spectrum of Compound **5**

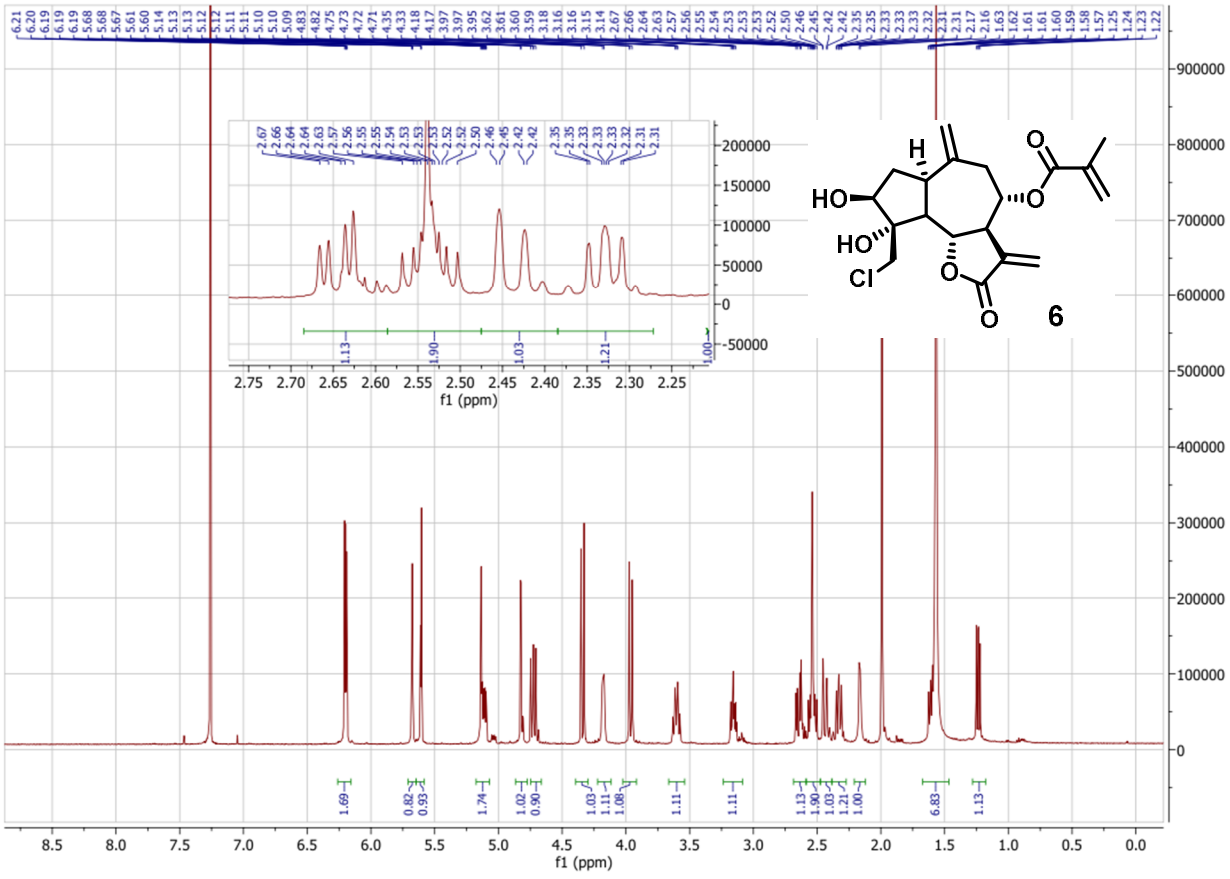

Figure S22: ^{1}H-NMR (500 MHz, $CDCl_3$) Spectrum of Compound **6**

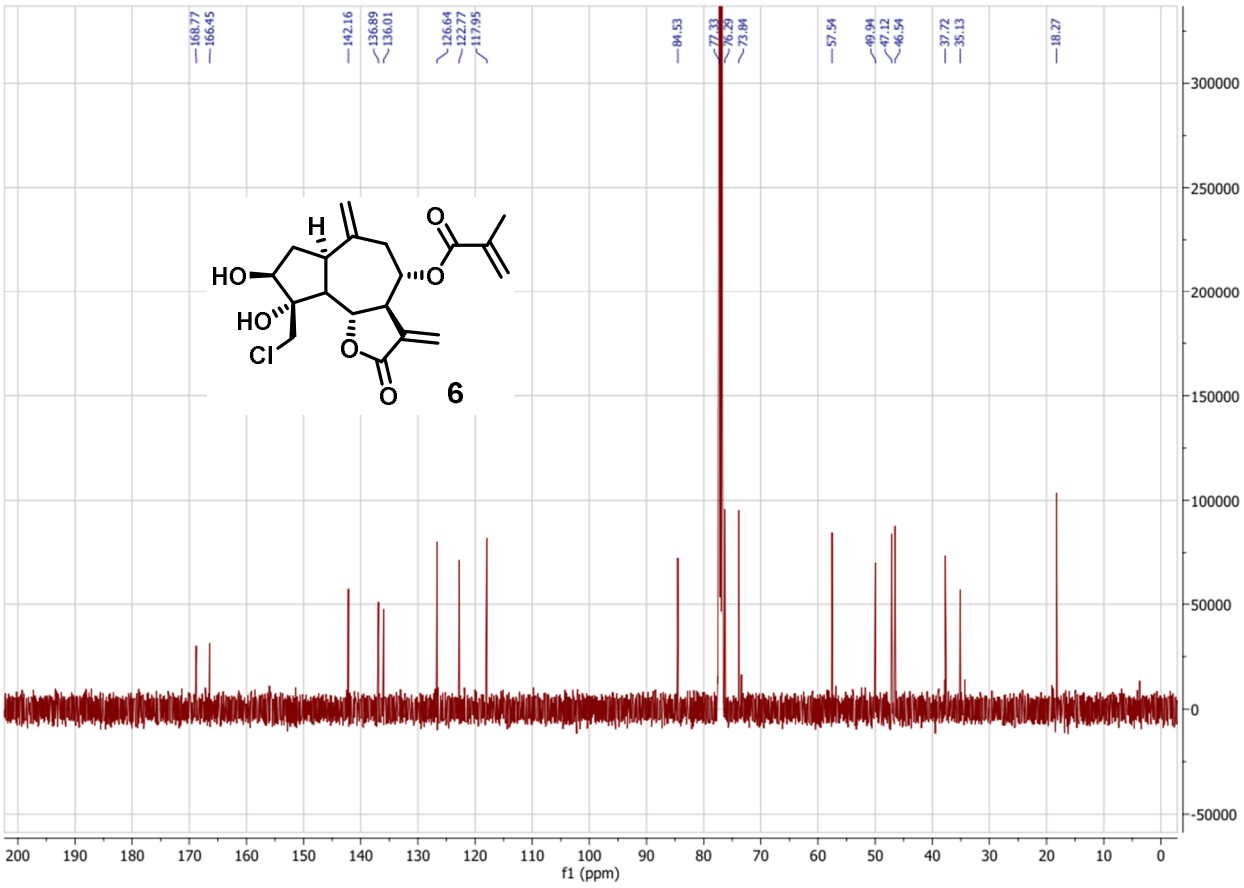

Figure S23: ^{13}C-NMR (125 MHz, $CDCl_3$) Spectrum of Compound **6**

Elemental Composition Report **Page 1**

Multiple Mass Analysis: 3 mass(es) processed
Tolerance = 5.0 PPM / DBE: min = -3.0, max = 120.0
Element prediction: Off
Number of isotope peaks used for i-FIT = 3

Monoisotopic Mass, Even Electron Ions
247 formula(e) evaluated with 3 results within limits (all results (up to 1000) for each mass)
Elements Used:
C: 0-20 H: 0-60 O: 0-6 Na: 0-1 35Cl: 0-1 37Cl: 0-1
Ignacio B
(ESI-20-707) Ignacio B (IB-Lin -A) 82 (3.551)

1: TOF MS ES+
8.20e+002

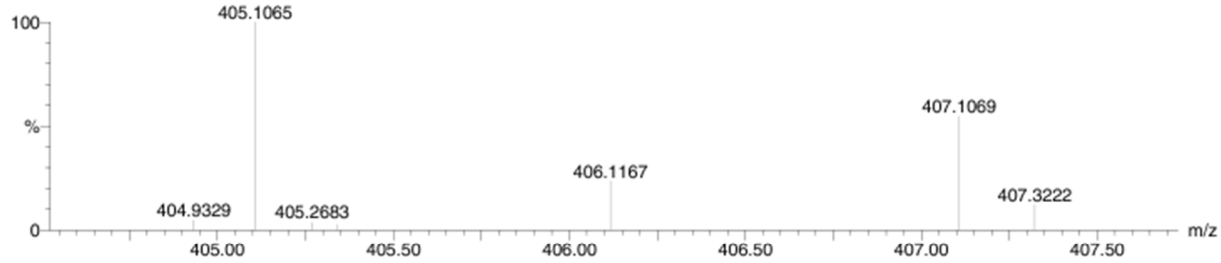

Minimum:	23.00				-3.0			
Maximum:	100.00		5.0	5.0	120.0			
Mass	RA	Calc. Mass	mDa	PPM	DBE	i-FIT	i-FIT (Norm)	Formula
405.1065	100.00	405.1050	1.5	3.7	6.5	43.7	0.6	C19 H25 O5 35Cl 37Cl
		405.1081	-1.6	-3.9	7.5	44.0	0.8	C19 H23 O6 Na 35Cl
406.1167	23.44	---						
407.1069	54.60	407.1051	1.8	4.4	7.5	32.3	0.0	C19 H23 O6 Na 37Cl

Figure S24: HRESI-MS Spectrum of Compound **6**

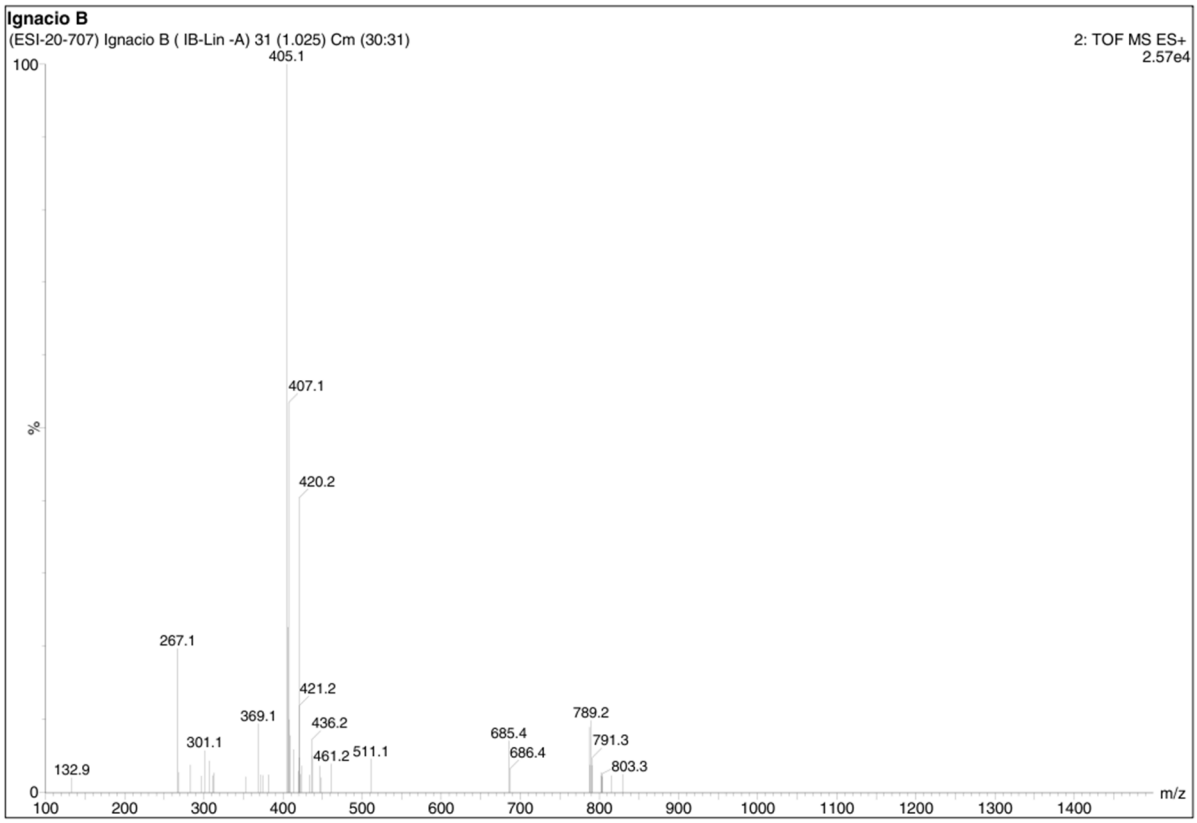

Figure S25: ESI-MS Spectrum of Compound **6**

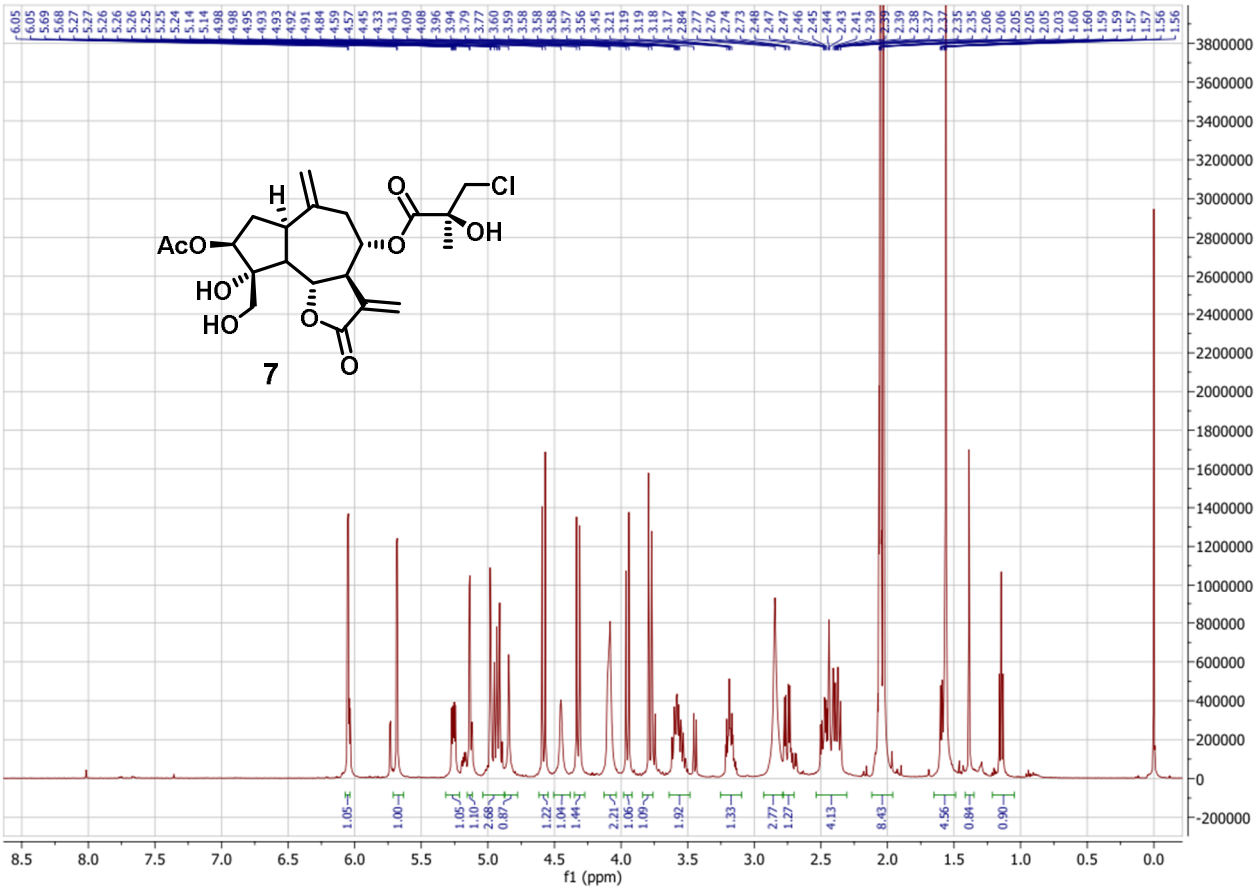

Figure S26: ^{1}H-NMR (500 MHz, Acetone-d6) Spectrum of Compound **7**

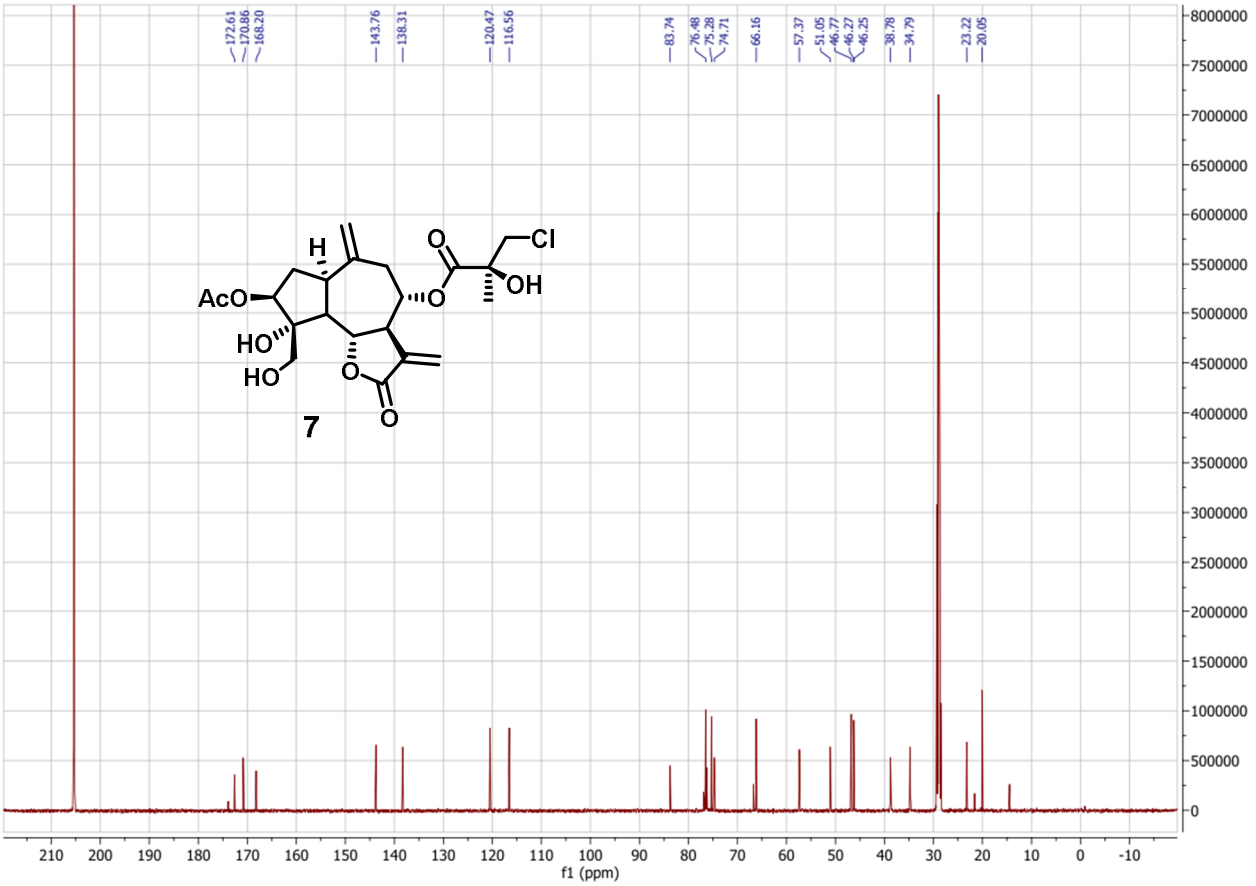

Figure S27: ^{13}C-NMR (125 MHz, Acetone-d6) Spectrum of Compound **7**

Elemental Composition Report **Page 1**

Multiple Mass Analysis: 4 mass(es) processed
Tolerance = 5.0 PPM / DBE: min = -3.0, max = 120.0
Element prediction: Off
Number of isotope peaks used for i-FIT = 3

Monoisotopic Mass, Even Electron Ions
525 formula(e) evaluated with 2 results within limits (all results (up to 1000) for each mass)
Elements Used:
C: 0-22 H: 0-60 O: 0-10 Na: 0-1 35Cl: 0-1 37Cl: 0-1

Ignacio B
(ESI-20-736) Ignacio B (IB -LIN -C) 24 (1.009)

1: TOF MS ES+
6.49e+003

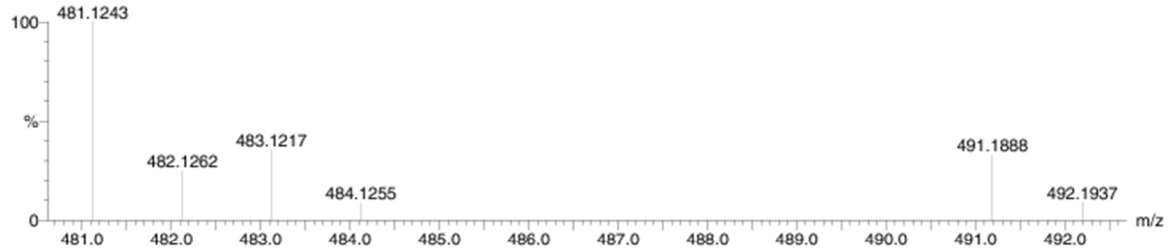

Minimum:	20.00				-3.0			
Maximum:	100.00		5.0	5.0	120.0			
Mass	RA	Calc. Mass	mDa	PPM	DBE	i-FIT	i-FIT (Norm)	Formula
481.1243	100.00	481.1241	0.2	0.4	7.5	26.7	0.0	C21 H27 O9 Na 35Cl
482.1262	24.85	---						
483.1217	35.43	483.1212	0.5	1.0	7.5	23.1	0.0	C21 H27 O9 Na 37Cl
491.1888	32.62	---						

Figure S28: HRESI-MS Spectrum of Compound **7**

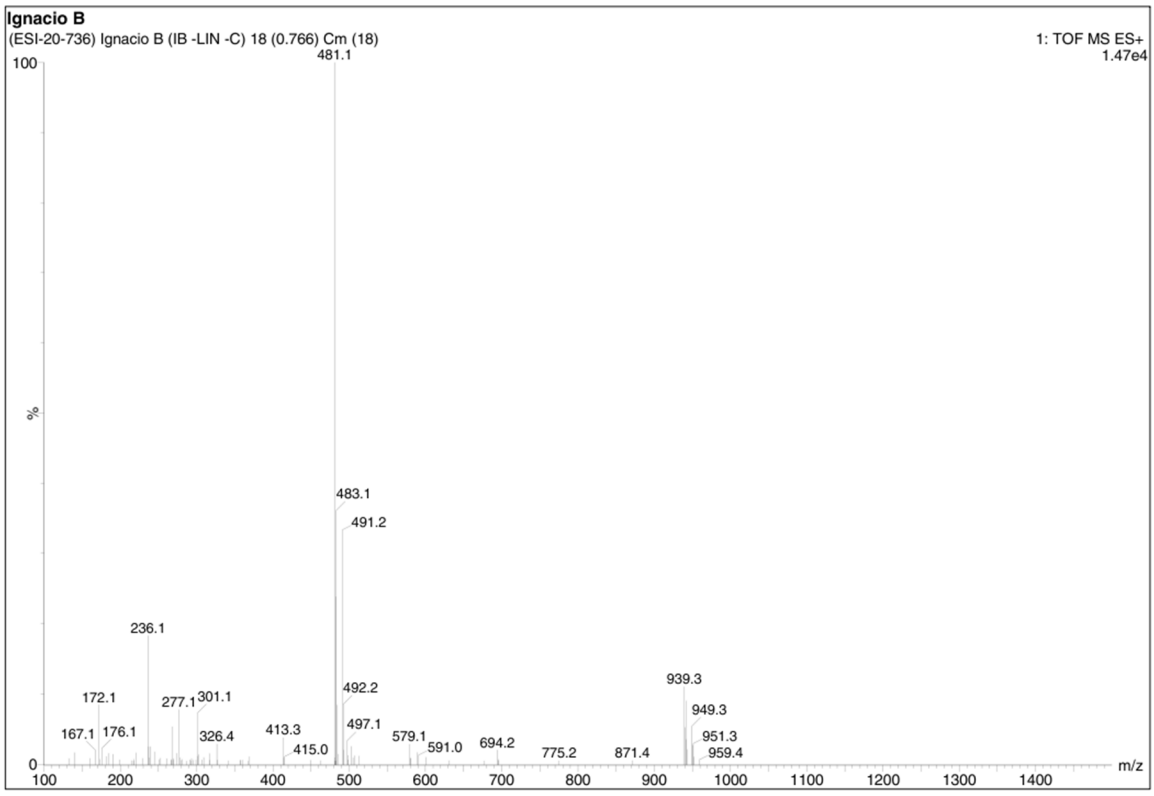

Figure S29: ESI-MS Spectrum of Compound **7**

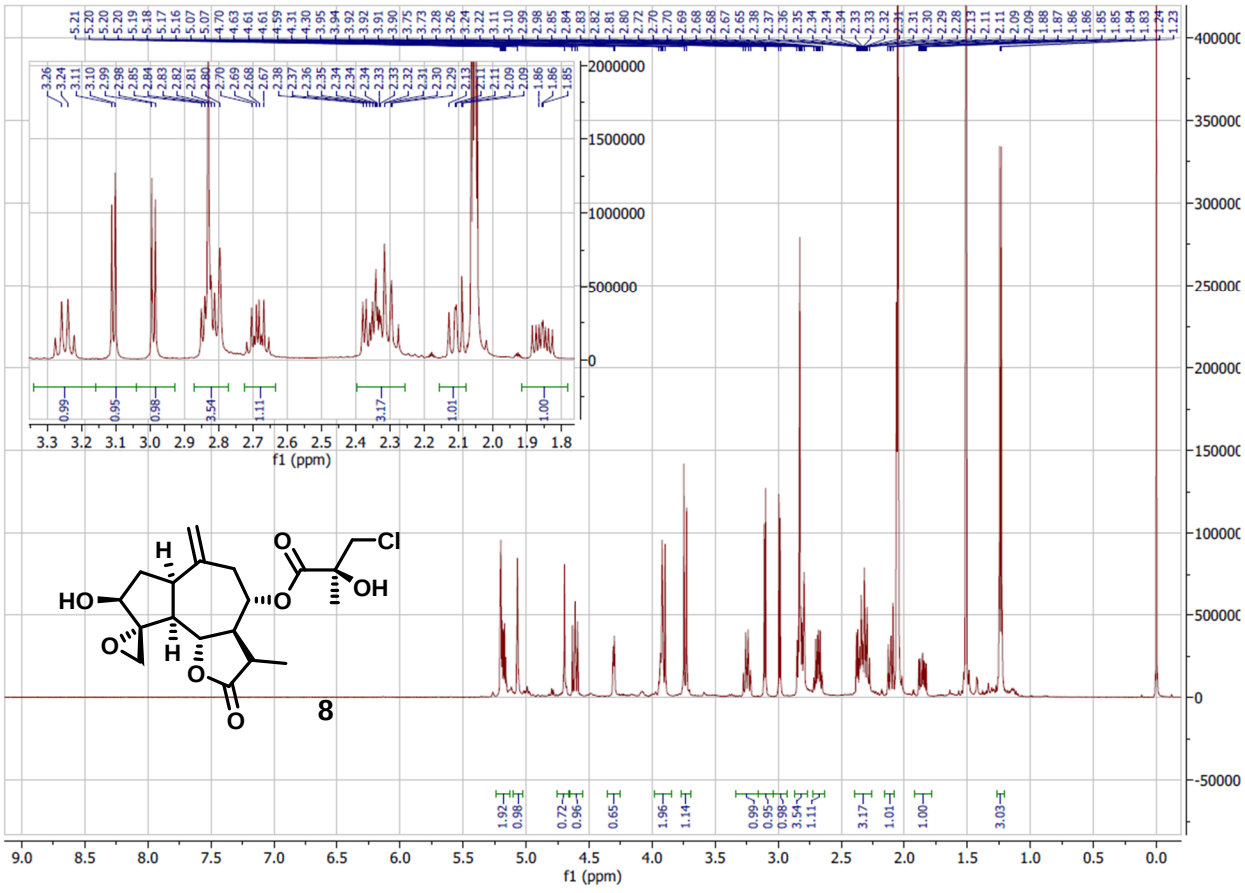

Figure S30: ^{1}H-NMR (500 MHz, Acetone-d6) Spectrum of Compound **8**

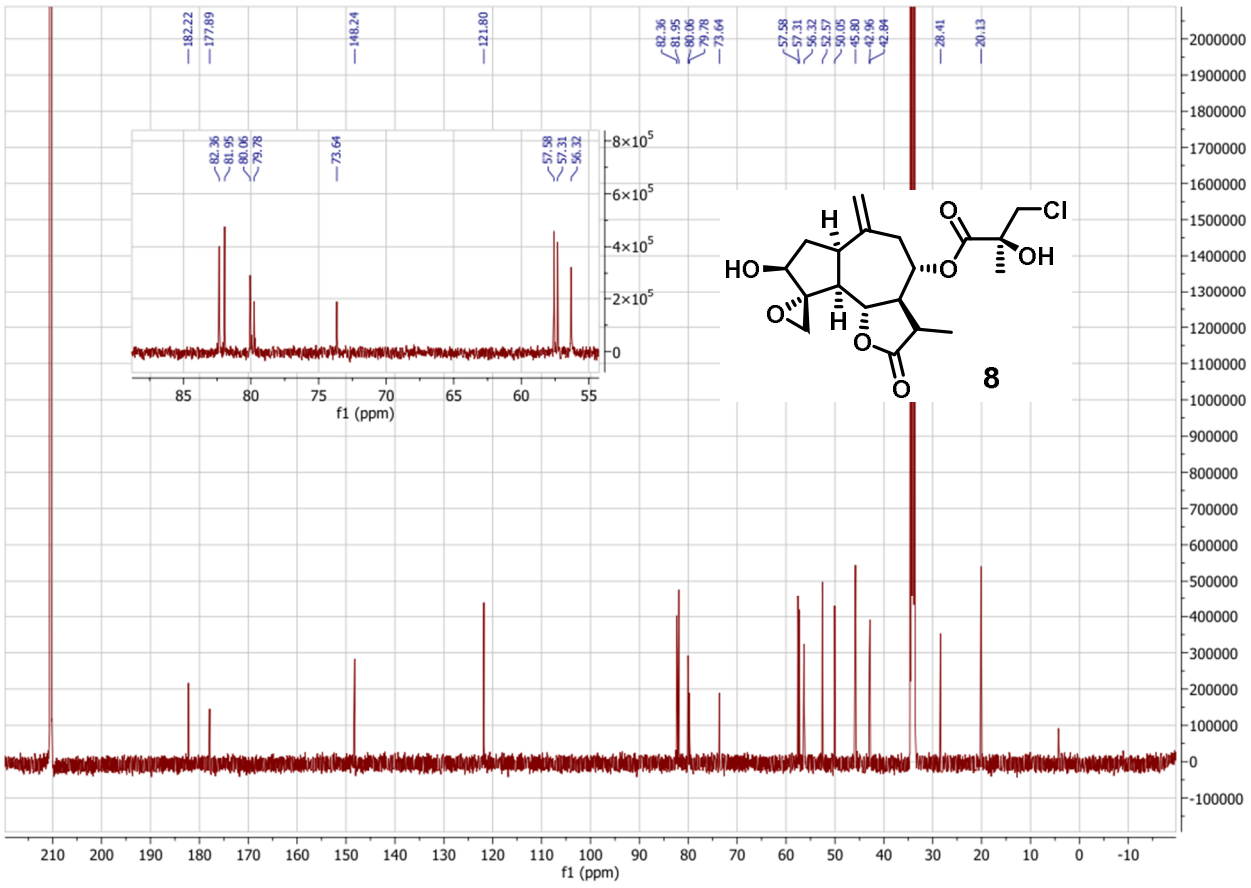

Figure S31: ^{13}C-NMR (125 MHz, Acetone-d6) Spectrum of Compound **8**

Elemental Composition Report **Page 1**

Multiple Mass Analysis: 2 mass(es) processed
Tolerance = 5.0 PPM / DBE: min = -3.0, max = 120.0
Element prediction: Off
Number of isotope peaks used for i-FIT = 3

Monoisotopic Mass, Even Electron Ions
117 formula(e) evaluated with 2 results within limits (all results (up to 1000) for each mass)
Elements Used:
C: 0-20 H: 0-25 O: 0-7 Na: 0-1 35Cl: 0-1 37Cl: 0-1

Ignacio B
(ESI-20-683) Ignacio B (IB -CL-24) 104 (4.490)

1: TOF MS ES+
2.78e+003

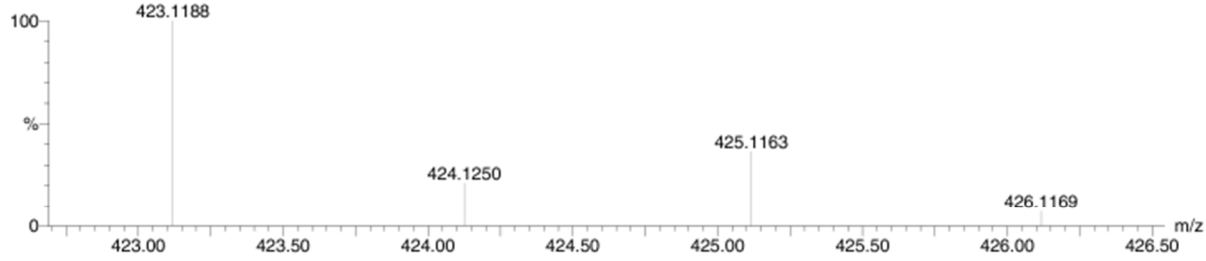

Minimum:	23.00				-3.0			
Maximum:	100.00		5.0	5.0	120.0			
Mass	RA	Calc. Mass	mDa	PPM	DBE	i-FIT	i-FIT (Norm)	Formula
423.1188	100.00	423.1187	0.1	0.2	6.5	24.9	0.0	C19 H25 O7 Na 35Cl
425.1163	36.40	425.1157	0.6	1.4	6.5	20.2	0.0	C19 H25 O7 Na 37Cl

Figure S32: HRESI-MS Spectrum of Compound **8**

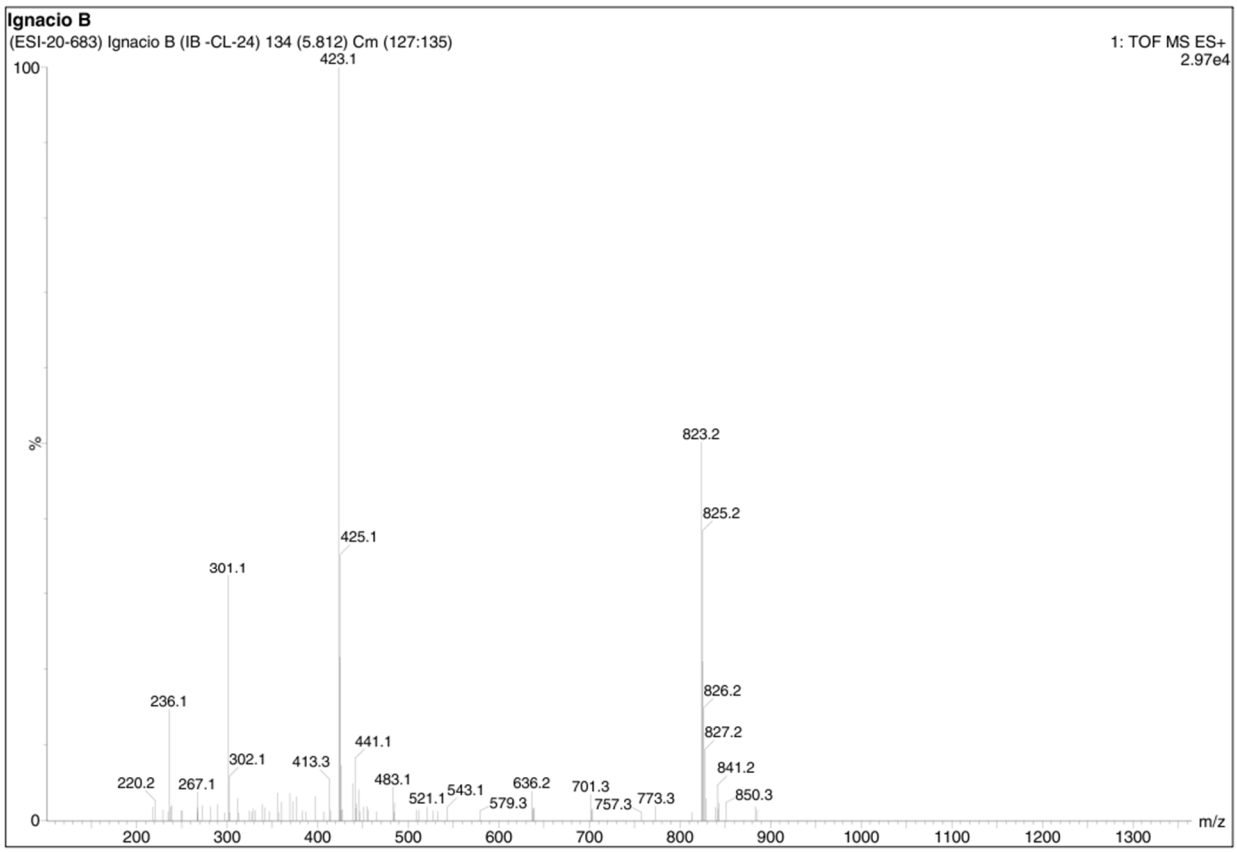

Figure S33: ESI-MS Spectrum of Compound **8**

International Journal of
Molecular Sciences

IMPACT FACTOR 6.208

Indexed in: PubMed

Article

Guanidine Derivatives Containing the Chalcone Skeleton Are Potent Antiproliferative Compounds against Human Leukemia Cells

Francisco Estévez-Sarmiento, Ester Saavedra, Ignacio Brouard, Jesús Peyrac, Judith Hernández-Garcés, Celina García, José Quintana and Francisco Estévez

Special Issue
Bioactive Compounds in Cancer, Inflammation and Related Diseases

Edited by
Dr. Guan-Jhong Huang

MDPI

https://doi.org/10.3390/ijms232415518

International Journal of
Molecular Sciences

MDPI

Article

Guanidine Derivatives Containing the Chalcone Skeleton Are Potent Antiproliferative Compounds against Human Leukemia Cells

Francisco Estévez-Sarmiento [1,*], Ester Saavedra [1,2], Ignacio Brouard [3], Jesús Peyrac [3], Judith Hernández-Garcés [4], Celina García [4], José Quintana [1] and Francisco Estévez [1]

[1] Departamento de Bioquímica y Biología Molecular, Fisiología, Genética e Inmunología, Instituto Universitario de Investigaciones Biomédicas y Sanitarias (IUIBS), Grupo de Química Orgánica y Bioquímica, Universidad de Las Palmas de Gran Canaria, Unidad Asociada al Consejo Superior de Investigaciones Científicas (CSIC), 35016 Las Palmas de Gran Canaria, Spain
[2] Instituto Canario de Investigación del Cáncer (ICIC), 35016 Las Palmas de Gran Canaria, Spain
[3] Instituto de Productos Naturales y Agrobiología, Consejo Superior de Investigaciones Científicas, 38206 La Laguna, Spain
[4] Instituto Universitario de Bio-Orgánica AG, Departamento de Química Orgánica, Universidad de La Laguna (Tenerife), 38200 San Cristóbal de La Laguna, Spain
* Correspondence: francisco.estevez103@alu.ulpgc.es or festevez1985@gmail.com; Tel.: +34-928-451443; Fax: +34-928-451441

Abstract: In this study, we investigated the effects of eleven synthetic guanidines containing the 1,3-diphenylpropenone core on the viabilities of six human cancer cells. The most cytotoxic compound against human cancer cells of this series contains a *N*-tosyl group and a *N*-methylpiperazine moiety **6f**. It was cytotoxic against leukemia cells (U-937, HL-60, MOLT-3, and NALM-6) with significant effects against Bcl-2-overexpressing U-937/Bcl-2 cells as well as the human melanoma SK-MEL-1 cell line. It exhibited low cytotoxicity against quiescent or proliferating human peripheral blood mononuclear cells. The IC_{50} value for the leukemia U-937 cells was 1.6 ± 0.6 μM, a similar value to that in the antineoplastic agent etoposide. The guanidine containing a *N*-phenyl substituent **6i** was also as cytotoxic as the guanidine containing the *N*-tosyl substituent and the *N*-methylpiperazine group **6f** against human U-937 leukemia cells and both synthetic guanidines were potent apoptotic inducers. Cell death was mediated by the activation of the initiator caspase-9 and the executioner caspase-3, and associated with the release of cytochrome *c*. These synthetic guanidines are potent cytotoxic compounds against several human leukemia cells and even the human melanoma cell line SK-MEL-1 and might be useful in the development of new strategies in the fight against cancer.

Keywords: apoptosis; caspases; cell cycle; cytotoxicity; hybrid chalcones; guanidines

Citation: Estévez-Sarmiento, F.; Saavedra, E.; Brouard, I.; Peyrac, J.; Hernández-Garcés, J.; García, C.; Quintana, J.; Estévez, F. Guanidine Derivatives Containing the Chalcone Skeleton Are Potent Antiproliferative Compounds against Human Leukemia Cells. *Int. J. Mol. Sci.* **2022**, *23*, 15518. https://doi.org/10.3390/ijms232415518

Academic Editor: Guan-Jhong Huang

Received: 31 October 2022
Accepted: 6 December 2022
Published: 8 December 2022

1. Introduction

The development of new hybrid cancer drugs by the combination of two or more biologically relevant "parent" molecules can improve bioactivity, specificity, and help overcome drug resistance. Incorporating a natural product's privileged structure such as chalcone as one of the parent molecules is an excellent starting point to develop new drugs [1]. Chalcones, consisting of a diaryl propenone system, are the major precursors for the biosynthesis of flavonoids and can interact with several cancer drug targets, exhibiting promising in vitro and in vivo activities against both drug-susceptible and drug-resistant cancers [2]. The chalcone core is considered an appropriate chemical entity to implement rational fragment-based drug discovery strategies in the search of novel anticancer agents [3]. These chemical entities are highly suitable for further optimization based on systematic functionalization of the starting fragment core, taking into account their pharmacological and physicochemical properties. Recently, numerous chalcone hybrids have been prepared

and evaluated as potential anticancer agents. Some of them have shown excellent potency against tumor cells in vitro and in vivo, indicating that these compounds may have therapeutic value [3,4].

Guanidines are versatile organosuperbases and are able to bind to carboxylates, phosphates, and metals. The guanidinium cation participates in special interactions between ligands and receptors or enzymes and substrates and may have important biological properties and chemical and pharmaceutical implications. They are of great interest in medicinal chemistry and constitute a key motif of many clinical drugs including the anti-diabetic drug dimethyldiguanide and the peptic ulcer drug cimetidine. Guanidine derivatives are also widely distributed in nature and have attracted a lot of attention due to their chemical diversity and broad biological activities [5,6].

The aim of this study was (i) to synthesize a series of benzyloxychalcones containing a trisubstituted guanidine functional group and (ii) to explore the effects of different substituents on the cytotoxic effects of guanidine functionality against six human cancer cell lines. These substituents included (i) the presence of a *p*-tosylsulfonamide or phenyl moiety on one of the nitrogen atoms of the guanidine functional group and (ii) the presence of different groups such as the isopropyl, diisopropyl, phenyl, or a heterocycle on another nitrogen atom of the guanidine functional group. In addition, we explored whether the most cytotoxic compounds induce cell death by apoptosis in leukemia cells.

2. Results

2.1. Synthesis

In the present study, we explored the effects of a collection of 11 trisubstituted guanidine-chalcone hybrids on viability of six human cancer cell lines. These compounds were prepared in an efficient one-pot process in which three reactions were carried out in the same solvent through the sequential addition of three reagents as indicated below. This atom-economy procedure incorporates almost all atoms of starting materials and reagents into the final product by the attachment of chemical building blocks. The azidochalcone **3** was prepared in a straightforward manner by a standard aldolic condensation procedure combining the acetophenone **1** with the benzaldehyde **2**. The azidochalcone **3** was treated with triphenylphosphine until the complete formation of iminophosphorane **4**. The isocyanate was then added to the iminophosphorane compound to produce carbodiimide **5**, which was immediately transformed into guanidine **6** by adding different amines (Scheme 1). This synthesis is based on a similar one described previously by Foster et al. [1]. Table 1 shows the chemical structures of the synthesized guanidine–chalcone hybrids **6a**–**6k** and the starting reagents.

Table 1. Azidochalcone, isocyanates, and amines as starting reagents to generate the corresponding guanidine–chalcone hybrids.

Chalcone	Isocyanate	Amine	Product
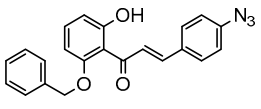 3	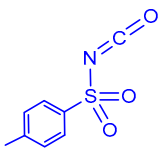		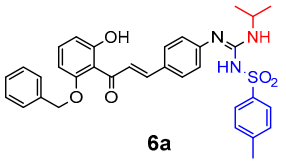 **6a**
			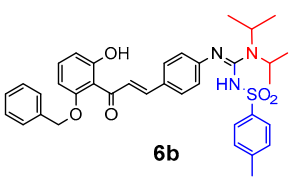 **6b**

Table 1. *Cont.*

Chalcone	Isocyanate	Amine	Product
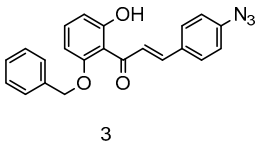 3	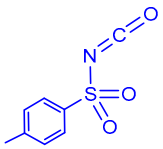		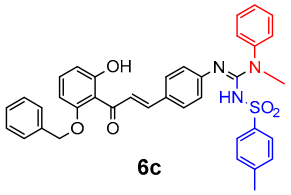 **6c**
			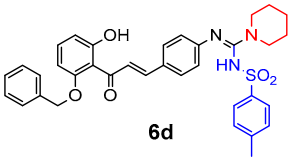 **6d**
			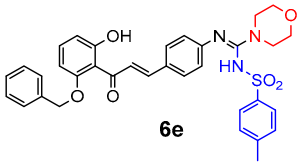 **6e**
			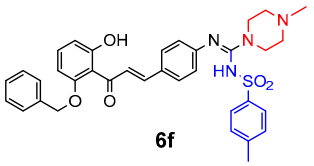 **6f**
		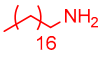	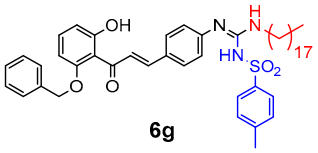 **6g**
			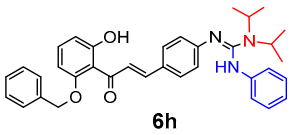 **6h**
			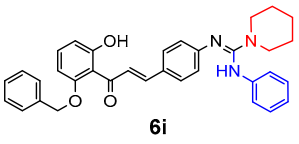 **6i**
	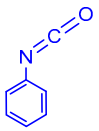		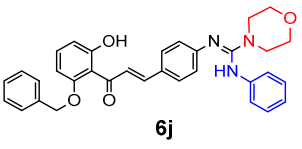 **6j**
			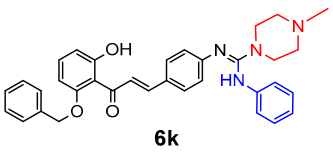 **6k**

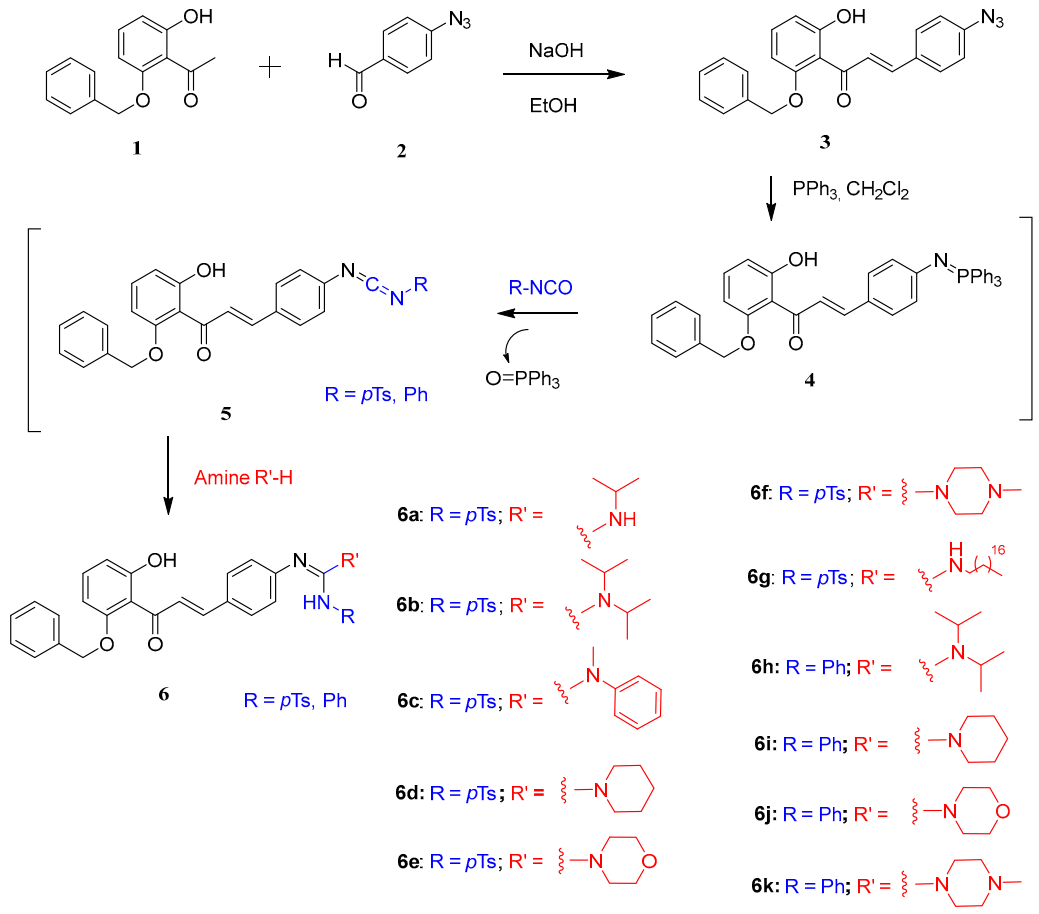

Scheme 1. Synthesis of trisubstituted guanidine–chalcone hybrids.

2.2. Hybrid Compounds Inhibit the Viability of Human Cancer Cells

The potential cytotoxicity of hybrid compounds containing the chalcone skeleton and a guanidine group was evaluated using several human cancer cells (Table 2). These cancer cells included the histiocytic lymphoma U-937, the acute promyelocytic leukemia HL-60, the acute lymphoblastic leukemia MOLT-3, the pre-B NALM-6, the cell line over-expressing the human Bcl-2 protein (U-937/Bcl-2), and the melanoma SK-MEL-1 cell line.

The studies of the effect on cell viability of this series of compounds revealed that in the case of hybrid compounds containing the *p*-tosylsulfonyl group, the cytotoxicity was dependent on the corresponding amine. As shown in Table 2, the isopropylamino derivative **6a** and the phenylmethylamino derivative **6c** were more potent than the corresponding diisopropylamino derivative **6b**. The cytotoxicity increased in the following order: diisopropylamino **6b** < isopropylamino **6a** ~ phenylmethylamino **6c**, except for MOLT-3 cells, in which the three compounds showed similar IC_{50} values and for NALM-6 in which the most cytotoxic compound was the isopropylamino derivative **6a**. There was an important change in cytotoxicity for compounds with a heterocycle structure as a substituent, according to whether the amino group was from a piperidine **6d**, a morpholine **6e,** or a *N*-methylpiperazine **6f**. In these experiments, etoposide and doxorubicin were used as positive controls. In general, the most cytotoxic compound was the hybrid compound **6f**. The greatest differences in cytotoxicity were observed in U-937 cells in which the order of cytotoxicity was: **6f** > **6e** > **6d**. In MOLT-3 cells, these three derivatives were almost equally potent with IC_{50} values between 1.5 μM and 3.3 μM, and in U-937/Bcl-2 cells, the morpholine derivative **6e** showed similar potency to the piperazine derivative **6f**. As shown in Table 2, the *N*-methylpiperazine derivative **6f** was the most cytotoxic compound in all cell lines assayed including the melanoma cell line SK-MEL-1. The IC_{50} values were between 1.5 μM and 4.5 μM, similar to the antineoplastic etoposide, which showed IC_{50}

values of 1.8 ± 0.2 μM, 0.6 ± 0.2 μM, and 0.2 ± 0.1 μM for U-937, HL-60 and MOLT-3, respectively. However, the substitution of the cyclic amine **6f** for an amine containing a long (C18) aliphatic chain yielded a compound (hybrid compound **6g**) which was not cytotoxic against the cancer cell lines assayed, probably due to its low solubility.

Table 2. Effects on cell viability of hybrid compounds on human cancer cells.

	IC_{50} (μM)					
Compound	**U-937**	**HL-60**	**MOLT-3**	**NALM-6**	**U-937/Bcl-2**	**SK-MEL-1**
3	-	-	7.4 ± 0.4	11.6 ± 1.6	-	-
6a	11.4 ± 6.5	3.7 ± 1.6	2.9 ± 1.1	2.9 ± 0.5	2.9 ± 0.2	-
6b	18.5 ± 9.6	20.5 ± 9.5	2.0 ± 0.7	27.0 ± 0.8	11.7 ± 7.0	-
6c	9.5 ± 5.3	4.2 ± 0.5	2.5 ± 0.2	9.9 ± 3.1	4.2 ± 1.2	-
6d	-	28.5 ± 14.3	3.3 ± 0.6	6.6 ± 1.2	24.6 ± 5.4	-
6e	5.4 ± 2.1	3.8 ± 1.1	3.2 ± 1.5	3.1 ± 0.5	2.3 ± 0.9	14.3 ± 5.7
6f	1.6 ± 0.6	1.6 ± 1.0	1.5 ± 0.0	2.7 ± 0.0	2.2 ± 0.8	4.5 ± 0.4
6g	-	-	-	-	-	-
6h	10.6 ± 2.6	5.2 ± 0.9	4.3 ± 0.5	5.4 ± 0.2	14.0 ± 6.6	5.2 ± 1.0
6i	3.5 ± 1.1	3.2 ± 0.6	7.1 ± 1.3	10.8 ± 0.5	5.1 ± 1.8	13.8 ± 1.2
6j	8.6 ± 1.1	6.2 ± 1.7	1.8 ± 0.5	4.1 ± 0.5	11.7 ± 3.4	5.4 ± 0.8
6k	14.0 ± 1.1	11.4 ± 5.5	21.7 ± 6.5	24.8 ± 3.3	14.0 ± 5.1	-
Etoposide	1.8 ± 0.2	0.6 ± 0.2	0.2 ± 0.1	ND	ND	9.0 ± 3.0
Doxorubicin	0.1 ± 0.0	ND	ND	ND	ND	0.3 ± 0.1

Cells were cultured for 72 h and the IC_{50} values were determined as described in Section 4. Data are expressed as means ± SEM from the dose-response curves of 3–5 independent experiments with three determinations in each. - means not active, IC_{50} values > 30 μM. ND, not determined.

In the case of *p*-tosylsulfonyl derivatives, the most potent compound contains a *N*-methylpiperazine **6f** and the order of potency was: *N*-methylpiperazine **6f** > morpholine **6e** > piperidine **6d**, mainly in U-937 and SK-MEL-1. However, compounds **6e** and **6f** showed similar IC_{50} values in HL-60, NALM-6, and U-937/Bcl-2, and compounds **6d**, **6e,** and **6f** were equally potent against MOLT-3.

Among the *N*-phenyl derivatives, compound **6i** containing a piperidine ring was, in general, the most cytotoxic compound with IC_{50} values that were either less than (U-937, HL-60, MOLT-3, and U-937/Bcl-2) or close to (NALM-6, SK-MEL-1) 10 μM. The substitution of the piperidine **6i** ring by a *N*-methylpiperazine **6k** ring determined a decrease in cytotoxicity. In contrast, the substitution of the piperidine **6i** by a morpholine **6j** increased the cytotoxicity against MOLT-3, NALM-6, and SK-MEL-1.

In general, over expression of Bcl-2 did not confer protection against hybrid compounds-induced cytotoxicity since the IC_{50} values were similar or even lower than that for the parental U-937 cells. In U-937/Bcl-2 cells, the *p*-tosyl derivatives containing the morpholine ring **6e**, the phenyl group **6c,** and *N*-methylpiperazine **6f** were equally potent showing IC_{50} values between 2.2 ± 0.8 μM and 4.2 ± 1.2 μM. In these cells, the *N*-phenyl guanidine derivative containing the piperidine ring **6i** was equally cytotoxic as it was against the parental U-937 cell line. Most compounds assayed in MOLT-3 cells were equally potent, showing IC_{50} values below 10 μM. The exceptions were the *p*-tosyl derivative containing an octadecyl substituent **6g** and the *N*-phenylguanidine containing the *N*-methylpiperazine ring **6k**. A similar trend was observed in NALM-6 cells since most compounds showed similar IC_{50} values. The exception was the *p*-tosyl derivative **6b**, which showed low cytotoxicity against NALM-6. The substitution of the *p*-tosyl-sulfonyl group **6b** by a phenyl group **6h** increased the cytotoxicity five-fold (IC_{50} = 27.0 ± 0.8 μM vs. IC_{50} = 5.4 ± 0.2 μM). The piperidine derivative (compound **6i**) was more potent than the *p*-tosylsulfonyl derivative (compound **6d**) in U-937, U-937/Bcl-2, HL-60, and SK-MEL-1 cells.

The structure–activity relationship (SAR) reveals that the introduction of the guanidine group enhances the cytotoxicity of the chalcone skeleton in comparison with the azidochalcone **3**, and the results of the cytotoxicity assays of *p*-tosylsulfonyl derivatives revealed that the most potent compound contains a *N*-methylpiperazine ring and the order of potency was *N*-methylpiperazine > morpholine > piperidine.

The cytotoxicity assays of the *N*-phenyl derivatives series revealed that: (i) the hybrid compound **6i** containing a piperidine ring was, in general, the most cytotoxic compound showing IC_{50} values below 10 μM, except in NALM-6 (IC_{50} = 10.8 ± 0.5 μM) and SK-MEL-1 (IC_{50} = 13.8 ± 1.2 μM) cells; (ii) the substitution of the piperidine **6i** by a morpholine ring **6j** decreased the cytotoxicity against human U-937, HL-60, and U-937/Bcl-2 cells; and (iii) the substitution of the piperidine ring **6i** by a *N*-methylpiperazine ring **6k** decreased the cytotoxicity against all cell lines assayed.

The SAR against U-937 and HL-60 leukemia cells of this series of hybrid compounds containing the chalcone skeleton and a guanidine group is displayed graphically in Figure 1.

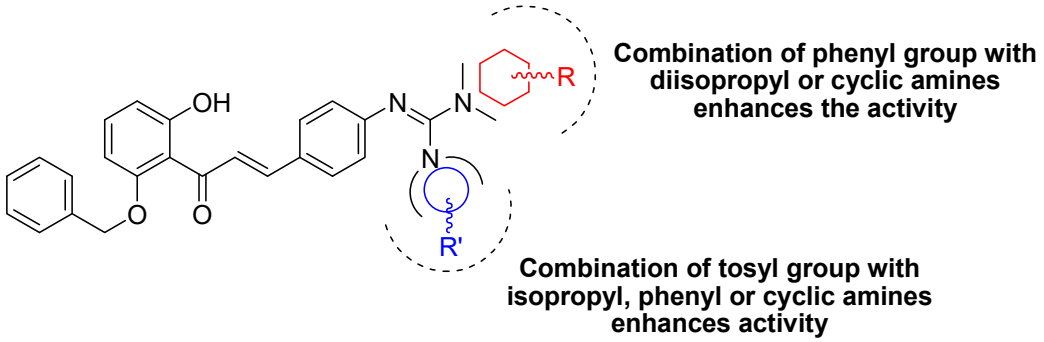

Figure 1. Structure–activity relationship of guanidines containing the 1,3-diphenylpropenone core against U-937 and HL-60 leukemic cells.

The results suggest that the main determinant of cytotoxicity in hybrid compounds containing the *p*-toluensulfonyl group is the presence of a *N*-methylpiperazine ring and the most cytotoxic compound was the hybrid compound **6f** in the six cell lines assayed. As shown in Table 2, compound **6f** showed similar IC_{50} values for U-937 and HL-60 to the values obtained with etoposide, which was included as a positive control. The human leukemia MOLT-3 cells and the cell line overexpressing Bcl-2 (U-937/Bcl-2) were also sensitive to these hybrid compounds. Compound **6i** was also as cytotoxic as compound **6f** in both U-937 and HL-60 cells. Representative concentration-dependent inhibition of cell viability curves of compounds **6f** and **6i** against U-937 are shown in Figure 2a. As visualized by phase-contrast microscopy, these compounds induced significant morphological changes and an important reduction in the number of cells (Figure 2b). To determine the potential selectivity of hybrid compounds **6f** and **6i** against human leukemia cells, we compared the effect against human mononuclear cells (PBMC) obtained from healthy donors. Proliferating and quiescent lymphocytes showed lower cytotoxicity even at 10 μM hybrid compounds for 24 h. Fresh and proliferating PBMC were more resistant to the cytotoxic effects of these compounds (Figure 2c).

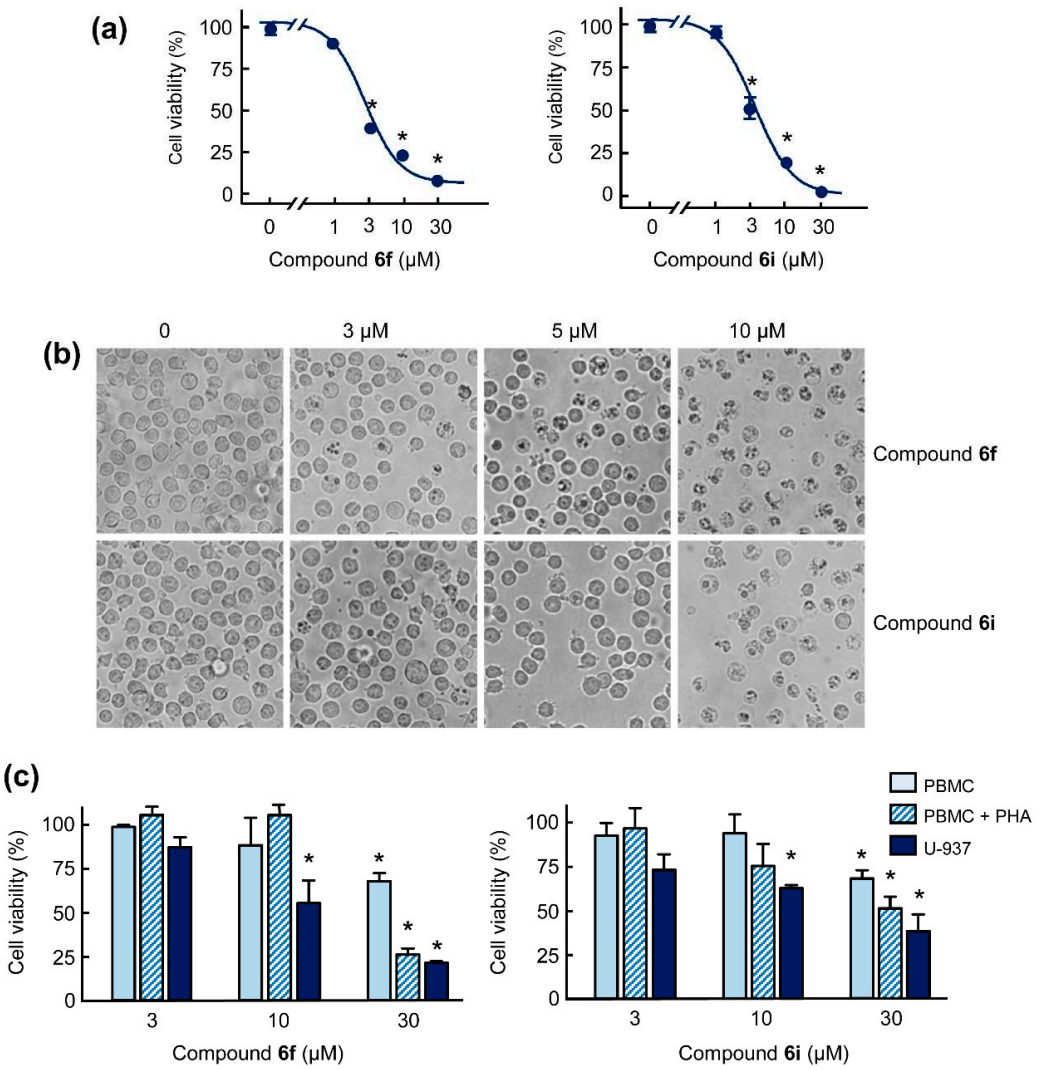

Figure 2. (**a**) Dose-response study of hybrid chalcone–guanidines on human U-937 leukemia cell viability. Cells were cultured in the presence of increasing concentrations of selected guanidines for 72 h, and thereafter cell viability was determined by the MTT assay. (**b**) Photomicrographs of morphological changes visualized with an inverted phase-contrast microscope after treatment of U-937 cells with the specified guanidine for 24 h. (**c**) Differential effects of guanidines on cell viability of normal peripheral blood mononuclear cells (PBMC) versus U-937 cells. Human leukemia and quiescent and phytohemagglutinin-activated PBMC (PBMC (+PHA)) cells from healthy human origin were cultured in the presence of the specified concentrations of guanidines for 24 h. Values represent means ± SE of three independent experiments each performed in triplicate. * $p < 0.05$, significantly different from the corresponding control.

2.3. Hybrid Compounds Induce Changes in Cell Cycle in Human U-937 Leukaemia Cells

Although the compounds **6f** and **6i** were the most cytotoxic against human cancer cells, we were interested in knowing whether other compounds of this series were able to affect the cell cycle. To explore this, U-937 cells were incubated with 10 μM of selected compounds **6c**, **6e**, **6f**, **6h**, **6i,** and **6j** for 24 h, and analyzed by flow cytometry after propidium iodide staining. As shown in Table 3, guanidine **6e** induced an arrest at the G_2-M phase of the cell cycle. The percentage of control cells in G_2-M phase was approximately 14%, which increased to 27% and this was accompanied by a significant decrease in cells in the G_1 phase. This suggests that the effects on viability may be caused at least in part by an arrest of the cell cycle. The percentage of sub-G_1 (i.e., apoptotic cells) increased until 23.5% (~10-fold), 11.9% (~5-fold), 25.1% (~10-fold), and 31.6% (~13-fold) by compounds **6c**, **6e**,

6f, and **6i**, respectively (Figure 3a). Representative histograms of flow cytometry after propidium iodide labelling are shown in Figure 3b. To confirm that the decrease in viability triggered by **6f** and **6i** was caused by apoptosis induction, treated cells were double stained with annexin V-FITC and propidium iodide and subjected to flow cytometry. The number of annexin V-FITC positive cells increased 11-fold (3.5% vs. 38%) and 10-fold (3.5% vs. 36%) for compounds **6f** and **6i**, respectively, in U-937 cells confirming that these specific guanidines are potent apoptosis inducers (Figure 3c). Interestingly, dose-response studies revealed that PBMC were more resistant toward compounds **6f** and **6i**. The number of annexin V-FITC positive cells hardly increased with respect to control after treatment with 3 μM of compounds **6f** and **6i**, but increased 3-fold (9.3% vs. 27%) and 1.4-fold (9.3% vs. 13%) with respect to control after treatment with 10 μM compounds **6f** and **6i**, respectively (Figure 3d).

Table 3. Effect of guanidines on cell cycle phases distribution in U-937 leukemia cells.

	%Sub-G_1	%G_1	%S	%G_2-M
Control	2.4 ± 0.4	54.4 ± 0.4	29.0 ± 0.7	14.2 ± 0.2
6c	23.5 ± 1.2 *	37.4 ± 0.3 *	27.0 ± 0.7	11.4 ± 0.4
6e	11.9 ± 0.2 *	36.5 ± 2.3 *	23.6 ± 0.5 *	27.3 ± 2.0 *
6f	25.1 ± 2.6 *	35.2 ± 3.8 *	28.3 ± 0.2	10.8 ± 1.6
6h	7.2 ± 1.1 *	53.7 ± 0.4	29.5 ± 0.3	9.2 ± 0.5 *
6i	31.6 ± 4.5 *	35.9 ± 2.1 *	23.6 ± 2.4 *	8.4 ± 0.1 *
6j	4.7 ± 0.6	51.3 ± 1.1	32.0 ± 0.4	11.5 ± 0.1

Cells were cultured with 10 μM of the indicated compounds for 24 h and the cell cycle phase distributions were determined by flow cytometry. The values are means ± S.E. of two independent experiments with three determinations in each. Asterisks indicate a significant difference ($p < 0.05$) compared with the corresponding controls.

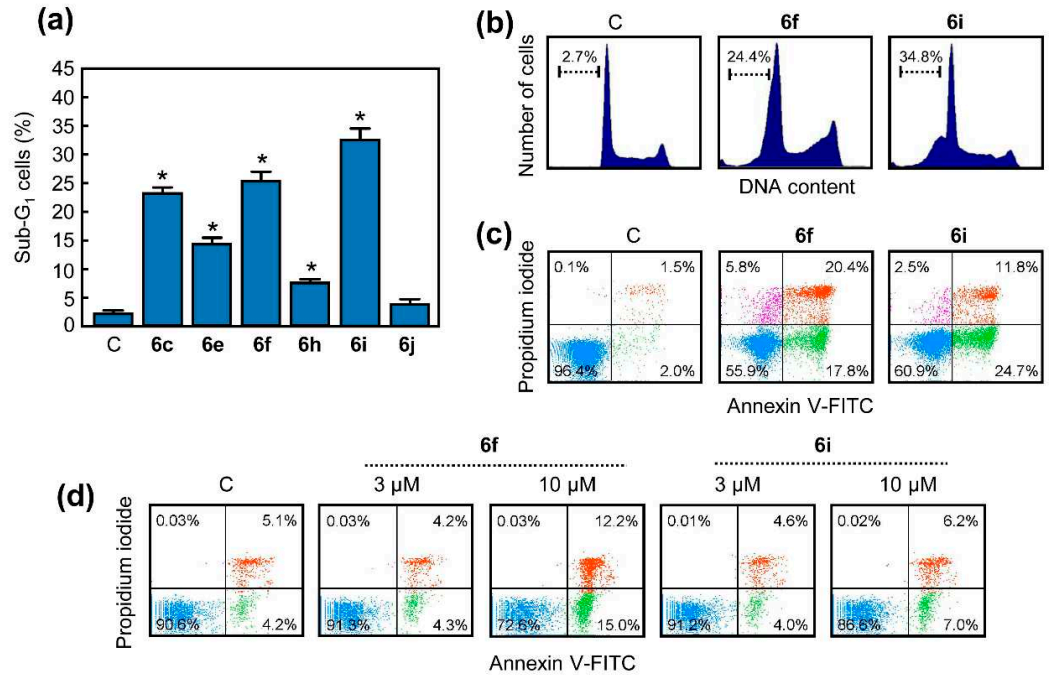

Figure 3. Increase in percentage of apoptotic cells (sub-G_1 fraction) due to hybrid compounds and externalization of phosphatidylserine by compounds **6f** and **6i** in U-937 cells. (**a**) Cells were incubated with 10 μM of specified chalcone–guanidines for 24 h and apoptotic cells were quantified as percentage

of cells in the sub-G_1 region using flow cytometry after propidium iodide staining. * indicates $p < 0.05$ for comparison with untreated control, C. (**b**) Representative histograms of flow cytometry using propidium iodide staining of cells incubated in the presence of 10 μM of the indicated compound for 24 h. The percentage of sub-G_1 cells is shown. (**c**) Cells were incubated as indicated in (**b**) and quantified by flow cytometry after double staining with annexin V-FITC and propidium iodide. Cells in the lower right quadrant show positive annexin V-FITC, which indicates phosphatidylserine translocation on the outside of the plasma membrane, and negative propidium iodide staining, which demonstrates intact cell membranes, both features of early apoptosis. Cells appearing in the top right quadrant are double positive for annexin V-FITC and propidium iodide and are undergoing late apoptosis. Data are representative of three independent experiments. (**d**) PBMC were incubated with increasing concentrations of compounds **6f** and **6i** for 24 h and quantified by flow cytometry after double staining with annexin V-FITC and propidium iodide.

2.4. Hybrid Compounds Induce Caspase Activation, PARP Cleavage, and Cytochrome c Release in Human U-937 Leukemia Cells

To determine whether the mechanism of cell death triggered by compounds **6f** and **6i** was associated with caspase activation, the enzyme activities of caspases-3/7, -8, and -9 were determined in lysates using tetrapeptide substrates. As shown in Figure 4a, maximal caspase-3/7 and -9 activities were detected after 24 h of treatment with 10 μM of both guanidines in U-937 cells, while caspase-8 was less activated. Caspase-3/7 and caspase-9 activities increased approximately three-fold and two-fold after treatment with guanidines **6f** and **6i**, respectively.

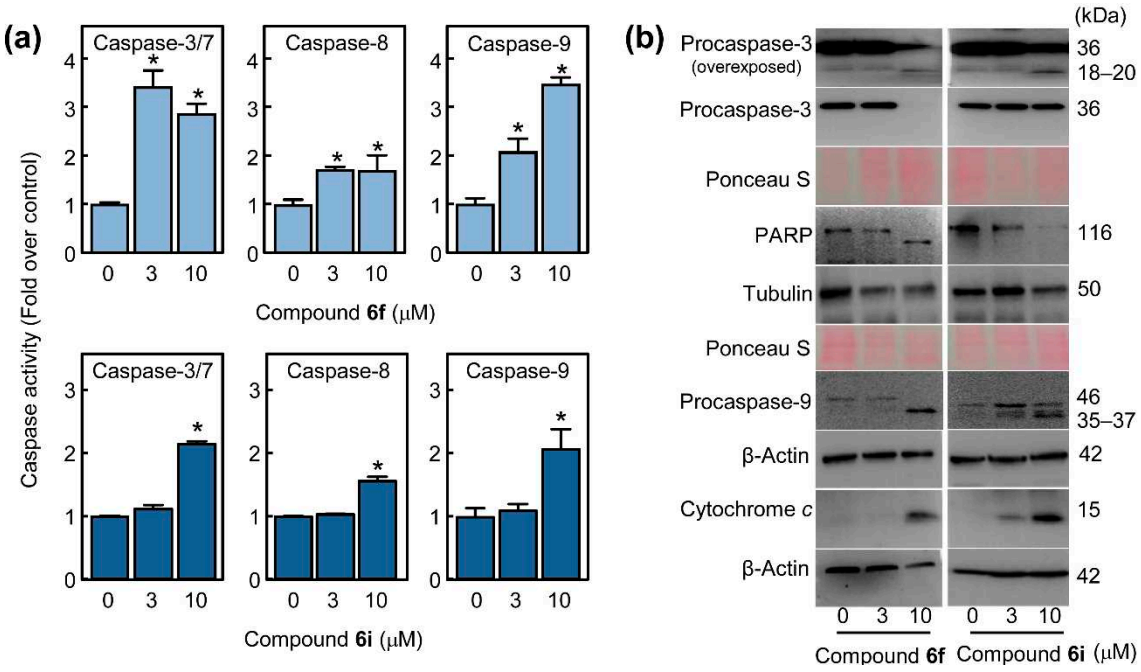

Figure 4. Processing of caspases and PARP (poly(ADP-ribose)polymerase) and mitochondrial cytochrome *c* release in the apoptosis induced by hybrid compounds on leukemia cells. (**a**) Caspase activation induced by guanidines. U-937 cells were treated with the indicated concentrations of compounds and cell lysates were assayed for caspase-3/7, -8, and -9 activities. Results are expressed as n–fold increases in caspase activity compared with the control. Values represent the means ± SE of three independent experiments each performed in triplicate. * indicates $p < 0.05$ for comparison with untreated control. (**b**) U-937 cells were incubated with the indicated concentrations of guanidines for 24 h and the cleavage of caspases and PARP and cytochrome *c* release were analyzed by immunoblotting. β-Actin and tubulin were used as loading controls. Equal loading was also controlled by staining the membranes with Ponceau S before antibody detection.

An indicator of caspase activation is the cleavage of poly(ADP-ribose)polymerase (PARP). This enzyme is involved in DNA repair and PARP cleavage is considered a hallmark of cell death. To explore whether guanidines **6f** and **6i** induced PARP cleavage, lysates of treated cells were analyzed by immunoblotting. As shown in Figure 4b, the full-length PARP protein dramatically decreased after 24 h of treatment with 10 μM of both guanidines indicating the processing of this protein. In accordance with PARP cleavage, the executioner caspase-3 was processed, as detected by the generation of a fragment of 18–20 kDa in the immunoblots. In a similar way as the enzymatic assays, the immunoblot experiments also revealed pro-caspase-9 processing suggesting that PARP cleavage might be attributable to pro-caspase-9 cleavage followed by caspase-3 activation.

Since caspase-9 activation is dependent on the release of cytochrome *c* from the intermembrane space of mitochondria to cytosol, we explored whether the cell death induced by selected guanidines involves cytochrome *c* release. To this end, dose-response experiments were performed and cytosolic fractions were analyzed by Western blot after 24 h of treatment with increasing concentrations of guanidines. As shown (Figure 4b), the level of cytochrome *c* increased in the cytosolic fraction in accordance with the processing and activation of pro-caspase-9. These results indicate that guanidines induce cytochrome *c* release and the processing and activation of caspases.

3. Discussion

In the present report, we synthesized a series of chalcone hybrids containing trisubstituted guanidines and explored the potential effects on human cancer cell viability. We found that the *p*-tosyl derivative containing a *N*-methylpiperazine **6f** was the most potent cytotoxic compound against the six cell lines assayed. It seems that the main determinant of this cytotoxicity is the nature of the heterocycle since the *N*-methylpiperazine derivative was more potent than the morpholine or piperidine derivatives. The second most potent inhibitor of cell viability, at least against leukemia cells, was the *N*-phenyl derivative **6i**. Interestingly, dose-response studies revealed that quiescent PBMC and proliferating PBMC were more resistant than the human leukemia U-937 cell line against the cytotoxicity triggered by the most potent guanidines. It is a remarkable finding that PBMC show increased apoptosis resistance toward guanidines **6f** and **6i** since the increases in the percentages of annexin V-FITC positive cells compared with the control were lower than in U-937 cells. The effects on cell viability and the mechanisms involved in cell death induction of these specific compounds have not been investigated to date. Our results demonstrated that at least one of the guanidines, compound **6e** containing a *N*-tosyl group and a morpholine ring, blocks proliferation of leukemia cells by arresting the cells in the G_2-M phase of the cell cycle. This suggests that compound **6e** might target cyclin-dependent kinase 1 (CDK1) which is a stimulator of cell cycle progression. CDK1 inhibition induces cell cycle arrest in the G_2-M phase and apoptosis and targeting CDK1 has showed promising results for cancer treatment in different preclinical models [7]. Another possibility might be that compound **6e** can bind tubulin and therefore interfere with the mitotic process as described for chalcone derivatives [8]. Further research is needed to confirm the specific target/s of this compound.

Cell cycle analysis revealed that inhibition of cell viability by the other hybrid compounds (compounds **6c**, **6f**, **6h**, and **6i**) was not caused by a significant cell cycle arrest in any phase. The experiments presented here, using U-937 cells as a model, supported apoptosis as the main cytotoxicity pathway induced by two specific guanidines, **6f** and **6i**, containing the chalcone skeleton. This was supported by an increase in the percentage of sub-G_1 and annexin V-FITC positive cells, caspase activation, and PARP cleavage. During apoptosis, caspases cause PARP cleavage and inactivation [9]. PARP protein is normally involved in DNA repair and is a known substrate for caspase-3. Moreover, these guanidines induced a concentration-dependent release of mitochondrial cytochrome *c* and this was in accordance with the activation of caspase-9 and caspase-3 determined by the enzymatic analysis and the immunoblots experiments. Mitochondrial outer membrane permeabilization is the

critical step for the intrinsic pathway of apoptosis [10]. This pathway involves the cytosolic release of apoptogenic factors that normally reside in the mitochondrial intermembrane space such as cytochrome *c* [11]. These results suggest that cell death induction triggered by these specific compounds occurs via the intrinsic apoptotic pathway.

It is known that overexpression of Bcl-2 protein protects the cells because it prevents the release of the pro-apoptotic protein cytochrome *c* from the mitochondria to the cytosol, apoptosome formation, and the consequent activation of caspase-9 [12]. Bcl-2 is frequently overexpressed in lymphomas and leukemias [13]. Therefore, this protein is a potential target in therapy. Previous reports have shown that multisite Bcl-2 phosphorylation induced by anti-mitotic drugs may inhibit Bcl-2 [14]. For example, helenalin, a naturally occurring sesquiterpene lactone, is able to induce cell death in cells overexpressing Bcl-2 and this effect could be due to the inactivation of Bcl-2 protein or, alternatively, this compound could trigger a pathway that bypasses mitochondria [15]. In addition, etoposide, but not staurosporine, bypasses the chemoresistance conferred by Bcl-2 in Hep3B hepatoma cells [16]. Our experiments demonstrate that guanidines are cytotoxic against human leukemia U-937 cells that overexpress Bcl-2. These results strongly suggest that selected guanidines kill cancer cells mainly through induction of apoptotic cell death. Future studies will be necessary to determine whether additional pathways of cell death are involved in U-937 cells.

4. Materials and Methods

4.1. Reagents

Compounds used as starting material and reagents were obtained from Aldrich Chemical Co. (St. Louis, MO, USA) or other chemical companies and utilized without further purification. ^{1}H and ^{13}C NMR spectra were obtained on a Bruker Ascen 500 spectrometer model with standard pulse sequences operating at 500 MHz in ^{1}H and 125 MHz in ^{13}C NMR. $CDCl_3$ was used as the solvent. Chemical shifts (δ) are given in ppm upfield from tetramethylsilane as internal standard, and coupling constants (*J*) are reported in hertz. EIMS and HREIMS were recorded on a Micromass model Autospec (70 eV) spectrometer. Column chromatography was carried out on silica gel 60 (Merck 230–400 mesh) and analytical thin layer chromatography (TLC) was performed using silica gel aluminum sheets. The starting materials 1-(2-(benzyloxy)-6-hydroxyphenyl)ethan-1-one (**1**) and 4-azidobenzaldehyde (**2**) were synthesized following the procedures described in the literature [17,18]. Acrylamide, bisacrylamide, ammonium persulfate, and *N*,*N*,*N*′,*N*′-tetramethylethylenediamine were from Bio-Rad (Hercules, CA, USA). Antibodies for caspase-3 (#ADI-AAP-113, 1:2000 dilution) and for caspase-9 (#9502) were purchased from Stressgen-ENZO (Victoria, BC, Canada) and Cell Signaling Technology (Beverly, MA, USA), respectively. Anti-PARP (poly(ADP-ribose) polymerase, #551024, 1:5000 dilution) and anti-cytochrome *c* (#556433, 1:1000 dilution) were from BD Pharmingen (San Diego, CA, USA). Monoclonal anti-β-actin (#A2228, 1:3000 dilution) and anti-tubulin (#2125, 1:1000 dilution) were from Sigma (Saint Louis, MO, USA) and Cell Signaling Technology (Beverly, MA, USA), respectively. Horseradish peroxidase-conjugated secondary antibodies (NA9310 and NA9340, 1:10,000 dilution) were from GE Healthcare Bio-Sciences AB (Little Chalfont, U.K.). PVDF membranes were from Millipore (Temecula, CA). All other chemicals were obtained from Sigma (Saint Louis, MO, USA).

4.2. General Procedure for the Synthesis of Hybrid Molecules

4.2.1. Synthesis of Chalcone 3

A mixture of the 1-(2-(benzyloxy)-6-hydroxyphenyl)ethan-1-one (5–10 mmol, 1 equiv.) and the corresponding 4-azidobenzaldehyde (1 equiv.) in EtOH (20–40 mL) was stirred at room temperature and a 50% aqueous solution of NaOH (5–8 mL) was added. The reaction mixture was stirred at room temperature until the starting materials were consumed. HCl (10%) was then added until neutrality was reached. Precipitated chalcone was filtrated and purified using column chromatography (60% yield).

4.2.2. General Method One-Pot Synthesis of Guanidines (**6a**–**6k**)

Triphenylphosphine (1.1 equiv.) was added at room temperature to a solution of azido-chalcone 3 (1 equiv.) in CH_2Cl_2. After 60 min, the isocyanate reagent (1.1 equiv.) was added. The reaction was followed by TLC until total consumption of the iminophosphorane. The appropriated amine (2 equiv.) was then added and the mixture was allowed to react for an additional 1 h. CH_2Cl_2 was removed in vacuo, and the residue was purified on silica gel MeOH–CH_2Cl_2 (5:95) to give the desired product a 40–75% yield. In some cases, additional preparative TLC developed with CH_2Cl_2–MeOH (95:5) was required. ^{1}H-NMR, ^{13}C-NMR and mass spectra of synthetic compounds are shown in Figures S1–S48 in Supplementary Materials.

4.3. Cell Culture and Cytotoxicity Assays

U-937, HL-60, MOLT-3, NALM-6, and SK-MEL-1 cells were from DSMZ (German Collection of Microorganisms and Cell Cultures, Braunschweig, Germany). U-937/Bcl-2 cells were kindly provided by Dr. Jacqueline Bréard (INSERM U749, Faculté de Pharmacie Paris-Sud, Châtenay-Malabry, France). The U-937 is a pro-monocytic, human promyelocytic leukemia cell line that was isolated from a histiocytic lymphoma. HL-60 is a human acute myeloid leukemia cell line. MOLT-3 is a human acute lymphoblastic leukemia cell line. NALM-6 is a human B cell precursor leukemia. SK-MEL-1 is a human melanoma cell line growing singly or in clumps (occasional giant, polynucleated cell) in suspension. Cells were cultured in RPMI 1640 medium containing 10% (*v*/*v*) heat-inactivated fetal bovine serum, 100 µg/mL streptomycin, and 100 U/mL penicillin, incubated at 37 °C in a humidified atmosphere containing 5% CO_2 as described [19]. The doubling times of the cell lines were 24 h in HL-60, 30 h in U-937, U-937/Bcl-2, 40 h in MOLT-3 and NALM-6, and several days in SK-MEL-1 cells. Human peripheral blood mononuclear cells (PBMC) were isolated from heparin-anticoagulated blood of healthy volunteers by centrifugation with Ficoll-Paque Plus (GE Healthcare Bio-Sciences AB, Uppsala, Sweden). PBMC were also stimulated with phytohemagglutinin (2 µg/mL) for 48 h before the experimental treatment. The trypan blue exclusion method was used for counting the cells by a hemocytometer with 95% viability in all the experiments. Compounds were dissolved in dimethyl sulfoxide (DMSO) and kept under dark conditions at 25 °C. Before each experiment, the compounds were dissolved in culture media at 37 °C and the final concentration of DMSO did not exceed 0.3% (*v*/*v*). The cytotoxicity of the synthetic compounds was evaluated by colorimetric 3-(4,5-dimethyl-2-thiazolyl-)-2,5-diphenyl-2*H*-tetrazolium bromide (MTT) assay as previously described [20]. Briefly, cells (5000 per well) were incubated with increasing concentrations of compounds for 72 h into a 96-well plate. Then, the supernatants were removed and 0.5 mg/mL MTT was added and incubated for 4 h at 37 °C. Sodium dodecyl sulfate (10% *w*/*v*) in 0.05 M HCl was added to solubilize the reaction products and the absorbance was measured at 570 nm with a reference wavelength of 570 nm using an ELISA reader (Bio-Rad, Hercules, CA, USA). The IC_{50} values (concentrations inducing a 50% inhibition of cell viability) were determined graphically for each experiment by a nonlinear regression using the curve fitting routine implemented within the software Prism 5.0 (GraphPad, La Jolla, CA, USA).

4.4. Quantification of Sub-G_1 Cells and Analysis of Cell Cycle and Apoptosis by Flow Cytometry

Cells (2.5×10^5) were centrifuged for 10 min at 500× *g*, washed with cold PBS, fixed with ice-cold 75% ethanol and stored at −20 °C overnight. Samples were then centrifuged at 500× *g* for 10 min at 4 °C, washed with PBS, resuspended in 200 µL of PBS containing 100 µg/mL RNase and 50 µg/mL propidium iodide and incubated for 1 h in the dark. The DNA content was analyzed by flow cytometry with a BD FACSVerse™ cytometer (BD Biosciences, San Jose, CA, USA). Apoptosis was also evaluated by flow cytometric analysis of double-staining annexin V-FITC and propidium iodide cells as previously described [21].

4.5. Assay of Caspase Activity

Caspase activity was determined by measuring proteolytic cleavage of specific chromogenic substrates as previously described [22]. Briefly, cells were treated with the specified guanidines for 24 h, harvested by centrifugation (1000× *g* for 5 min at 4 °C), washed twice with PBS, resuspended in lysis buffer (50 mM HEPES, pH 7.4, 0.1 mM EDTA, 1 mM dithiothreitol, and 0.1% Chaps), spun (17,000× *g* for 10 min at 4 °C) and the supernatants were normalized by protein concentration and used to determine enzyme activity. The net increase in absorbance at 405 nm after incubation at 37 °C was indicative of caspase activity. The colorimetric substrates were DEVD-*p*NA (for caspase-3 like protease activity), IETD-*p*NA (for caspase-8 activity), and LEHD-*p*NA (for caspase-9 activity).

4.6. Western Blot Analysis

For whole cell lysates, cells were harvested by centrifugation (500× *g*, 10 min, 4 °C), washed twice with PBS, and pellets were resuspended in lysis buffer (1% Triton X-100, 10 mM sodium fluoride, 2 mM EDTA, 20 mM Tris-HCl (pH 7.4), 2 mM tetrasodium pyrophosphate, 10% glycerol, 137 mM NaCl, and 20 mM sodium β-glycerophosphate), with the protease inhibitors phenylmethylsulfonyl fluoride (PMSF, 1 mM), aprotinin, leupeptin, and pepstatin A (5 μg/mL each) and kept on ice for 15 min. Cells were sonicated on ice 5 times (5 s each, with intervals between each sonication of 5 s) with a Braun Labsonic 2000 microtip sonifier and centrifuged (11,000× *g*, 10 min, 4 °C). For subcellular fractionation, cells were washed twice with PBS and then resuspended in ice-cold buffer (20 mM HEPES (pH 7.5), 250 mM sucrose, 10 mM KCl, 1.5 mM $MgCl_2$, 1 mM EDTA, 1 mM EGTA, and 1 mM dithiothreitol containing protease inhibitors (0.1 mM PMSF and 1 μg/mL leupeptin, aprotinin, and pepstatin A)). After 15 min on ice, cells were lysed by pushing them several times through a 29-gauge needle, and the lysate was centrifuged at 1000× *g* for 5 min at 4 °C. The resulting supernatant fraction was centrifuged at 15,000× *g* for 20 min at 4 °C, and the resulting supernatant was used as the cytosolic fraction. The Bradford method was used to determine protein concentration. The samples loaded in sodium dodecyl sulfate-polyacrylamide gel (from 7.5 to 15% depending on the molecular weight of interest) were prepared with the same protein amount and boiled for 5 min. The proteins were transferred to poly(vinylidene difluoride) membranes for 20 h at 20 V. The membranes were blocked with 10% nonfat milk in Tris-buffered saline (50 mM Tris-HCl (pH 7.4), 150 mM NaCl) containing 0.1% Tween-20 (TBST) for 1 h, followed by incubation with specific antibodies against caspase-3, PARP, caspase-9, β-actin, tubulin, and cytochrome *c* overnight at 4 °C. Membranes were washed three times with TBST and incubated for 1 h with the specific secondary antibody and the antigen-antibodies complexes were visualized by enhanced chemiluminescence using the manufacturer's protocol.

4.7. Statistical Analysis

Statistical differences between means were tested using (i) Student's *t*-test (two samples) or (ii) one-way analysis of variance (ANOVA) (three or more samples) with a posteriori pairwise comparisons of means carried out using Tukey's test. A significance level of $p < 0.05$ was used.

5. Conclusions

In summary, we designed and synthesized a series of trisubstituted guanidines containing a 1,3-diphenylpropenone core and different substituents on the guanidine functional group taking advantage of a one-pot procedure involving three sequential reactions. The SARs revealed that (i) the presence of a piperazine ring in *p*-toluensulfonyl guanidines generated a more cytotoxic response than the corresponding isopropylamino, diisopropylamino, piperidine, morpholine, or phenylamino derivatives and (ii) the presence of a piperidine ring in *N*-phenylguanidines enhanced the cytotoxicity in comparison with the corresponding diisopropylamino, morpholine, and *N*-methylpiperazine derivatives. The most cytotoxic compounds were the *p*-toluensulfonylguanidine containing a

N-methylpiperazine and the *N*-methyl-*N*-phenylguanidine containing a piperidine ring against the human leukemia cells. Both compounds showed less cytotoxicity against human peripheral blood mononuclear cells, suggesting that they may have potential therapeutic value. These compounds induce cell death by apoptosis, which was associated with cytochrome *c* release, caspase activation, and PARP cleavage while the over-expression of the anti-apoptotic protein Bcl-2 did not block cell viability inhibition.

Supplementary Materials: The following supporting information can be downloaded at: https://www.mdpi.com/article/10.3390/ijms232415518/s1. The following are available online, spectral and analytical data for hybrid compounds.

Author Contributions: Conceptualization, F.E.; methodology, F.E.-S., E.S., J.P., J.H.-G., C.G., J.Q. and F.E.; software, F.E.-S., E.S., I.B., J.P., J.Q. and F.E.; validation, I.B., J.Q., and F.E.; formal analysis, F.E.-S., I.B., C.G., J.Q. and F.E.; investigation, F.E.-S., E.S., I.B., J.P., J.H.-G., C.G., J.Q. and F.E.; resources, I.B., C.G., J.Q. and F.E.; data curation, F.E.-S., I.B., C.G., J.Q. and F.E.; writing—original draft preparation, F.E.-S., I.B., J.Q. and F.E.; writing—review and editing, F.E.-S., I.B., J.Q. and F.E.; visualization, F.E.-S., E.S., I.B., J.P., J.H.-G., C.G., J.Q. and F.E.; supervision, F.E.-S., I.B., J.Q. and F.E.; project administration, F.E. All authors have read and agreed to the published version of the manuscript.

Funding: This research was funded by the Spanish Ministry of Science, Innovation, and Universities and the European Regional Development Fund (PGC2018-094503-B-C21 and PGC2018-094503-B-C22).

Institutional Review Board Statement: Not applicable.

Informed Consent Statement: Not applicable.

Data Availability Statement: Data is contained within the article or Supplementary Materials.

Acknowledgments: We thank Jacqueline Bréard (INSERM U749, Faculté de Pharmacie Paris-Sud., Châtenay-Malabry, France) for supplying U-937/Bcl-2 cells. E.S. was supported by the Fundación Instituto Canario de Investigación del Cáncer.

Conflicts of Interest: The authors declare no conflict of interest.

References

1. Chen, C.; Yu, J.; Fleck, B.A.; Hoare, S.R.; Saunders, J.; Foster, A.C. Phenylguanidines as selective nonpeptide melanocortin-5 receptor antagonists. *J. Med. Chem.* **2004**, *47*, 4083–4088. [CrossRef] [PubMed]
2. Shukla, S.; Sood, A.K.; Goyal, K.; Singh, A.; Sharma, V.; Guliya, N.; Gulati, S.; Kumar, S. Chalcone Scaffolds as Anticancer Drugs: A Review on Molecular Insight in Action of Mechanisms and Anticancer Properties. *Anticancer Agents Med. Chem.* **2021**, *21*, 1650–1670. [CrossRef] [PubMed]
3. Ashour, H.F.; Abou-Zeid, L.A.; El-Sayed, M.A.; Selim, K.B. 1,2,3-Triazole-Chalcone hybrids: Synthesis, in vitro cytotoxic activity and mechanistic investigation of apoptosis induction in multiple myeloma RPMI-8226. *Eur. J. Med. Chem.* **2020**, *189*, 112062. [CrossRef] [PubMed]
4. Rodríguez, I.; Saavedra, E.; Del Rosario, H.; Perdomo, J.; Quintana, J.; Prencipe, F.; Oliva, P.; Romagnoli, R.; Estévez, F. Apoptosis pathways triggered by a potent antiproliferative hybrid chalcone on human melanoma cells. *Int. J. Mol. Sci.* **2021**, *22*, 13462. [CrossRef]
5. Berlinck, R.G.S.; Bernardi, D.I.; Fill, T.; Fernandes, A.A.G.; Jurberg, I.D. The chemistry and biology of guanidine secondary metabolites. *Nat. Prod. Rep.* **2021**, *38*, 586–667. [CrossRef]
6. Berlinck, R.G.; Burtoloso, A.C.; Kossuga, M.H. The chemistry and biology of organic guanidine derivatives. *Nat. Prod. Rep.* **2008**, *25*, 919–954. [CrossRef]
7. Wijnen, R.; Pecoraro, C.; Carbone, D.; Fiuji, H.; Avan, A.; Peters, G.J.; Giovannetti, E.; Diana, P. Cyclin dependent kinase-1 (CDK-1) inhibition as a novel therapeutic strategy against pancreatic ductal adenocarcinoma (PDAC). *Cancers* **2021**, *13*, 4389. [CrossRef]
8. Liu, W.; He, M.; Li, Y.; Peng, Z.; Wang, G. A review on synthetic chalcone derivatives as tubulin polymerisation inhibitors. *J. Enzym. Inhibin. Med. Chem.* **2022**, *37*, 9–38. [CrossRef]
9. Curtin, N.J.; Szabo, C. Poly(ADP-ribose) polymerase inhibition: Past, present and future. *Nat. Rev. Drug. Discov.* **2020**, *19*, 711–736. [CrossRef]
10. Galluzzi, L.; Vitale, I.; Aaronson, S.A.; Abrams, J.M.; Adam, D.; Agostinis, P.; Alnemri, E.S.; Altucci, L.; Amelio, I.; Andrews, D.W.; et al. Molecular mechanisms of cell death: Recommendations of the Nomenclature Committee on Cell Death 2018. *Cell Death Differ.* **2018**, *25*, 486–541. [CrossRef]
11. Kalkavan, H.; Green, D.R. MOMP, cell suicide as a BCL-2 family business. *Cell Death Differ.* **2018**, *25*, 46–55. [CrossRef] [PubMed]

12. Correia, C.; Lee, S.H.; Meng, X.W.; Vincelette, N.D.; Knorr, K.L.; Ding, H.; Nowakowski, G.S.; Dai, H.; Kaufmann, S.H. Emerging understanding of Bcl-2 biology: Implications for neoplastic progression and treatment. *Biochim. Biophys. Acta* **2015**, *1853*, 1658–1671. [CrossRef] [PubMed]
13. Kaloni, D.; Diepstraten, S.T.; Strasser, A.; Kelly, G.L. BCL-2 protein family: Attractive targets for cancer therapy. *Apoptosis* **2022**. [CrossRef] [PubMed]
14. Ruvolo, P.; Deng, X.; May, W. Phosphorylation of Bcl2 and regulation of apoptosis. *Leukemia* **2001**, *15*, 515–522. [CrossRef]
15. Dirsch, V.M.; Stuppner, H.; Vollmar, A.M. Helenalin triggers a CD95 death receptor-independent apoptosis that is not affected by overexpression of Bcl-x(L) or Bcl-2. *Cancer Res.* **2001**, *61*, 5817–5823.
16. Yoo, S.H.; Yoon, Y.G.; Lee, J.S.; Song, Y.S.; Oh, J.S.; Park, B.S.; Kwon, T.K.; Park, C.; Choi, Y.H.; Yoo, Y.H. Etoposide induces a mixed type of programmed cell death and overcomes the resistance conferred by Bcl-2 in Hep3B hepatoma cells. *Int. J. Oncol.* **2012**, *41*, 1443–1454. [CrossRef]
17. Smith, J.A.; Maloney, D.J.; Hecht, S.M.; Lannigan, D.A. Structural basis for the activity of the RSK-specific inhibitor, SL0101. *Bioorg. Med. Chem.* **2007**, *15*, 5018–5034. [CrossRef]
18. Duval, R.; Kolb, S.; Braud, E.; Genest, D.; Garbay, C. Rapid discovery of triazolobenzylidene-thiazolopyrimidines (TBTP) as CDC25 phosphatase inhibitors by parallel click chemistry and in situ screening. *J. Comb. Chem.* **2009**, *11*, 947–950. [CrossRef]
19. Saavedra, E.; Del Rosario, H.; Brouard, I.; Quintana, J.; Estévez, F. 6′-Benzyloxy-4-bromo-2′-hydroxychalcone is cytotoxic against human leukaemia cells and induces caspase-8- and reactive oxygen species-dependent apoptosis. *Chem. Biol. Interact.* **2019**, *298*, 137–145. [CrossRef]
20. Mosmann, T. Rapid colorimetric assay for cellular growth and survival: Application to proliferation and cytotoxicity assays. *J. Immunol. Methods* **1983**, *65*, 55–63. [CrossRef]
21. Estévez-Sarmiento, F.; Hernández, E.; Brouard, I.; León, F.; García, C.; Quintana, J.; Estévez, F. 3′-Hydroxy-3,4′-dimethoxyflavone-induced cell death in human leukaemia cells is dependent on caspases and reactive oxygen species and attenuated by the inhibition of JNK/SAPK. *Chem. Biol. Interact.* **2018**, *288*, 1–11. [CrossRef] [PubMed]
22. Estévez, S.; Marrero, M.T.; Quintana, J.; Estévez, F. Eupatorin-induced cell death in human leukemia cells is dependent on caspases and activates the mitogen-activated protein kinase pathway. *PLoS ONE* **2014**, *9*, e112536. [CrossRef] [PubMed]

Supplementary Materials

Guanidine Derivatives Containing the Chalcone Skeleton Are Potent Antiproliferative Compounds against Human Leukemia Cells

Francisco Estévez-Sarmiento [1,*], Ester Saavedra [1,2], Ignacio Brouard [3], Jesús Peyrac [3], Judith Hernández-Garcés [4], Celina García [4], José Quintana [1] and Francisco Estévez [1]

[1] Departamento de Bioquímica y Biología Molecular, Fisiología, Genética e Inmunología, Instituto Universitario de Investigaciones Biomédicas y Sanitarias (IUIBS), Grupo de Química Orgánica y Bioquímica, Universidad de Las Palmas de Gran Canaria, Unidad Asociada al Consejo Superior de Investigaciones Científicas (CSIC), 35016 Las Palmas de Gran Canaria, Spain
[2] Instituto Canario de Investigación del Cáncer (ICIC), 35016 Las Palmas de Gran Canaria, Spain
[3] Instituto de Productos Naturales y Agrobiología, Consejo Superior de Investigaciones Científicas, 38206 La Laguna, Spain
[4] Instituto Universitario de Bio-orgánica AG, Departamento de Química Orgánica, Universidad de La Laguna (Tenerife), 38206 San Cristóbal de La Laguna, Spain

* Correspondence: francisco.estevez103@alu.ulpgc.es or festevez1985@gmail.com; Tel.: +34-928-451443; Fax: +34-928-451441

Table of Contents

1. NMR spectroscopic and mass-spectrometric data

*(E)-3-(4-azidophenyl)-1-(2-(benzyloxy)-6-hydroxyphenyl)prop-2-en-1-one (**3**):*

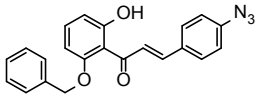

^{1}H-NMR (500 MHz, $CDCl_3$) δ 13.53 (s, 1H); 7.82 (d, *J* = 15.6 Hz, 1H); 7.69 (d, *J* = 15.6 Hz, 1H); 7.55-7.46 (m, 2H); 7.46-7.36 (m, 4H); 7.11-7.02 (m, 2H); 6.88-6.79 (m, 2H); 6.65 (dd, *J* = 8.4, 1.0 Hz, 1H); 6.54 (dd, *J* = 8.3, 1.1 Hz, 1H); 5.12 (s, 2H). ^{13}C-NMR (125 MHz, $CDCl_3$) δ 194.2, 165.6, 160.2, 142.1, 141.6, 136.1, 135.6, 132.0, 130.0, 128.9, 128.7, 128.6, 127.2, 119.2, 111.7, 111.4, 102.2, 71.4. HRMS (ESI-FT-ICR) m/z: 394.1165 $[M+Na]^+$; calcd. for $C_{22}H_{17}N_3NaO_3$: 394.1168.

*N-((Z)-N'-(4-((E)-3-(2-(benzyloxy)-6-hydroxyphenyl)-3-oxoprop-1-en-1-yl)phenyl)-N-isopropylcarbamimidoyl)-4-methylbenzenesulfonamide (**6a**):*

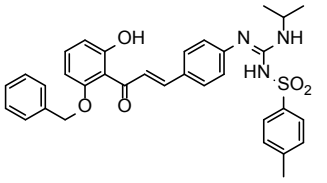

^{1}H-NMR (500 MHz, $CDCl_3$) δ 13.50 (s, 1H), 9.01 (s, 2H), 7.91-7.79 (m, 3H), 7.67 (d, *J* = 15.5 Hz, 1H), 7.51 (d, *J* = 6.4 Hz, 2H), 7.48-7.36 (m, 4H), 7.29 (d, *J* = 8.0 Hz, 2H), 7.05 (d, *J* = 8.2 Hz, 2H), 6.95 (d, *J* = 8.0 Hz, 2H), 6.66 (d, *J* = 8.4 Hz, 1H), 6.56 (d, *J* = 8.2 Hz, 1H), 5.13 (s, 2H), 4.58 (s, 1H), 4.14 (bm, 1H), 2.42 (s, 3H), 1.12 (d, *J* = 6.5 Hz, 6H). ^{13}C-NMR (125 MHz, $CDCl_3$) δ 194.1, 165.7, 160.3, 152.6, 142.1, 141.4, 140.9, 136.9, 136.3, 135.6, 133.8, 130.0, 129.2, 128.9, 128.9, 128.7, 128.4, 126.0, 124.9, 111.6, 111.5, 102.2, 71.5, 43.7, 22.7, 21.5. HRMS (ESI-FT-ICR) m/z: 606.2034 $[M+Na]^+$; calcd. for $C_{33}H_{33}N_3NaO_5S$: 606.2039. (65% yield).

*N-((Z)-N'-(4-((E)-3-(2-(benzyloxy)-6-hydroxyphenyl)-3-oxoprop-1-en-1-yl)phenyl)-N,N-diisopropylcarbamimidoyl)-4-methylbenzenesulfonamide (**6b**):*

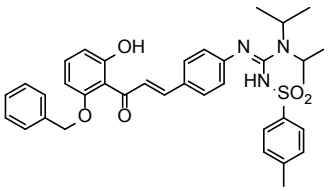

^{1}H-NMR (500 MHz, $CDCl_3$) δ 13.61 (s, 1H), 8.16 (s, 1H), 7.82 (d, *J* = 15.6 Hz, 1H), 7.73 (d, *J* = 8.2 Hz, 2H), 7.67 (d, *J* = 15.5 Hz, 1H), 7.55-7.48 (m, 2H), 7.41 (d, *J* = 8.4 Hz, 1H), 7.38 (dd, *J* = 4.9, 2.2 Hz, 3H), 7.15 (d, *J* = 7.6 Hz, 2H), 6.92 (d, *J* = 8.5 Hz, 2H), 6.66 (dd, *J* = 8.4, 1.0 Hz, 1H), 6.61-6.52 (m, 3H), 5.12 (s, 2H), 3.68 (p, *J* = 6.7 Hz, 2H), 2.35 (s, 3H), 1.18 (d, *J* = 6.7 Hz, 12H). ^{13}C-NMR (125 MHz, $CDCl_3$) δ. 194.2, 165.6, 160.2, 155.3, 142.4, 142.1, 142.0, 140.4, 136.1, 135.7, 131.5, 129.7, 129.1, 128.9, 128.8, 128.6, 126.9, 126.4, 121.5, 111.6, 111.5, 102.2, 71.4, 49.2, 21.5, 20.8. HRMS (ESI-FT-ICR) m/z: 648.2509 $[M+Na]^+$; calcd. for $C_{36}H_{39}N_3NaO_5S$: 648.2508. (72% yield).

*N-((Z)-N'-(4-((E)-3-(2-(benzyloxy)-6-hydroxyphenyl)-3-oxoprop-1-en-1-yl)phenyl)-N-methyl-N-phenylcarbamimidoyl)-4-methylbenzenesulfonamide (**6c**):*

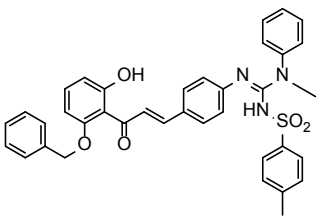

^{1}H-NMR (500 MHz, $CDCl_3$) δ 13.47 (s, 1H); 8.76 (s, 1H); 7.84 (d, *J* = 8.3 Hz, 1H); 7.82 (d, *J* = 8.3 Hz, 1H); 7.70 (d, *J* = 15.5 Hz, 1H); 7.53 (d, *J* = 15.6 Hz, 1H); 7.50-7.43 (m, 2H); 7.39 (t, *J* = 8.3 Hz, 1H); 7.36-7.33 (m, 2H); 7.33-7.29 (m, 1H); 7.29-7.26 (m, 2H); 7.04 (dd, *J* = 8.4, 7.2 Hz, 2H); 6.99-6.90 (m, 1H); 6.85 (dd, *J* = 8.5, 1.2 Hz, 2H); 6.69 (d, *J* = 8.6 Hz, 2H); 6.64 (d, *J* = 8.5 Hz, 1H); 6.53 (d, *J* = 8.3 Hz, 1H); 6.39 (d, *J* = 8.6 Hz, 2H); 5.11 (s, 2H); 3.31 (s, 3H); 2.43 (s, 3H). ^{13}C-NMR (125 MHz, $CDCl_3$) δ 194.2, 165.5, 160.2, 156.3, 143.3, 142.6, 142.1, 140.2, 139.2, 135.6, 131.9, 129.7, 129.4, 129.0, 128.8, 128.6, 128.5, 127.3, 126.5, 126.4, 126.4, 125.7, 123.6, 111.7, 111.5, 102.3, 71.4, 41.1, 21.5. HRMS (ESI-FT-ICR) m/z: 654.2035 $[M+Na]^+$; calcd. for $C_{37}H_{33}N_3NaO_5S$: 654.2039. (60% yield).

*(Z)-N'-(4-((E)-3-(2-(benzyloxy)-6-hydroxyphenyl)-3-oxoprop-1-en-1-yl)phenyl)-N-tosylpiperidine-1-carboximidamide (**6d**):*

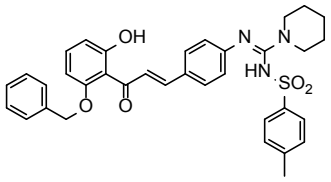

^{1}H-NMR (500 MHz, $CDCl_3$) δ 13.59 (s, 1H), 8.61 (s, 1H), 7.82 (d, *J* = 15.6 Hz, 1H), 7.74-7.69 (m, 2H), 7.66 (d, *J* = 15.6 Hz, 1H), 7.54-7.48 (m, 2H), 7.42-7.35 (m, 3H), 7.15 (d, *J* = 8.1 Hz, 2H), 6.95 (d, *J* = 8.6 Hz, 2H), 6.65 (dd, *J* = 8.4, 1.0 Hz, 1H), 6.60-6.53 (m, 3H), 5.13 (s, 2H), 3.28 (t, *J* = 5.3 Hz, 4H), 2.35 (s, 3H), 1.65 (s, 1H), 1.58 (m, 2H), 1.53 (m, 4H). ^{13}C-NMR (125 MHz, $CDCl_3$) δ 194.2, 165.6, 160.2, 154.8, 142.3, 142.2, 140.8, 140.3, 140.3, 136.1, 135.7, 131.1, 129.8, 129.3, 128.9, 128.7, 128.5, 126.9, 126.2, 119.8, 111.5, 102.2, 71.4, 48.3, 25.3, 24.0, 21.4. HRMS (ESI-FT-ICR) m/z: 632.2193 $[M+Na]^+$; calcd. for $C_{35}H_{35}N_3NaO_5S$: 632.2195. (68% yield).

*(Z)-N'-(4-((E)-3-(2-(benzyloxy)-6-hydroxyphenyl)-3-oxoprop-1-en-1-yl)phenyl)-N-tosylmorpholine-4-carboximidamide (**6e**):*

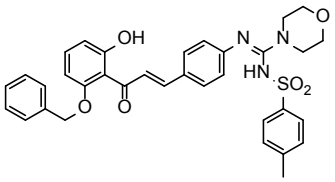

^{1}H-NMR (500 MHz, $CDCl_3$) δ 13.53 (s, 1H); 8.75 (s, 1H); 7.83 (d, *J* = 15.6 Hz, 1H); 7.73 (d, *J* = 8.2 Hz, 2H); 7.66 (d, *J* = 15.5 Hz, 1H); 7.56-7.47 (m, 2H); 7.44-7.34 (m, 4H); 7.19 (d, *J* = 8.1 Hz, 2H); 6.99 (d, *J* = 8.6 Hz, 2H); 6.70-6.60 (m, 3H); 6.55 (dd, *J* = 8.3, 1.0 Hz, 1H); 5.13 (s, 2H); 3.61 (t, *J* = 4.8 Hz, 4H); 3.34 (d, *J* = 4.9 Hz, 4H); 2.37 (s, 3H). ^{13}C-NMR (125 MHz, $CDCl_3$) δ 194.1, 165.6, 160.2, 155.0, 142.6, 141.8, 140.0, 136.2, 135.7, 131.8, 129.9, 129.4, 128.9, 128.7, 128.5, 127.4, 126.3, 120.3, 111.7, 111.5, 102.2, 71.4, 66.0, 47.3, 21.5. HRMS (ESI-FT-ICR) m/z: 634.1989 $[M+Na]^+$; calcd. for $C_{34}H_{33}N_3NaO_6S$: 634.1988. (73% yield).

*(Z)-N'-(4-((E)-3-(2-(benzyloxy)-6-hydroxyphenyl)-3-oxoprop-1-en-1-yl)phenyl)-4-methyl-N-tosylpiperazine-1-carboximidamide (**6f**):*

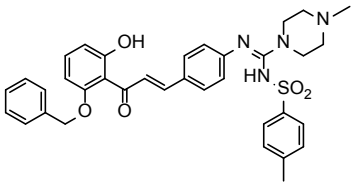

^{1}H-NMR (500 MHz, $CDCl_3$) δ 13.54 (s, 1H); 8.70 (s, 1H); 7.82 (d, *J* = 15.5 Hz, 1H); 7.72 (d, *J* = 8.3 Hz, 2H); 7.66 (d, *J* = 15.6 Hz, 1H); 7.56-7.46 (m, 2H); 7.43-7.35 (m, 4H); 7.17 (d, *J* = 8.1 Hz, 2H); 6.96 (d, *J* = 8.6 Hz, 2H); 6.65 (dd, *J* = 8.4, 1.0 Hz, 1H); 6.63-6.59 (m, 2H); 6.55 (dd, *J* = 8.3, 1.0 Hz, 1H); 5.12 (s, 2H); 3.36 (t, *J* = 5.0 Hz, 4H); 2.35 (d, *J* = 7.5 Hz, 7H); 2.26 (s, 3H). ^{13}C-NMR (125 MHz, $CDCl_3$) δ 193.1, 164.6, 159.2, 153.8, 141.4, 141.0, 139.3, 139.1, 135.1, 134.7, 130.4, 128.8, 128.3, 127.8, 127.7, 127.5, 126.2, 125.2, 119.1, 110.6, 110.4, 101.2, 70.4, 53.0, 45.8, 44.7, 20.4. HRMS (ESI-FT-ICR) m/z: 623.2317 [M-H]; calcd. for $C_{35}H_{35}N_4O_5S$: 623.2328. (75% yield).

*N-((Z)-N'-(4-((E)-3-(2-(benzyloxy)-6-hydroxyphenyl)-3-oxoprop-1-en-1-yl)phenyl)-N-octadecylcarbamimidoyl)-4-methylbenzenesulfonamide (**6g**):*

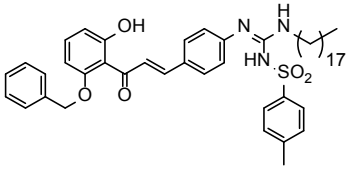

^{1}H-NMR (500 MHz, $CDCl_3$) δ 13.48 (s, 1H), 9.08 (s, 1H), 7.89-7.80 (m, 3H), 7.67 (d, *J* = 15.6 Hz, 1H), 7.55-7.48 (m, 2H), 7.47-7.36 (m, 4H), 7.28 (d, *J* = 8.0 Hz, 2H), 7.09-7.02 (m, 2H), 6.97 (s, 2H), 6.67 (dd, *J* = 8.4, 1.0 Hz, 1H), 6.56 (dd, *J* = 8.4, 1.1 Hz, 1H), 5.13 (s, 2H), 3.29 (q, *J* = 6.6 Hz, 2H), 2.42 (s, 3H), 1.45 (s, 2H), 1.24 (d, *J* = 12.2 Hz, 30H), 0.88 (t, *J* = 6.9 Hz, 3H). ^{13}C-NMR (125 MHz, $CDCl_3$) δ 194.16, 165.71, 160.32, 153.47, 142.16, 141.3, 140.89, 136.8, 136.35, 135.64, 134.1, 130.04, 129.26, 128.98, 128.87, 128.73, 126.09, 125.1, 111.65, 111.56, 102.25, 71.51, 41.77, 31.95, 30.95, 29.73, 29.68, 29.61, 29.50,

29.39, 29.34, 29.23, 26.75, 22.72, 21.52, 14.15. HRMS (ESI-FT-ICR) m/z: 816.4393 $[M+Na]^+$; calcd. for $C_{48}H_{63}N_3O_5NaS$: 816.4386. (72% yield).

*(E)-2-(4-((E)-3-(2-(benzyloxy)-6-hydroxyphenyl)-3-oxoprop-1-en-1-yl)phenyl)-1,1-diisopropyl-3-phenylguanidine (**6h**):*

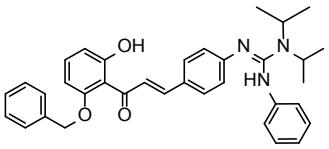

^{1}H-NMR (500 MHz, $CDCl_3$) δ 13.73 (s, 1H); 7.74 (d, *J* = 15.5 Hz, 1H); 7.69 (d, *J* = 15.5 Hz, 1H); 7.47 (dd, *J* = 8.0, 1.5 Hz, 2H); 7.35 (t, *J* = 8.3 Hz, 1H); 7.36-7.22 (m, 5H); 7.21-7.14 (m, 2H); 6.91 (m, 3H); 6.87-6.79 (m, 2H); 6.69-6.59 (m, 3H); 6.52 (d, *J* = 8.2 Hz, 1H); 5.10 (s, 2H); 3.91 (p, *J* = 6.8 Hz, 2H); 1.32 (d, *J* = 6.8 Hz, 12H). ^{13}C-NMR (125 MHz, $CDCl_3$) δ 194.2, 174.3, 165.5, 160.2, 150.4, 149.1, 144.4, 135.7, 135.5, 129.9, 129.0, 128.8, 128.5, 128.4, 127.9, 124.2, 122.0, 120.8, 119.6, 111.9, 111.4, 102.2, 71.3, 47.8, 21.5. HRMS (ESI-FT-ICR) m/z: 548.2914 [M]; calcd. for $C_{35}H_{38}N_3O_3$: 548.2913. (48% yield).

*(E)-N'-(4-((E)-3-(2-(benzyloxy)-6-hydroxyphenyl)-3-oxoprop-1-en-1-yl)phenyl)-N-phenylpiperidine-1-carboximidamide (**6i**):*

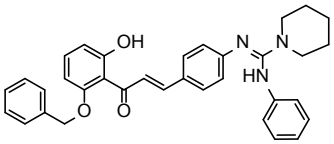

^{1}H-NMR (500 MHz, $CDCl_3$) δ 13.67 (s, 1H), 7.80 (d, *J* = 15.5 Hz, 1H), 7.73 (d, *J* = 15.5 Hz, 1H), 7.47 (d, *J* = 7.4 Hz, 2H), 7.36 (m, 2H), 7.20-7.34 (m, 5H), 7.06-6.84 (m, 5H), 6.77 (d, *J* = 8.1 Hz, 2H), 6.64 (dd, *J* = 8.4, 1.0 Hz, 1H), 6.53 (dd, *J* = 8.3, 1.0 Hz, 1H), 5.10 (s, 2H), 3.34 (s, 4H), 1.61 (brm, 6H). ^{13}C-NMR (125 MHz, $CDCl_3$) δ 194.2, 165.6, 160.2, 143.9, 135.7, 130.1, 129.4, 128.8, 128.8, 128.7, 128.5, 128.4, 124.9, 122.3, 111.8, 111.4, 102.1, 71.4, 47.7, 25.3, 24.6. HRMS (ESI-FT-ICR) m/z: 532.2604 [M]; calcd. for $C_{34}H_{34}N_3O_3$: 532.2600. (60% yield).

*(E)-N'-(4-((E)-3-(2-(benzyloxy)-6-hydroxyphenyl)-3-oxoprop-1-en-1-yl)phenyl)-N-phenylmorpholine-4-carboximidamide (**6j**):*

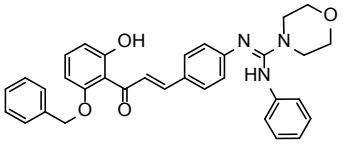

^{1}H-NMR (500 MHz, $CDCl_3$) δ 13.72 (s, 1H); 7.80 (d, *J* = 15.6 Hz, 1H), 7.71 (d, *J* = 15.5 Hz, 1H), 7.51-7.43 (m, 2H), 7.42-7.24 (m, 6H), 7.23-7.10 (m, 1H), 7.01 (m, 5H), 6.75 (d, J = 8.0 Hz, 2H), 6.64 (dd, *J* = 8.4, 1.0 Hz, 1H), 6.53 (dd, *J* = 8.3, 1.0 Hz, 1H), 5.10 (s, 2H), 3.72 (q, *J* = 4.7, 4.0 Hz, 4H), 3.42-3.32 (m, 4H). ^{13}C-NMR (125 MHz, $CDCl_3$) δ 194.2, 165.6, 160.2, 143.5, 135.8, 132.9, 132.1, 132.1, 132.0, 131.9, 131.9, 130.1, 129.5, 128.9, 128.7, 128.5, 128.5, 128.4, 122.9, 111.8, 111.4, 102.2, 71.4, 66.3, 47.0. HRMS (ESI-FT-ICR) m/z: 534.2397 [M]; calcd. for $C_{33}H_{32}N_3O_4$: 534.2393. (52% yield).

*(E)-N'-(4-((E)-3-(2-(benzyloxy)-6-hydroxyphenyl)-3-oxoprop-1-en-1-yl)phenyl)-4-methyl-N-phenylpiperazine-1-carboximidamide (**6k**):*

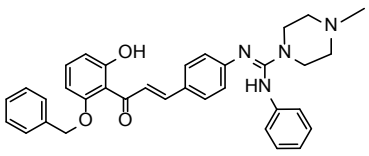

^{1}H-NMR (400 MHz, $CDCl_3$) δ 13.69 (s, 1H), 7.79 (d, *J* = 15.5 Hz, 1H), 7.70 (d, *J* = 15.5 Hz, 1H), 7.47 (d, *J* = 7.0 Hz, 2H), 7.40-7.15 (m, 7H), 7.06 (t, *J* = 7.4 Hz, 1H), 6.97 (m, 4H), 6.77 (d, *J* = 8.1 Hz, 2H), 6.63 (dd, *J* = 8.4, 1.0 Hz, 1H), 6.52 (dd, *J* = 8.4, 1.0 Hz, 1H), 5.09 (s, 2H), 3.43 (s, 4H), 2.46 (s, 4H), 2.34 (s, 3H). ^{13}C-NMR (101 MHz, $CDCl_3$) δ 194.2, 165.6, 160.2, 143.4, 135.8, 135.6, 130.0, 129.8, 129.5, 128.9, 128.8, 128.7, 128.6, 128.6, 128.6, 128.5, 125.6, 123.4, 119.9, 111.7, 111.4, 102.1, 71.4, 54.1, 46.6, 45.9. HRMS (ESI-FT-ICR) m/z: 547.2708 $[M^+]$; calcd. for $C_{34}H_{35}N_4O_3$: 547.2709. (58% yield).

2. NMR and Mass Spectra:

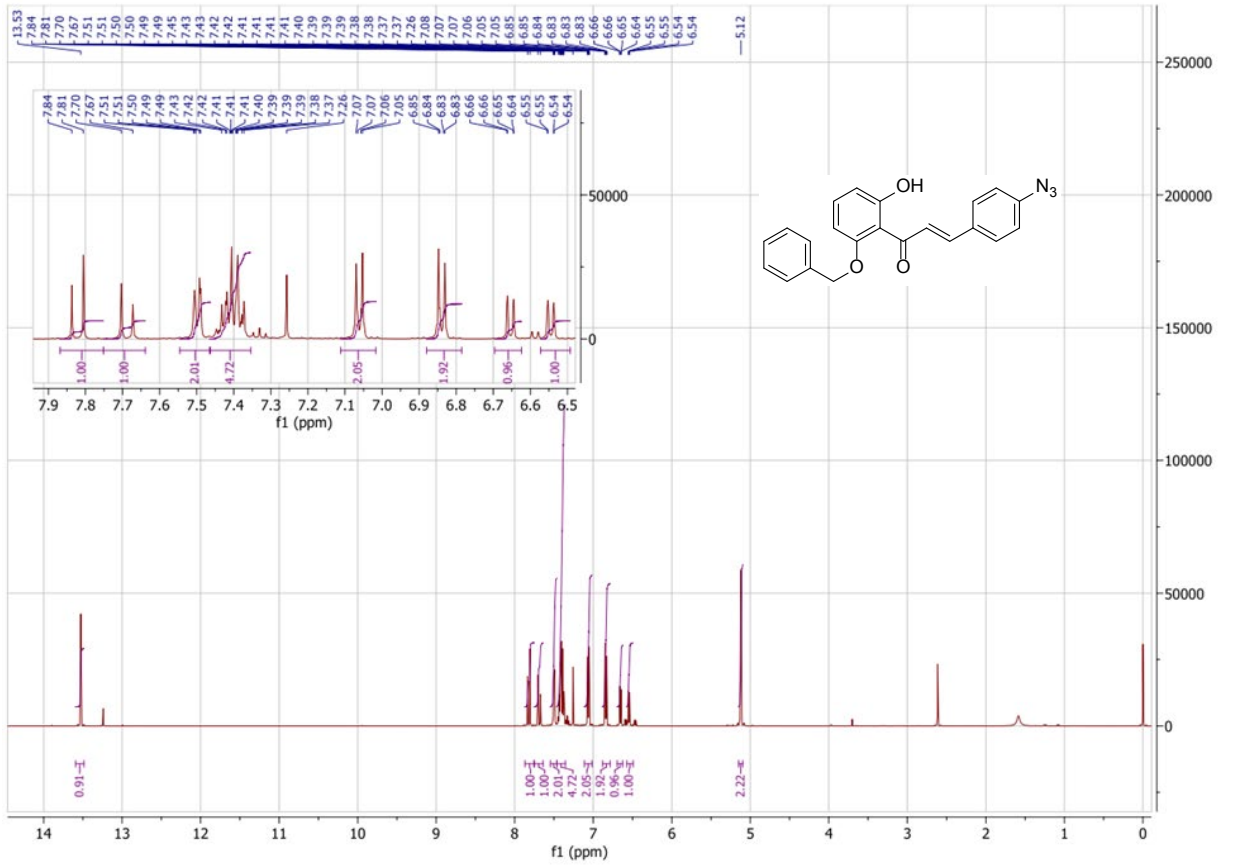

Figure S1: ^{1}H-NMR (500 MHz, $CDCl_3$) Spectrum of compound **3**

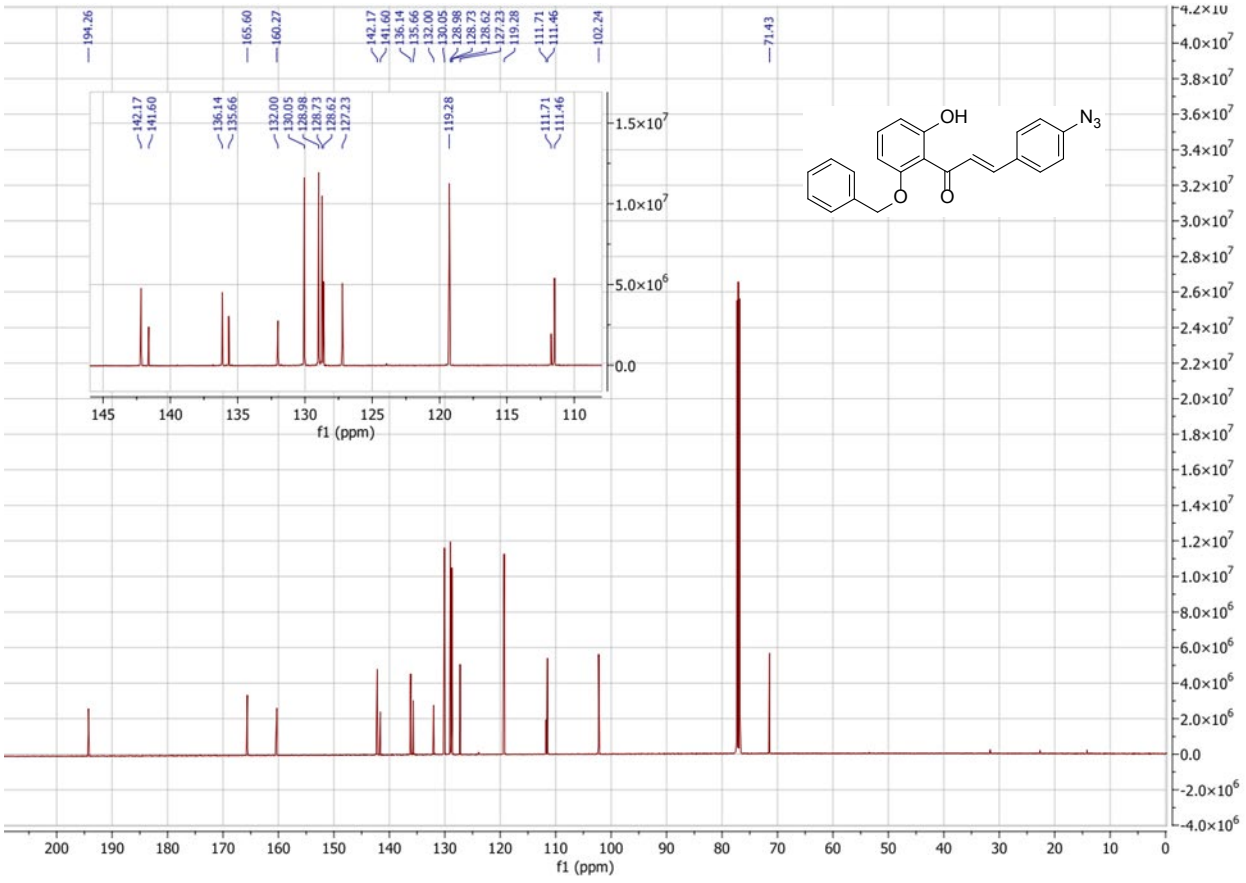

Figure S2: ^{13}C-NMR (125 MHz, $CDCl_3$) Spectrum of compound **3**

Elemental Composition Report Page 1

Multiple Mass Analysis: 2 mass(es) processed
Tolerance = 5.0 PPM / DBE: min = -3.0, max = 120.0
Element prediction: Off
Number of isotope peaks used for i-FIT = 3

Monoisotopic Mass, Even Electron Ions
1095 formula(e) evaluated with 3 results within limits (all results (up to 1000) for each mass)
Elements Used:
C: 0-60 H: 0-60 N: 0-3 O: 0-16 Na: 0-1

Inaki
(ESI-19) (992) Inaki (IB-JP 22) 54 (2.331)

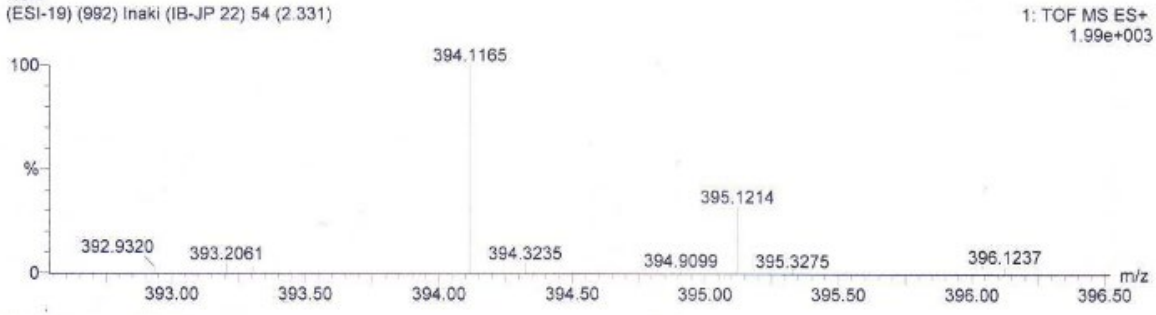

Minimum:	20.00				-3.0			
Maximum:	100.00		5.0	5.0	120.0			
Mass	RA	Calc. Mass	mDa	PPM	DBE	i-FIT	i-FIT (Norm)	Formula
394.1165	100.00	394.1168	-0.3	-0.8	15.5	32.6	0.0	C22 H17 N3 O3 Na
		394.1173	-0.8	-2.0	-2.5	37.6	5.0	C9 H25 N O14 Na
395.1214	32.01	395.1219	-0.5	-1.3	10.5	24.1	0.0	C19 H20 N2 O6 Na

Figure S3: HRESI-MS Spectrum of compound **3**

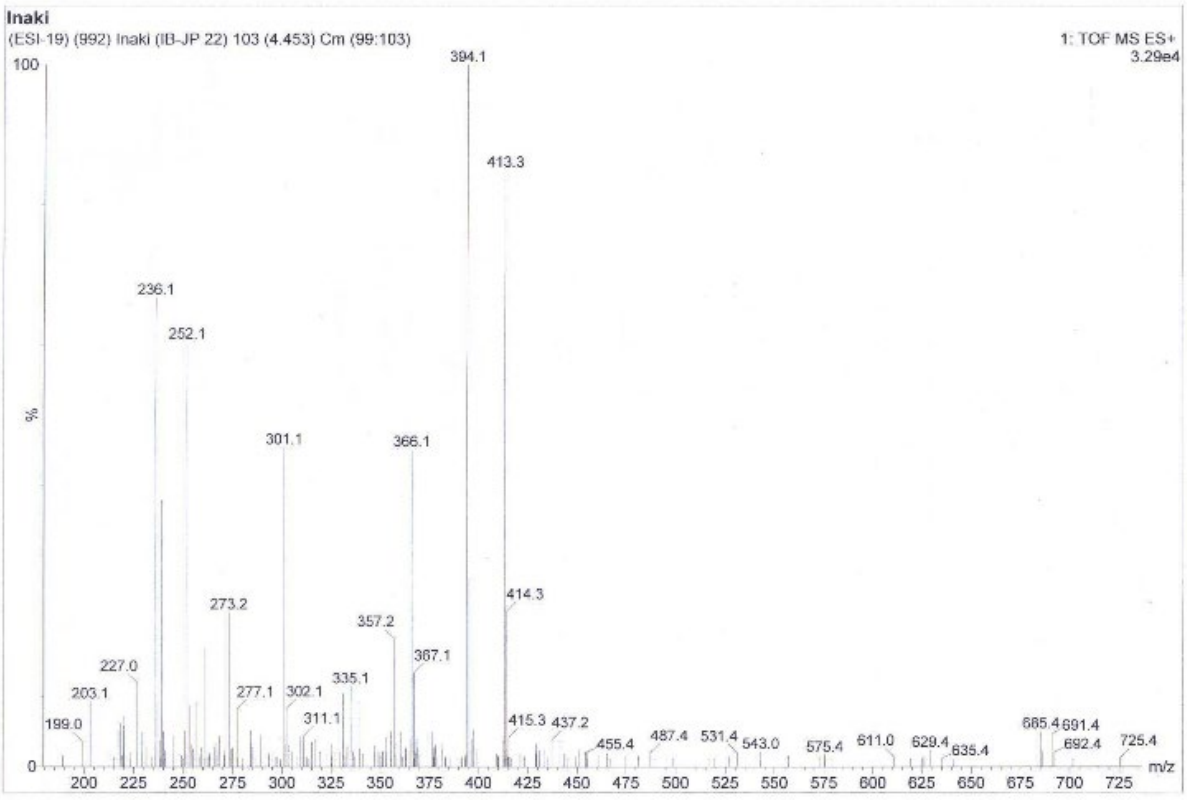

Figure S4: ESI-MS Spectrum of compound **3**

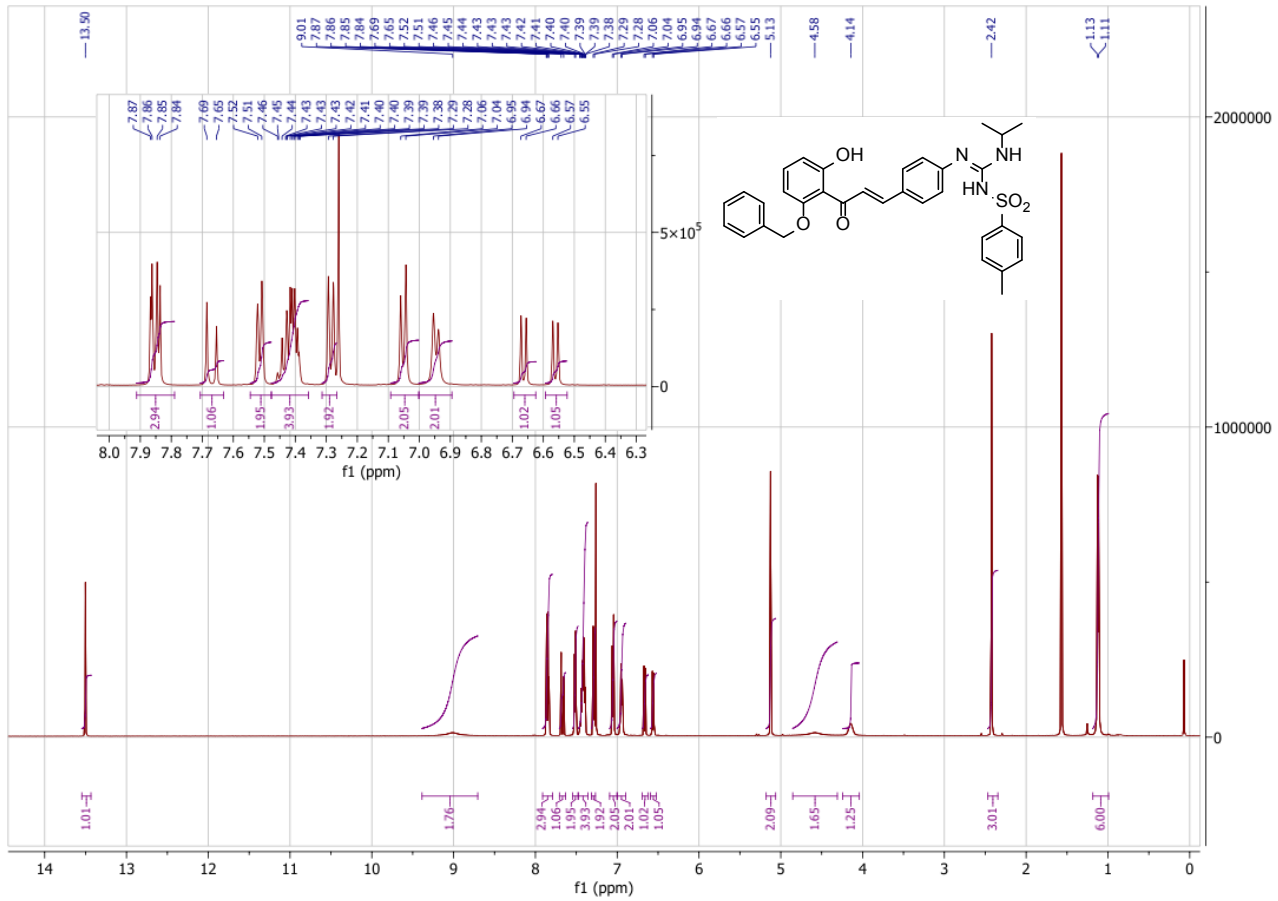

Figure S5: ^{1}H-NMR (500 MHz, $CDCl_3$) Spectrum of compound **6a**

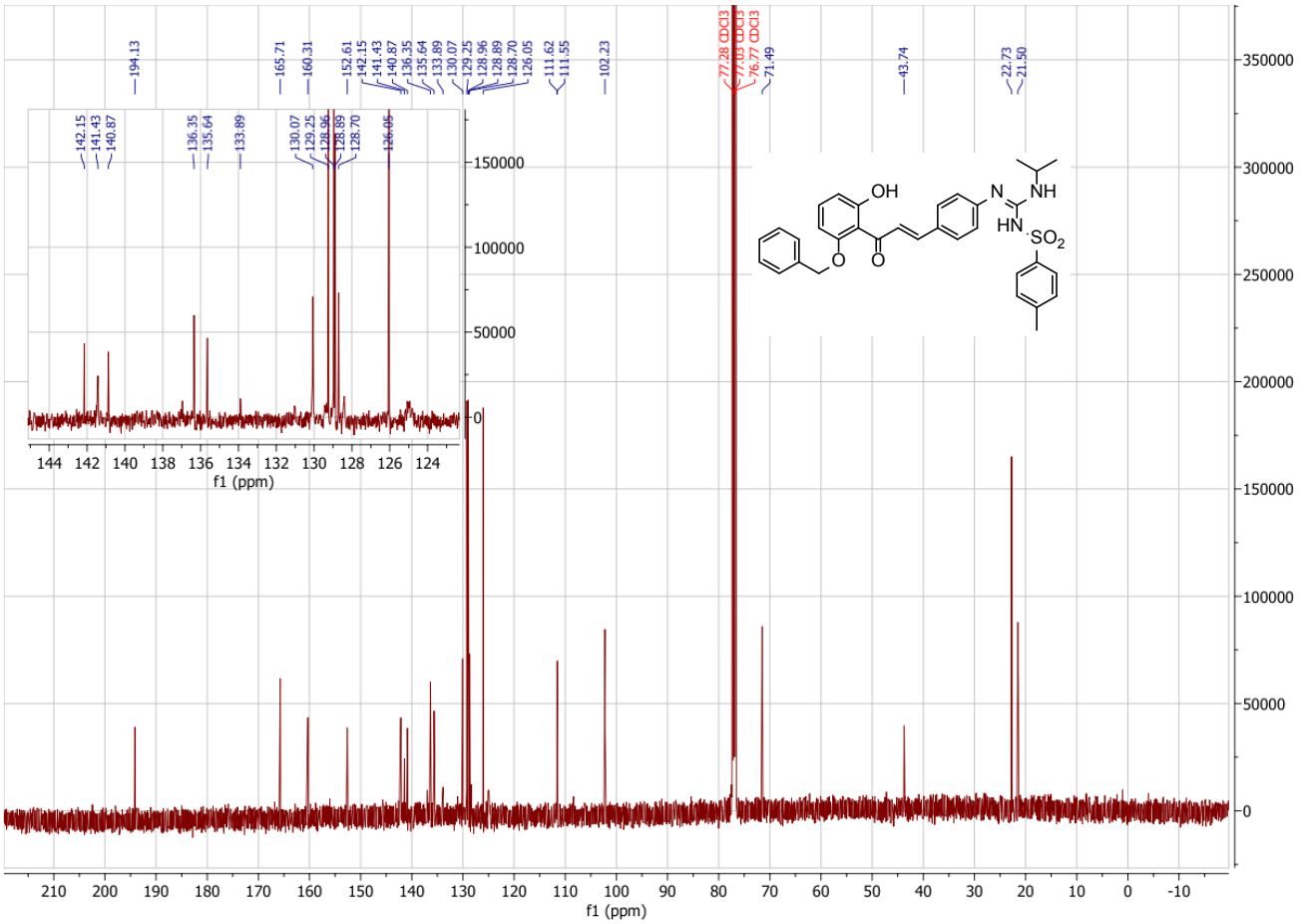

Figure S6: ^{13}C-NMR (125 MHz, $CDCl_3$) Spectrum of compound **6a**

Elemental Composition Report Page 1

Tolerance = 5.0 PPM / DBE: min = -10.0, max = 1000.0
Element prediction: Off
Number of isotope peaks used for i-FIT = 2

Monoisotopic Mass, Even Electron Ions
2930 formula(e) evaluated with 12 results within limits (all results (up to 1000) for each mass)
Elements Used:
C: 0-60 H: 0-100 N: 0-4 O: 0-12 Na: 0-1 S: 0-2

ESI (17-066) Inaki (IB-333) 10 (0.347) 2: TOF MS ES+ 2.05e+003

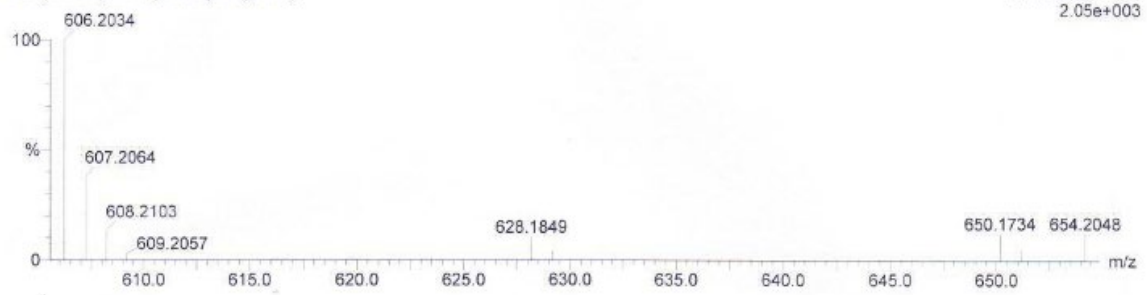

Minimum:	60.00				-10.0		
Maximum:	100.00		100.0	5.0	1000.0		
Mass	RA	Calc. Mass	mDa	PPM	DBE	i-FIT	Formula
606.2034	100.00	606.2038	-0.4	-0.7	25.5	13.3	C39 H32 N3 S2
		606.2029	0.5	0.8	26.5	6.9	C38 H28 N3 O5
		606.2039	-0.5	-0.8	18.5	0.5	C33 H33 N3 O5 Na S
		606.2043	-0.9	-1.5	7.5	7.4	C26 H40 N O11 S2
		606.2045	-1.1	-1.8	27.5	13.3	C41 H29 N O3 Na
		606.2019	1.5	2.5	4.5	14.4	C24 H41 N O11 Na S2
		606.2014	2.0	3.3	22.5	7.8	C37 H33 N3 Na S2
		606.2009	2.5	4.1	12.5	2.5	C29 H36 N O11 S
		606.2063	-2.9	-4.8	21.5	2.8	C35 H32 N3 O5 S
		606.2005	2.9	4.8	23.5	3.2	C36 H29 N3 O5 Na
		606.2004	3.0	4.9	30.5	21.2	C42 H28 N3 S
		606.2064	-3.0	-4.9	14.5	2.8	C29 H33 N3 O10 Na

Figure S7: HRESI-MS Spectrum of compound **6a**

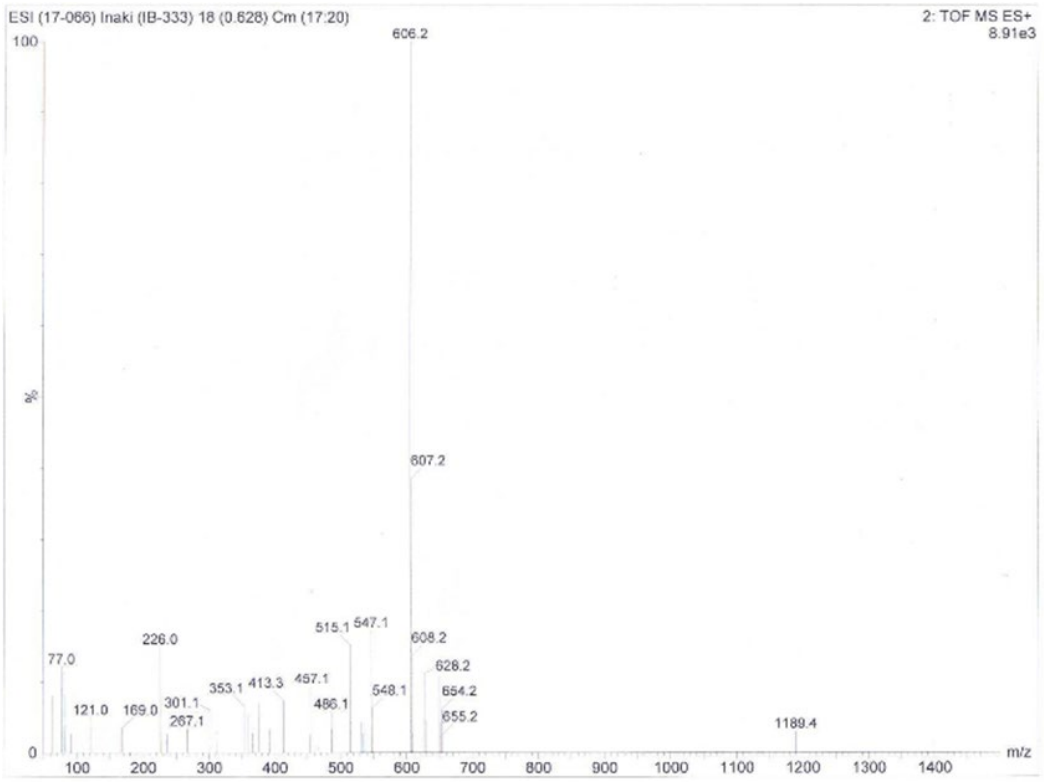

Figure S8: ESI-MS Spectrum of compound **6a**

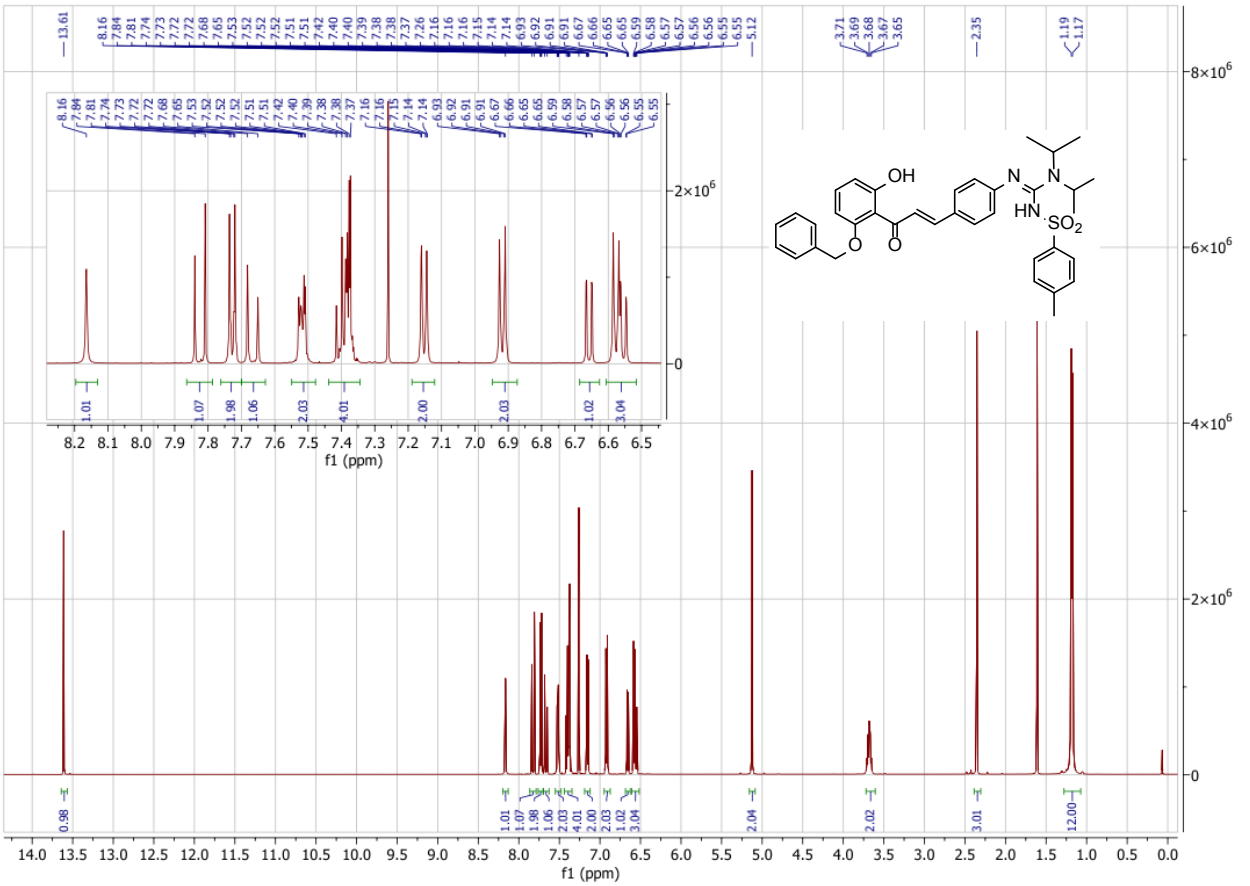

Figure S9: ^{1}H-NMR (500 MHz, $CDCl_3$) Spectrum of compound **6b**

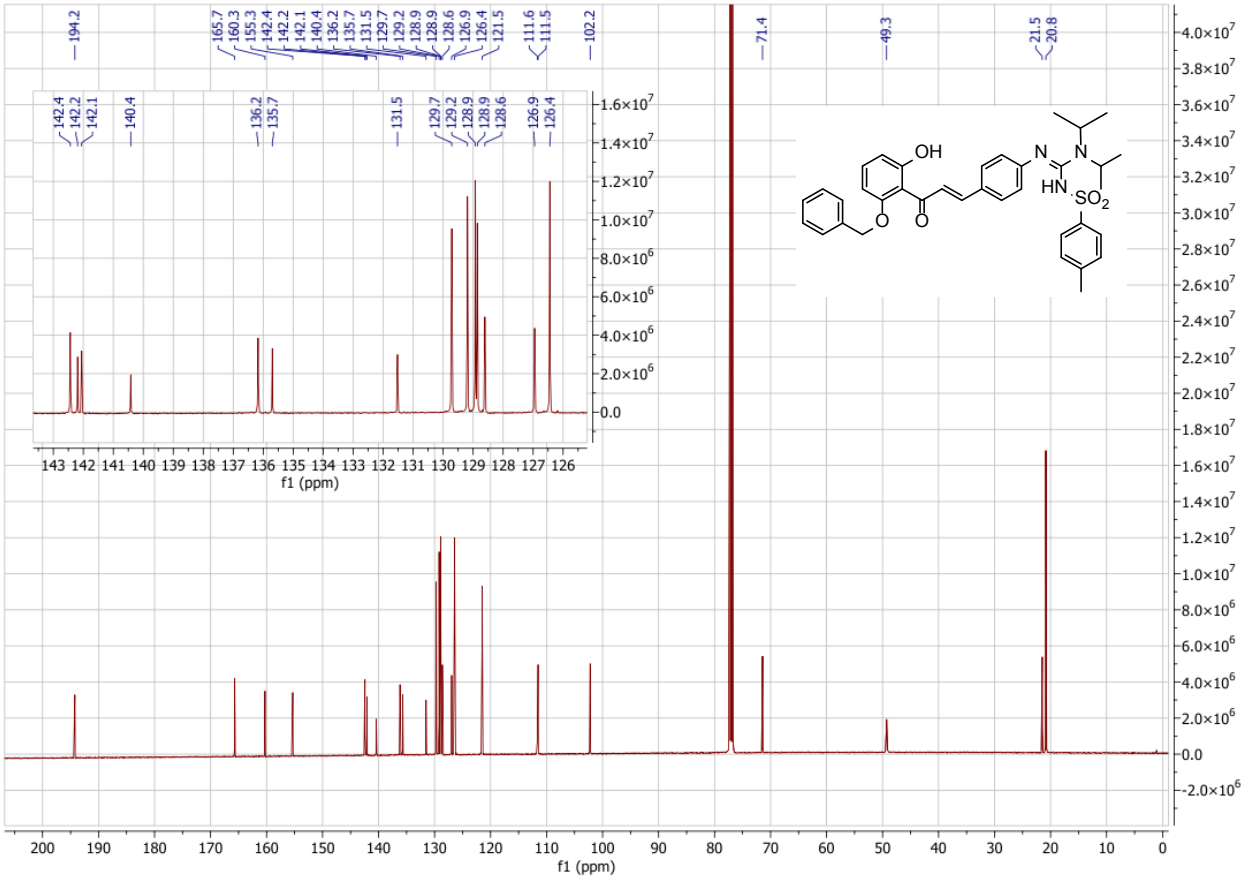

Figure S10: ^{13}C-NMR (125 MHz, $CDCl_3$) Spectrum of compound **6b**

Elemental Composition Report Page 1

Tolerance = 5.0 PPM / DBE: min = -10.0, max = 1000.0
Element prediction: Off
Number of isotope peaks used for i-FIT = 2

Monoisotopic Mass, Even Electron Ions
3090 formula(e) evaluated with 11 results within limits (all results (up to 1000) for each mass)
Elements Used:
C: 0-60 H: 0-100 N: 0-4 O: 0-12 Na: 0-1 S: 0-2

ESI (17-057) Inaki (IB-324) 59 (2.568) 1: TOF MS ES+ 1.57e+003

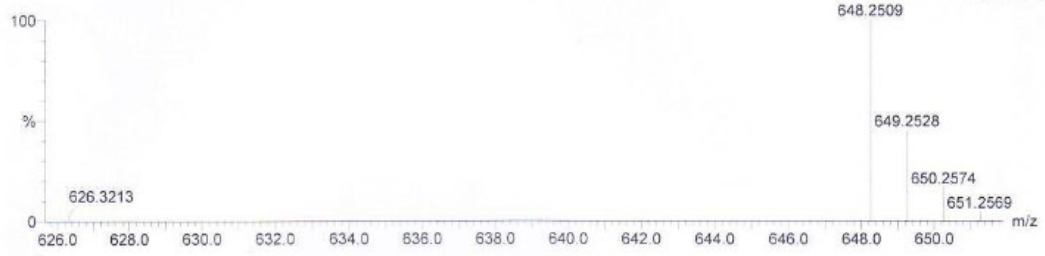

Minimum:	60.00				-10.0		
Maximum:	100.00		100.0	5.0	1000.0		
Mass	RA	Calc. Mass	mDa	PPM	DBE	i-FIT	Formula
648.2509	100.00	648.2508	0.1	0.2	18.5	0.7	C36 H39 N3 O5 Na S
		648.2507	0.2	0.3	25.5	2.8	C42 H38 N3 S2
		648.2512	-0.3	-0.5	7.5	12.8	C29 H46 N O11 S2
		648.2515	-0.6	-0.9	27.5	2.8	C44 H35 N O3 Na
		648.2498	1.1	1.7	26.5	0.7	C41 H34 N3 O5
		648.2488	2.1	3.2	4.5	19.8	C27 H47 N O11 Na S2
		648.2532	-2.3	-3.5	21.5	0.1	C38 H38 N3 O5 S
		648.2533	-2.4	-3.7	14.5	7.2	C32 H39 N3 O10 Na
		648.2483	2.6	4.0	22.5	1.0	C40 H39 N3 Na S2
		648.2479	3.0	4.6	12.5	7.0	C32 H42 N O11 S
		648.2539	-3.0	-4.6	30.5	5.8	C46 H34 N O3

Figure S11: HRESI-MS Spectrum of compound **6b**

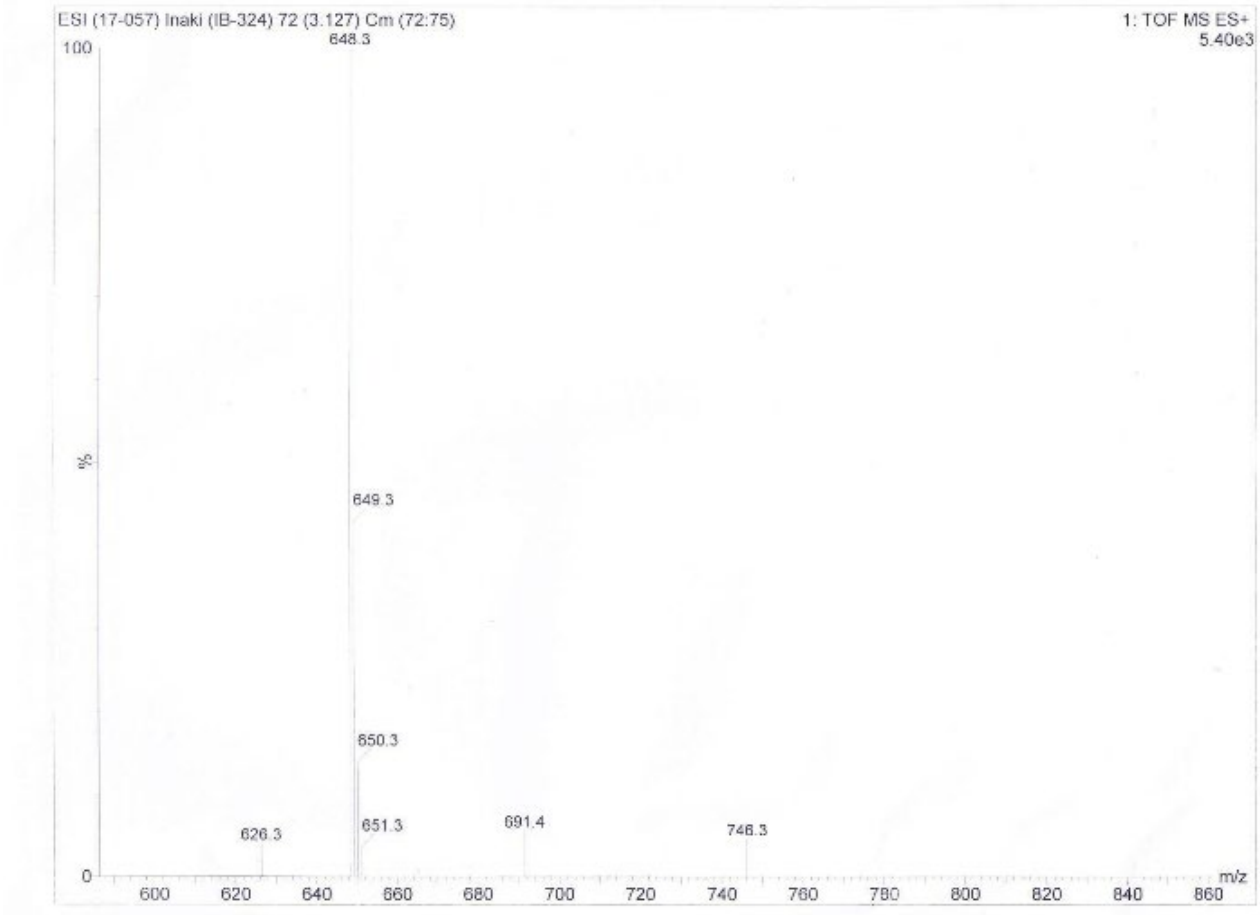

Figure S12: ESI-MS Spectrum of compound **6b**

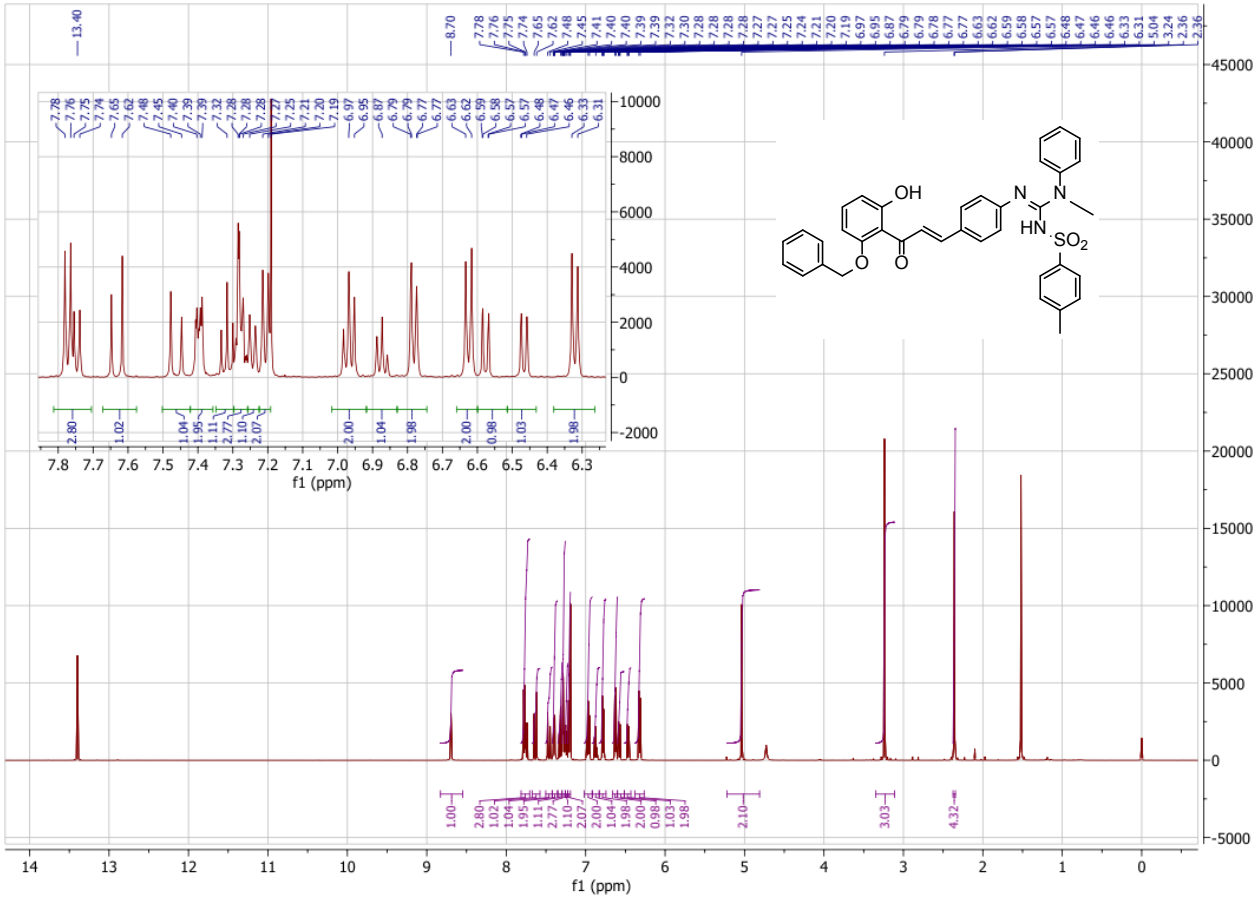

Figure S13: ^{1}H-NMR (500 MHz, $CDCl_3$) Spectrum of compound **6c**

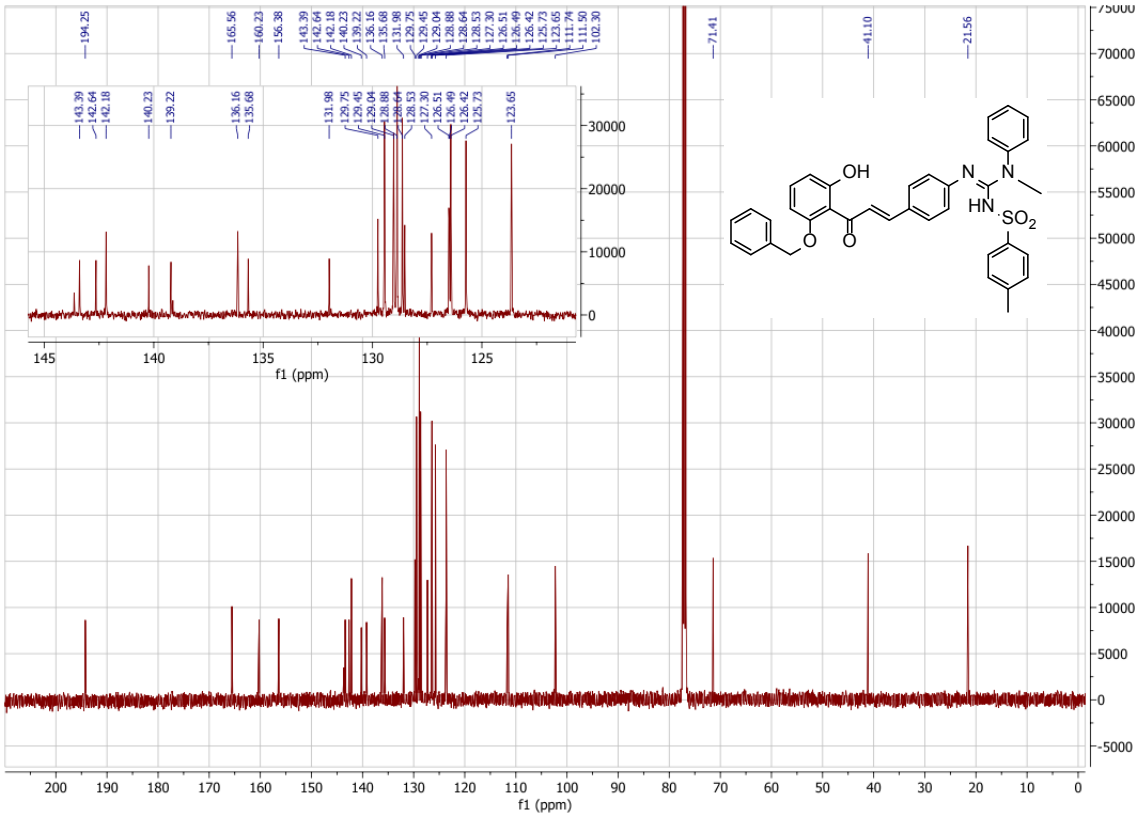

Figure S14: ^{13}C-NMR (125 MHz, $CDCl_3$) Spectrum of compound **6c**

Elemental Composition Report Page 1

Tolerance = 5.0 PPM / DBE: min = -10.0, max = 1000.0
Element prediction: Off
Number of isotope peaks used for i-FIT = 2

Monoisotopic Mass, Even Electron Ions
3103 formula(e) evaluated with 12 results within limits (all results (up to 1000) for each mass)
Elements Used:
C: 0-60 H: 0-100 N: 0-4 O: 0-12 Na: 0-1 S: 0-2

ESI (17-065) Inaki (IB-332) 55 (1.916) 2: TOF MS ES+ 9.86e+002

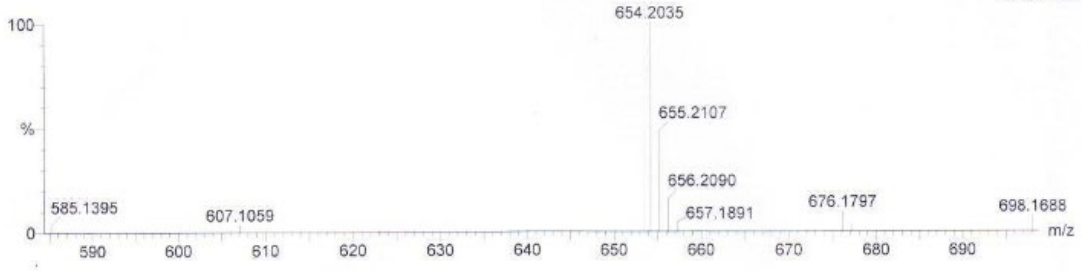

Minimum:	60.00				-10.0		
Maximum:	100.00		100.0	5.0	1000.0		
Mass	RA	Calc. Mass	mDa	PPM	DBE	i-FIT	Formula
654.2035	100.00	654.2038	-0.3	-0.5	29.5	0.7	C43 H32 N3 S2
		654.2039	-0.4	-0.6	22.5	1.3	C37 H33 N3 O5 Na S
		654.2029	0.6	0.9	30.5	0.1	C42 H28 N3 O5
		654.2043	-0.8	-1.2	11.5	10.8	C30 H40 N O11 S2
		654.2045	-1.0	-1.5	31.5	0.7	C45 H29 N O3 Na
		654.2019	1.6	2.4	8.5	15.9	C28 H41 N O11 Na S2
		654.2014	2.1	3.2	26.5	0.2	C41 H33 N3 Na S2
		654.2009	2.6	4.0	16.5	6.6	C33 H36 N O11 S
		654.2063	-2.8	-4.3	25.5	0.3	C39 H32 N3 O5 S
		654.2064	-2.9	-4.4	18.5	6.7	C33 H33 N3 O10 Na
		654.2005	3.0	4.6	27.5	0.4	C40 H29 N3 O5 Na
		654.2004	3.1	4.7	34.5	2.2	C46 H28 N3 S

Figure S15: HRESI-MS Spectrum of compound **6c**

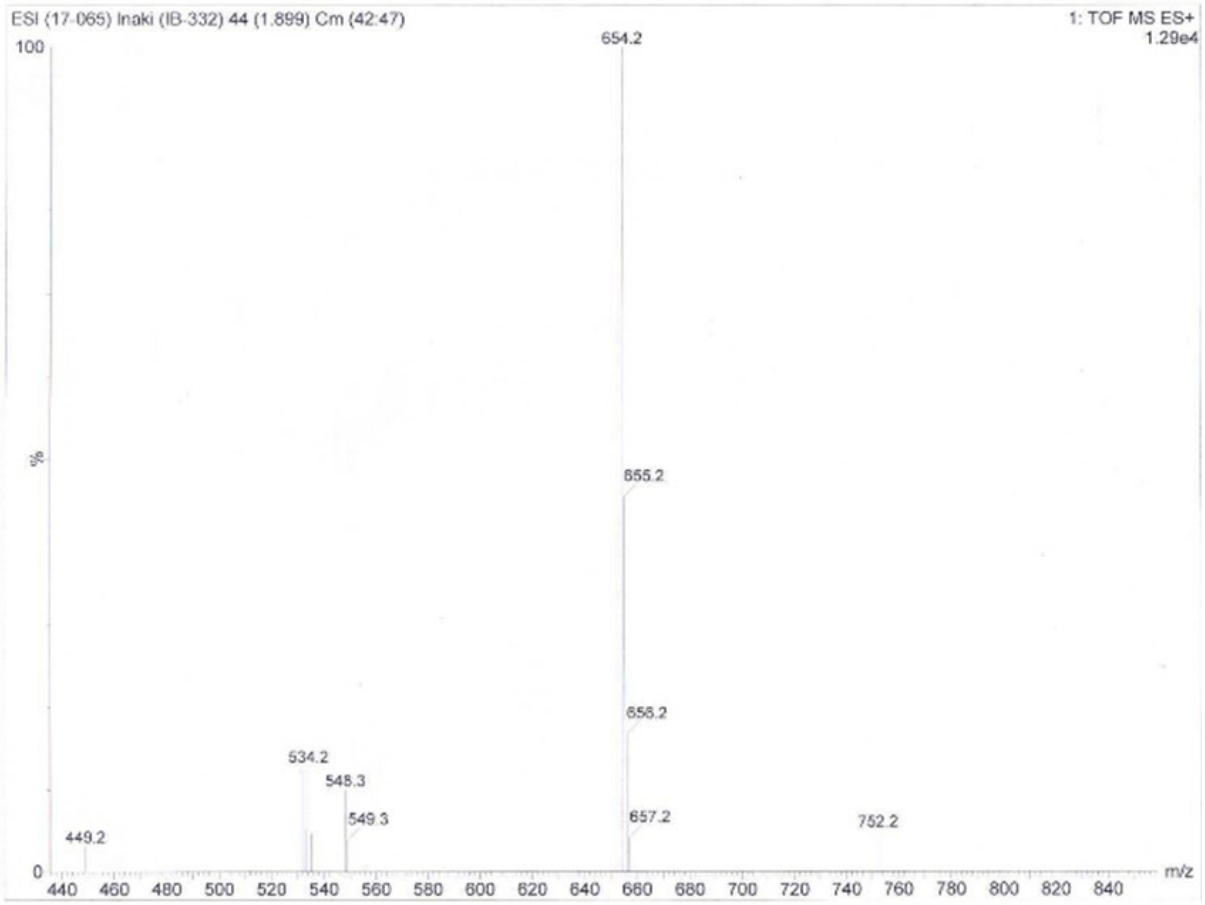

Figure S16: ESI-MS Spectrum of compound **6c**

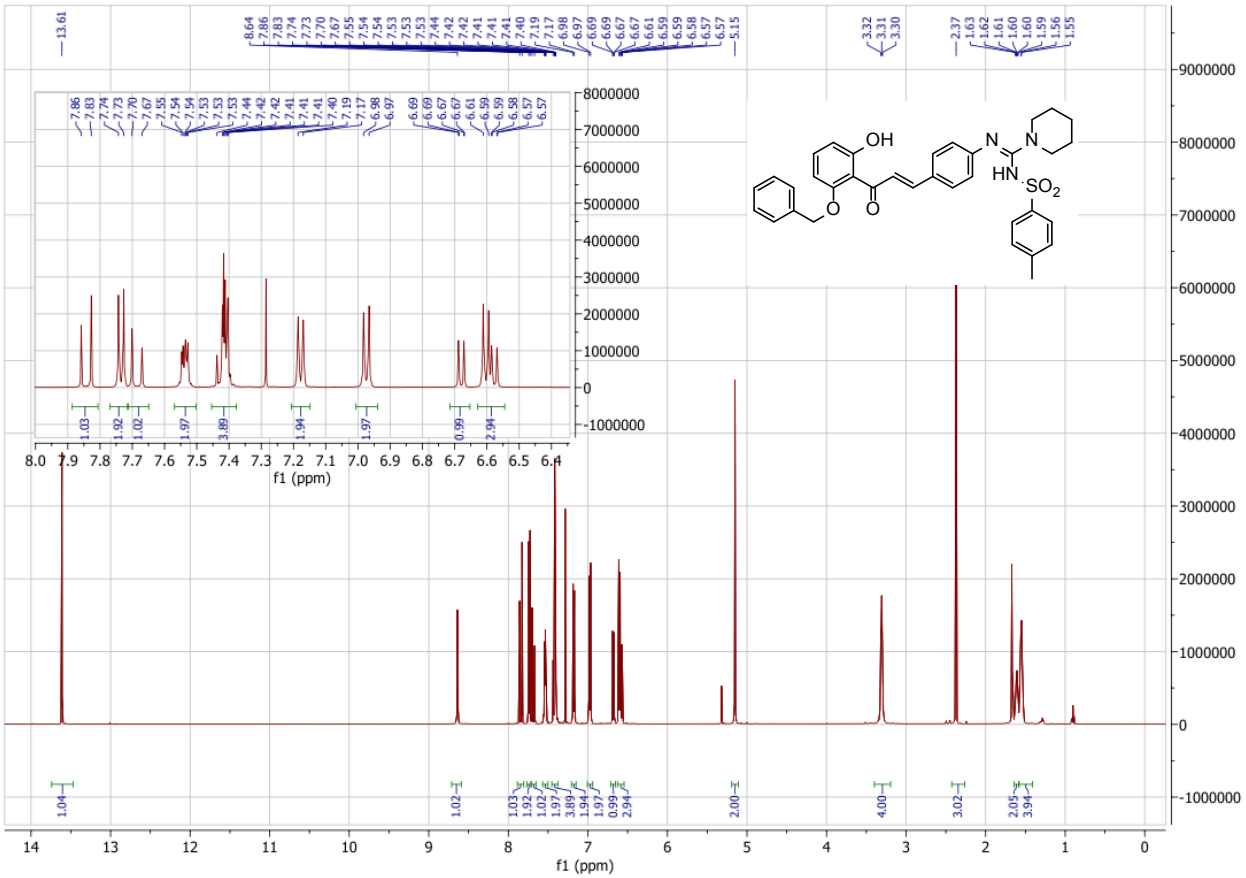

Figure S17: ^{1}H-NMR (500 MHz, $CDCl_3$) Spectrum of compound **6d**

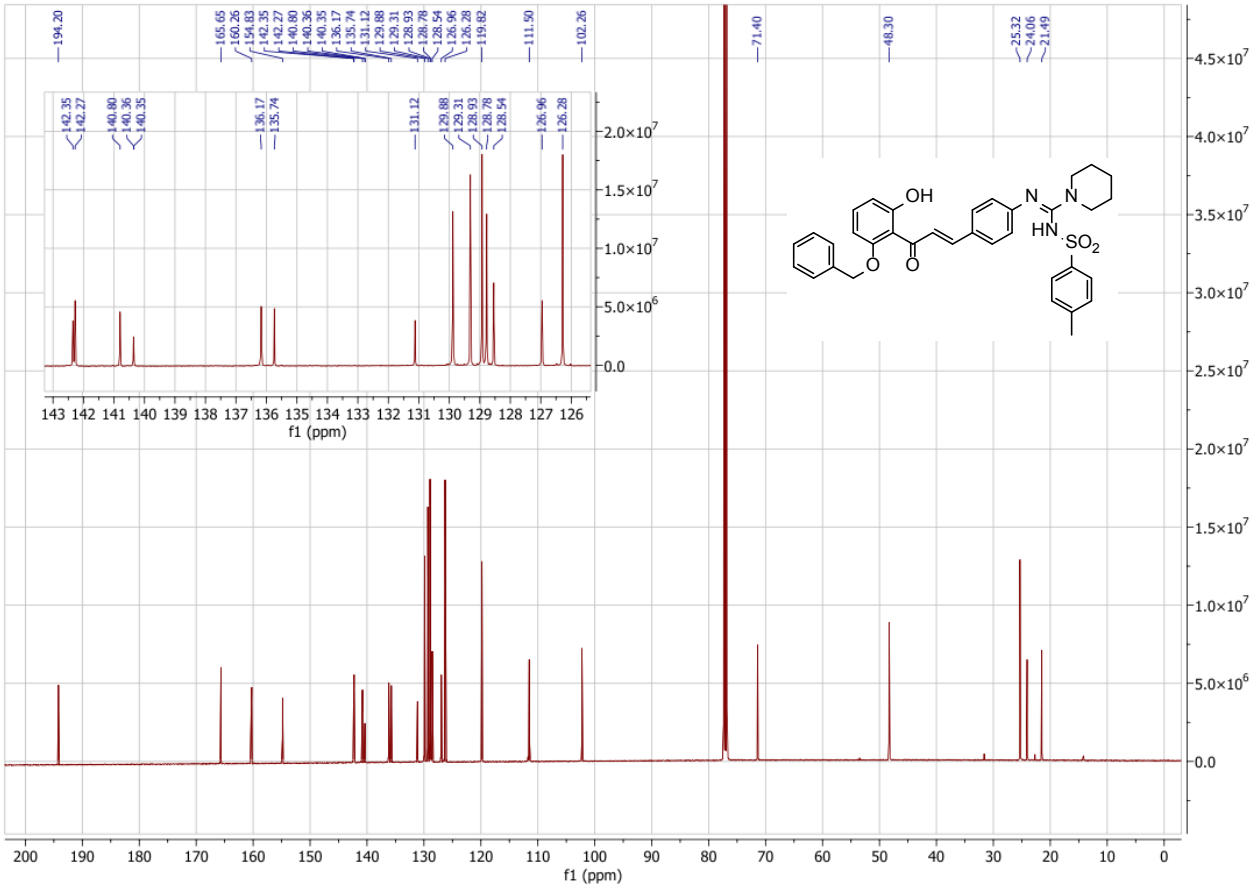

Figure S18: ^{13}C-NMR (125 MHz, $CDCl_3$) Spectrum of compound **6d**

Elemental Composition Report Page 1

Tolerance = 5.0 PPM / DBE: min = -10.0, max = 1000.0
Element prediction: Off
Number of isotope peaks used for i-FIT = 2

Monoisotopic Mass, Even Electron Ions
3037 formula(e) evaluated with 11 results within limits (all results (up to 1000) for each mass)
Elements Used:
C: 0-60 H: 0-100 N: 0-4 O: 0-12 Na: 0-1 S: 0-2

ESI (17-058) Inaki (IB-325) 5 (0.172) 2: TOF MS ES+ 1.35e+003

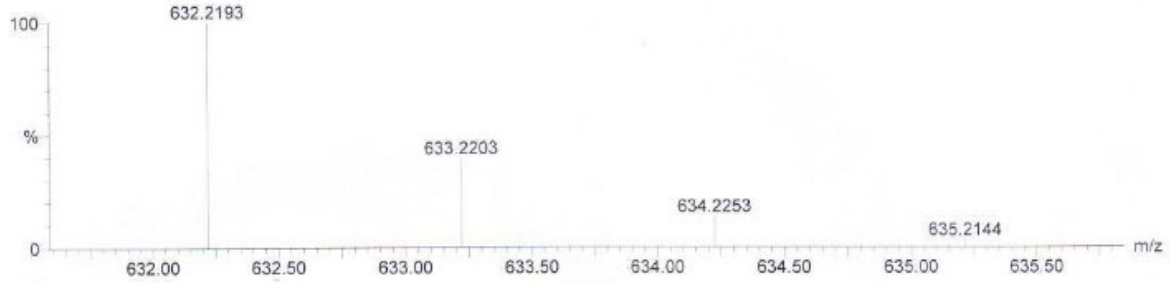

Minimum:	60.00				-10.0		
Maximum:	100.00		100.0	5.0	1000.0		
Mass	RA	Calc. Mass	mDa	PPM	DBE	i-FIT	Formula
632.2193	100.00	632.2194	-0.1	-0.2	26.5	9.3	C41 H34 N3 S2
		632.2195	-0.2	-0.3	19.5	0.5	C35 H35 N3 O5 Na S
		632.2199	-0.6	-0.9	8.5	3.8	C28 H42 N O11 S2
		632.2185	0.8	1.3	27.5	5.1	C40 H30 N3 O5
		632.2202	-0.9	-1.4	28.5	9.3	C43 H31 N O3 Na
		632.2175	1.8	2.8	5.5	7.8	C26 H43 N O11 Na S2
		632.2170	2.3	3.6	23.5	5.6	C39 H35 N3 Na S2
		632.2219	-2.6	-4.1	22.5	2.3	C37 H34 N3 O5 S
		632.2220	-2.7	-4.3	15.5	1.3	C31 H35 N3 O10 Na
		632.2166	2.7	4.3	13.5	1.1	C31 H38 N O11 S
		632.2161	3.2	5.1	24.5	2.5	C38 H31 N3 O5 Na

Figure S19: HRESI-MS Spectrum of compound **6d**

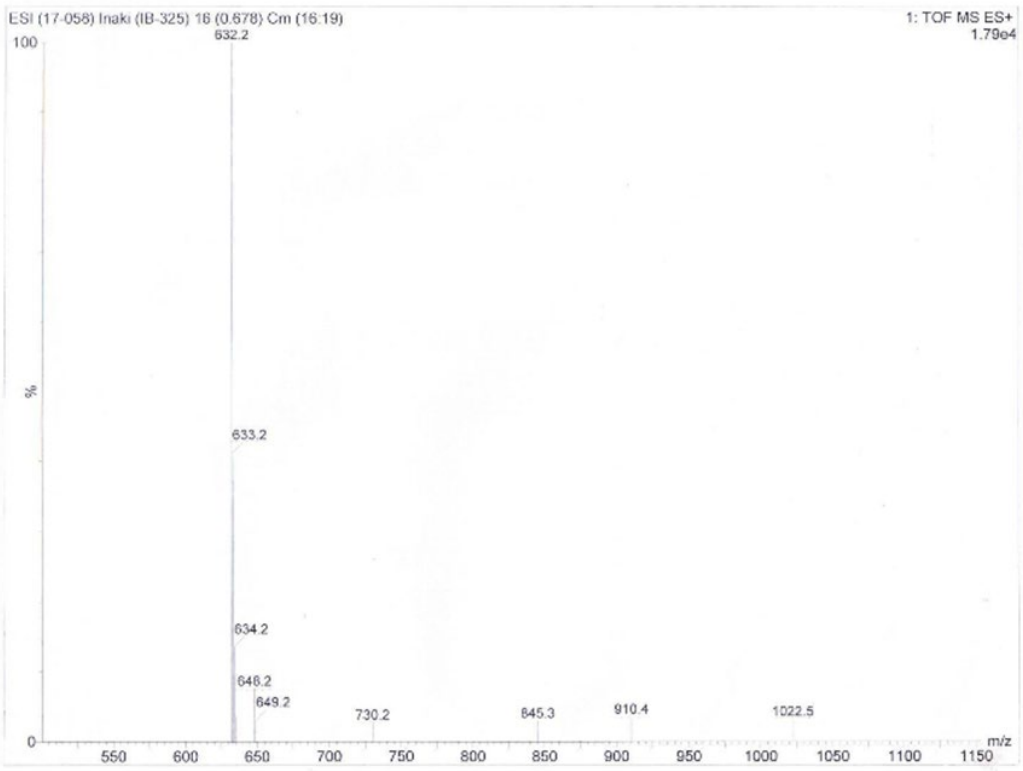

Figure S20: ESI-MS Spectrum of compound **6d**

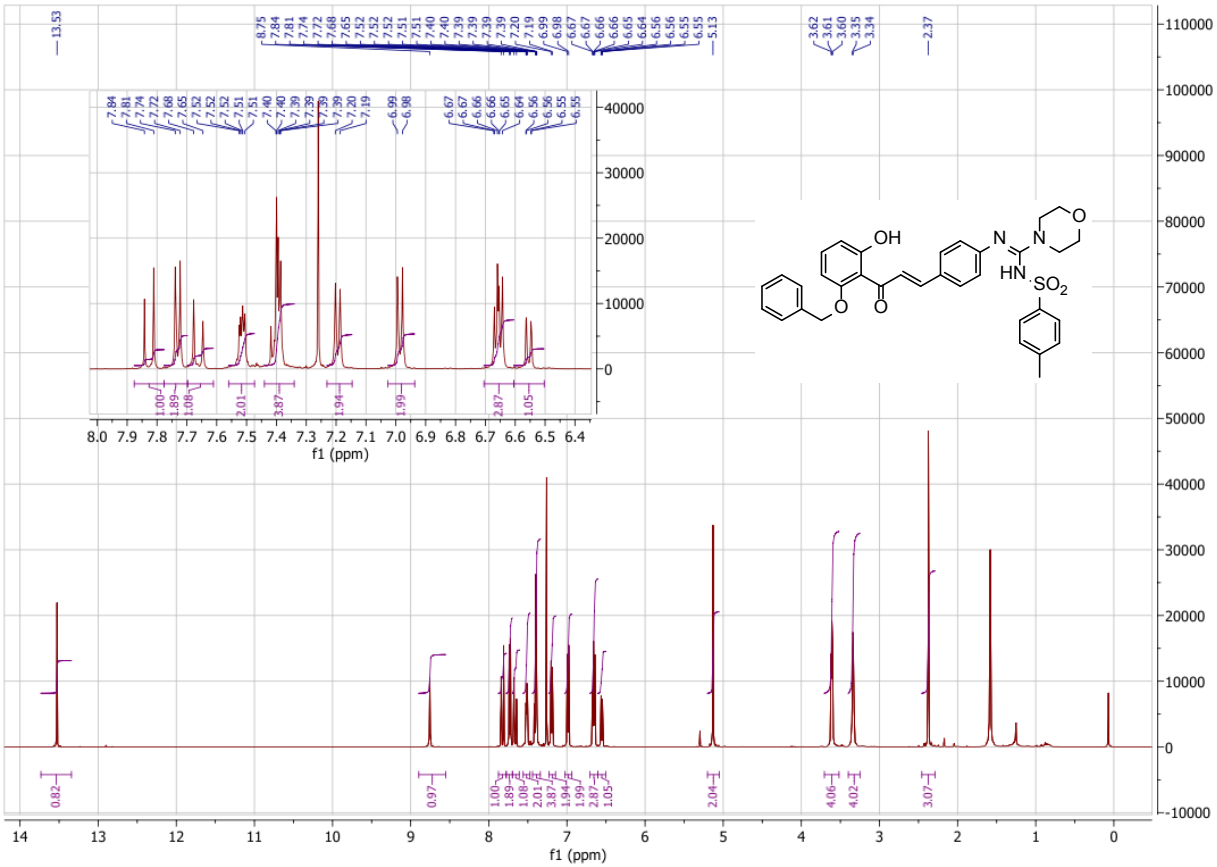

Figure S21: ^{1}H-NMR (500 MHz, $CDCl_3$) Spectrum of compound **6e**

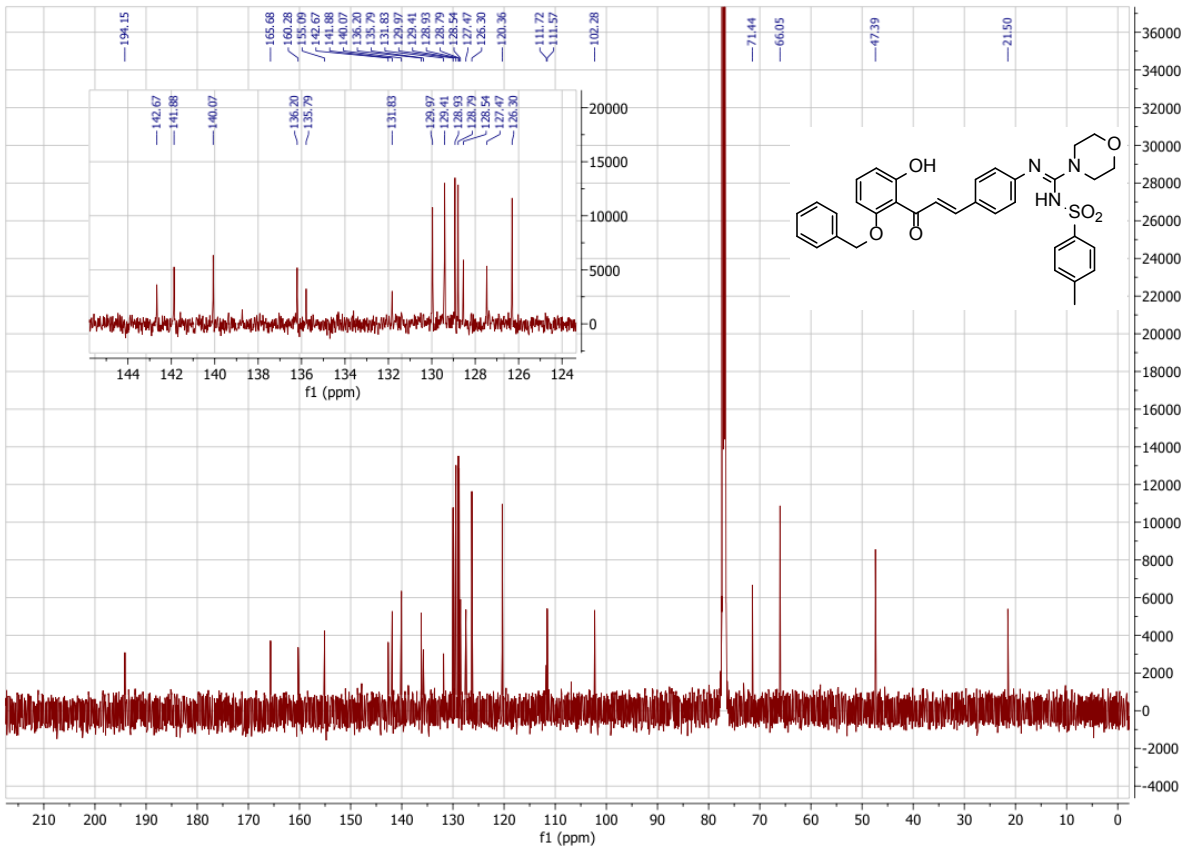

Figure S22: ^{13}C-NMR (125 MHz, $CDCl_3$) Spectrum of compound **6e**

Elemental Composition Report Page 1

Tolerance = 5.0 PPM / DBE: min = -10.0, max = 1000.0
Element prediction: Off
Number of isotope peaks used for i-FIT = 2

Monoisotopic Mass, Even Electron Ions
3043 formula(e) evaluated with 11 results within limits (all results (up to 1000) for each mass)
Elements Used:
C: 0-60 H: 0-100 N: 0-4 O: 0-12 Na: 0-1 S: 0-2

ESI (17-059) Inaki (IB-326) 77 (3.367) 1: TOF MS ES+ 2.61e+003

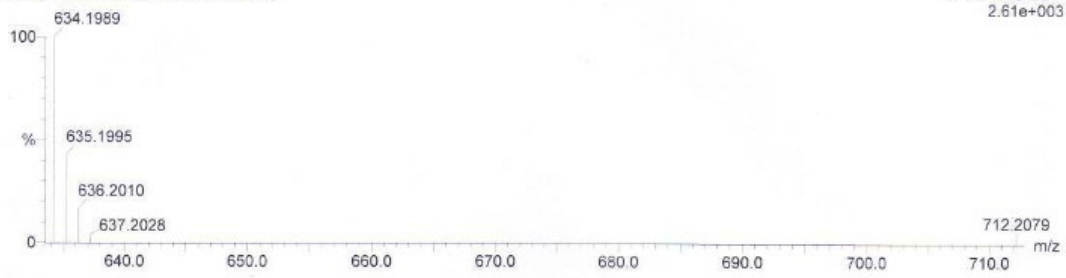

Minimum:	60.00				-10.0		
Maximum:	100.00		100.0	5.0	1000.0		
Mass	RA	Calc. Mass	mDa	PPM	DBE	i-FIT	Formula
634.1989	100.00	634.1988	0.1	0.2	19.5	1.3	C34 H33 N3 O6 Na S
		634.1987	0.2	0.3	26.5	4.7	C40 H32 N3 O S2
		634.1992	-0.3	-0.5	8.5	23.3	C27 H40 N O12 S2
		634.1994	-0.5	-0.8	28.5	4.8	C42 H29 N O4 Na
		634.1978	1.1	1.7	27.5	1.1	C39 H28 N3 O6
		634.1968	2.1	3.3	5.5	36.0	C25 H41 N O12 Na S2
		634.2012	-2.3	-3.6	22.5	0.3	C36 H32 N3 O6 S
		634.2013	-2.4	-3.8	15.5	13.4	C30 H33 N3 O11 Na
		634.1963	2.6	4.1	23.5	1.6	C38 H33 N3 O Na S2
		634.2018	-2.9	-4.6	31.5	10.0	C44 H28 N O4
		634.1958	3.1	4.9	13.5	12.7	C30 H36 N O12 S

Figure S23: HRESI-MS Spectrum of compound **6e**

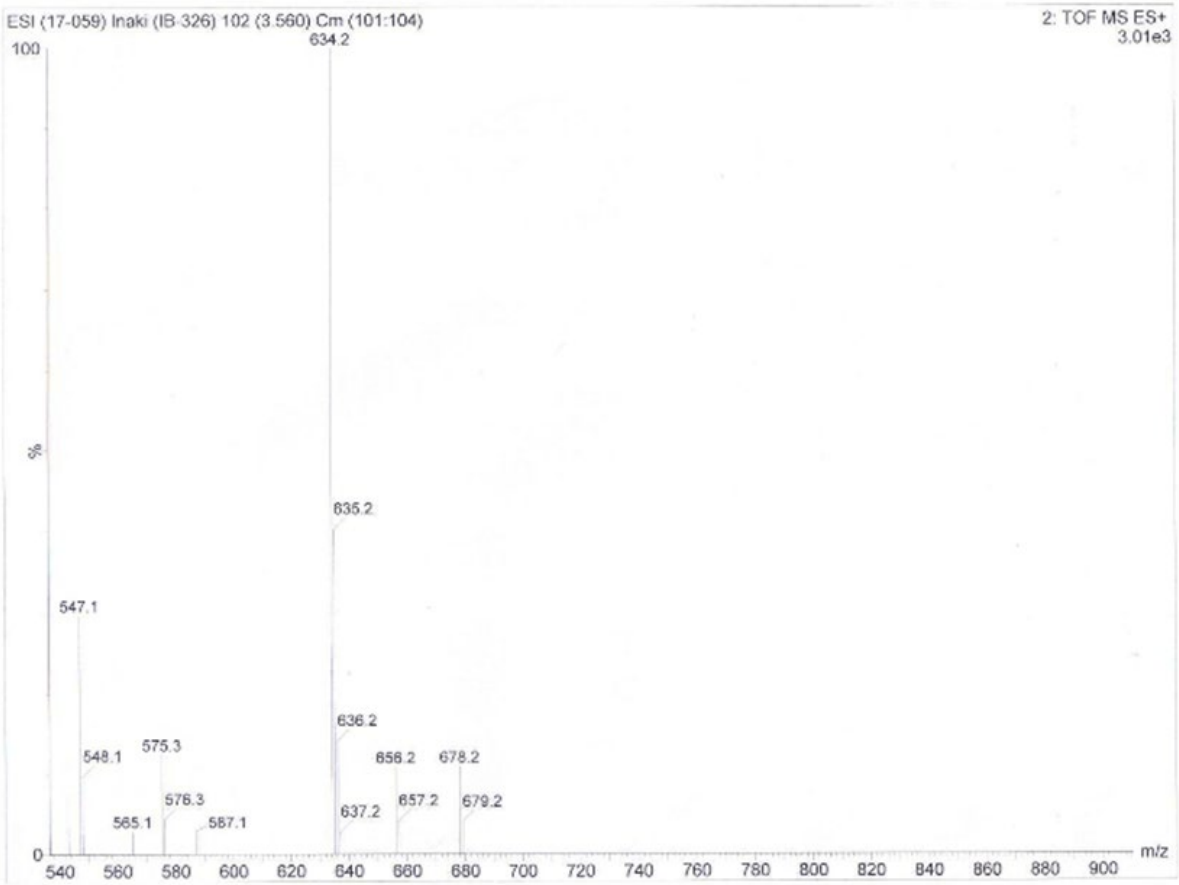

Figure S24: ESI-MS Spectrum of compound **6e**

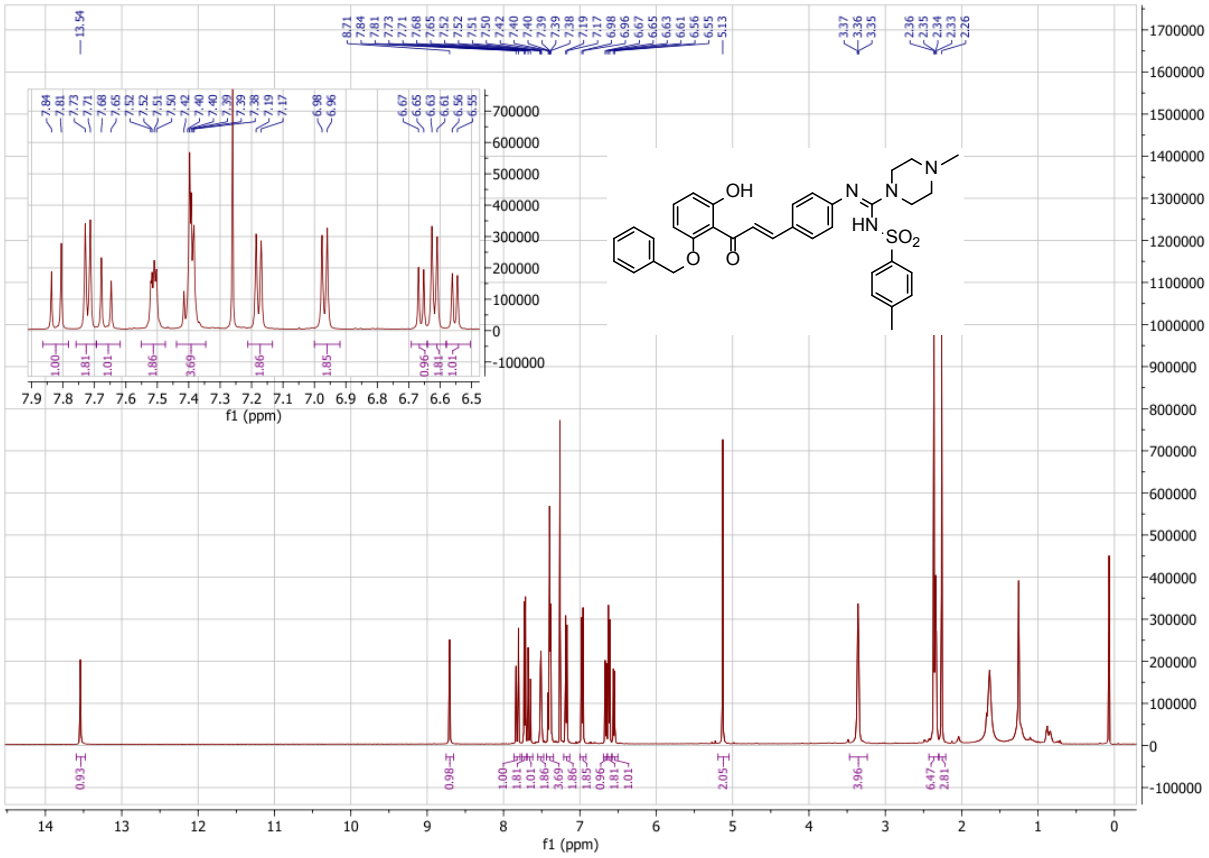

Figure S25: ^{1}H-NMR (500 MHz, $CDCl_3$) Spectrum of compound **6f**

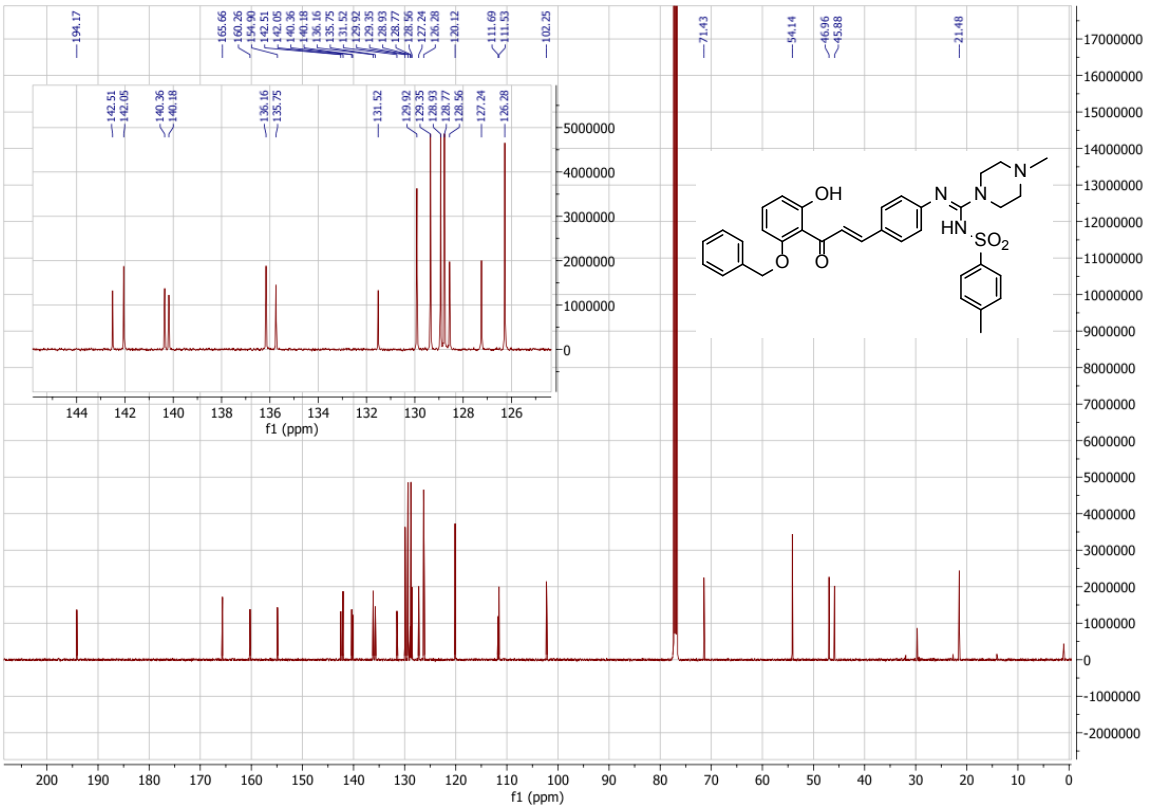

Figure S26: ^{13}C-NMR (125 MHz, $CDCl_3$) Spectrum of compound **6f**

Elemental Composition Report Page 1

Multiple Mass Analysis: 2 mass(es) processed
Tolerance = 5.0 PPM / DBE: min = -10.0, max = 1000.0
Element prediction: Off
Number of isotope peaks used for i-FIT = 2

Monoisotopic Mass, Even Electron Ions
6921 formula(e) evaluated with 34 results within limits (all results (up to 1000) for each mass)
Elements Used:
C: 0-70 H: 0-90 N: 0-5 O: 0-20 Na: 0-1 S: 0-1

ESI (16-435) Inaki (IB JP-44 F5) 8 (0.330) 1: TOF MS ES- 1.16e+004

Minimum:	40.00				-10.0		
Maximum:	100.00		100.0	5.0	1000.0		
Mass	RA	Calc. Mass	mDa	PPM	DBE	i-FIT	Formula
623.2317	100.00	623.2316	0.1	0.2	8.5	148.2	C28 H40 O14 Na
		623.2315	0.2	0.3	15.5	20.1	C34 H39 O9 S
		623.2311	0.6	1.0	26.5	7.1	C41 H32 N2 O3 Na
		623.2309	0.8	1.3	-0.5	418.0	C20 H44 N2 O16 Na S
		623.2328	-1.1	-1.8	20.5	4.6	C35 H35 N4 O5 S
		623.2329	-1.2	-1.9	13.5	92.2	C29 H36 N4 O10 Na
		623.2304	1.3	2.1	17.5	19.0	C33 H36 N4 O5 Na S
		623.2333	-1.6	-2.6	2.5	319.5	C22 H43 N2 O16 S
		623.2300	1.7	2.7	7.5	226.3	C25 H39 N2 O16
		623.2335	-1.8	-2.9	29.5	22.0	C43 H31 N2 O3
		623.2340	-2.3	-3.7	11.5	95.9	C30 H39 O14
		623.2294	2.3	3.7	25.5	0.9	C38 H31 N4 O5
		623.2293	2.4	3.9	-1.5	550.9	C17 H43 N4 O18 S
		623.2291	2.6	4.2	12.5	46.6	C32 H40 O9 Na S
		623.2344	-2.7	-4.3	21.5	0.8	C38 H36 N2 O3 Na S
624.2357	44.09	624.2356	0.1	0.2	12.5	15.1	C30 H39 N3 O8 Na S
		624.2361	-0.4	-0.6	-5.5	227.1	C17 H47 N O19 Na S
		624.2361	-0.4	-0.6	28.5	29.8	C44 H34 N O S
		624.2362	-0.5	-0.8	21.5	1.2	C38 H35 N O6 Na
		624.2351	0.6	1.0	2.5	128.2	C22 H42 N O19
		624.2364	-0.7	-1.1	7.5	89.9	C23 H38 N5 O15
		624.2346	1.1	1.8	20.5	0.8	C35 H34 N3 O8

Figure S27: HRESI-MS Spectrum of compound **6f**

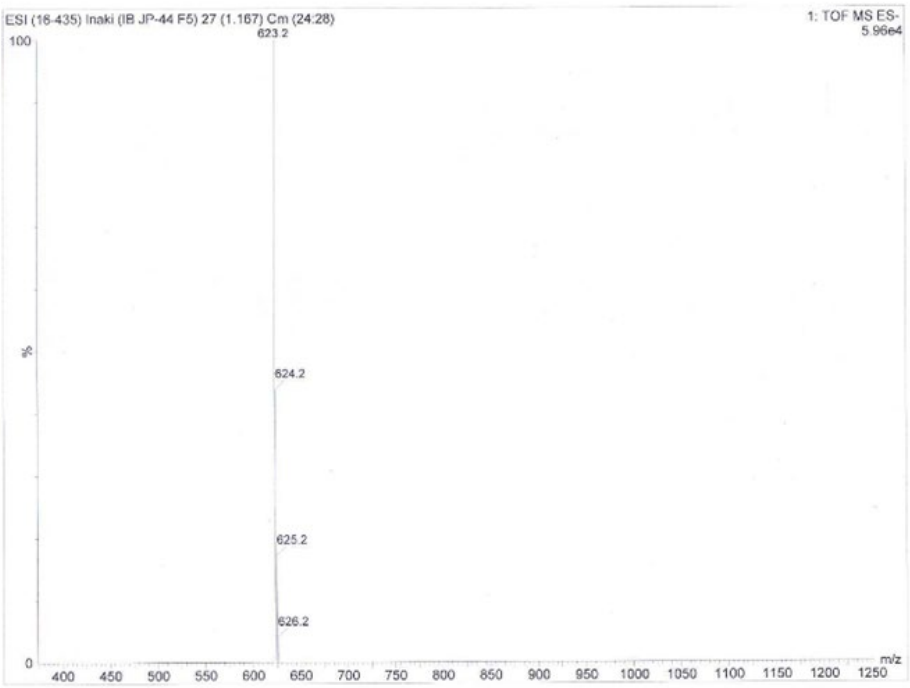

Figure S28: ESI-MS Spectrum of compound **6f**

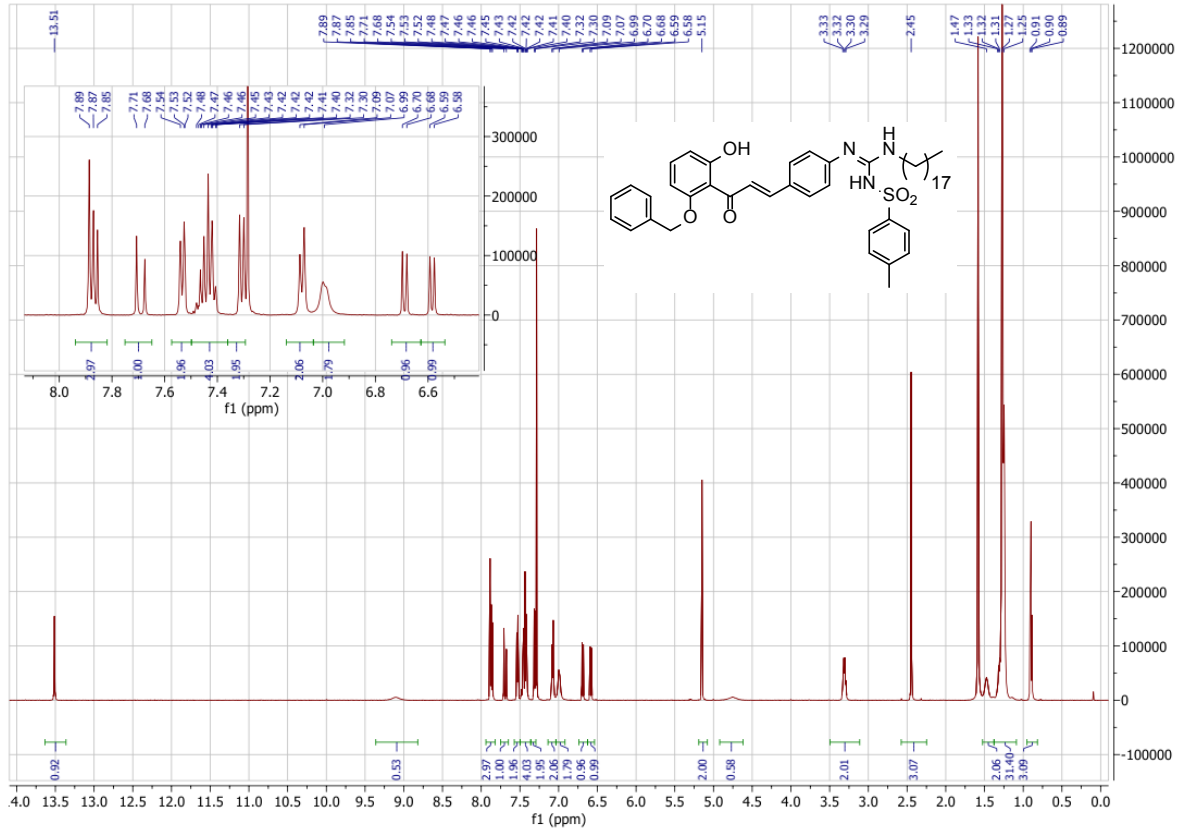

Figure S29: ^{1}H-NMR (500 MHz, $CDCl_3$) Spectrum of compound **6g**

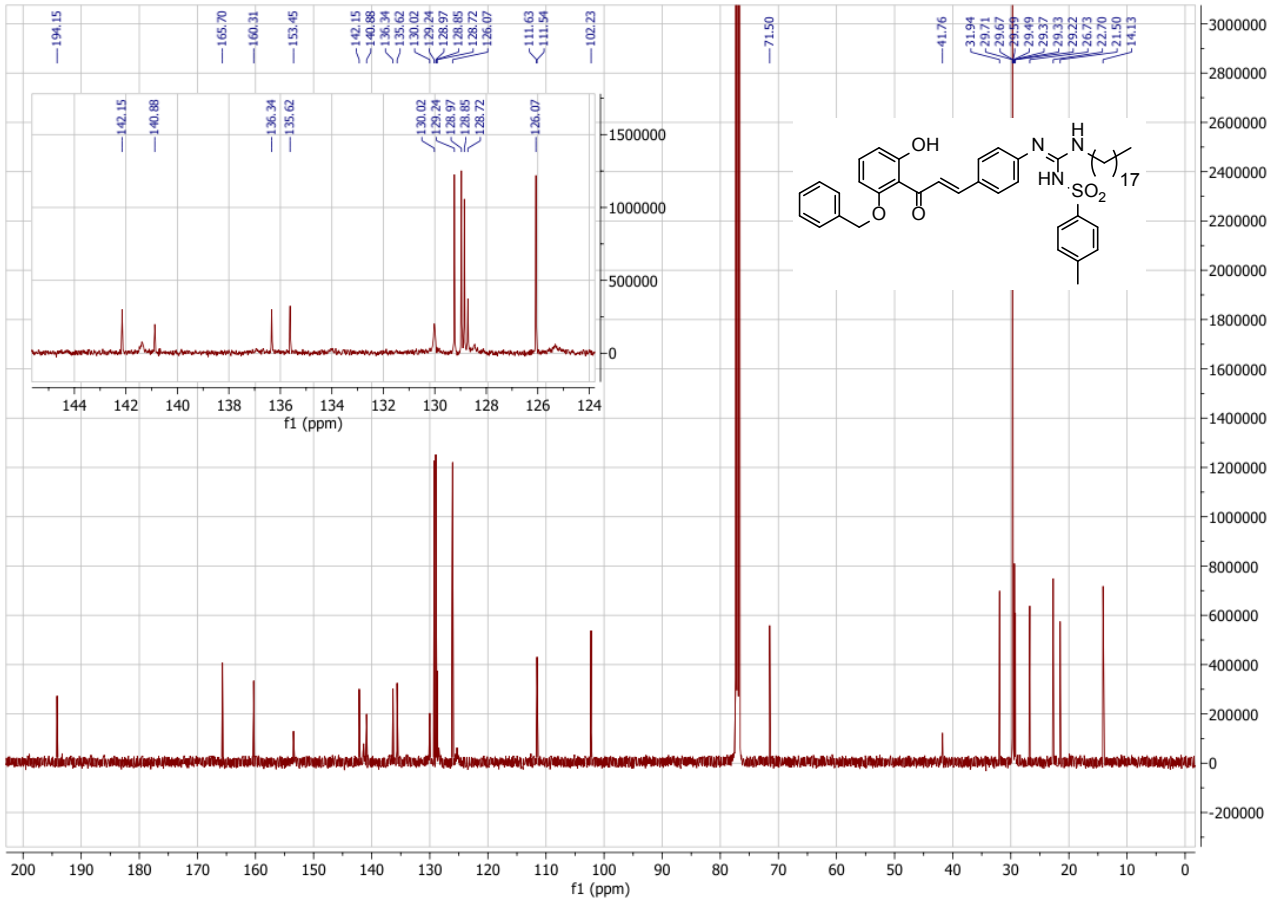

Figure S30: ^{13}C -NMR (125 MHz, $CDCl_3$) Spectrum of compound **6g**

Elemental Composition Report Page 1

Tolerance = 5.0 PPM / DBE: min = -10.0, max = 1000.0
Element prediction: Off
Number of isotope peaks used for i-FIT = 2

Monoisotopic Mass, Even Electron Ions
3182 formula(e) evaluated with 14 results within limits (all results (up to 1000) for each mass)
Elements Used:
C: 0-60 H: 0-100 N: 0-4 O: 0-12 Na: 0-1 S: 0-2

ESI (17-067) Inaki (IB-335) 87 (3.033) 2: TOF MS ES+ 2.01e+003

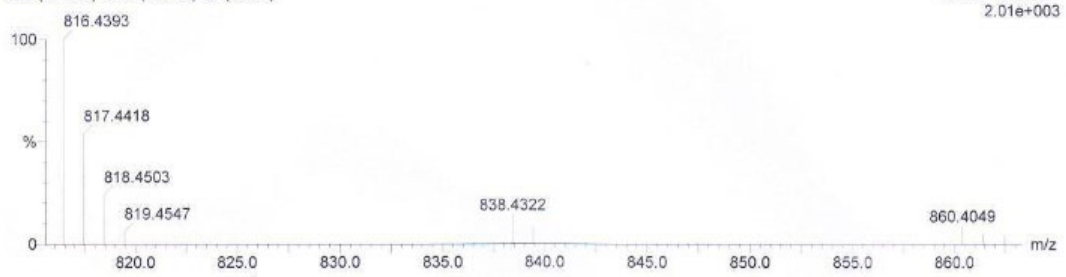

Minimum:	60.00				-10.0		
Maximum:	100.00		100.0	5.0	1000.0		
Mass	RA	Calc. Mass	mDa	PPM	DBE	i-FIT	Formula
816.4393	100.00	816.4393	0.0	0.0	27.5	10.2	C56 H59 N O3 Na
		816.4390	0.3	0.4	7.5	3.0	C41 H70 N O11 S2
		816.4386	0.7	0.9	18.5	0.8	C48 H63 N3 O5 Na S
		816.4385	0.8	1.0	25.5	10.2	C54 H62 N3 S2
		816.4410	-1.7	-2.1	21.5	2.6	C50 H62 N3 O5 S
		816.4376	1.7	2.1	26.5	5.8	C53 H58 N3 O5
		816.4411	-1.8	-2.2	14.5	0.8	C44 H63 N3 O10 Na
		816.4417	-2.4	-2.9	30.5	14.9	C58 H58 N O3
		816.4366	2.7	3.3	4.5	6.7	C39 H71 N O11 Na S2
		816.4420	-2.7	-3.3	13.5	0.1	C45 H67 N3 O5 Na S2
		816.4361	3.2	3.9	22.5	6.4	C52 H63 N3 Na S2
		816.4426	-3.3	-4.0	22.5	6.0	C53 H63 N O3 Na S
		816.4357	3.6	4.4	12.5	0.8	C44 H66 N O11 S
		816.4352	4.1	5.0	23.5	3.1	C51 H59 N3 O5 Na

Figure S31: HRESI-MS Spectrum of compound **6g**

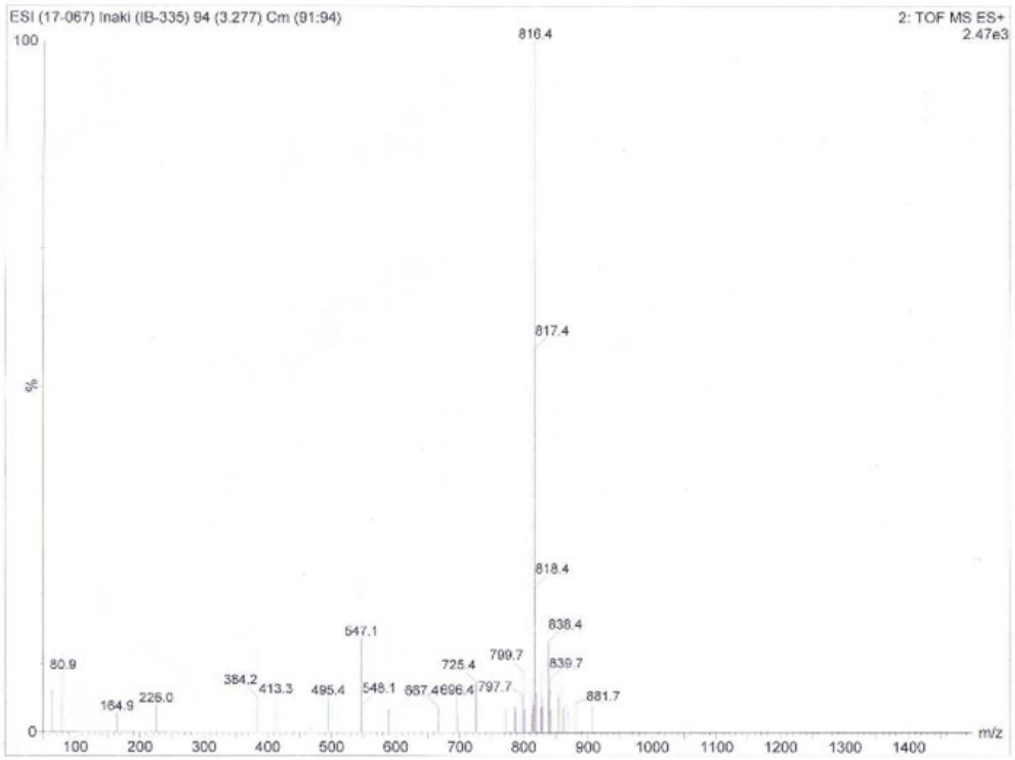

Figure S32: ESI-MS Spectrum of compound **6g**

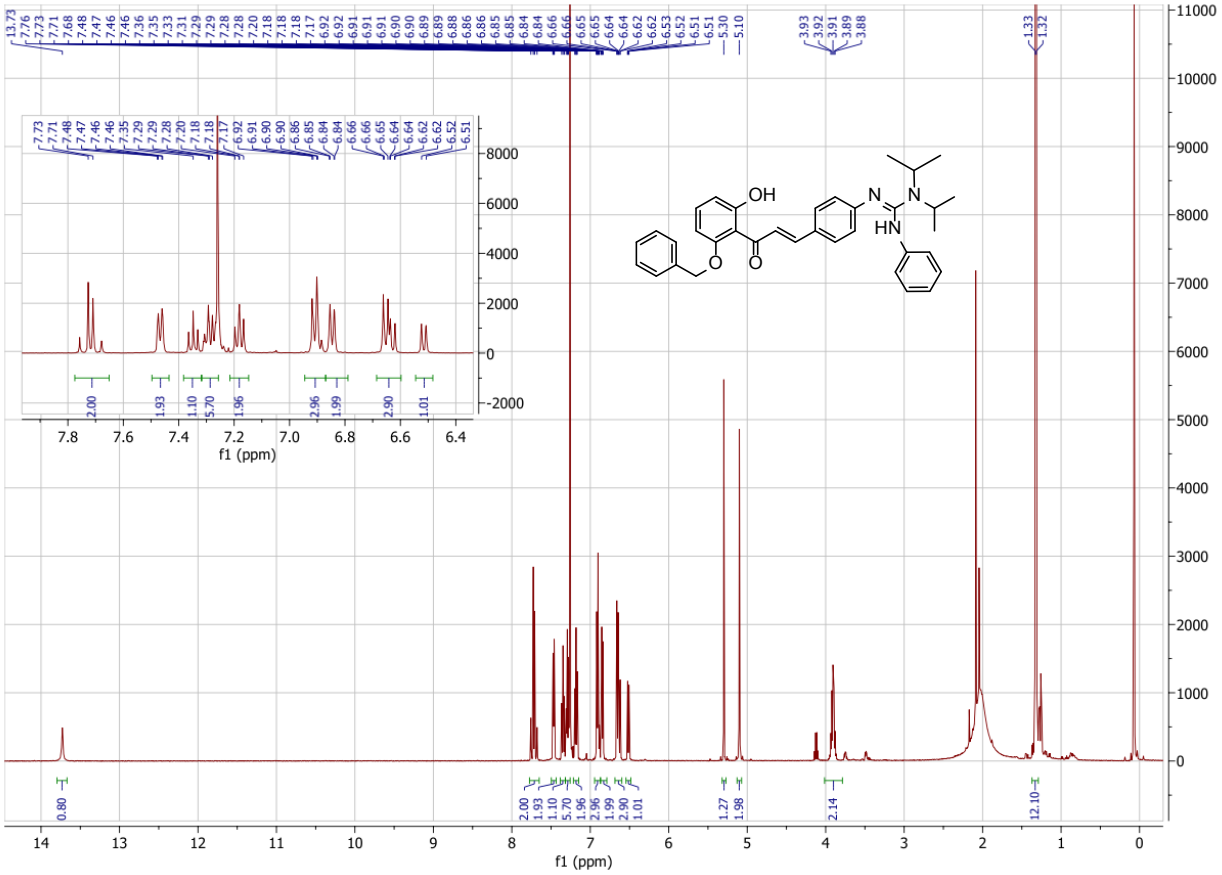

Figure S33: ^{1}H-NMR (500 MHz, $CDCl_3$) Spectrum of compound **6h**

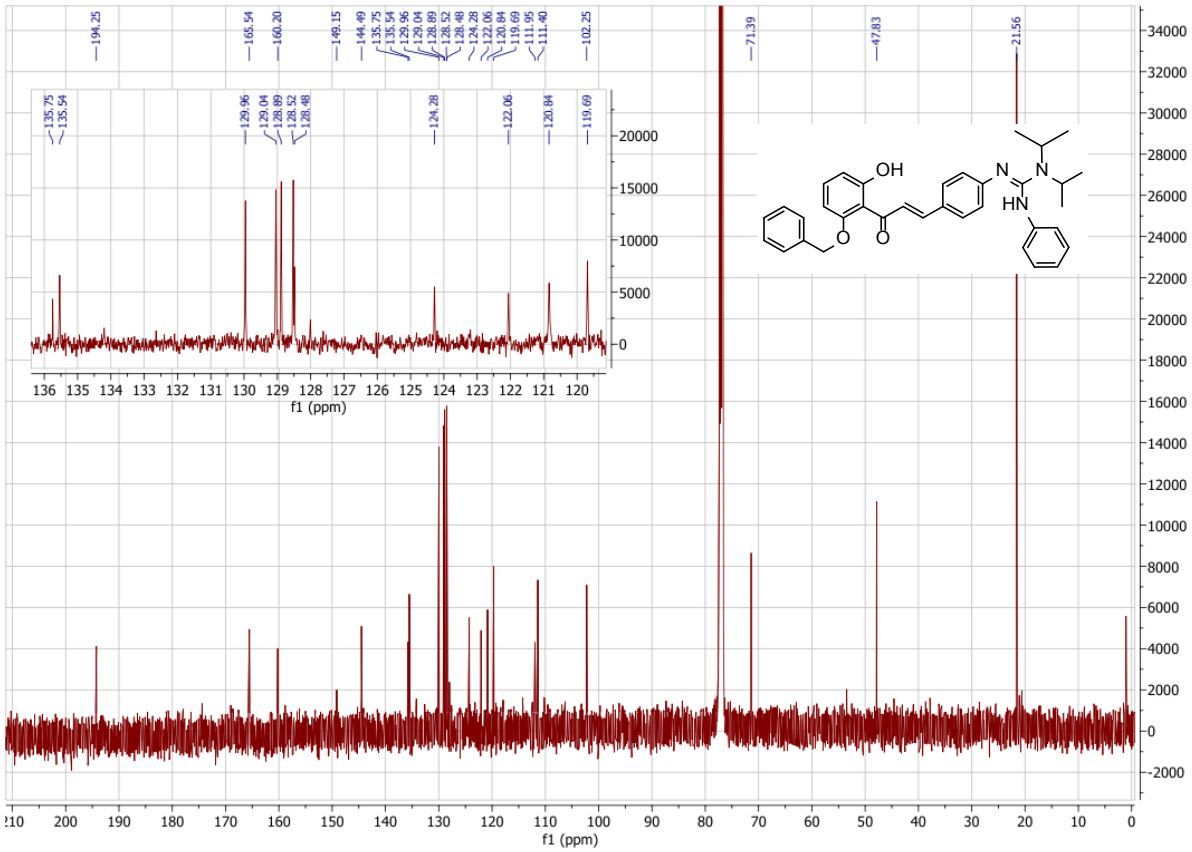

Figure S34: ^{13}C -NMR (125 MHz, $CDCl_3$) Spectrum of compound **6h**

Elemental Composition Report Page 1

Multiple Mass Analysis: 2 mass(es) processed
Tolerance = 5.0 PPM / DBE: min = -10.0, max = 1000.0
Element prediction: Off
Number of isotope peaks used for i-FIT = 2

Monoisotopic Mass, Even Electron Ions
5504 formula(e) evaluated with 21 results within limits (all results (up to 1000) for each mass)
Elements Used:
C: 0-60 H: 0-100 N: 0-4 O: 0-12 Na: 0-1 S: 0-2
ESI (17-061) Inaki (IB-327) 29 (1.011)

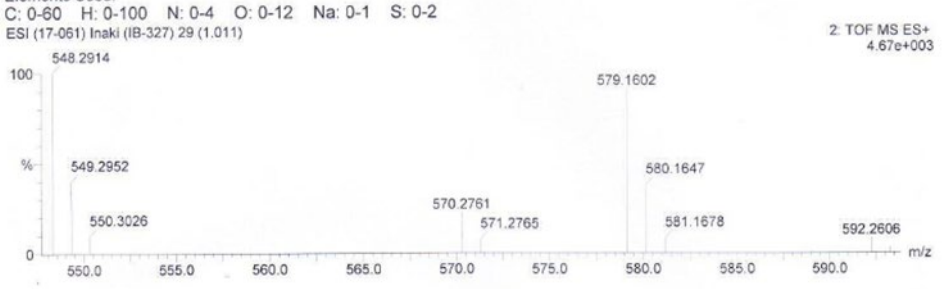

Minimum:	60.00				-10.0		
Maximum:	100.00		100.0	5.0	1000.0		
Mass	RA	Calc. Mass	mDa	PPM	DBE	i-FIT	Formula
548.2914	100.00	548.2913	0.1	0.2	18.5	0.2	C35 H38 N3 O3 •
		548.2923	-0.9	-1.6	10.5	7.2	C30 H43 N3 O3 Na S
		548.2903	1.1	2.0	-3.5	92.5	C21 H51 N O9 Na S2
		548.2927	-1.3	-2.4	-0.5	63.3	C23 H50 N O9 S2
		548.2929	-1.5	-2.7	19.5	4.2	C38 H39 N O Na
		548.2893	2.1	3.8	4.5	37.8	C26 H46 N O9 S
		548.2889	2.5	4.6	15.5	1.4	C33 H39 N3 O3 Na
		548.2887	2.7	4.9	-4.5	134.0	C18 H50 N3 O11 S2
579.1602	90.67	579.1600	0.2	0.3	13.5	21.2	C28 H32 N2 O6 Na S2
		579.1606	-0.4	-0.7	22.5	0.0	C36 H28 O4 Na S
		579.1596	0.6	1.0	30.5	7.4	C41 H23 O4
		579.1610	-0.8	-1.4	35.5	16.1	C42 H19 N4
		579.1591	1.1	1.9	14.5	39.9	C27 H28 N2 O11 Na
		579.1590	1.2	2.1	21.5	2.7	C33 H27 N2 O6 S
		579.1615	-1.3	-2.2	17.5	23.4	C29 H27 N2 O11
		579.1586	1.6	2.8	32.5	8.0	C40 H20 N4 Na
		579.1619	-1.7	-2.9	27.5	2.0	C37 H24 N4 Na S
		579.1583	1.9	3.3	12.5	40.0	C25 H31 N4 O8 S2
		579.1624	-2.2	-3.8	16.5	10.1	C30 H31 N2 O6 S2
		579.1625	-2.3	-4.0	9.5	64.7	C24 H32 N2 O11 Na S

Figure S35: HRESI-MS Spectrum of compound **6h**

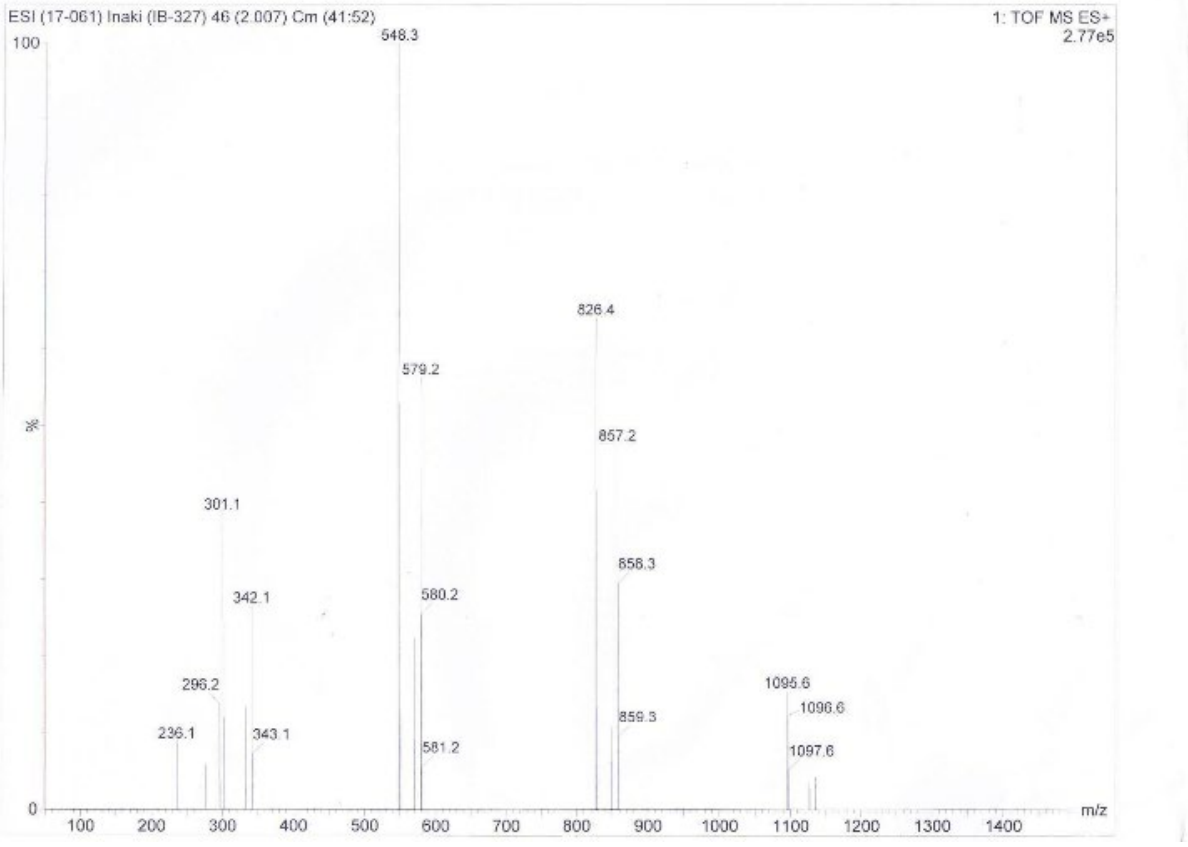

Figure S36: ESI-MS Spectrum of compound **6h**

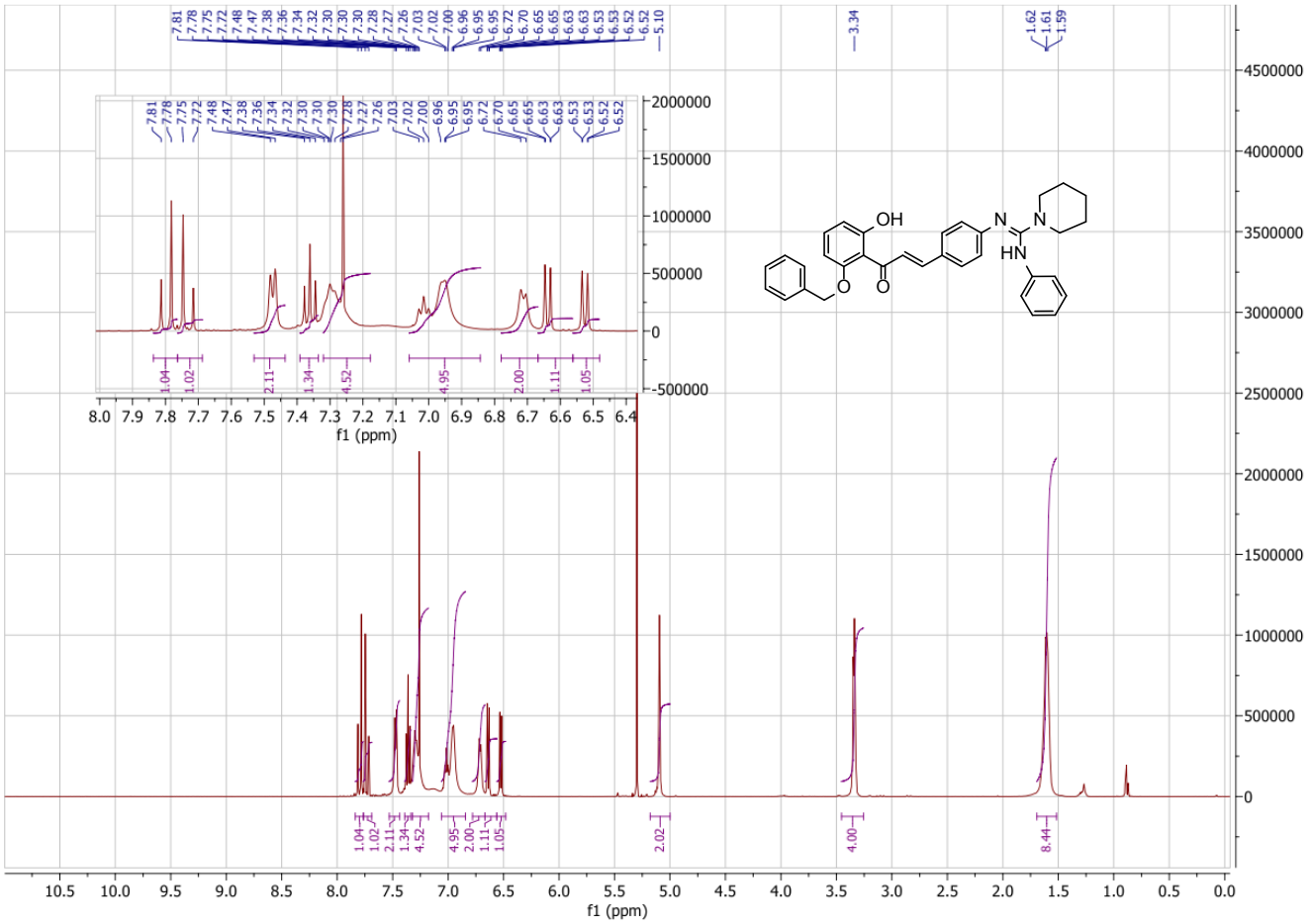

Figure S37: ^{1}H-NMR (500 MHz, $CDCl_3$) Spectrum of Compound **6i**

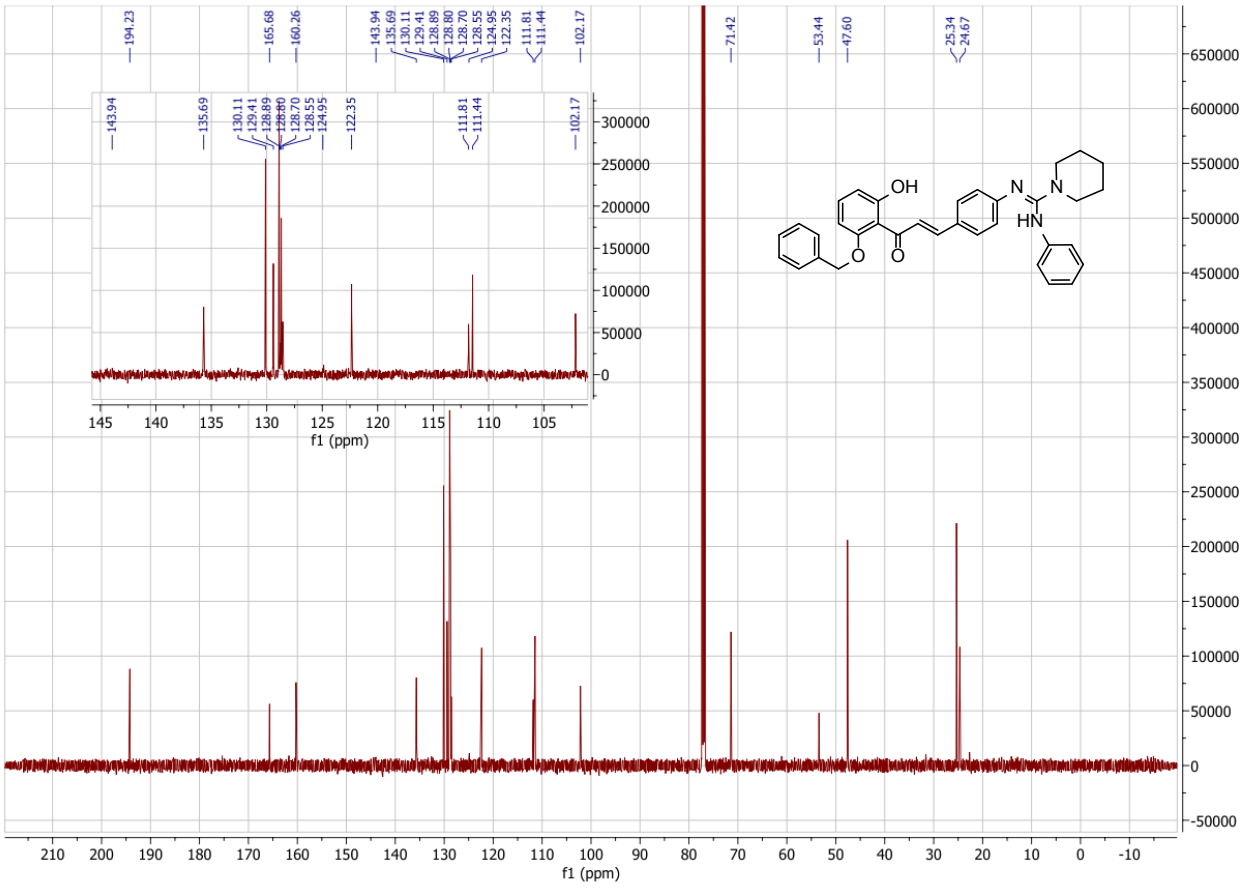

Figure S38: ^{13}C-NMR (125 MHz, $CDCl_3$) Spectrum of Compound **6i**

Elemental Composition Report **Page 1**

Tolerance = 5.0 PPM / DBE: min = -10.0, max = 1000.0
Element prediction: Off
Number of isotope peaks used for i-FIT = 2

Monoisotopic Mass, Even Electron Ions
2601 formula(e) evaluated with 6 results within limits (all results (up to 1000) for each mass)
Elements Used:
C: 0-60 H: 0-100 N: 0-4 O: 0-12 Na: 0-1 S: 0-2

ESI (17-063) Inaki (IB-329) 70 (2.444) 2: TOF MS ES+ 8.67e+002

Minimum:	60.00				-10.0		
Maximum:	100.00		100.0	5.0	1000.0		
Mass	RA	Calc. Mass	mDa	PPM	DBE	i-FIT	Formula
532.2604	100.00	532.2600	0.4	0.8	19.5	0.5	C34 H34 N3 O3
		532.2610	-0.6	-1.1	11.5	4.2	C29 H39 N3 O3 Na S
		532.2614	-1.0	-1.9	0.5	18.6	C22 H46 N O9 S2
		532.2616	-1.2	-2.3	20.5	0.0	C37 H35 N O Na
		532.2590	1.4	2.6	-2.5	25.2	C20 H47 N O9 Na S2
		532.2580	2.4	4.5	5.5	12.5	C25 H42 N O9 S

Figure S39: HRESI-MS Spectrum of Compound **6i**

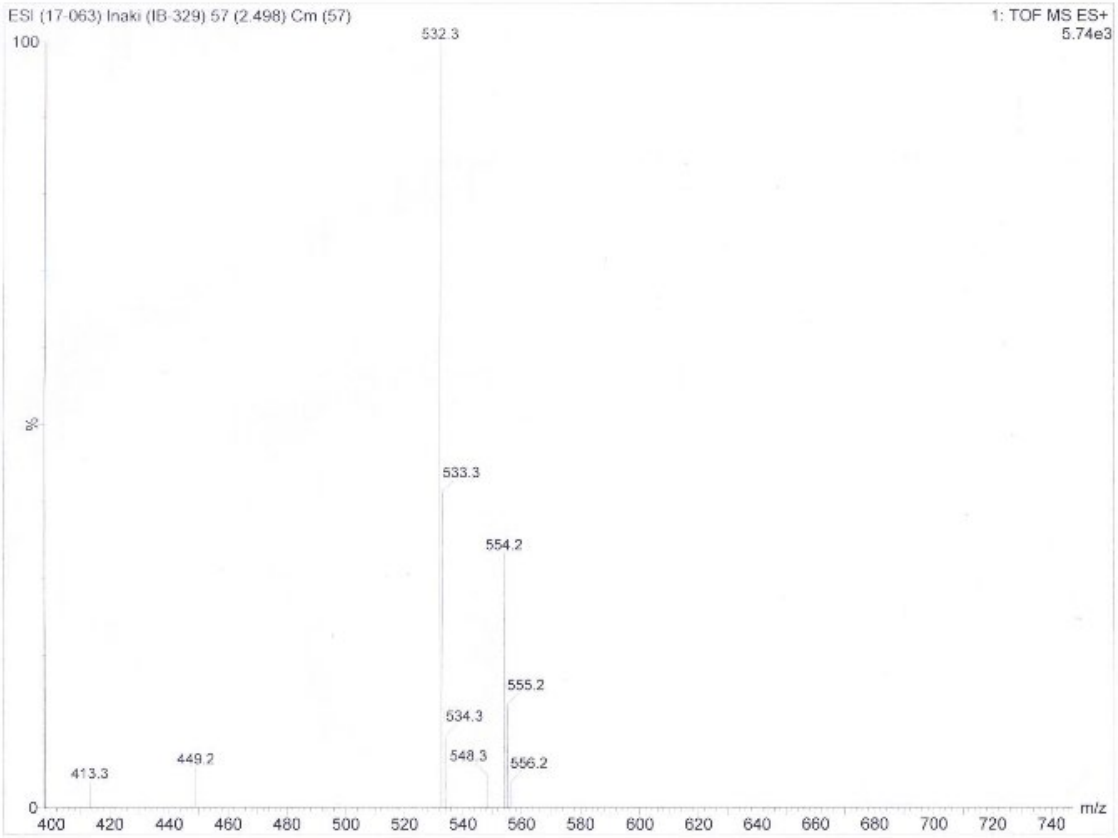

Figure S40: ESI-MS Spectrum of Compound **6i**

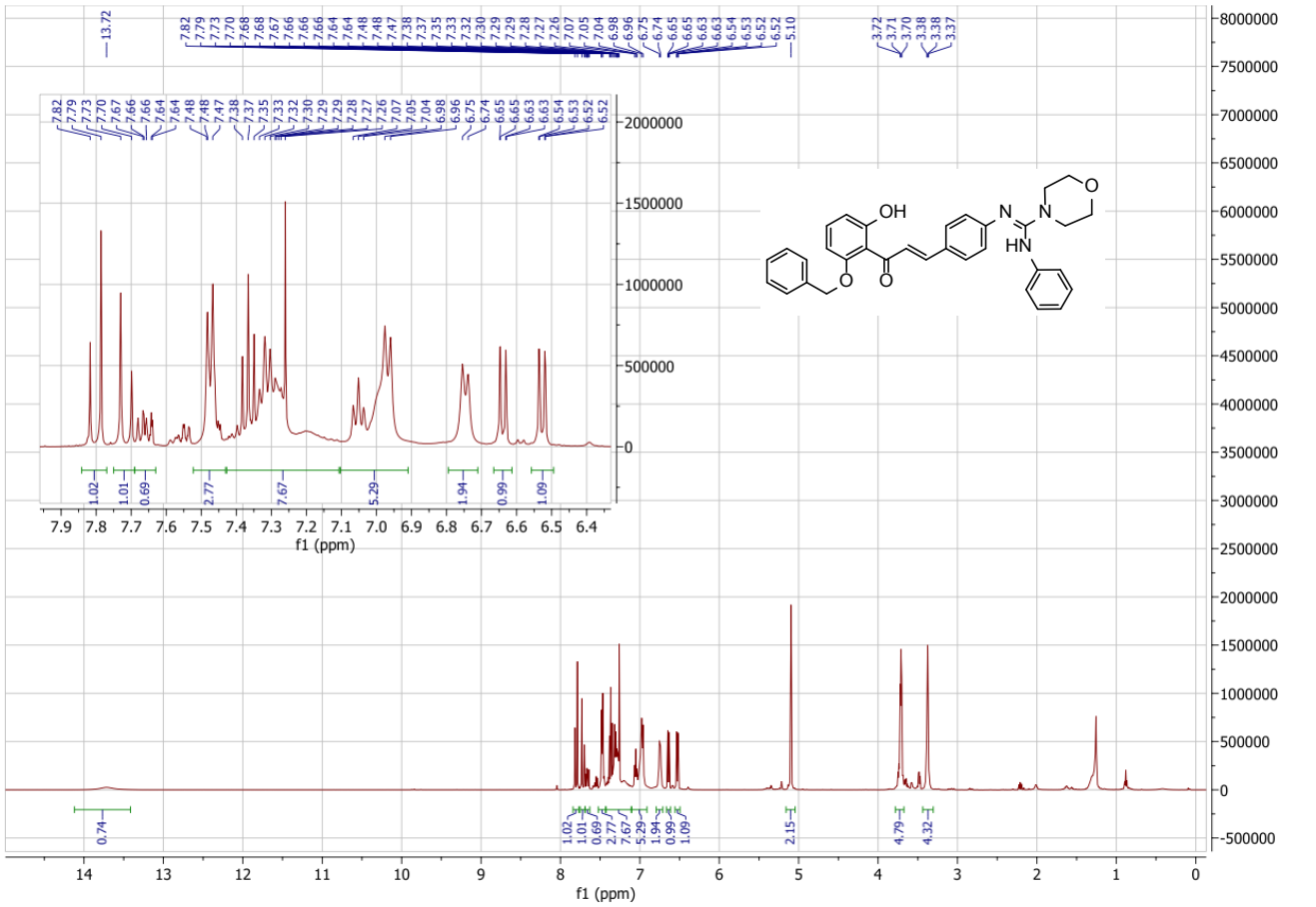

Figure S41: ^{1}H-NMR (500 MHz, $CDCl_3$) Spectrum of Compound **6j**

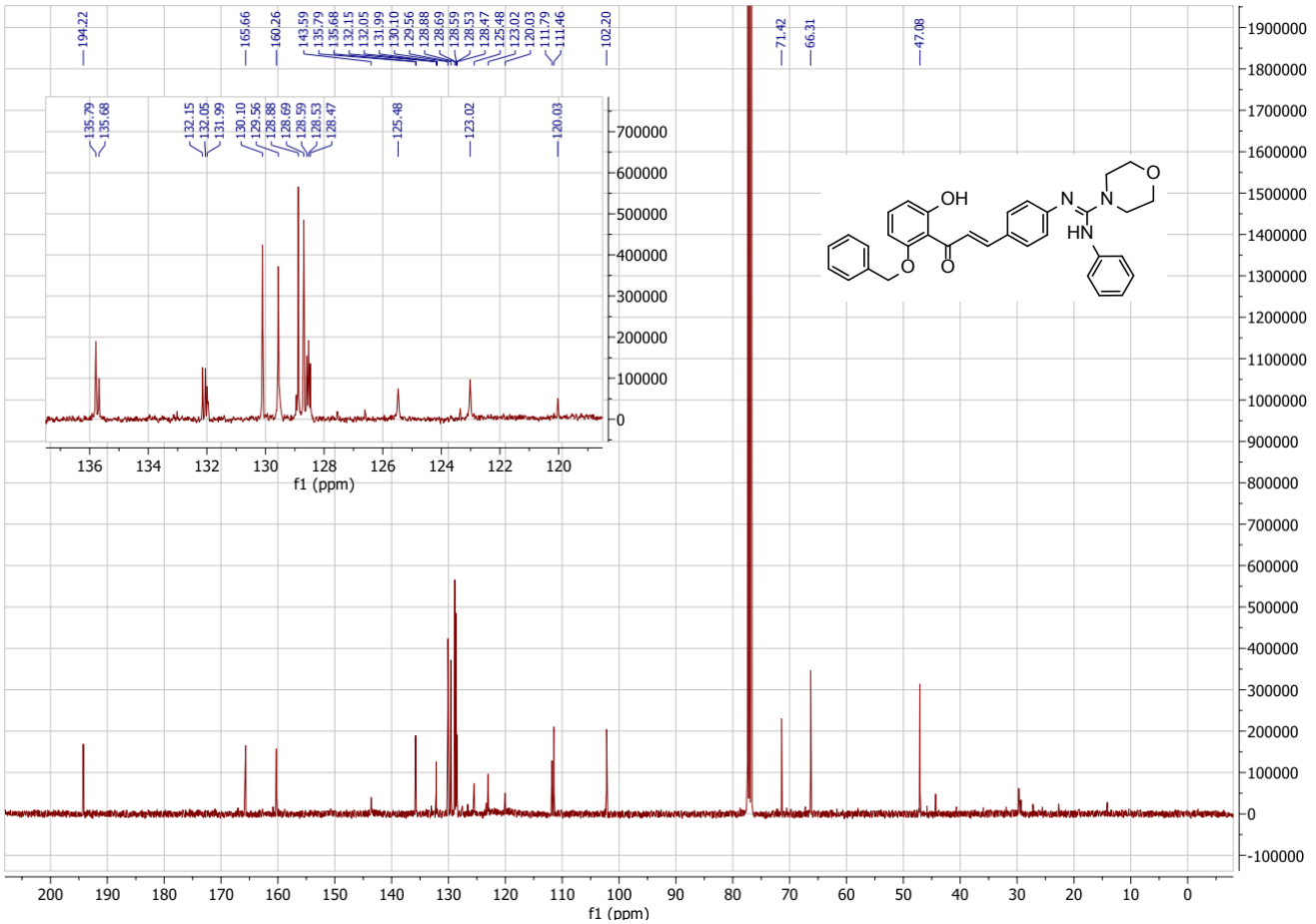

Figure S42: ^{13}C-NMR (125 MHz, $CDCl_3$) Spectrum of Compound **6j**

Elemental Composition Report **Page 1**

Tolerance = 5.0 PPM / DBE: min = -10.0, max = 1000.0
Element prediction: Off
Number of isotope peaks used for i-FIT = 2

Monoisotopic Mass, Even Electron Ions
2611 formula(e) evaluated with 6 results within limits (all results (up to 1000) for each mass)
Elements Used:
C: 0-60 H: 0-100 N: 0-4 O: 0-12 Na: 0-1 S: 0-2

ESI (17-064) Inaki (IB-330) 13 (0.454) 2: TOF MS ES+ 8.71e+002

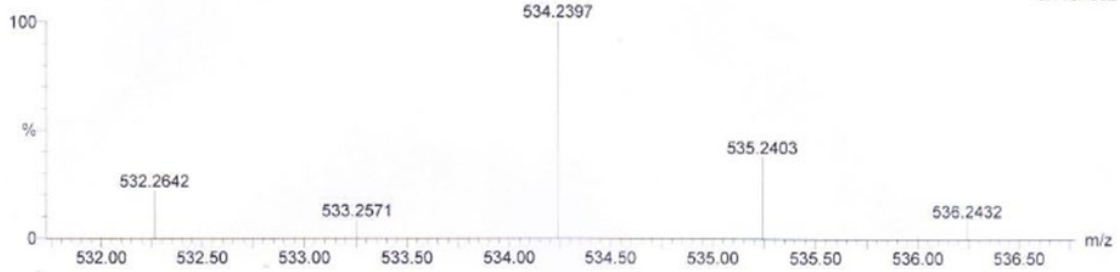

Minimum:	60.00				-10.0		
Maximum:	100.00		100.0	5.0	1000.0		
Mass	RA	Calc. Mass	mDa	PPM	DBE	i-FIT	Formula
534.2397	100.00	534.2393	0.4	0.7	19.5	0.1	C33 H32 N3 O4 +
		534.2402	-0.5	-0.9	11.5	1.2	C28 H37 N3 O4 Na S
		534.2407	-1.0	-1.9	0.5	11.9	C21 H44 N O10 S2
		534.2409	-1.2	-2.2	20.5	1.1	C36 H33 N O2 Na
		534.2383	1.4	2.6	-2.5	17.6	C19 H45 N O10 Na S2
		534.2373	2.4	4.5	5.5	6.9	C24 H40 N O10 S

Figure S43: HRESI-MS Spectrum of Compound **6j**

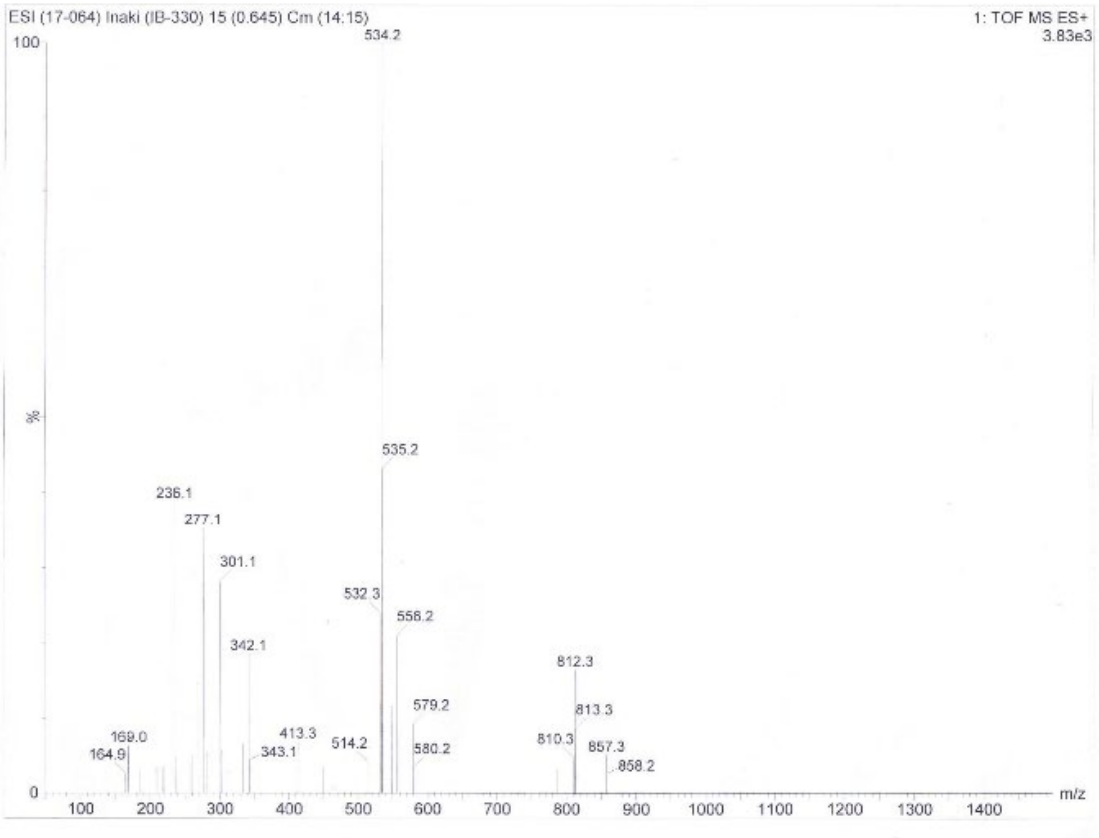

Figure S44: ESI-MS Spectrum of Compound **6j**

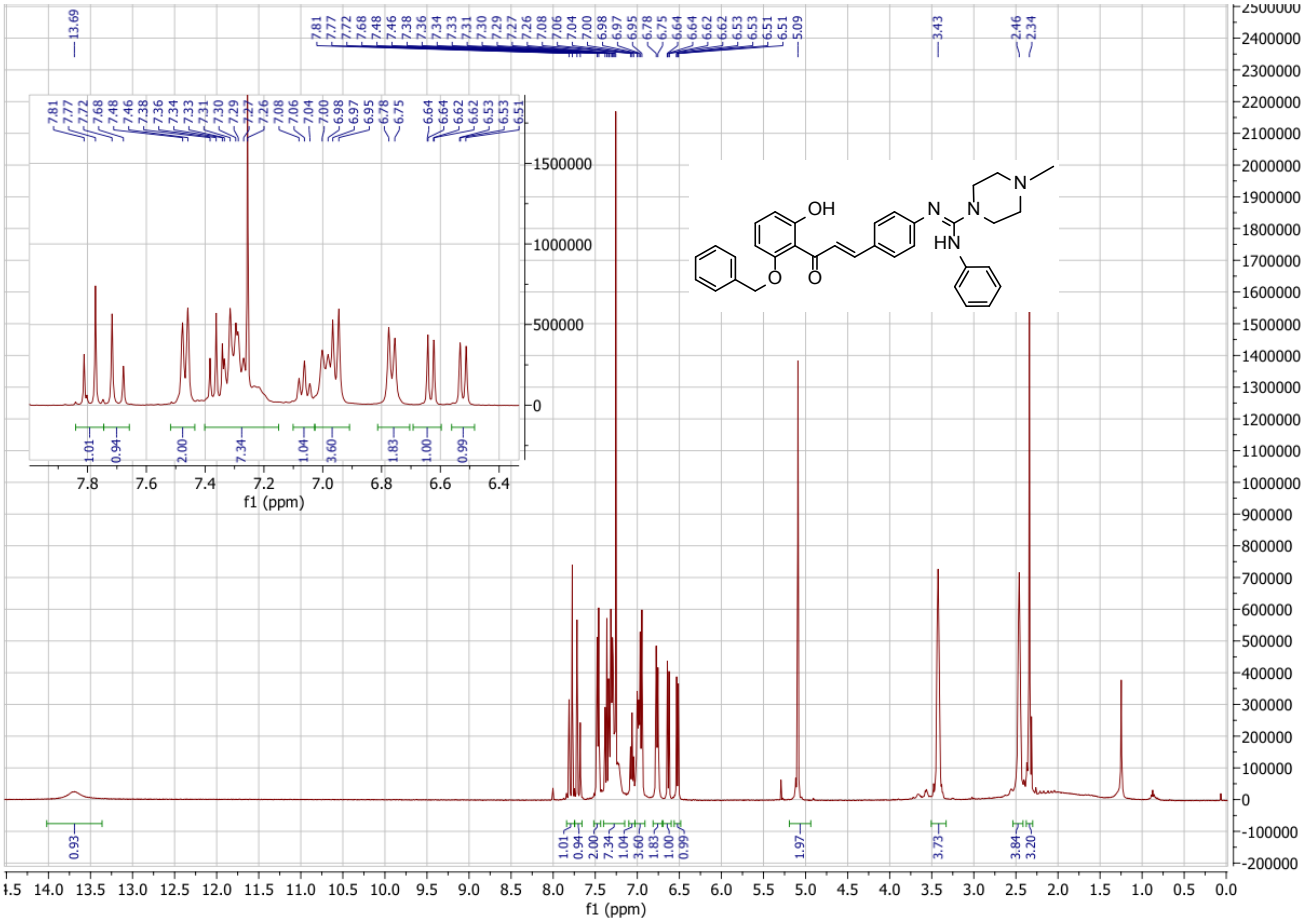

Figure S45: ^{1}H -NMR (500 MHz, $CDCl_3$) Spectrum of compound **6k**

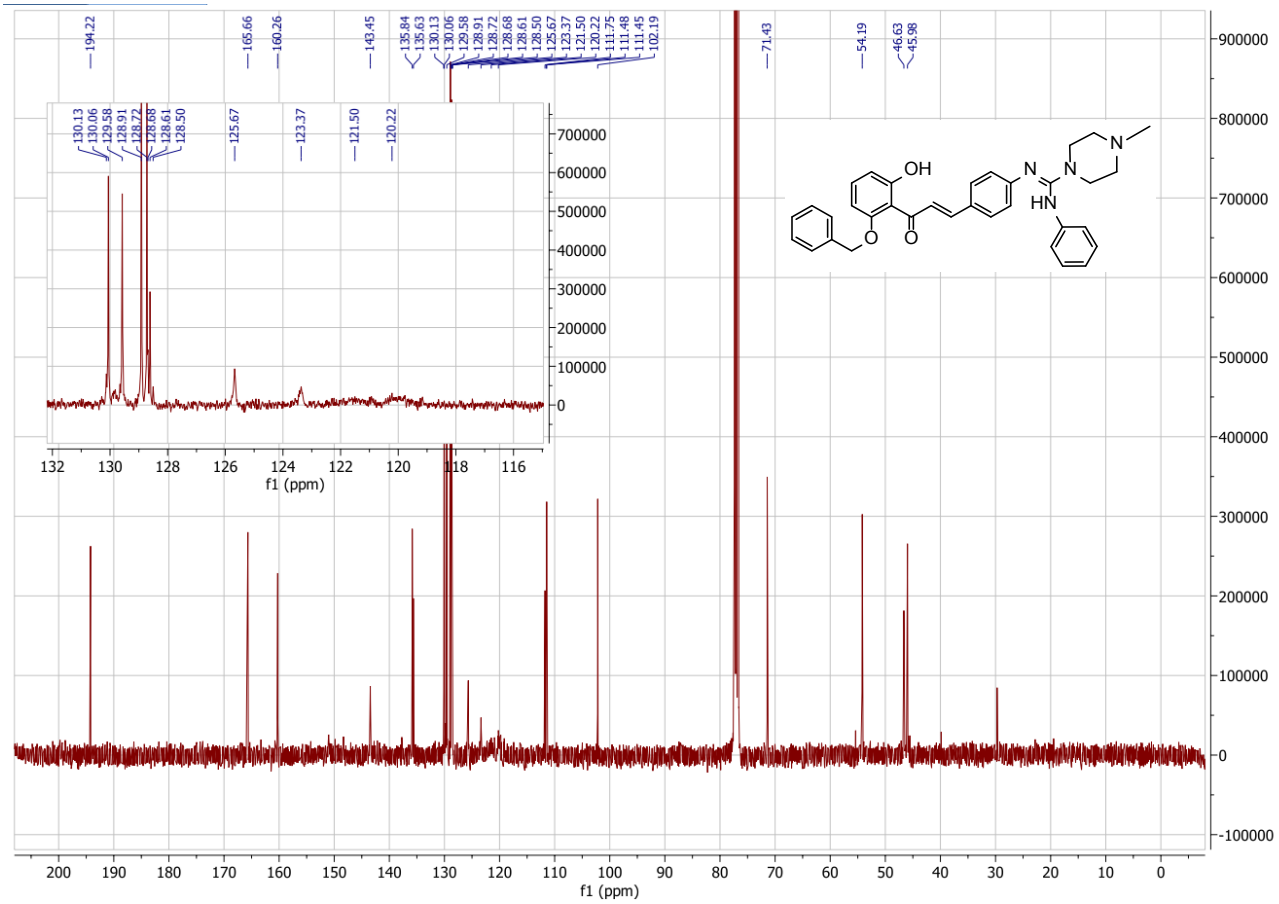

Figure S46: ^{13}C -NMR (125 MHz, $CDCl_3$) Spectrum of compound **6k**

Elemental Composition Report Page 1

Tolerance = 5.0 PPM / DBE: min = -10.0, max = 1000.0
Element prediction: Off
Number of isotope peaks used for i-FIT = 2

Monoisotopic Mass, Even Electron Ions
2682 formula(e) evaluated with 13 results within limits (all results (up to 1000) for each mass)
Elements Used:
C: 0-60 H: 0-100 N: 0-4 O: 0-12 Na: 0-1 S: 0-2
ESI (17-060) Inaki (IB-328) 147 (6.405)

1: TOF MS ES+
3.96e+003

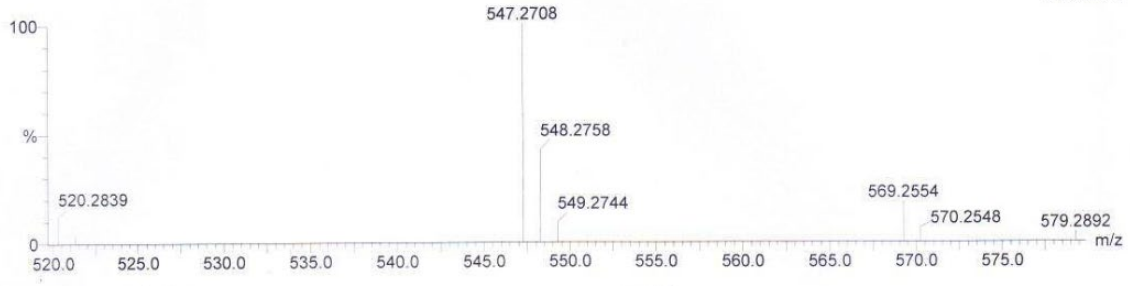

Minimum:	60.00				-10.0		
Maximum:	100.00		100.0	5.0	1000.0		
Mass	RA	Calc. Mass	mDa	PPM	DBE	i-FIT	Formula
547.2708	100.00	547.2709	-0.1	-0.2	19.5	2.0	C34 H35 N4 O3
		547.2705	0.3	0.5	6.5	33.5	C28 H44 O7 Na S
		547.2704	0.4	0.7	13.5	1.8	C34 H43 O2 S2
		547.2699	0.9	1.6	-2.5	113.3	C20 H48 N2 O9 Na S2
		547.2719	-1.1	-2.0	11.5	18.3	C29 H40 N4 O3 Na S
		547.2696	1.2	2.2	14.5	8.2	C33 H39 O7
		547.2723	-1.5	-2.7	0.5	83.2	C22 H47 N2 O9 S2
		547.2725	-1.7	-3.1	20.5	0.1	C37 H36 N2 O Na
		547.2689	1.9	3.5	5.5	55.9	C25 H43 N2 O9 S
		547.2730	-2.2	-4.0	2.5	83.6	C24 H44 O12 Na
		547.2730	-2.2	-4.0	9.5	19.3	C30 H43 O7 S
		547.2685	2.3	4.2	16.5	8.0	C32 H36 N4 O3 Na
		547.2683	2.5	4.6	-3.5	154.6	C17 H47 N4 O11 S2

Figure S47: HRESI-MS Spectrum of Compound **6k**

ESI (17-060) Inaki (IB-328) 154 (6.720) Cm (150:162)

1: TOF MS ES+
5.72e4

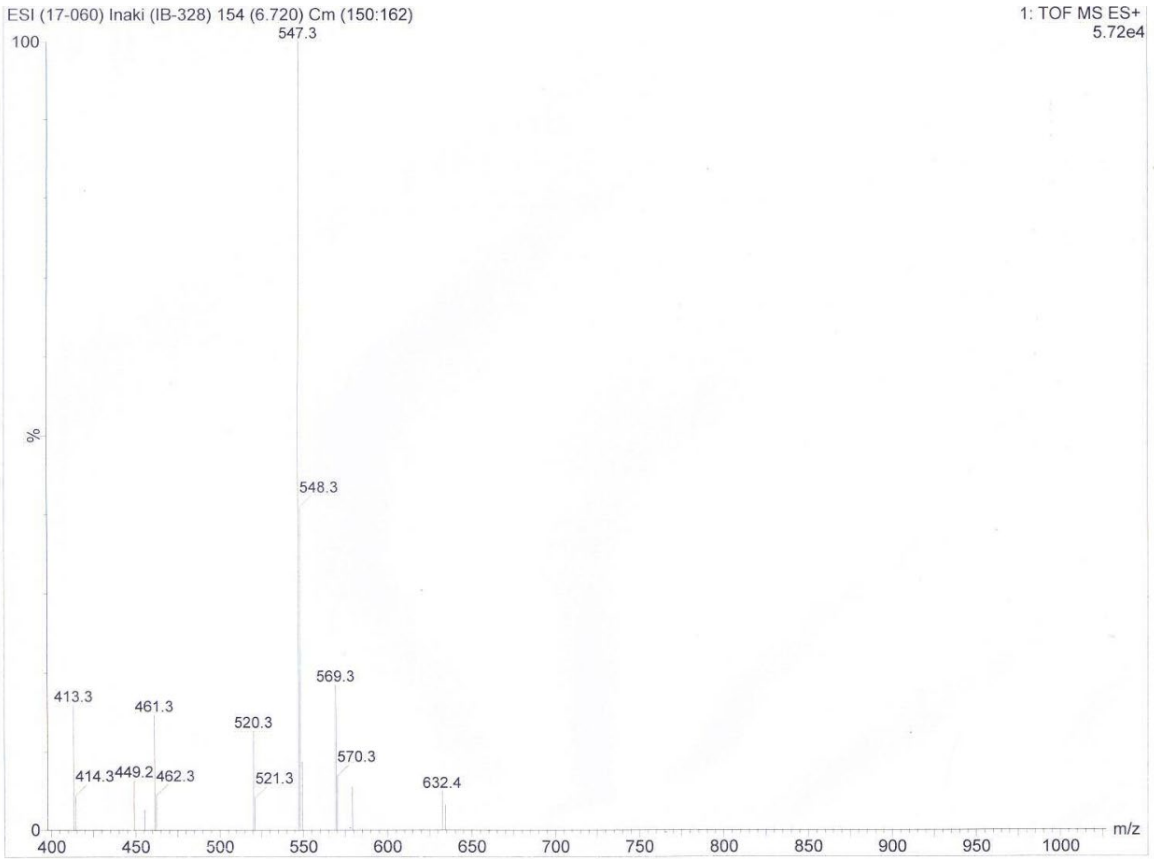

Figure S48: ESI-MS Spectrum of Compound **6k**

Contraportada: Microfotografía óptica de contraste de fases de un campo representativo de células de melanoma humano SK-MEL-1.

Esta Tesis es el resultado de una línea de investigación conjunta entre el Departamento de Bioquímica y Biología Molecular, Fisiología, Genética e Inmunología de la Universidad de Las Palmas de Gran Canaria, Unidad Asociada al CSIC, y el Consejo Superior de Investigaciones Científicas a través del Instituto de Productos Naturales y Agrobiología. En esta Tesis hemos explorado compuestos naturales y sintéticos derivados de quince átomos de carbono que afectan a la viabilidad de varias líneas celulares de cáncer humanas y determinado sus relaciones estructura-actividad. Los compuestos estudiados incluyen flavonoides, lactonas sesquiterpénicas del grupo de las guayanolidas y compuestos híbridos constituidos por guanidinas trisustituidas conteniendo un núcleo 1,3-difenilpropenona. Los estudios del mecanismo de acción de algunos de estos compuestos revelan que bloquean las células en la fase G_2-M del ciclo celular y modulan vías de señalización de muerte celular regulada. Los resultados presentados aquí sientan las bases científicas para explorar la potencial utilidad de estos compuestos y/o sus derivados solos o en combinación en el campo de la Oncología.